Identifying mechanisms and biomarkers predictive of efficacy of vaccines against opioid use disorders and overdose

A DISSERTATION

SUBMITTED TO THE FACULTY OF THE GRADUATE SCHOOL

OF THE UNIVERSITY OF MINNESOTA

BY

Bethany Crouse

IN PARTIAL FULFILLMENT OF THE REQUIREMENTS

FOR THE DEGREE OF

DOCTOR OF PHILOSOPHY

Advisor, Marco Pravetoni

August 2022

Acknowledgements:

I would like to thank the following people:

My advisor Dr. Marco Pravetoni for accepting me into the lab, for providing financial and intellectual support for my project, and for providing many opportunities for collaboration and mentorship over four years of research. My committee members Drs. Tanya Freedman, Pam Skinner, and Andy Harris for guidance and helpful suggestions regarding my work and career path. My current and former lab members Dr. April Huseby Kelcher, Dr. Carly Baehr, Dustin Hicks, Valeria Gradinati, Christine Robinson, Dr. Mariah Wu, Dagny Hemisdottir, Daihyun Song, Yue Zhang, Fatima Hamid, Pedro Silva, Diego Luengas, Dr. Cheryl Marker, Dr. Mike Raleigh, Josie Conn, Dr. Stefano Persano, Maria Guevara Lopez, and Aaron Khaimraj for experimental advice, technical and emotional support, and providing a fun lab environment to keep spirits up. Our collaborators Drs. Mark LeSage, Alonso Guedes, Angela Birnbaum, Sabita Roy, Li Zhang, Jay Evans, Shannon Miller and others from the University of Montana for invaluable research support and contributions to the work presented here. Yorie Smart and the PharmacNeuroImmunology NIH T32 training program for providing financial support and opportunities for career development. The University of Minnesota core facilities including University Imaging Center, University Flow Cytometry Resource, the Genomics Center, and the Informatics Institute for technical and research assistance. The Department of Pharmacology for accepting me into their program and providing guidance along the way.

Finally, I would like to thank my family members Rhonda Crouse, Jeremy Crouse, Jerico Crouse, and Sean Adamson, who provided constant emotional support and encouragement.

Abstract:

Opioid use disorders (OUD) and overdose are public health crises that are worsening despite the availability of approved pharmacotherapies. Active immunization with anti-opioid conjugate vaccines is a novel therapeutic strategy to treat OUD and prevent overdose. To date, clinical studies suggest that efficacy of anti-drug conjugate vaccines is limited to a subset of individuals who can produce optimal antibody responses. To increase positive treatment outcomes and clinical success, this research program investigated several complementary strategies to increase OUD vaccine efficacy. First, mechanisms of optimal anti-opioid vaccine response are investigated by elucidating the immunological mechanisms behind a previously established interleukin-4 (IL-4) mediated increase in vaccine efficacy. These studies found that depletion of IL-4 resulted in a Type I IL-4R mediated increase in germinal center formation and germinal center T cell response which leads to increased opioid-specific antibody secreting cells, and that vaccine efficacy is dependent on a balanced Th_1/Th_2 T cell response in mice. Next, these results provided a blueprint for next generation anti-fentanyl vaccine formulations incorporating novel adjuvants targeting toll-like receptors (TLRs). These data show that a TLR7/8 agonist adjuvant increases vaccine efficacy in rodent and porcine models of fentanyl misuse and overdose. Third, vaccine design and immunization paradigms were assessed to optimize the efficacy of a novel carfentanil vaccine alone and in combination with a lead fentanyl vaccine. Longer linker lengths and a co-administered bivalent immunization strategy were associated with increased vaccine efficacy. Then, environmental factors contributing to the immune response are investigated by testing whether changes in the gastrointestinal microbiome would affect vaccine efficacy and whether these specific changes in the microbiome could be utilized as biomarkers. These studies revealed that changes in the microbiome in specific pathogen free or immune-

experienced rodents did not affect efficacy of anti-oxycodone or anti-fentanyl vaccines. Finally, exploratory studies were performed to identify putative biomarkers that may be predictive of anti-opioid vaccine response in preclinical and clinical investigations. These studies indicate that pre-immunization concentration of IL-4 is correlated with vaccine efficacy in genetically diverse mice, and that specific cytokines may be of interest as indicators of immune response in human patients. Overall, the findings outlined in this research program support the use of novel adjuvants and predictive biomarkers to increase clinical efficacy of vaccines to treat OUD and overdose.

Table of Contents:

List of Figures

List of Tables

Chapter 1: Introduction

Opioid pharmacology. Opioids have been used as a medication for pain relief for thousands of years. The opium poppy (from which naturally occurring opioids are derived) was reported to have been cultivated as early as 3400 BC in Mesopotamia, and records show that ancient Egyptians used opium for pain relief [(1), reviewed in (2)]. Opioids canonically produce their effects by signaling through the mu, kappa, or delta opioid receptors (MOR, KOR, and DOR), which are 7-transmemberane G-protein coupled receptors that are found within the CNS and in peripheral tissues. Signaling through opioid receptors leads to activation of β-arrestin and $G_{i/o}$ signaling, which causes potassium efflux, inhibits calcium influx, and inhibits downstream cyclic-AMP production and second messengers. This can lead to a myriad of tissue-dependent physiological effects. For example, opioid signaling in the presynaptic terminal of nociceptive C fibers and A delta fibers inhibit the release of pain neurotransmitters such as glutamate and substance P, while opioid signaling in presynaptic GABA neurons prevents inhibitory GABA signals on dopaminergic neurons, leading to an increase in dopamine which causes an opioid's rewarding and reinforcing effects [reviewed in (3)]. Additionally, opioid receptor activation in the preBötzinger Complex and nucleus tractus solitarii can lead to respiratory depression (4)—a common and dangerous adverse effect which can be fatal. Many commonly prescribed opioids, including morphine, oxycodone, hydrocodone, and fentanyl, exert most of their pharmacological effects by binding to the MOR (3). These medications have varying potency and efficacy at the MOR, with fentanyl being 80x more potent than morphine (3). While opioids are critically important medications for control of moderate to severe pain, they are also extremely addictive due to their action at dopaminergic neurons.

History of opioid use disorder and overdose. Recent data suggests opioid use disorders (OUD) affect over 2 million people in the United States, and over 40 million individuals worldwide (5). Those with OUD are at high risk for opioid overdose, with over 75% of the 100,306 drug overdoses in the United States being attributed to opioids in the 12 months ending in April 2021 (6). The SARS-CoV-2 pandemic has further increased both fatal and non-fatal overdoses attributed to opioids alone or in combination with other drugs of abuse (7-11). The rise in OUD and overdose has become a public health crisis, which began in the 1990s with increased availability of prescription opioids such as oxycodone and the belief that opioids were not addictive when prescribed to pain patients. A second wave of opioid misuse began in 2010 following the increased availability and low cost of heroin, which caused heroin use to increase almost 5-fold. More recently, a third wave of opioid misuse has followed the increased availability of cheap, synthetic opioids such as fentanyl. Due of its extremely high potency and its use as an adulterant in street drug mixtures, unintentional and intentional consumption of fentanyl has led to a 10-fold increase in opioid overdose deaths over the last 10 years [reviewed in (12)]. The opioid public health crisis has also become an enormous economic burden. It was estimated that in 2017, the total cost of the opioid crisis in the United States was $1.02 trillion (13) when accounting for health care ($31.3 billion), OUD treatment ($3.5 billion), criminal justice costs ($14.8 billion), lost productivity ($100 billion), reduced quality of life ($390.0 billion), and life lost to opioid overdose ($480.7 billion).

Medications for OUD and overdose. Current medications for OUD (MOUD) include the MOR agonist methadone, the partial agonist buprenorphine, and the antagonist naltrexone. Agonist or partial agonist therapy with methadone or buprenorphine, known as maintenance therapy, prevents withdrawal and attenuates craving by replacing the misused opioid with a longer acting, less rewarding opioid [reviewed in (14)]. While

methadone has an estimated 64.1% treatment retention (15), it also has severe side effects such as respiratory depression and cardiac arrhythmia (14). Furthermore, both methadone and buprenorphine [which has an estimated treatment retention of 54.1% (15)] have the potential for diversion for illicit use. Because of these shortcomings, these medications must be given daily in the office of a licensed physician which complicates patient compliance, particularly for individuals in rural areas or without access to reliable transportation (12, 14). On the other hand, antagonist therapy with naltrexone blocks the MOR binding site which prevents the rewarding effects from the misused opioid. This treatment option has a retention rate of 41% (15), with hindered compliance due to the fact that opioid users must be abstinent from opioid use for 7-14 days before initiating naltrexone therapy, leading to unpleasant withdrawal symptoms (12, 14). Extended-release formulations of buprenorphine and naltrexone are now FDA-approved, which may increase retention and improved treatment outcomes (12, 14). Additionally, combinations of agonists and antagonists, such as the buprenorphine and naloxone combination Suboxone, have mitigated some concerns for diversion (14). These pharmacological treatments can be combined with cognitive behavioral therapy or counseling, although it is unclear whether this improves treatment outcomes compared to MOUD alone (16-18).

The gold standard for treatment of opioid overdose is the MOR antagonist naloxone. This medication can be administered intravenously (i.v), intramuscularly (i.m), or intranasally (i.n) and can reverse overdose in a matter of minutes; however, this is contingent on the availability of naloxone to the bystanders of an overdose situation, and their ability to properly administer it within a short timeframe (19). Furthermore, naloxone may be insufficient to reverse the effects of highly potent opioids such as fentanyl or its analogues, such as carfentanil. Fentanyl has a quick onset of action, making it difficult to administer naloxone in the time before fatal overdose occurs (12), and fentanyl's high

potency often leads to a return of opioid overdose symptoms even after apparent recovery, known as “re-narcotization” (20). Finally, fentanyl has been shown to induce muscle rigidity in the chest, known as “wooden chest syndrome”, which is mediated by cholinergic and α_1-adrenergic receptors and is insufficiently reversed by administration of a MOR antagonist (21-23). Because of the limitations of current pharmacotherapies of OUD and overdose, novel therapeutic options to treat OUD and overdose are urgently needed.

Vaccines against OUD. Active immunization with an anti-opioid conjugate vaccine is a novel therapeutic strategy that may be used alone or in combination with currently available MOUD. Anti-opioid vaccines consist of an opioid-based hapten structure conjugated to a large immunogenic carrier protein and formulated with an adjuvant such as aluminum hydroxide (alum) to stimulate an immune response. Active immunization stimulates the production of opioid-specific antibodies which neutralize the drug and prevent its distribution to the brain, inhibiting opioid-induced effects. The first record of anti-opioid vaccines appeared in the 1970s when two groups demonstrated proof of principle that active immunization with a morphine-based vaccine could attenuate the effects of morphine (24) and heroin (25). Since then, anti-opioid vaccines targeting oxycodone and hydrocodone (26-36), morphine and heroin (37-52), fentanyl (37, 38, 40, 53-57), and fentanyl analogues (57-61) have been developed and characterized for preclinical efficacy, selectivity and safety. Vaccines against opioids have been shown to reduce opioid-induced pharmacological effects such as locomotor activity (41, 42, 47, 62-64), antinociception (26-31, 33, 34, 36-46, 50-57, 59-63, 65-76), respiratory depression and bradycardia (33, 34, 54, 55, 59, 61, 68), and lethality (29, 39) using a variety of animal models and drug administration paradigms. Additionally, anti-opioid vaccines have been shown to attenuate acquisition and dose-escalation of opioid-self administration behavior (30, 32, 35, 49, 55, 69, 74, 77), reinstatement of opioid-self administration after extinction

(47, 64, 69), decrease opioid-induced conditioned place preference (46, 63, 69), and attenuate opioid vs. food choice in rats (56, 67) and rhesus monkeys (56, 78). Polyclonal antibody responses produced by anti-opioid vaccines have been shown to have high affinity toward the target opioid (30, 37, 38, 44-47, 49, 52, 53, 55-57, 59, 60, 64-67, 78, 79) with low cross-reactivity to off-target molecules (33, 35, 39, 45, 47, 49, 52, 54, 55, 57, 64, 67), including MOUD. In fact, anti-opioid vaccines given in combination with regular or extended-release naltrexone were found to be more efficacious in preventing opioid-induced motor activity, antinociception, and respiratory depression compared to either treatment alone (80, 81), further highlighting the ability of anti-opioid vaccines to be used in combination with MOUD to improve treatment outcomes. This extensive preclinical efficacy and safety data has led to testing an oxycodone vaccine (OXY-sKLH) in an ongoing Phase Ia/Ib clinical trial (NCT04458545).

Clinical findings of vaccines for substance use disorders (SUD). To date, clinical trials testing vaccines for substance use disorders (SUD) have had mixed results. While some Phase II trials for nicotine vaccines have shown promising efficacy in increasing smoking cessation rates, several large Phase III trials failed to meet their primary efficacy endpoints [reviewed in (82)]. However, clinical trials of both anti-nicotine (83) and anti-cocaine vaccines (84) have found that significant efficacy in obtaining drug abstinence was achieved in individuals who produced high titers of high affinity antibodies. In an anti-cocaine vaccine trial, it was found that individuals with greater than 43 μg/mL cocaine-specific serum IgG concentrations had increased cocaine-free urine and a >50% reduction of cocaine use overall, but only 38% of subjects attained this serum antibody concentration (84). This highlights the large individual variability in immune response between patients, and the importance of investigating strategies to increase vaccine efficacy to overcome variability and enhance clinical success. These strategies can include examining

molecular mechanisms associated with OUD vaccine response, evaluating novel adjuvants to increase antibody production, modifying vaccine design and immunization paradigms, investigating the influence of environmental factors that affect the immune system, and discovering predictive biomarkers to identify patients most likely to response to anti-opioid vaccination.

Immunological mechanisms underlying an immune response to vaccines. Investigations into the mechanisms of vaccine response are critical to identify immunological targets for adjuvants and biomarkers and to determine the type of immune response necessary for optimal vaccine efficacy. In general, protein antigens introduced through intramuscular or intranasal immunization are phagocytosed by antigen-presenting cells such as dendritic cells (DCs) and processed for antigen presentation on major histocompatibility complex (MHC) I or II receptors on the cell surface, while simultaneously trafficking to the draining lymph node or other secondary lymphoid organ (SLO) (85). Once in the lymph node, dendritic cells present the processed antigen to activate naïve CD4+ T cells through the T cell receptor (TCR) and produce signals for the T cell to become CD4+ follicular helper T cells (T_{fh}) or T helper (Th) cells (85). There are various subtypes of Th cells, including Th_1, Th_2, Th_{17}, and Th_9, which have varying functions in different pathogen contexts (86, 87). Meanwhile, intact antigen can be presented to naïve B cells through their B cell receptor (BCR) through interactions with dendritic cells, macrophages, or follicular dendritic cells (FDCs). Antigen-specific B cells can also bind to the target antigen and act as antigen presenting cells, or can be activated by either cross-linking of BCRs or by presence of cognate CD4+ T cells. Activated B and T cells form a germinal center (GC) in the SLO, where activated B cells participate in somatic hypermutation in the GC dark zone to increase the affinity of their BCR to the target antigen. B cells then traffic to the GC light zone, where they test their affinity for the target antigen through interactions

with FDCs and receive survival and differentiation signals through interactions with both FDCs and cognate T cells. T cells can produce signals in the form of cytokines such as interleukin (IL)-2, IL-4, and IL-21 which instruct the B cell to class-switch their antibody constant region (Fc) from IgM and IgD to IgE, IgA, or IgG, which can also be further categorized into IgG_1, $IgG_{2a,}$ and IgG_3 subclasses. After increasing BCR affinity through several rounds of somatic hypermutation, B cells can differentiate into antibody-producing plasma cells, or into memory B cells which are reserved for repeat antigen encounter [reviewed in (88-91)]. When introduced to polysaccharide antigens, humoral responses can also be "T cell independent" wherein small GCs are formed outside of the B cell follicle and generally produce low-affinity IgM antibodies (92). In addition to humoral responses through antibody production, immunization can also lead to cell-mediated immunity, such as the activation of CD8+ cytotoxic T cells and natural killer (NK) cells (93). Since OUD vaccines are thought to primarily depend on the production of antibodies, the majority of research into OUD vaccine mechanisms has focused on humoral responses.

Mechanisms of OUD vaccine efficacy. Mechanisms of OUD vaccine efficacy are relatively understudied. Published literature has shown that OUD vaccines rely on T cell dependent B cell activation and germinal center formation in SLOs. Mice without functional CD4+ T cells do not develop protective antibody responses to an OXY-sKLH vaccine (27), and immunization with OXY-sKLH in wild-type (WT) mice led to increases in GC B cells and T cells after immunization (94), suggesting that GC formation is critical for vaccine efficacy. Furthermore, immunization with opioid-based haptens conjugated to T cell independent antigens such as ficoll or dextran did not elicit an antibody response supporting the hypothesis that cross-linking is not sufficient for vaccine efficacy against small molecules (27). Additionally, it was found that antibody-mediated effector functions are not necessary for vaccine efficacy after drug challenge (95). In these studies, mice

with genetic deletions for the FcγRI-IV, which contribute to IgG-mediated effector functions, were immunized with an anti-oxycodone vaccine (OXY-sKLH), challenged with oxycodone, and compared to WT mice. There were no differences in antibody titers or efficacy in response to oxycodone challenge between the two sets of mice, suggesting that antibody effector functions do not contribute to vaccine efficacy. Furthermore, a separate study involved immunizing mice with OXY-sKLH and depleting phagocytotic cells such as macrophages and granulocytes immediately before challenge with oxycodone. Macrophage or granulocyte depletion did not affect vaccine efficacy, suggesting these cell populations are not important for neutralization of the target drug after challenge (95). Immunization of toll like receptor 4 (TLR4) deficient mice with OXY-sKLH led to impaired antibody responses, suggesting that TLR4, and perhaps other TLRs, are important for vaccine response (31). Investigations into conjugate vaccine design such as varying carrier protein and linker length have had mixed results as to whether certain carrier proteins or a longer linker length is beneficial for vaccine efficacy through enhanced engagement of B and T cell populations (28, 31, 55, 96). Finally, factors such as age, sex, and strain have been investigated in the context of vaccine efficacy in mice (72, 97). Other environmental and genetic factors, such as microbiome or comorbid conditions, have yet to be assessed. These studies investigating the mechanisms behind OUD vaccine efficacy are critical for rational vaccine design, however more studies are needed to fully understand how to optimize vaccine response. Additionally, further exploration into factors that impact vaccine efficacy such as specific cell populations, signaling pathways, or environmental or genetic conditions could result in identification of putative biomarkers in clinical studies.

Adjuvants for SUD vaccines. Most first-generation SUD vaccine formulations, including those tested in clinical trials, have used aluminum hydroxide (alum) as an

adjuvant. Alum is currently the most widely used adjuvant in FDA-approved vaccine formulations and is often chosen due to its known efficacy and safety profile (98). However, since current clinical studies suggest alum alone may not be enough to produce a sufficient antibody response, additional adjuvants and novel delivery platforms have been investigated with OUD vaccines to increase the antibody response after immunization. In preclinical studies, OUD vaccines have been tested with MF59 (97), LTA1 and dmLT (99), TLR agonists CpG ODN (37, 73) and MPLA (31), Advax (37), complete Freund's (31), and ALF (42) with varying success, although many of these adjuvants are not suitable for translation to clinical studies due to cost, patent rights, or toxicity. More recently, our lab investigated whether the addition of immunomodulators, including an anti-IL2R monoclonal antibody (mAb), anti-IL-7R mAb, anti-IL-4 mAb, anti-ICOSL mAb, or anti-PD-L1 mAb would increase the immune response to an anti-oxycodone vaccine (OXY-sKLH). It was found that the addition of a depleting IL-4 mAb increased oxycodone-specific IgG titers, increased subclass switching from IgG_1 to IgG_{2a}, and increased efficacy of the vaccine after drug challenge (94). Administration of a model antigen with IL-4 depletion also led to an increase in GC-T_{fh} cells. These studies were replicated with an IL-4 genetic knockout mouse, but results were not replicated when administering a non-depleting IL-4 antibody (94). IL-4 has previously been shown to be crucial for B cell proliferation and GC formation in a variety of contexts (100-106), making it an unusual finding that depletion of IL-4 would increase vaccine efficacy. Therefore, elucidating the mechanisms behind the increase in efficacy after IL-4 depletion at both the cellular and molecular level to may help determine factors that contribute to optimal vaccine efficacy.

IL-4 is an incredibly pleotropic cytokine that is produced by T cells (particularly Th_2 cells), natural killer T (NKT) cells, mast cells, innate lymphoid cells, eosinophils, and

basophils (107). IL-4 can signal through either the type I or type II IL-4 receptors (IL-4R). The type I receptor consists of the IL-4Rα and the IL-2R common gamma chain (γ_c) and can only be activated in response to IL-4. This receptor complex is found on most lymphocytes and myeloid cells. Downstream of this receptor is signal transducer and activator of transcription (STAT)6 and insulin receptor substrate (IRS)-2. The type II receptor consists of the IL-4Rα and the IL-13Rα1, and this receptor complex can signal in response to IL-4 or IL-13. The type II receptor is found on most myeloid and non-hematopoietic cells, and canonically signals downstream through STAT6 [reviewed in (108)]. IL-4 is extremely important for the protection against parasites and helminth worms (109-111), and has more recently been shown to be critical for GC formation in many contexts (100-106, 112, 113). Activation of IL-4 signaling leads to a variety of effects, including inducing macrophage transcription programs and polarization (114), Th_2 cell differentiation (115), mast cell and eosinophil proliferation (116), stimulation of GC B cells (104), class switching to IgE (113, 117), and skewing the memory cell vs. plasma cell choice in activated B cells (100, 101, 104, 112). Immunizing IL-4 deficient mice (102, 104), mice with STAT6 deficient B cells (103), antibody-based depletion of IL-4 (102, 106), or depletion of cells that produce IL-4 (102) leads to smaller or misshapen GCs with less GC B cells and altered gene expression, which leads to impaired antibody responses and decreased vaccine efficacy. On the other hand, a handful of studies have suggested that depletion of IL-4 can positively affect GC formation and increase vaccine efficacy (118-120). These contradicting reports suggest that the role of IL-4 in the GC may be dependent on antigen context. A recent paper further highlights the complex role of IL-4 in the GC by showing that the IL-4R can both activate signaling in some cell populations, while also acting as a decoy to sequester IL-4 away from the GC in other cell populations, such as FDCs (101). This multi-faceted and often contradictory role of IL-4 during immunization is

mirrored by findings seen with OUD vaccines, and investigating the changes in vaccine response after IL-4 depletion may elucidate important novel mechanisms for targeted adjuvant delivery, such as with selected TLR agonists.

TLRs are a group of pattern recognition receptors (PRRs) on innate immune cells that respond to pathogen associated molecular patterns (PAMPs) to stimulate the immune response early in infection (121). Because immunization starts with delivery of the antigen in the periphery where innate immune cells are found, TLRs and other PRRs are common targets for adjuvants in novel vaccine formulations. There are currently 13 known TLRs, all of which produce a distinct immune profile in response to stimulation by specific ligands (122). Stimulation of some TLRs can produce primarily cytotoxic cell responses, while others produce CD4+ T cell responses and humoral immunity (123). OUD vaccines have been tested with adjuvants targeting TLR3 (37), TLR4 (31, 42, 124), and TLR9 (37, 73), alone or in combination with other adjuvants, with variable results. Some TLR agonists are also associated with systemic toxicity and adverse effects, limiting their use as adjuvants, including several that target TLR2, TLR3, TLR7, and TLR8 [reviewed in (125)]. Recent efforts have been made to produce novel TLR agonists that retain their robust immunostimulatory properties while limiting systemic toxicity. If successful, these novel TLR agonists could be a source of new, targeted adjuvants without current cost and patent considerations to be used in clinical trials with OUD and other SUD vaccines to increase their immunogenicity without increasing the adverse effect profile.

Biomarkers. Another strategy to increase the efficacy and success of clinical implementation of OUD vaccines is to use personalized medicine to stratify patients into those most likely to produce high antibody titers in response to vaccination by identifying predictive biomarkers of vaccine efficacy. In this scenario, a simple blood draw or saliva

sample could be used to identify genetic or cellular biomarkers that would inform clinicians whether the patient would be a good candidate for immunization or instead be given a traditional pharmacotherapy. Many vaccine studies have found correlates of protection through simple assays or genetic testing (126). In fact, several studies have demonstrated that single nucleotide polymorphisms (SNPs) of IL-4 and its downstream signaling molecules may be a predictor of response to vaccines for Hepatitis B (127, 128), Japanese encephalitis virus (129), measles (130), tetanus and diphtheria (131), and streptococcus pneumoniae (132). For OUD vaccines, preclinical studies have demonstrated that pre-immunization frequency of opioid-specific naïve B cells correlated positively with opioid-specific serum IgG titers post-vaccination (133). Currently, there is only 1 OUD vaccine in phase I clinical trial (NCT04458545). Pre-immunization samples from the patients in this trial offer a unique opportunity for exploratory biomarker identification of OUD vaccine efficacy in human subjects. Additionally, since the target population for OUD vaccines are those with a current substance use disorder, the use of opioids or potential concurrent conditions, such as dysbiosis, nutritional deficiency, or infections such as HIV or HBV from IV drug use may affect their resulting immune response. Therefore, comparing the immune profile between drug-naïve individuals and those with OUD may be informative for exploratory identification of biomarkers that may positively or negatively impact the immune response.

The research program presented within this thesis had the intention to identify methods to increase OUD vaccine efficacy. These strategies include the elucidation of cellular and molecular mechanisms underlying the increase in efficacy seen after administration of OUD vaccines with IL-4 depletion to determine fundamental processes involved in OUD vaccine efficacy. The information gained from these mechanistic studies was then used to identify and test appropriate novel adjuvants suitable for clinical

translation in combination with a lead fentanyl vaccine. Additionally, elements of vaccine design and administration including testing linker length and bivalent immunization strategies are investigated to determine the effects on vaccine efficacy in the context of a novel carfentanil vaccine. In an attempt to explore environmental factors that may influence vaccine efficacy, the effects of microbiome and housing condition were investigated in rodents. Finally, exploratory studies aimed at identifying putative predictive biomarkers for OUD vaccines were performed in both preclinical and clinical settings. With these putative biomarkers in mind, a biomarker identification pipeline was developed for future OUD vaccine clinical trials to validate these predictive biomarkers as clinical studies progress.

Chapter 2: Role of interleukin-4 signaling in anti-opioid vaccine efficacy

The goal of this study was to identify cellular and molecular mechanisms associated with increased OUD vaccine efficacy after depletion of IL-4 during immunization. These experiments tested the molecular role of IL-4 signaling in increasing vaccine efficacy and the role of IL-4 during cellular events of germinal center formation. Identifying mechanisms of increased vaccine efficacy are critical for rational selection of novel adjuvants and biomarkers to increase vaccine efficacy in clinical studies.

This chapter contains data from the following paper that has been published:

Crouse B, Robinson C, Huseby Kelcher A, Laudenbach M, Abrahante JE, Pravetoni M. Mechanisms of interleukin 4 mediated increase in efficacy of vaccines against opioid use disorders, *NPJ Vaccines* (2020).

The rest of the data is unpublished. The following people contributed to this data:

Crouse B, Hicks D, Baehr C, Pravetoni M.

Experiments may be interspersed for clarity and logical flow.

Author Contributions: BC planned and conducted experiments and analyzed data, CR conducted experiments, AHK conducted experiments, ML conducted experiments, JEA analyzed RNA-sequencing data, DH developed and characterized key antibodies for determining the role of IgG subclass in vaccine efficacy, CB developed oxycodone-specific hybridomas and sequenced their BCRs, MP assisted with method development, interpretation of data and editing.

INTRODUCTION

Opioid use disorders (OUD) affect over 2 million people in the United States and 27 million people worldwide (134, 135). In 2016, 46,400 deaths occurred due to opioid misuse in the US, and up to 80,000 fatal overdoses per year are projected by 2025 (136). Although approved medication assisted treatment (MAT) consisting of pharmacological agonists and antagonists of opioid receptors is available, these medications display suboptimal clinical efficacy due to side effects, regulatory hurdles that limit patient access, and the potential for diversion and abuse (137-141). As an alternative or complementary option to MAT, anti-opioid vaccines are an emerging strategy to counteract OUD and overdose (142-144). Active immunization with opioid-based small molecule haptens conjugated to immunogenic carriers elicit production of drug-specific polyclonal antibodies, which selectively bind to the target drug in the blood and prevent its distribution to the brain (27, 38, 41, 54). Preclinical studies have provided proof of efficacy, selectivity, and safety for this approach to reduce drug-seeking behavior and to prevent respiratory depression, bradycardia, and fatal overdose (30, 32, 34, 42, 54, 65). Although the efficacy of anti-opioid vaccines has not been tested in humans, clinical trials for vaccines against cocaine and nicotine showed that a subset of immunized patients produced sufficient levels of high affinity serum IgG antibodies required to achieve vaccine efficacy against nicotine and cocaine (83, 84, 145). These data suggest that vaccine efficacy against drugs of abuse is attainable, but that our understanding of the immunological mechanisms underlying anti-drug antibody responses needs to be further explored. To support the translation of anti-opioid vaccines, efforts are needed to draft a rational blueprint for vaccine development by further understanding the immunological mechanisms underlying optimal vaccine-induced antibody responses against drugs of abuse.

To date, the immunological mechanisms of vaccines against OUD and substance use disorder (SUD) are relatively understudied. We have previously demonstrated that generation of effective anti-opioid antibodies requires $CD4^+$ T cell dependent B cell activation by showing that depletion of $CD4^+$ T cells or immunization of T cell receptor α (TCRα) subunit knockout mice blunted antibody responses and vaccine efficacy against opioids (27, 133). Analysis of B cell subsets after vaccination showed that early germinal center (GC) formation correlated with antibody titers and vaccine efficacy against oxycodone and nicotine (133, 146). Generally, GC formation involves the activation of B cells and cognate $CD4^+$ T cells within the spleen or lymph node follicles, which is mediated by antigen presenting cells (APCs) such as dendritic cells, macrophages, or B cells. Within the GC microenvironment, antigen-specific B cells undergo clonal expansion and affinity maturation to increase antibody specificity for the target antigen (89). Depending upon molecular signals such as cytokines and co-stimulatory molecules (e.g., CD40), B cells can also undergo class switching recombination of their constant antibody fragments (F_c), which results in different antibody effector functions (89). Within the GC, $CD4^+$ T helper (Th) cells will also differentiate into Th_1, Th_2, $Th_{17,}$ T follicular helper (T_{fh}), and GC-T_{fh} subsets which coordinate B cell responses to different antigens (86, 147). In this context, B and T cell responses to vaccines can be shaped by the incorporation of adjuvants to achieve successful immunization (98, 148). Pre-clinical studies have already shown that the efficacy of vaccines against SUD is enhanced by adjuvants such as aluminum salts (alum) and toll-like receptor 4 (TLR4) or TLR9 agonists (31, 39, 73, 97). In contrast to more traditional adjuvants, this study focuses on the use of cytokine-targeting immunomodulators as a strategy to enhance GC formation and to increase vaccine efficacy against drugs of abuse.

Our team previously tested whether the efficacy of a candidate vaccine against oxycodone was enhanced by immunomodulators of IL-4, IL-7R (CD127), IL-2R (CD25), programmed death-ligand 1 (PD-L1), or inducible T cell co-stimulator ligand (ICOSL), some of which have been used or tested clinically for other indications (149-153). This screening strategy found that administration of a neutralizing anti-IL-4 monoclonal antibody (αIL-4 mAb), but not a non-neutralizing αIL-4 mAb (94), increased the efficacy of a vaccine against oxycodone in mice. This effect was replicated in IL-$4^{-/-}$ mice (94). The increased efficacy was associated with class switching from IgG_1 to IgG_{2a} and IgG_3 and differentiation of $CD4^+$ T cells toward T_{fh} and GC-T_{fh} cell subsets (94), which are needed for GC formation and B cell activation (86). This is consistent with the hypothesis that anti-opioid vaccine efficacy relies primarily on generating high levels of high affinity opioid-specific antibodies. Treatment with an αIL-4 mAb also improved responses to a tetanus toxoid, diphtheria, acellular pertussis (TDaP) vaccine (94), further supporting this approach for increasing efficacy of other recombinant protein or conjugate vaccines. These data support the hypothesis that IL-4 is both a pharmacological target to increase vaccine efficacy and a biomarker to enhance and predict vaccine efficacy against opioids and other targets, warranting more studies of the IL-4 biology in the context of anti-drug vaccines.

The IL-4 signaling pathway consists of type I and type II receptor complexes. The type I receptor complex involves the IL-4 receptor (IL-4R) binding to the common gamma chain (γ_c), which signals only in response to IL-4. The type II receptor consists of a complex of the IL-4R and IL-13 receptor (IL-13R), which can be activated by either IL-4 or IL-13. Type I receptors are expressed on most immune cells, while type II receptors are expressed on limited immune cell subsets of myeloid origin and several non-hematopoietic cell populations, including fibroblasts and epithelial cells (108). The IL-4 signaling pathway

is involved in early GC formation in secondary lymphoid organs (103, 104, 154), antibody class switching (113, 117), Th_2 differentiation (115), macrophage activation (114), and mucosal/allergic responses (116). Although the source of IL-4 during GC formation is still debated, it has been shown that natural killer T cells (NKT cells) and $CD4^+$ T cells produce IL-4 after vaccination (102-105, 118). Previous literature suggests that IL-4 is involved in several processes within GC formation, including mediating the transition from centroblasts to centrocytes (103), class-switching (113), and memory cell differentiation (112). In contrast, IL-13's role in GC formation is largely unexplored. IL-4 has also been shown to inhibit GC formation in some contexts (102, 103, 110), demonstrating that the role of IL-4 may vary according to the nature or category of antigenic stimuli (94, 103, 104, 110, 118, 119, 132, 154). Therefore, the seemingly pleiotropic role of IL-4 during GC formation is not yet fully uncovered, and its role in modulating the efficacy of conjugate vaccines and antibody responses against small molecules is unknown. Furthermore, the relative contribution of type I vs. type II receptors and the role of IL-13 in mediating the efficacy of anti-drug vaccines has not been elucidated.

This study extended our previous findings that blockade of IL-4 increases the efficacy of anti-opioid vaccines, which generalized to different opioid conjugate vaccine formulations containing structurally different haptens and carrier proteins, and occurred in both males and females. To further dissect the molecular mechanisms, we tested the effect of depletion or deletion of downstream signaling components on vaccine efficacy against oxycodone. Surprisingly, we did not see enhanced efficacy upon deletion of IL-4R or its downstream effectors, signal transducer and activator of transcription 6 (STAT6) or insulin receptor substrate 2 (IRS-2). Depletion of IL-13 also did not change vaccine efficacy, suggesting that while IL-4 and its type I receptors were implicated in the increase in vaccine efficacy, IL-13 and type II IL-4 receptors were not. The effect of IL-4 depletion

on vaccine efficacy was associated with enhanced number and size of GCs after immunization. We then tested the specific effects of IL-4 depletion on lymphocyte populations involved in GC formation. We have previously found that depletion of IL-4 was associated with an increase in GC-T_{fh} cells (94), which was supported in this study by changes in transcriptome signatures found in activated $CD4^+$ T cells. In contrast, NKT cells, a population of cells that are important for early GC events including IL-4 secretion (102), were not necessary for vaccine efficacy. IL-4 depletion did not influence oxycodone-specific B cell affinity maturation or class switching to IgE. IgG_{2a}, a subclass previously associated with increased OUD vaccine efficacy, did not display increased efficacy compared to IgG_1. Finally, IL-4 depletion was shown to increase short lived oxycodone-specific antibody-secreting cells, but not long-lived plasma cell formation. In summary, these studies support the use of molecular adjuvants targeting IL-4 to improve vaccine efficacy against opioids and potentially other drugs of abuse, as well as the use of IL-4, but not IL-13 or IL-4R, as a biomarker of vaccine efficacy for patient stratification or in personalized therapy against OUD or SUD.

MATERIALS AND METHODS

Drugs. Oxycodone hydrochloride (HCl) and fentanyl citrate were obtained from either Sigma Aldrich (St. Louis, MO) or the NIDA drug supply program (RTI, NC).

Immunomodulators. Anti-IL-4 (αIL-4) monoclonal antibody (rat anti-mouse IgG_1, clone 11b11, Cat. No. BE0045) was obtained from Bio X cell (West Lebanon, NH). αIL-13 monoclonal antibody (mouse anti-human IgG_1) was generously donated by Genentech (San Francisco, CA) under MTA OR-217400.

Ethics statement. Pre-clinical studies were performed according to the Guide for the Care and Use of Laboratory Animals of the National Institutes of Health. Animal protocols were approved by the Hennepin Healthcare Research Institute and University of Minnesota Animal Care and Use Committees. Animals were euthanized by AAALAC-approved CO_2 inhalation chambers, and efforts were made to minimize suffering.

Mice. Six- to eight-week old male and female Balb/c and C57BL/6 mice, IL-4 receptor$^{-/-}$ (IL-4R$^{-/-}$, BALB/c-*Il4ra*^{tm1Sz}/J, stock no. 003514), STAT6$^{-/-}$ (C.129S2-*Stat6*^{tm1Gru}/J, stock no. 002828), or IL-4R Y500F (C.129X1-*Il4ra*^{tm1Tch}/J, stock no. 007680) mice were obtained from Jackson Laboratory (Bar Harbor, ME) or Harlan Laboratories (Madison, WI). CD1d$^{-/-}$ mice were generously donated by Drs. Stephen Jameson and Kris Hogquist at the University of Minnesota Center for Immunology. Mice were group housed under a 14/10 hour standard light/dark cycle and fed standard mouse chow *ad libitum*. Testing occurred during the light phase.

Hapten synthesis and conjugate vaccines. The oxycodone-based hapten containing a tetraglycine linker at the C6 position (OXY) and the fentanyl-based hapten (F) containing an analogous linker were synthesized as previously described (26, 54), and conjugated to native keyhole limpet hemocyanin (KLH, Thermo Fisher, Rockford, IL), GMP grade subunit KLH (sKLH, Biosyn, Carlsbad, CA), or diphtheria cross reactive material (CRM, Fina Biosolutions, LLC., Rockville, MD) using carbodiimide chemistry as previously described (27, 54). For use as a coating antigen in ELISA, OXY and F haptens were conjugated to either chicken ovalbumin (OVA) or bovine serum albumin (BSA). Briefly, 5 mM OXY or F haptens were activated with 104 mM EDAC in 0.1 M MES buffer pH 5. Because of its high hydrophobicity, the F hapten was dissolved in the presence of 10% DMSO. The reaction mixture was stirred for 10 minutes at room temperature (RT). Native KLH, sKLH, or CRM were then added to a final concentration of 2.8 mg/mL and stirred for

3 hours at room temperature. MES buffer was exchanged with PBS buffer pH 7.2 using an Amicon filter unit (MilliporeSigma, Merck, Burlington, MA) with 100 or 50 kDa molecular cutoff for sKLH and CRM conjugates respectively, and resuspended to a final concentration of 2.5 mg/mL before storage at 4°C. 250 mM sucrose was added as a stabilizing agent to MES and PBS buffers used for CRM conjugates. Haptenation ratio of OVA, BSA, and CRM conjugates was measured by MALDI-TOF analysis (AB SCIEX 5800, Foster City, CA), while KLH and sKLH conjugate formations were confirmed by Dynamic Light Scattering (DLS) as described (27). The unconjugated carrier protein and the conjugate vaccines were adsorbed to aluminum adjuvant (Alhydrogel '85', 2%, Brenntag Biosector, Denmark) as described in each experimental section.

Active immunization studies. Anti-opioid vaccines were administered either i.m. or s.c. on days 0, 14 and 28. For studies involving the i.m route, mice were immunized in the hind leg at two sites. In all studies, mice received either the unconjugated carrier protein as a control (KLH, sKLH, or CRM) or the test vaccine (OXY-KLH, OXY-sKLH, F-sKLH, or F-CRM). In most studies, immunomodulators (αIL-4, αIL-13, or both) were administered i.p. on days -2 and 1 at a dose of 0.5 mg per injection as described (94). Blood was collected via facial vein on days 14 and 34 for antibody analysis, unless otherwise noted. Mice were challenged s.c. on day 35 with either oxycodone (2.5-5.0 mg/kg) or fentanyl (0.05 mg/kg). Thirty minutes post-drug challenge, vaccine efficacy in reducing opioid-induced behavioral effects was measured by the hot plate test of centrally-mediated nociception as described (34). After collection of the behavioral endpoint, blood and brain were collected and analyzed by triple quadrupole LC/MS (Agilent) or a single quadrupole GC/MS (Agilent) as described (54). Experiment-specific details are described in figure legends or individual result sections, as well as in Table 1. To test the cellular and molecular mechanisms underlying vaccine efficacy, mice were immunized once, and then sacrificed at 7-10 days

for either analysis of spleen sections by immunofluorescent staining or RNA sequencing in $CD4^+$ T cells isolated from the spleen and lymph nodes.

Table 1. Experimental design

Experiment	Treatment	Dose & Route*	Adjuvant	Challenge Dose
Effect of αIL-4 and sex on anti-oxycodone vaccines	sKLH, OXY-sKLH	60 µg, i.m	Alum	5.0 mg/kg oxycodone
Test anti-oxycodone vaccines in $IL\text{-}4R^{-/-}$ and $STAT6^{-/-}$ mice	KLH, OXY-KLH	60 µg, s.c	Alum	2.25 mg/kg oxycodone
Effect of αIL-4/αIL-13 on anti-oxycodone vaccines	sKLH, OXY-sKLH	60 µg, i.m	Alum	2.25 mg/kg oxycodone
Effect of αIL-13 dosing on anti-oxycodone vaccines	sKLH, OXY-sKLH	60 µg, i.m	Alum	2.25 mg/kg oxycodone
Effect of αIL-4 on germinal center formation (immunofluorescence)	sKLH, OXY-sKLH	60 µg, i.m	Alum	N/A
Test anti-oxycodone vaccines in $CD1d^{-/-}$ mice	sKLH, OXY-sKLH	60 µg, i.m	Alum	5.0 mg/kg oxycodone
Effect of αIL-4 and anti-oxycodone vaccines on $CD4^+$ T cell transcriptome by RNA-sequencing	sKLH, OXY-sKLH	75 µg, i.m	Alum	N/A
Effect of αIL-4 on anti-fentanyl vaccines	sKLH, CRM, F-sKLH, F-CRM	50 µg, i.m	Alum	0.05 mg/kg fentanyl

*In all experiments, αIL-4 and αIL-13 given i.p at 0.5 mg per dose, except when otherwise noted.

Passive immunization study: Balb/c mice were passively immunized intraperitoneally (i.p) with 40 mg/kg of appropriate monoclonal antibody, which has previously been shown to protect against the effects of oxycodone (155). Twenty-four hours later, mice were bled via facial vein to determine antibody concentration using biolayer interferometry. One hour later, mice were challenged with 2.25 mg/kg oxycodone, s.c. After 30 minutes, mice were

euthanized and blood and brain were collected to determine oxycodone concentration via LCMS/MS analysis.

Antibody analysis. Opioid-specific IgG titers were measured by ELISA as described (94). Briefly, 96-well ELISA plates (Costar 9018 EIA/RIA, Jackson ImmunoResearch Laboratories Inc., West Grove, PA) were coated with 5 ng/well of unconjugated chicken ovalbumin (OVA) or OXY hapten conjugated to OVA in carbonate buffer at pH 9.6 overnight. For fentanyl-specific antibody titers, plates were coated with BSA, or fentanyl hapten conjugated to BSA at 5 ng/well. The following day, plates were blocked with 1% gelatin. Mouse serum was added to wells starting at a 1:200 dilution and serially diluted, and plate were incubated for 2 hours. Primary antibodies were then incubated overnight with 1:30,000 goat-anti-mouse IgG (Jackson ImmunoResearch, Cat. No. 115-035-008), 1:35,000 IgG_1 (Alpha Diagnostic International, Inc., Cat. No. 40126-GAF-BLK), or 1:7500 IgG_{2a} (Alpha Diagnostic International, Cat. No. 40127-GAF-BLK) conjugated to horseradish peroxidase to measure titers of oxycodone- or fentanyl-specific total IgG or individual IgG subclasses. For IgE ELISAs, plates were coated with 5 ng/well OXY-OVA or IgE capture antibody (Biotechne, Cat. No. MAB9935-100). Serum was diluted starting at 1:50, and primary antibodies were incubated with 1:5000 anti-IgE antibody conjugated to HRP (VWR, Cat. No. 100242-786). Purified mouse IgE (Biolegend, Cat. No. 401701) was used to obtain a concentration curve. SIGMAFAST OPD substrate (Sigma-Aldrich, St. Louis, MO) was used to develop plates.

Immunofluorescent staining. Spleens were collected and immediately frozen in OCT buffer (Fisher Scientific) in a plastic cassette using liquid nitrogen and stored at -80ºC. Blocks were sliced into 10 µm sections using a cryostat, placed onto slides, and left to dry for 30 minutes. A hydrophobic barrier was drawn around sections using a PAP Pen (Fisher Scientific). Sections were fixed in 4% PFA for 15 minutes, washed, and then blocked in

5% rat serum + 0.5% IGEPAL in PBS for 1 hour at room temperature. A primary antibody cocktail including 1:50 dilution GL7-FITC (Biolegend, clone GL7, Cat. No. 144603), 1:100 dilution CD21/35-PE (Biolegend, clone 7E9, Cat. No. 123409), and 1:100 dilution IgD-AF647 (Biolegend, clone 11-26c.2a, Cat. No. 405707) in blocking solution was added to sections overnight at room temperature. Slides were then washed and one drop of Fluoroshield mounting medium with DAPI stain (Abcam) was added and a coverslip was placed on top.

Fluorescence Microscopy. Images were acquired with a Zeiss Axio.Observer Z1 motorized microscope equipped with a Plan-Apochromat 20x/0.80 NA objective and a QuantEM:512SC electron multiplying CCD camera (Photometrics). The light source was an HXP-120 mercury halide lamp and the following channels were collected sequentially (excitation/emission bands, in nm): DAPI (335-383/420-470), EGFP (450-490/500-550), phycoerythrin (559-585/600-690) and Cy5 (625-655/665-715). The large field of view was automatically tiled and stitched using ZEN 2.5 software (Zeiss). Pixel size was 800x800 nm. Germinal centers and follicles were quantified by manual counting by two independent counters. Counters were blinded to all treatment conditions. $GL7^+$ fluorescent area was outlined and measured using Fiji software (156).

RNA sequencing. Spleens and lymph nodes were processed into a single cell suspension as previously described (133). Cells were stained for viability (V450 Ghost Dye™, Tonbo Biosciences, Cat. No. 13-0863-T100), CD90.2 (PerCP-eFluor710, eBioscience clone 30-H12, Cat. No. 46-0903-82), CD4 (APC-eFluor780, eBioscience clone RM4-5, Cat. No. 47-0042-82), CD44 (FITC, Biolegend clone 1M7, Cat. No. 103021), CD8a (BV510, BD Bioscience clone 53-6.7, Cat. No. 563-068), B220 (PE-Cy7, Biolegend, clone RA3-6B2, Cat. No. 103221), F4/80 (PE-Cy7, eBioscience clone BM8, Cat. No. 25-4801-82) CD11b (PE-Cy7, Biolegend clone M1/70, Cat. No. 101215) and CD11c (PE-

Cy7, eBioscience clone N418, Cat. No. 25-0114-82). All antibodies were diluted 1:100, except for CD90.2, which was diluted 1:500, and the viability dye, which was diluted 1:1000. Cells were sorted for activated $CD4^+$ T cells, described as Ghost Dye^- $CD11b^-$ $CD11c^-$ $F4/80^-$ $B220^-$ $CD8a^-$ $CD90.2^+$ $CD4^+$ $CD44^+$, using a BD FACSAria II. RNA was extracted from sorted cells using chloroform/trizol and collected using an RNA isolation kit (Qiagen, Hilden, Germany). Samples were processed using a Clontech pico mammalian RNA library preparation (Takara Bio, Mountain View, California). Libraries were sequenced on an Illumina NextSeq with 75 pair-end sequencing with samples acquiring an average of 30 million reads per sample. Results were analyzed using Reactome Pathway Analysis to analyze DEG involvement with different cellular processes (157).

BCR Sequencing. BCR sequencing of previously characterized hybridomas generated from mice immunized with OXY-sKLH or OXY-sKLH+αIL-4(155) was carried out as previously described (158). Briefly, 1-5 million cells were pelleted in a microfuge tube via centrifugation at 2,000 rpm. Cells were washed with 1 mL PBS, pelleted, and frozen at -80ºC until processed. To extract RNA, pellets were thawed, and RNA was extracted using RNeasy Mini kit (Qiagen, Hilden, Germany). RNA was reverse transcribed with Maxima First Strand cDNA synthesis kit (Thermo Fisher, Waltham. MA). cDNA was amplified via PCR using Q5 High-Fidelity DNA polymerase. PCR product was then purified using a QIAquick PCR purification kit (Qiagen, Hilden, Germany). Amplified DNA was sent for Sanger sequencing at the University of Minnesota Genomics Center. Heavy chain sequences were aligned to germline mouse heavy chain sequences using IgBlast, and mutations in CDR1 and CDR2 regions were quantified.

Expression of oxycodone-specific monoclonal antibodies. Oxycodone-binding mAb [clone HY1-3G8 (155)] V_H and V_L sequences were cloned into pcDNA3.4 mammalian

expression vectors (Genscript). The CMV promoter driven pcDNA3.4 expression vector was modified to contain a Kozak consensus sequence preceding an open-reading frame (ORF) with a murine IGHV signal peptide (MGWSCIILFLVATATGVHS), or a murine IGKV signal peptide (METDTLLLWVLLLWVPGSTG) for the antibody heavy and light chain expression vector, respectively. The heavy chain ORF terminates with a murine IgG_1 or IgG_{2a} constant region (Accession # P01857 and P01863), and the light chain vector ORF terminates with a murine IgK constant region (Accession # P01834). The IgG_{2a} sequence was mutated using site-directed mutagenesis to introduce L234A, L235A, and P329G mutations (IgG_{2a}-LALA-PG) to block FcγRI-IV binding as previously described (159). Oxycodone-specific mAbs were produced via transient expression in the Expi293 or ExpiCHO expression system (ThermoFisher Catalog # A14635 and A29133) according to manufacturer instructions. Transfections were performed using a 2.5:1 ratio of LC vector:HC vector, with 1 µg of total vector DNA/mL of culture volume. Cell culture supernatant was harvested 7-10 days following transfection, and mAb was purified from filtered cell culture supernatant via liquid chromatography on an ÄKTA pure with a HiTrap Protein G HP column (Cytiva Product # 29048581), and buffer exchanged into PBS, pH 7.4.

ELISPOT. ELISPOT was performed using Mabtech Mouse IgG ELISpot^{BASIC} kit (HRP). PVDF membrane ELISPOT plates were pretreated with 35% EtOH for 1 minute and then washed 5x with sterile water. Plates were then coated with 5 µg/mL OXY-OVA or 15 µg/mL IgG capture antibody overnight for detection of oxycodone-specific IgG secreting cells or total IgG secreting cells, respectively. The following day, plate was washed 5x with PBS before being blocked with DMEM+10% FBS. Meanwhile, spleens and lymph nodes from immunized mice were collected and processed to a single cell suspension. Cells were washed 3 times with ClonaCell Medium A (StemCell). Cells were counted and plated in

triplicate in ClonaCell Medium A at a density of 200,000 cells/well for OXY-OVA coated wells and 50,000 cells/well for IgG coated wells. Plates were incubated overnight at 37ºC+5% CO_2 and spots were visualized using TMB substrate according to the manufacturer's instructions. Images were acquired with an CTL BioSpot S5 Core Analyzer and analyzed using ImmunoSpot 7 software (Cell Technology Limited, Shaker Heights, OH).

Biolayer Interferometry. Antibody avidity assays were performed on an Octet Red 96e instrument (Sartorius). Serum samples from immunized mice on day 25 (analyte) and biotinylated antigen, OXY-Biotin, (ligand) were diluted in PBS. Assays were performed by loading OXY-Biotin onto pre-hydrated streptavidin sensors at 0.1 µg/ml (loading step 60 sec) followed by 60 sec baseline. Sensors were then moved into analyte for 180 sec for association, followed by a 300 sec dissociation step. All steps were performed at room temperature with shaking at 1000 rpm. Serum samples were run at 1:200 dilution in PBS. Dissociation rate (K_{diss}) and response values were calculated using Sartorius HT analysis software version 11.1.3.50. All data was inspected for quality of fit to the calculated curve (R^2>0.95). Monoclonal serum antibody concentrations were calculated by fitting response values to a standard curve produced with an oxycodone-specific monoclonal antibody.

Flow Cytometry. On day 100, bone marrow was analyzed for oxycodone-specific long-lived plasma cells. Bone marrow was extracted from femurs, processed to a single cell suspension, and stained extracellularly for APC-eFluor780 CD90.2 (eBioscience), APC-eFluor780 F4/80 (eBioscience), APC-eFluor780 Ly-6G (eBioscience), APC-eFluor780 CD11c (eBioscience), and BV650 CD138 (Biolegend). Cells were permeabilized using a BD Cytofix/Cytoperm kit, and stained with PE-AF647 decoy, OXY-Biotin-Streptavidin-PE, and Pacific Orange F(ab')2 (H+L) (Invitrogen). Oxycodone-specific plasma cells were

defined as singlets that were CD90.2$^-$F4/80$^-$Ly6G$^-$CD11c$^-$Decoy$^-$Ig$^+$OXY$^+$CD138$^+$ cells. All fluorophores were diluted 1:100 for staining. Oxycodone-specific bait and decoy reagents were produced as previously described (133).

Data Analysis. Statistical analyses were performed using Prism version 9.2.0 (GraphPad, La Jolla, CA). Mean antibody titers or concentrations, drug concentrations, and percent maximum possible effect (MPE%) on the hot plate were analyzed by one-way ANOVA followed by Tukey's multiple comparisons post hoc test. The relationship between opioid-specific antibodies, serum opioid concentrations, and brain opioid concentrations were analyzed via two-tailed Pearson correlation after determination of normality using D'Agostino-Pearson's test. Germinal center data, somatic hypermutation data, and affinity maturation were analyzed using a Mann-Whitney nonparametric U test. ELISPOT data were analyzed using Student's T test. In RNA-sequencing studies, data were collected and analyzed via gopher-pipelines. Briefly, 2 x 50bp FastQ paired end reads (n=33.5 Million average per sample) were trimmed using Trimmomatic (v 0.33) enabled with the optional "-q" option; 3bp sliding-window trimming from 3' end requiring minimum Q30. Quality control on raw sequence data for each sample were performed with FastQC. Read mapping was performed via Hisat2 (v2.1.0) using the mouse genome (mm10) as reference. Gene quantification was done via Feature Counts for raw read counts. Differentially expressed genes were identified using the edgeR (negative binomial) feature in CLCGWB (Qiagen, Redwood city, CA) using raw read counts. Statistical analysis was obtained by filtering genes on edgeR with at least 1.5-fold differential expression, a p-value < 0.05 and a minimum average of 5 reads per group for any one gene.

RESULTS

Neutralization of IL-4 enhances anti-opioid antibody responses in male and female mice*.* Previous studies show concurrent administration of an IL-4 depleting monoclonal antibody (αIL-4) with an anti-oxycodone vaccine increased concentrations of antibody-bound oxycodone in serum, decreased oxycodone concentration in the brain, and resulted in greater efficacy in reducing oxycodone-induced behavioral effects (94). The increased vaccine efficacy against oxycodone was correlated with higher oxycodone-specific IgG antibody titers and their class switching from IgG_1 to IgG_{2a} in male Balb/c and C57Bl/6 mice (94). In a first experiment, these previous findings were expanded by testing the effect of αIL-4 administration in male and female mice. Since the effect of αIL-4 administration was previously established with anti-oxycodone vaccines (94), a lead anti-oxycodone vaccine consisting of an oxycodone-based hapten (OXY) conjugated to subunit keyhole limpet hemocyanin (sKLH) or native KLH was used as a model for these studies. Both OXY-KLH and OXY-sKLH are effective in preventing oxycodone-distribution to the brain, and reducing oxycodone-induced antinociception, motor activity, respiratory depression, and bradycardia as well as acquisition of oxycodone intravenous self-administration (27, 31-34). While oxycodone-specific IgG titers were increased in female mice shortly after the first immunization compared to male mice (Day 14, data not shown), no differences were found after the third and last immunization (**Figure 1A**). Co-administration of αIL-4 with OXY-sKLH increased both IgG_1 and IgG_{2a} compared to the vaccine alone in both male and female mice at 34 days (**Figure 1B and C**). When challenged with oxycodone (5.0 mg/kg, s.c), significant increases in serum oxycodone concentrations were found in both male and female mice treated with αIL-4 compared to mice receiving the vaccine alone (**Figure 1D**)**.** These data suggest that IL-4-based mechanisms of vaccine enhancement are conserved between sexes. While brain

oxycodone concentrations were reduced in all groups compared to the control (**Figure 1E**), no significant differences in brain concentrations were found across treatment groups. In contrast to serum (**Figure 1D**), the lack of differences in the efficacy of various vaccine formulations in reducing drug distribution to the brain may be related to the respective pharmacokinetics of unbound (free) oxycodone and antibody-bound oxycodone. For instance, serum opioid-specific antibodies are expected to bind free drug, which prolongs the opioid's half-life and protects it from metabolism or clearance. This preserves differences in serum drug concentration across treatment groups, which may not be as evident in the brain. Higher individual serum IgG antibody titers were significantly correlated with decreased brain oxycodone concentrations (**Figure 1F**), indicating that titers may be used as immune correlates of vaccine efficacy in lieu of significant differences in brain opioid concentration. In fact, it has been previously shown that oxycodone-specific serum IgG antibody titers are predictive of vaccine efficacy against oxycodone in mice and rats (94, 133, 146). Significant correlations were also found between antibody titers versus serum concentrations as well as brain concentrations versus serum concentration, indicating that serum oxycodone concentration is also a parameter of vaccine efficacy (data not shown). Future studies may address the interplay of sex and genetic polymorphisms related to IL-4 signaling in the context of vaccine efficacy.

Deletion of STAT6 or the IL-4R does not increase vaccine efficacy against opioids. Because pharmacological or genetic ablation of IL-4 increases vaccine efficacy against opioids (94), this study further tested whether genetic ablation of individual downstream signaling components could recapitulate this effect. Canonical IL-4 signaling occurs through the IL-4R, which leads to phosphorylation of JAK1/3 and downstream phosphorylation of either STAT6 or insulin receptor substrates (IRS) (108). Here, IL-4R$^{-/-}$

and STAT6$^{-/-}$ mice were immunized with OXY-KLH and compared to wild-type mice receiving OXY-KLH plus αIL-4. Despite an initial increase in oxycodone-specific serum IgG titers after the first immunization in IL-4R$^{-/-}$ and STAT6$^{-/-}$ mice (**Figure 2A**), antibody levels were below those of mice receiving OXY-KLH and αIL-4 after the third vaccination (**Figure 2B**). Immunizing IL-4R$^{-/-}$ and STAT6$^{-/-}$ mice with OXY-KLH did not yield an IgG_{2a} to IgG_1 response ratio equivalent to wild-type mice immunized with OXY-KLH and αIL-4 (**Figure 2C**). When challenged with oxycodone, mice receiving OXY-KLH plus αIL-4 showed an increased serum oxycodone concentration compared to the OXY-KLH, indicating higher efficacy, while STAT6$^{-/-}$ and IL-4R$^{-/-}$ mice did not (**Figure 2D**). Brain oxycodone levels were significantly decreased in all groups compared to control (**Figure 2E**).

These results suggest that while IL-4 depletion increases vaccine efficacy, lack of functional IL-4R or STAT6 does not. To further explain the relationship between blocking IL-4 and IL-4R ablation, we administered OXY-KLH plus αIL-4 to IL-4R$^{-/-}$ mice. To ensure that potential differences were not due to genetic or behavioral differences, wild-type mice from different vendors were included as a control (**Figure 2F**). In this experiment, wild-type mice responded similarly to the combination of OXY-KLH and αIL-4, regardless of supplier. However, the combination of OXY-KLH and αIL-4 in IL-4R$^{-/-}$ mice did not yield increased IgG titers compared to wild-type mice receiving OXY-KLH and αIL-4, suggesting that the IL-4R is necessary for the increased efficacy associated with depletion of IL-4.

Blockage of IL-13 does not increase vaccine efficacy. Since the IL-4R was necessary for the efficacy of OXY-KLH plus αIL-4, we hypothesized that the increased vaccine efficacy was mediated by IL-13 activating type II IL-4Rs. To test this alternative hypothesis, mice were immunized with OXY-sKLH in combination with either αIL-4, a neutralizing anti-

IL-13 mAb (αIL-13), or both, to differentiate the effects of type I vs. type II IL-4R signaling. While dual IL-4/IL-13 depletion increased the early antibody response (**Figure 3A**), after the third immunization, αIL-13 did not increase oxycodone-specific IgG titers compared to the vaccine alone (**Figure 3B**). Furthermore, dual cytokine depletion did not have a greater effect on IgG titers than IL-4 depletion. A similar trend was found when measuring the ratio of IgG_{2a} to IgG_1 (**Figure 3C**). The lack of effect by αIL-13 was confirmed at several concentrations and dosing schedules of the αIL-13 antibody (**Figure 4**). In response to an oxycodone challenge, groups given αIL-4 showed increased serum concentrations of oxycodone (**Figure 3D**) and decreased concentrations of oxycodone in the brain (**Figure 3E**). Groups given αIL-13 did not display significant differences in serum or brain oxycodone concentrations when compared to the vaccine alone, and dual IL-4/IL-13 depletion did not produce any additive increases in efficacy when compared to αIL-4 administration. These data demonstrate that αIL-13 does not increase vaccine efficacy, suggesting vaccine efficacy is modulated by IL-4 signaling through the type I IL-4R. Additional studies testing vaccine efficacy against opioids in IL-$13R^{-/-}$ or IL-4/IL-$4R^{-/-}$ mice are needed to further confirm these findings.

Ablation of IL-4R mediated IRS signaling does not increase vaccine efficacy. We previously hypothesized that the increase in vaccine efficacy after IL-4 depletion was due to loss of IRS signaling downstream of the IL-4 receptor (160). To test this, WT mice or mice with a Y500F mutation in the IL-4R that prevents IRS2 phosphorylation downstream of the IL-4R (IL-4R Y500F) were immunized with OXY-KLH. Heterozygous littermates (IL-4R/IL-4R Y500F) were immunized to test whether reduced IRS signaling would produce an equivalent increase in vaccine efficacy. A group of WT mice was immunized with OXY-sKLH with antibody-based IL-4 depletion as a positive control. After 3 immunizations, IL-4R Y500F and IL4R/IL4R Y500F mice did not show increased oxycodone-specific IgG

antibody titers (**Figure 5A**) or a similar IgG_{2a}:IgG_1 ratio (**Figure 5B**) compared to WT. 30 min after oxycodone challenge, brain:serum ratio of oxycodone in IL4R Y500F and IL4R/IL4R Y500F mice was comparable to WT mice without IL-4 depletion (**Figure 5C**). These data suggest that deletion of IRS signaling downstream of the IL-4R does not increase vaccine efficacy.

Neutralization of IL-4 enhances germinal center formation after vaccination against opioids. We have previously shown by means of antigen-based magnetic enrichment paired with flow cytometry in lymph nodes that the combination of a model antigen plus αIL-4 increased $CD4^+$ T cell differentiation toward T_{fh} and GC-T_{fh} subsets, suggesting an enhancement of GC formation (94). The current study directly studied GC formation by fluorescent immunohistochemistry in murine spleens 10 days after a single immunization with OXY-sKLH with or without αIL-4. Follicles were outlined and defined as $IgD^+CD21/35^+$ areas, which are markers of follicular B cells and follicular dendritic cells, respectively (161). Follicular B cells developing into GC B cells downregulate expression of IgD and upregulate expression of GL7 (161), so GCs were defined as $GL7^{high}$/ IgD^{low} areas within the follicle (**Figure 6A**). While the number of follicles between mice vaccinated with and without αIL-4 was not different (**Figure 6B**), there was a significant increase in GCs per follicle in mice administered αIL-4 (**Figure 6C**). Consistently, the GL7 positive fluorescent area was increased in αIL-4-treated mice (**Figure 6D**). These data indicate that IL-4 depletion enhances anti-opioid vaccine efficacy by increasing the number and size of GCs in secondary lymphoid organs. These findings extend previous studies which demonstrated that greater efficacy of drug-conjugate vaccines against oxycodone and nicotine is correlated with increased frequency of hapten-specific $GL7^{high}$ GC B cells in lymph nodes and spleens in mice, as measured by antigen-based magnetic enrichment paired with flow cytometry (133, 146).

Natural Killer T (NKT) cells are not necessary for vaccine efficacy against opioids. Because CD1d-restricted NKT cells are one of the main sources of IL-4 during early vaccination events (102), we hypothesized that depletion or deletion of NKT cells would yield equivalent results to depletion or deletion of IL-4. Vaccination of wild-type and $CD1d^{-/-}$ mice with OXY-sKLH showed no difference in oxycodone-specific IgG antibody titers after a first immunization (**Figure 7A**) or after two additional boosts (**Figure 7B**). In response to an oxycodone challenge, wild-type and $CD1d^{-/-}$ mice showed no differences in serum or brain oxycodone distribution (**Figure 7C and D**) suggesting that NKT cells are not necessary for successful vaccination against opioids.

Transcriptome analysis of activated $CD4^+$ T cells reveals a distinct molecular signature associated with IL-4 depletion. $CD4^+$ T cell subset polarization is greatly influenced by IL-4 signaling (86, 87, 89), consistent with our previous finding that αIL-4 skewed T cell differentiation toward GC formation (94). To conduct a preliminary evaluation of gene expression changes associated with administration of αIL-4, RNA-sequencing was performed in sorted activated $CD4^+$ T cells after immunization with OXY-sKLH with or without αIL-4. When comparing all differentially regulated genes (DEGs), administration of αIL-4 led primarily to an upregulation of RNA expression (**Figure 8A**). Over 500 DEGs were found to be unique to the OXY-sKLH plus αIL-4 formulation compared to the vaccine alone (**Figure 8D**), which was the greatest change in gene expression when comparing any two groups to each other (sKLH control, OXY-sKLH, OXY-sKLH+αIL-4). While no specific major pathway was revealed, analysis of all 934 DEGs in the OXY-sKLH vs. OXY-sKLH+αIL-4 group suggested increased inflammatory signaling, metabolism, transcription, and signal transduction, consistent with increased T cell proliferation and differentiation triggered by immunization (**Figure 8B**). The heatmap of top 50 DEGs for each group further support these findings (**Figure 8C**). These data

suggest that the combination of an anti-opioid vaccine and αIL-4 administration uniquely affects gene transcription in the $CD4^+$ T cell compartment, supporting the need for future studies of antigen-specific $CD4^+$ T cell subsets to further elucidate the cellular and molecular mechanisms associated with αIL-4-mediated enhancement of vaccines against opioids or other drug of abuse.

IL-4 depletion does not change somatic hypermutation or affinity maturation. IL-4 is involved in somatic hypermutation and affinity maturation of B cells in the GC to produce high affinity antibodies (104, 162). To determine whether depletion of IL-4 during anti-opioid immunization affects these processes, BCRs were sequenced from hybridomas previously isolated from mice that were immunized with OXY-sKLH with or without an IL-4 depleting antibody. BCR heavy chain sequences were compared to germline sequences using IgBlast, and mutations in complementary determining regions (CDR) 1 and 2 were quantified. There was no significant difference in the number of mutations after anti-oxycodone immunization with or without IL-4 depletion, indicating that IL-4 depletion had no effect on somatic hypermutation (**Figure 9A**). To further test this hypothesis, the dissociation rate (k_{diss}) was measured using biolayer interferometry in polyclonal serum samples as a correlate of antibody avidity from WT mice immunized with or without IL-4 depletion in Figure 5. There were no differences in antibody avidity between the two groups (**Figure 9B**), suggesting that affinity maturation is unaffected by IL-4 depletion during anti-opioid immunization.

Oxycodone-specific IgE was not detected in mice immunized with OXY-sKLH. Since IL-4 is known to induce class switching to IgE after immunization (113, 117), we hypothesized that IL-4 produced after vaccination with OXY-sKLH may induce a subset of opioid-specific IgE antibodies which is prevented by addition of an IL-4 depleting antibody.

Without the influence of IL-4, these B cells would instead class-switch to IgG, which led to the increased IgG titers in mice that were treated with the αIL-4 antibody. Mice were immunized with OXY-sKLH with or without IL-4 depletion on days 0, 14, and 28, and then sera were collected on day 34 for analysis oxycodone-specific and total IgE concentration. While total IgE was detected and did decrease in groups administered the αIL-4 mAb (**Figure 10A**), no oxycodone-specific IgE was detected in any groups (**Figure 10B**), indicating that opioid-specific IgE is not produced in response to OXY-sKLH immunization, and that a reduction in IgE class-switching is not the cause of the IL-4 depletion mediated increase in vaccine efficacy.

IgG_{2a} antibodies display equivalent efficacy to IgG_1 antibodies against drug challenge in mice. We have reported that depletion of IL-4 increases class switching to IgG_{2a} after anti-opioid immunization and increases vaccine efficacy after drug challenge (94, 160). To directly assess whether IgG_{2a} is responsible for the increase in vaccine efficacy, an anti-oxycodone mAb (155) was expressed recombinantly as murine IgG_1, $IgG_{2a,}$ or IgG_{2a} LALA-PG, the latter of which contains mutations to remove FcyRI-IV binding (159). Mice were passively immunized with recombinant mAb and then challenged with oxycodone 24 hours later. Blood was collected immediately before challenge, and no differences in antibody concentration were observed between groups (**Figure 11A**). Similarly, there were no differences in oxycodone concentration in the serum (**Figure 11B**) or brain (**Figure 11C**) between the passively immunized groups 30 minutes post-drug challenge. These data suggest that the increased class switching to IgG_{2a} does not cause the increase in efficacy seen after depletion of IL-4 during anti-opioid immunization, and further supports previous studies reporting that antibody mediated effector functions do not play a role in opioid vaccine efficacy (95).

IL-4 depletion increases early antibody secreting B cells but not long-term B cell responses. Previous literature has suggested that IL-4 is involved in the memory cell vs. plasma cell choice in the germinal center (100, 101, 104, 112). To assess whether depletion of IL-4 increases the number of antibody secreting cells after anti-opioid vaccination, mice were immunized with or without IL-4 depletion on days 0, 14, and 28, and then spleens and lymph nodes were harvested to perform antigen-specific ELISPOT on day 35. One week after final immunization, there were no differences in total IgG secreting cells between mice immunized with OXY-sKLH and OXY-sKLH with an IL-4 depleting antibody (**Figure 12A**). Conversely, there was a significant increase in the proportion of oxycodone-specific IgG secreting cells compared to total IgG secreting cells (**Figure 12B**). A second cohort of mice was immunized in a similar fashion and then left until day 100 to assess whether this increase in early antibody-secreting cells led to an increase in oxycodone-specific long lived plasma cells (LLPCs) in the bone marrow. Analysis of bone marrow showed there was no significant difference in LLPCs in mice immunized with or without IL-4 depletion (**Figure 12C and D**). These data suggests that the depletion of IL-4 may results in an increase in plasmablast formation at day 35; however, this increase in early antibody secreting cells does not result in an increase in long-lived plasma cells at day 100, suggesting these plasmablasts are either short-lived and die during contraction of the immune response or do not home to the bone marrow after immunization.

Neutralization of IL-4 increases efficacy of anti-fentanyl vaccines. Our findings have shown that co-administration of OXY-sKLH with a depleting IL-4 antibody led to increased vaccine efficacy in preventing oxycodone-distribution to the brain, and reducing oxycodone-induced antinociception and respiratory depression (94). To examine the applicability of this strategy to other anti-opioid vaccine formulations, a final experiment

tested whether co-administration of αIL-4 would improve the efficacy of candidate anti-fentanyl vaccines containing a fentanyl-based hapten (F) conjugated to either the sKLH or CRM carrier proteins. The F-sKLH vaccine adsorbed on aluminum adjuvant is a first-generation formulation effective in preventing fentanyl distribution to the brain in mice and rats, as well as reducing fentanyl-induced respiratory depression in rats (54). Treatment with αIL-4 increased overall IgG titers in mice immunized with F-CRM, but not F-sKLH (**Figure 13A**). Mice treated with αIL-4 displayed increased IgG_1 and IgG_{2a} titers compared to mice receiving vaccine alone (**Figure 13B and C**). In response to a fentanyl challenge, F-CRM was more effective than F-sKLH in retaining fentanyl in serum, and F-CRM with αIL-4 was more effective than F-CRM alone (**Figure 13C**). Serum antibody titers positively correlated with increased serum concentrations (**Figure 13D**). All vaccinated groups displayed a significant reduction in brain fentanyl concentrations compared to control (**Figure 13E**). The difference in effect of αIL-4 between the two vaccine formulations may relate to the different immunogenicity profiles of sKLH and CRM. Previous reports from our group showed that anti-oxycodone vaccine formulations containing either KLH or CRM were not equally effective in inducing GC B cell responses and in reducing oxycodone's effects in mice and rats (27). Overall, these data suggest that αIL-4 is effective in improving the efficacy of vaccines against OUD.

DISCUSSION

Clinical evaluation of vaccines against SUD has shown proof of efficacy in a subset of immunized patients that achieved clinically meaningful antibody responses against the target drug of abuse (83, 84, 145). While high levels of high affinity antibodies generally correlate with increased efficacy, it is not fully understood whether individual variability

limits vaccine efficacy or whether the relatively low immunogenicity is inherent to drug-carrier conjugate vaccines. To accelerate translation, vaccine development efforts should be integrated with the analysis of underlying cellular and molecular mechanisms. A comprehensive approach would provide a blueprint for vaccine development as well as guide personalized strategies, patient stratification, and clinical management of patients with SUD.

Previous studies have shown that the efficacy of SUD vaccines could be increased by traditional adjuvant platforms, including TLR3, TLR4, TLR5, and TLR9 agonists, oil-in-water emulsions, aluminum salts, and squalene emulsions (31, 39, 73, 97, 163). Using a previously established molecular adjuvant strategy focused on modulating the adaptive immune response (94), this study demonstrated that αIL-4 increases efficacy of several anti-opioid vaccine formulations, suggesting that immunomodulation of IL-4 may be broadly applicable to other vaccines targeting small molecules, peptides, or purified protein subunits. These findings are consistent with reports that the depletion of IL-4 increases efficacy of vaccines against viruses in mice (119, 120). In the aforementioned studies, increased efficacy was attributed to increased IgG_1 and IgG_{2a} production and increased numbers of cytotoxic $CD8^+$ T cells. Furthermore, these studies found an increase in efficacy when blocking IL-4R and observed that IL-13 was detrimental to protective response. While we report a similar increase in antibody class switching, there was no observed effect of IL-13, and IL-4R was necessary for increased vaccine efficacy, suggesting a different mechanism than previous reports. These apparent discrepancies in the role of IL-4 in mediating vaccine efficacy against different targets may be due to inherent differences in structural and biophysical properties between antigens, such as conjugate vaccines, live attenuated viruses, or recombinant bacterial proteins. Interestingly, other studies have found that depletion of IL-4 attenuated disease

progression after *Leishmania major* (111) or *Pseudomonas aeruginosa* infection (164). While the mechanism was not fully explored, it was postulated that this outcome was due to the change in balance between Th_2 and Th_1 responses. Additional studies focusing on the effects of IL-4 depletion on the $CD4^+$ T cell compartment will help to determine if this mechanism plays a role in the IL-4 depletion-mediated increase in efficacy of anti-opioid vaccines.

When probing downstream signaling components of IL-4, the IL-4R was found to be required for the increase in efficacy mediated by IL-4 depletion, yet the absence of IL-13 had no effect on efficacy. These data suggest that type I IL-4R signaling plays a predominant role in modulating vaccine efficacy against drugs of abuse or small molecules. Previous studies found that genetic deletion of IL-4 similarly increased vaccine efficacy compared to pharmacologic inhibition (94). Here, depletion of IL-4 increased vaccine efficacy yet deletion of IL-4R did not. This apparently contradictory paradigm has been observed in previous studies when examining parasitic infections in IL-$4^{-/-}$ and IL-$4R^{-/-}$ mice. The discrepancy was attributed to IL-13 signaling (110, 165), although this was never directly tested. In contrast, we found no contribution of IL-13, suggesting a different mechanism in the context of anti-opioid vaccines. One hypothesis is that low levels of constitutive signaling through IL-4Rs may be necessary to maintain immune system integrity after vaccination, as IL-4 signaling has been shown to prevent apoptosis in T cells and B cells (166, 167). Further studies using dual IL-4/IL-13 deficient mice are needed to explore whether this hypothesis is correct. Deletion of STAT6 or IRS2 also did not increase vaccine efficacy, suggesting that the effect of IL-4 after vaccination that is attenuated by depletion is not mediated through canonical signaling downstream of Type I IL-4R. Some literature suggests that IL-4 may signal through STAT5 in certain contexts (168), making this a possible contributor to the increase in efficacy seen after IL-4 depletion; however

testing this hypothesis may be difficult due to the lack of highly-specific STAT5 pharmacological inhibitors and STAT5's role downstream of other signaling pathways including IL-2 family receptors (IL-2, IL-7, IL-9, and IL-15), GM-CSF, erythropoietin, thrombopoietin, epidermal growth factor, and platelet-derived growth factor (169). Another potential hypothesis is that the effect is mediated through inhibition of IL-4 signaling through a non-IL-4R based pathway, although there is no evidence to date of IL-4 signaling through a non-canonical receptor. One caveat to these studies is the use of full genetic deletion models to test the functions of IL-4 signaling. Not only can genetic manipulations lead to uncharacterized immune system deficiencies, but the elucidation of the increasingly complex and often opposing role of IL-4 signaling in different cell types (101, 104) makes one speculate that deletion of IL-4 signaling in all cell types may be hiding phenotypes specific to certain cell populations that would require more nuanced approaches to assess, such as conditional knockouts or adoptive transfer.

On a cellular level, αIL-4 administration increased the number and size of GCs after vaccination. Published literature shows that the depletion of IL-4 increases GC formation after secondary vaccination in some contexts (118). However, IL-4 depletion can also have a detrimental effect on GC formation during helminth infection (104). While the reasons behind these *in vivo* effects are not well established, a potential hypothesis is that both B cells and $CD4^+$ T cells require progressively different cytokine environments to thrive during different stages of GC formation in response to specific antigens (103, 105, 170). Accordingly, timely immunomodulation of specific cytokines (e.g., IL-4) may help to synchronize cellular and molecular events conducive to GC formation. A simpler hypothesis is that GC formation relies on a balanced $CD4^+$ T cell subset polarization, and that targeted modulation of cytokines can facilitate this balance.

Our laboratory has previously shown that the generation of effective anti-drug antibodies stems from $CD4^+$ T cell-dependent B cell activation, which involves GC formation (27, 133); however, the contribution of IL-4 to GC formation in the context of anti-opioid vaccination has not been fully established. To this end, this study tested whether other immune cells were involved in the effect of IL-4 blockade. Because NKT cells are one of the major sources of IL-4 after vaccination, we hypothesized that elimination of NKT cells would replicate the effect of IL-4 depletion, as it would similarly decrease IL-4 levels in the GC. However, loss of NKT cells through CD1d deletion did not influence the efficacy of anti-opioid vaccines, indicating that either these cells are not involved, or that the immune system has other compensatory mechanisms in place, such as IL-4 supplied from either T cells or basophils (107).

On a molecular level, depletion of IL-4 resulted in a distinct transcriptomic profile in activated $CD4^+$ T cells compared to the vaccine alone. While a limited number of DEGs were found, several inflammatory markers were upregulated, including complement component C3. C3 has been shown to be a general marker of inflammation (171), an important component of antigen presentation by follicular dendritic cells (172), and an intracellular signaling molecule in T cells which is necessary for Th_1 responses and costimulation (173, 174). Because complement-mediated antibody effector functions are involved in neutralization of viral particles and other antigens (175, 176), it is possible that an equivalent process is involved in counteracting opioid effects, or at least in mounting an effective response to active immunization. While it has been shown that Fc mediated antibody effector functions are not necessary for vaccine efficacy (95), the role of complement mediated antibody-mediated effector functions against SUD is still poorly understood.

IL-4 has been shown to be important for somatic hypermutation and affinity maturation in some contexts (104, 162). Studies in IL-4 deficient animals have shown a significant reduction in activation induced cytidine deaminase (AID) (104) and a reduction in affinity of antibodies to the target antigen. These changes were more pronounced in IgG_1 secreting B cells compared to IgG_{2a} secreting B cells (162). After OXY-sKLH immunization, we saw no differences in somatic hypermutation or affinity maturation when directly measuring the number of heavy chain mutations in the complementary determining regions of the BCR or by measuring antibody avidity via biolayer interferometry. Since the polyclonal antibody response consisted of both IgG_1 and IgG_{2a} antibodies, it is possible that there were differences in affinity maturation in the IgG_1 subset which were not detected due to compensation in affinity from the IgG_{2a} subset. Regardless, any changes in affinity that may be present in a subset of cells does not prevent an increase in efficacy after drug challenge, indicating that antibody affinity is not important for the increased efficacy in this specific context.

We have reported here and elsewhere (94) that increases in IgG_{2a} correlate with increases in vaccine efficacy after IL-4 depletion. Here, we directly tested whether IgG_{2a} antibodies have inherently greater capacity to protect against oxycodone after challenge by passively immunizing mice with mAbs that have identical binding sequences but different Fc regions. This study showed no difference between the mAbs in their efficacy to prevent oxycodone distribution to the brain, indicating that Fc portion is not relevant to vaccine efficacy at the time of drug challenge. We additionally tested an IgG_{2a} mAb with a L234A, L235A, P329G mutation that prevents binding to FcγRI-IV receptor [inhibiting antibody dependent effector functions (159)], which displayed similar efficacy to the unmutated IgG_{2a} mAb. This further reinforces previous reports that antibody mediated effector functions are not necessary for vaccine efficacy after drug challenge (95). One

alternative hypothesis for the correlation between IgG_{2a} production and increased vaccine efficacy is that an early IgG_{2a} response during immunization increases Fc mediated antigen presentation of immune complexes, which in turn increases overall antibody production. Another explanation is that rather than needing a Th_1 polarized response, adjuvants that can stimulate both Th_1 and Th_2 responses can engage non-overlapping populations of B and T cells, leading to an overall increase in antibody production. These results will be important for future vaccine design and adjuvant selection to pair Th_1 and Th_2 inducing adjuvants.

During GC formation, IL-4 has been implicated in the differentiation of antibody-secreting plasma cells and in the plasma vs. memory cell choice (101, 104). Since IL-4 depletion increases GC-T_{fh} cells in the GC which results in increased antibody titers, we hypothesized that the increased number of GC-T_{fh} cells leads to increased interactions with GC B cells, increasing survival and differentiation into plasma cells. We found that immunization with OXY-sKLH and a depleting IL-4 mAb increased the number of oxycodone-specific antibody secreting cells at day 35, visualized via ELISPOT. When determining whether the increase in plasmablast formation translated into an increase in long-lived plasma cells in the bone marrow, we found no significant difference in oxycodone-specific plasma cells at day 100. This suggests that the increase in plasmablasts caused by IL-4 depletion is transient, and these cells likely die during the contraction of the immune response, or alternatively they may become tissue-resident plasma cells in other organs.

Overall, these studies are consistent with a model where the increase in anti-opioid vaccine efficacy is modulated by type I IL-4 signaling, potentially involving inhibition of STAT5. Inhibition of signaling leads to increased germinal center formation in secondary

lymphoid organs after vaccination, in part through changes in the T cell signaling compartment. This change in T cell signaling does not lead to increased somatic hypermutation or affinity maturation in B cells after immunization, but does increase proportion of short-lived antibody-secreting cells, perhaps due to increased survival signals given within the GC after cognate interactions between opioid-specific B and T cells. These antibody secreting cells do not secrete opioid-specific IgE, but do secrete increased amounts of IgG_{2a}; however this increase in IgG_{2a} is not directly responsible for increased vaccine efficacy.

These results support the use of αIL-4 as a molecular adjuvant for vaccination against OUD and SUD. IL-4 depletion-mediated vaccine enhancement has now been verified with several opioid vaccine formulations, TDaP vaccines (94), and HIV vaccines (119). These results suggest that this strategy may be broadly applicable, particularly in vaccine formulations that require a strong neutralizing antibody response against challenging targets. The mechanisms uncovered during this investigation also provide a blueprint for next generation vaccine formulation in which adjuvants need to strongly stimulate T cells and provide a balanced Th_1/Th_2 response to increase the number and size of GCs after immunization, specifically through proliferation of T_{fh} cells and antibody secreting cells. In addition, as IL-4 polymorphisms correlated with antibody responses after vaccination against other targets (131, 132), these data support the hypothesis that IL-4, but not necessarily it's downstream signaling components, could be a putative biomarker predictive of vaccine efficacy used to identify patients that would benefit from clinical management using anti-opioid vaccines.

FIGURES

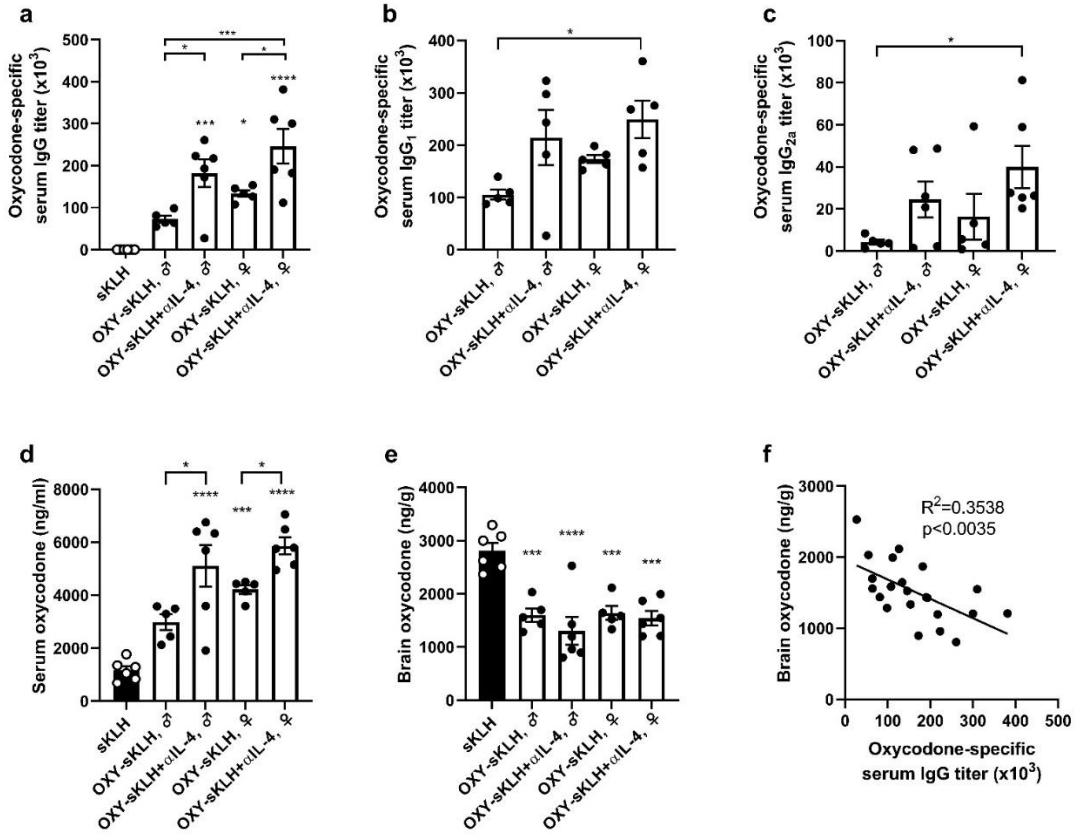

Figure 1. Effect of IL-4 depletion on anti-oxycodone vaccines in male and female mice. Male and female Balb/c mice were immunized on days 0, 14, and 28. A) Oxycodone-specific serum IgG antibody titers on day 34. Oxycodone-specific B) IgG_1 and C) IgG_{2a} subclass titers. After challenge with 5.0 mg/kg oxycodone, shown: D) serum and E) brain concentrations. F) Relationship between oxycodone-specific serum IgG antibody titers and brain oxycodone concentrations in vaccinated mice. Data are mean±SEM. Sample size: n=5-6 per group. Statistical analysis conducted by one-way ANOVA paired with Tukey's multiple comparisons post hoc test (A-E) or linear regression (F). Symbols: * $p \leq 0.05$, ** $p \leq 0.01$, *** $p \leq 0.001$, **** $p \leq 0.0001$ compared to control, or brackets to indicate differences between groups.

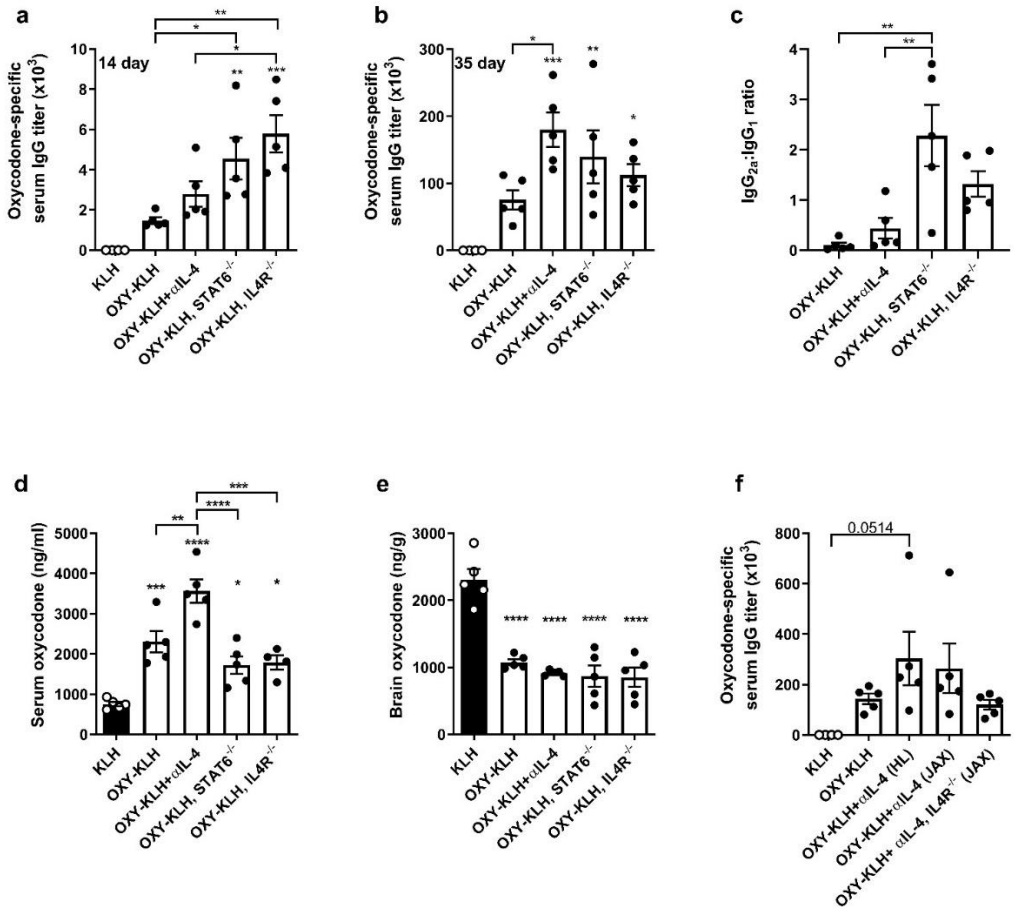

Figure 2. Deletion of downstream IL-4 signaling does not increase efficacy of an anti-oxycodone vaccine. Mice were immunized with either KLH or OXY-KLH on days 0, 14, and 28 and challenged s.c. with 2.25 mg/kg oxycodone on day 35. Oxycodone-specific antibody titers: A) IgG at 14 days, B) IgG at 35 days, and C) ratio of IgG_{2a} to IgG_1. At 30 minutes post-drug challenge, concentration of oxycodone in D) serum and E) brain. F) In a separate experiment, IL4R$^{-/-}$ mice were vaccinated with OXY-KLH and αIL-4, and controls included mice from Harlan (HL) and Jackson (JAX) laboratories. Data are mean±SEM. Sample size: n=5 per group. Statistical analysis conducted by one-way ANOVA paired with Tukey's multiple comparisons post hoc test. Statistical symbols: * p

≤ 0.05, ** p ≤ 0.01, *** p ≤ 0.001, **** p ≤ 0.0001 compared to control, or brackets to indicate differences between groups.

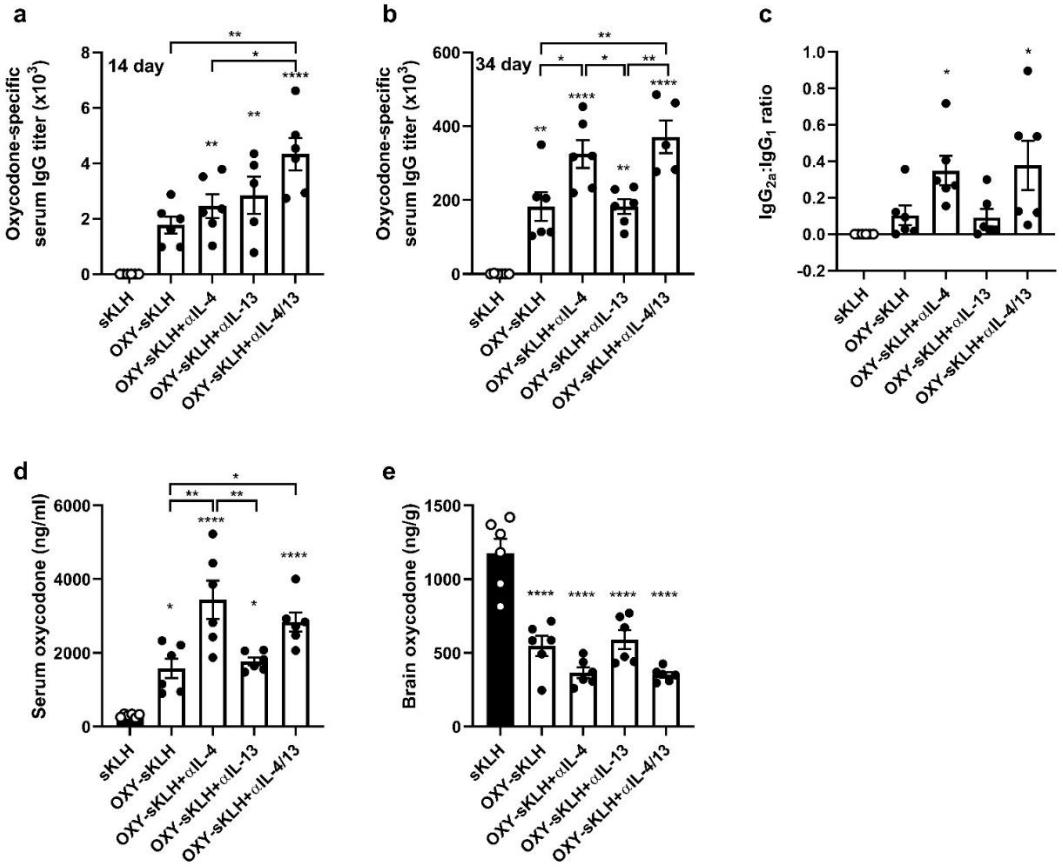

Figure 3. IL-13 does not modulate efficacy of anti-opioid vaccines. Balb/c mice were immunized on days 0, 14, and 28 with either sKLH or OXY-sKLH. Concurrently, αIL-4 mAb, αIL-13 mAb, or both were administered on days -2 and 1 at a dose of 0.5 mg per mAb per dose. Mice were challenged s.c. with 2.25 mg/kg oxycodone. Oxycodone-specific antibody titers expressed as: A) IgG at 14 days, B) IgG at 34 days, and C) ratio of IgG_{2a} to IgG_1. At 30 minutes post-drug challenge, concentration of oxycodone in D) serum and E) brain. Data are mean±SEM. Sample size: n=5-6 per group. Statistical analysis conducted by one-way ANOVA with Tukey's multiple comparisons post hoc test. Statistical symbols: * $p \leq 0.05$, ** $p \leq 0.01$, *** $p \leq 0.001$, **** $p \leq 0.0001$ compared to control, or brackets to indicate differences between groups.

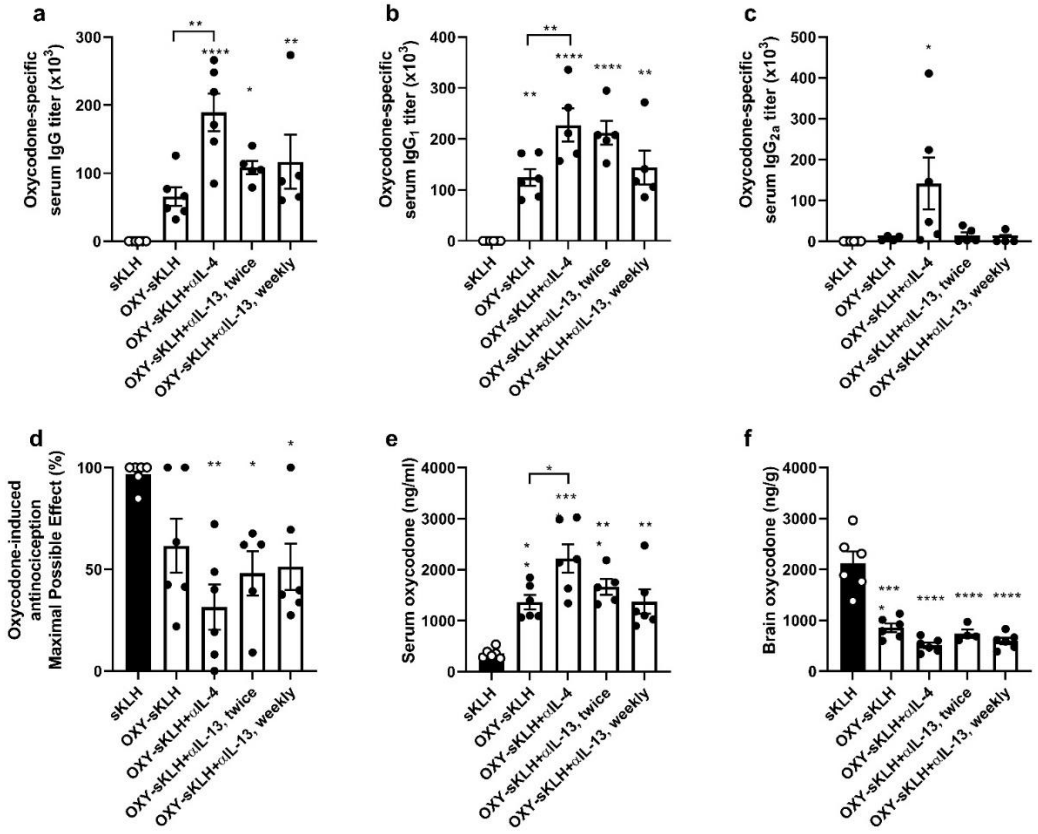

Figure 4. Depletion of IL-13 did not alter vaccine efficacy against oxycodone. Mice were immunized on days 0, 14, and 28 with either sKLH or OXY-sKLH. Concurrently, mice immunized with OXY-sKLH were also treated with: 1) αIL-4 on days -2 and 1, 2) αIL-13 on days -2 and 1, or 3) αIL-13 once per week. αIL-4 was administered at a dose of 0.5 mg per injection as previously described (94). αIL-13 was administered at a dose of 0.1 mg per injection based on Genentech's recommendations. After vaccination, oxycodone-specific serum antibody titers: A) IgG, B) IgG_1, C) IgG_{2a}. After *in vivo* oxycodone challenge, shown effect of vaccination on: D) decreasing oxycodone-induced antinociception percent maximum possible effect (%MPE), E) increasing opioid concentration in the serum, and F) decreasing oxycodone distribution to the brain. Data are mean±SEM. Sample size: n=5-6/group. Statistical analysis conducted by one-way ANOVA paired with Tukey's

multiple comparisons post hoc test. Statistical symbols: * $p \leq 0.05$, ** $p \leq 0.01$, **** $p \leq 0.0001$ compared to control, or brackets to indicate differences between groups.

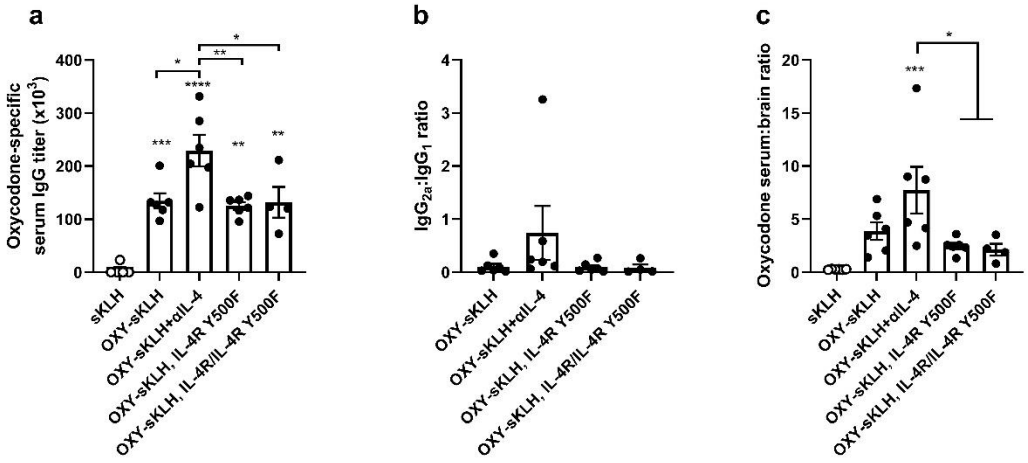

Figure 5. Ablation of IL-4 dependent IRS signaling does not increase vaccine efficacy after OXY-sKLH immunization. WT Balb/c mice (n=6/group) were immunized on days 0, 14, and 28 with OXY-sKLH with or without IL-4 depletion with a αIL-4 mAb and compared to mice with a homozygous deficiency in IL-4 dependent IRS signaling (IL-4R Y500F) or their heterozygous littermates (IL-4R/IL-4R Y500F). Blood was collected via facial vein on day 34 to measure A) oxycodone-specific serum IgG titers, or B) ratio of IgG_{2a}:IgG_1 subclass titers. On day 35, mice were challenged with 2.25 mg/kg oxycodone. Thirty minutes later, blood and brain were collected to measure concentration of oxycodone in each, expressed as C) serum:brain oxycodone ratio. Data are mean±SEM. Sample size: n=4-6/group. Statistical analysis conducted by one way ANOVA with Tukey's multiple comparisons post hoc test. Statistical symbols: * p<0.05, ** p<0.01, *** p<0.001, **** p<0.0001 compared to control, or brackets to indicate differences between groups.

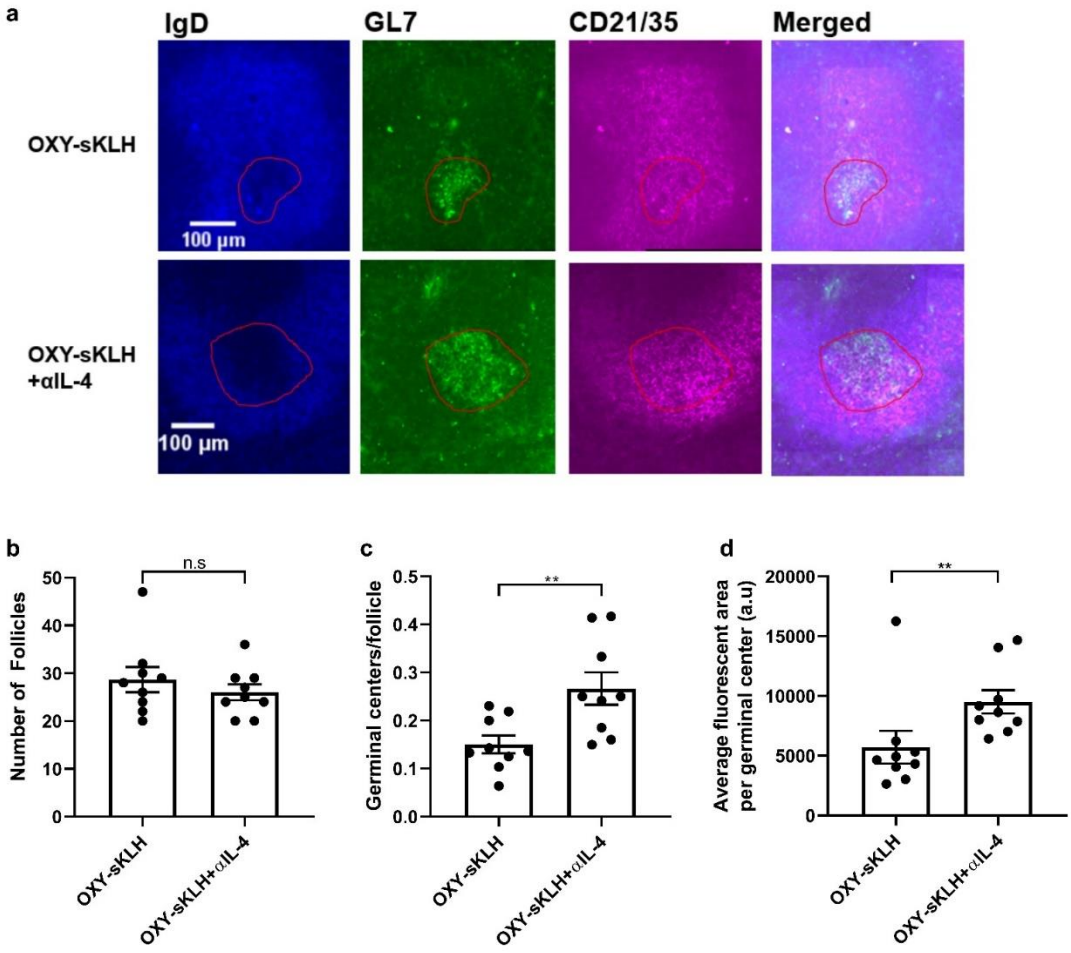

Figure 6. Depletion of IL-4 increases germinal center formation. Cryosections of spleens from mice vaccinated with OXY-sKLH ± αIL-4 were stained for $GL7^{+}$ germinal center B cells, IgD^{+} follicular B cells, and $CD21/35^{+}$ follicular dendritic cells. Slides were imaged at 20x magnification with a Zeiss widefield fluorescence microscope. A) Representative image of germinal centers and surrounding follicle from mice immunized with OXY-sKLH ± αIL-4. Germinal centers are outlined in red. At 10 days post-vaccination: B) overall number of follicles per imaged spleen section, C) germinal centers per follicle, and D) average $GL7^{high}$ fluorescent area per germinal center was measured. Data are mean±SEM. Sample size: n=3 mice per group x 3 slides per mouse, with slices at least

100 μm apart. Statistical analysis conducted by Mann-Whitney U test. Symbols: ** $p \leq 0.01$.

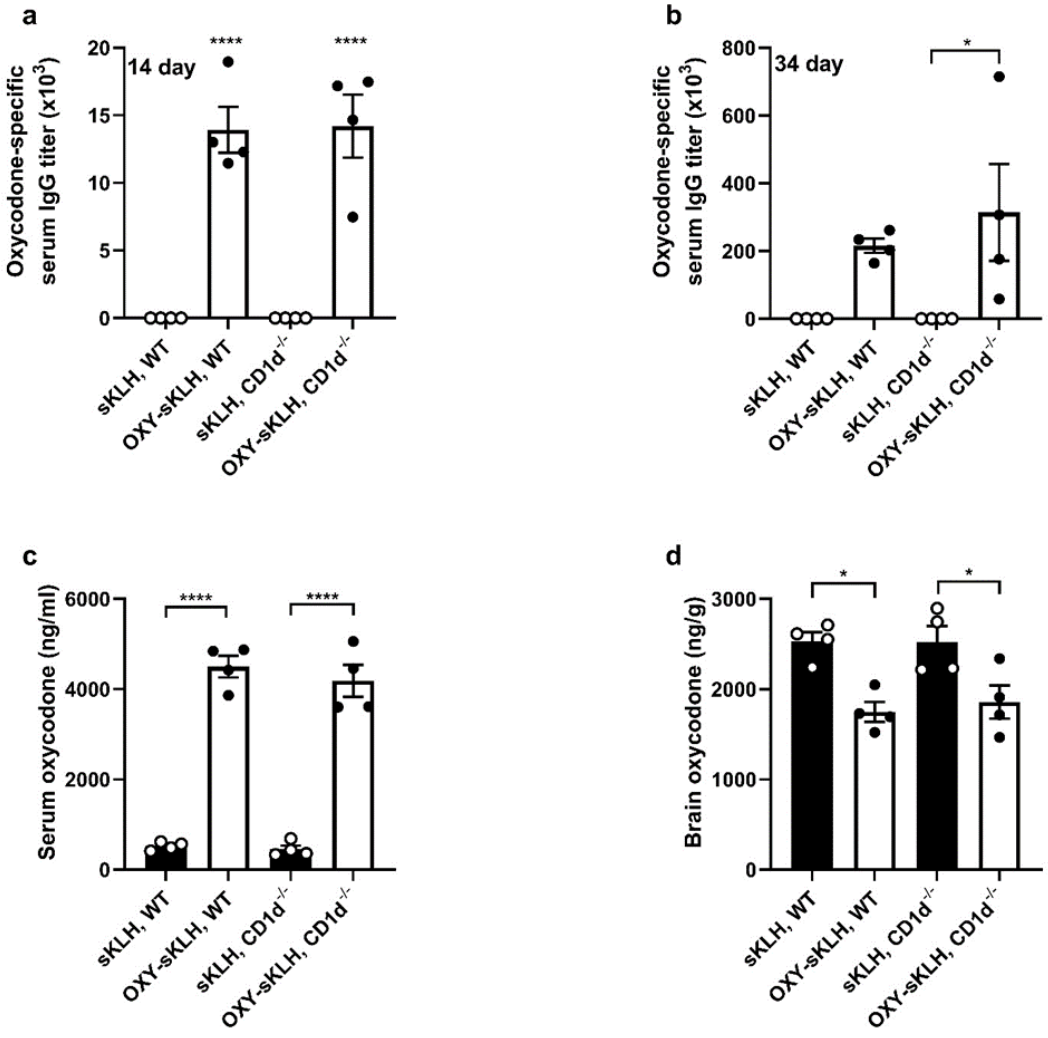

Figure 7. Deletion of NKT cells does not increase efficacy of anti-opioid vaccines. Wild-type or CD1d$^{-/-}$ C57BL/6 mice were immunized with either sKLH or OXY-sKLH on days 0, 14, and 28. After immunization, oxycodone-specific antibody titers expressed as A) IgG at 14 days and B) IgG at 34 days. On day 35, mice were challenged s.c with 5 mg/kg oxycodone and C) serum oxycodone concentration and D) brain oxycodone concentration were measured 30 minutes post-challenge. Data are mean±SEM. Sample size: n=4 per group. Statistical analysis conducted by one-way ANOVA with Tukey's

multiple comparisons post hoc test. Symbols: * $p \leq 0.05$, **** $p \leq 0.0001$ compared to control, or brackets to indicate differences between groups.

a

Groups Compared	Genes Upregulated	Genes Downregulated	Total Differentially Expressed Genes
sKLH vs. **OXY-sKLH**	86	627	713
sKLH vs. **OXY-sKLH+αIL-4**	294	59	353
OXY-sKLH vs. **OXY-sKLH+αIL-4**	860	74	934

b

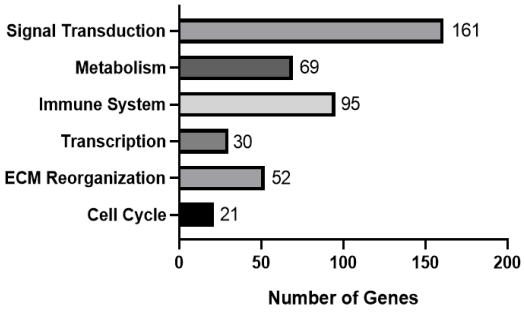

d

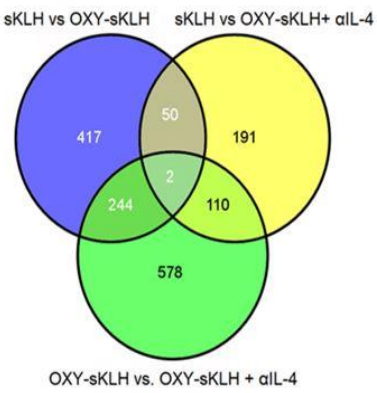

c

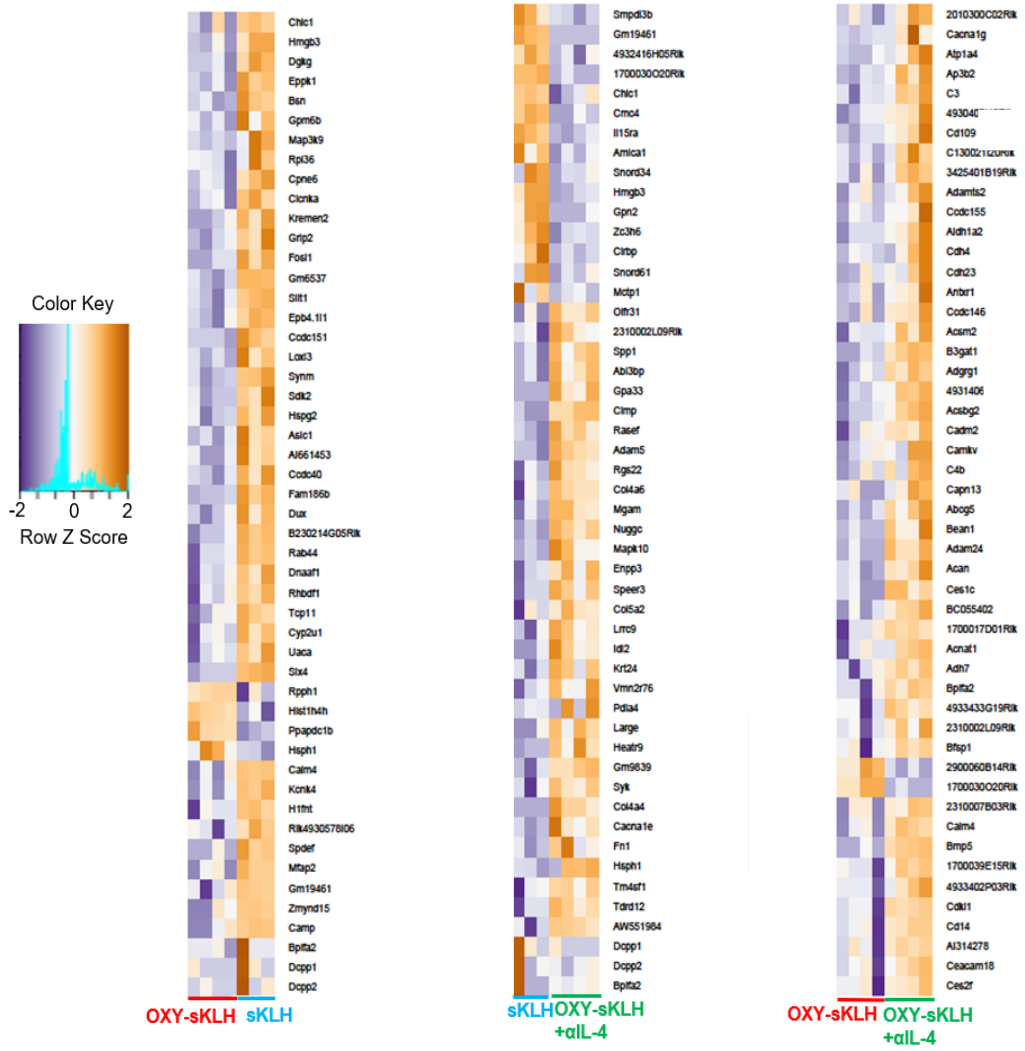

Figure 8. Effect of IL-4 depletion on global mRNA expression in activated CD4$^+$ T cells. Mice were immunized once with either sKLH or OXY-sKLH, and αIL-4 was administered on days -2 and 1. On day 7, T cells from spleen and lymph nodes were isolated for analysis by RNA sequencing. A) Table quantifying total upregulated and downregulated genes between groups. B) Graph showing number of DEGs related to common cell processes between OXY-sKLH and OXY-sKLH plus αIL-4. C) Comparison of top 50 up- and down-regulated genes between sKLH vs. OXY-sKLH, sKLH vs. OXY-sKLH plus αIL-4, and OXY-sKLH vs. OXY-sKLH plus αIL-4. D) Venn diagram showing similarities of DEGs between groups. Sample size: n= 3-4 per group. Statistical analysis conducted by edgeR on CLC Genomics Workbench for genes with at least 1.5-fold differential expression with a p-value ≤0.05 and an average of ≥ 5 reads per sample.

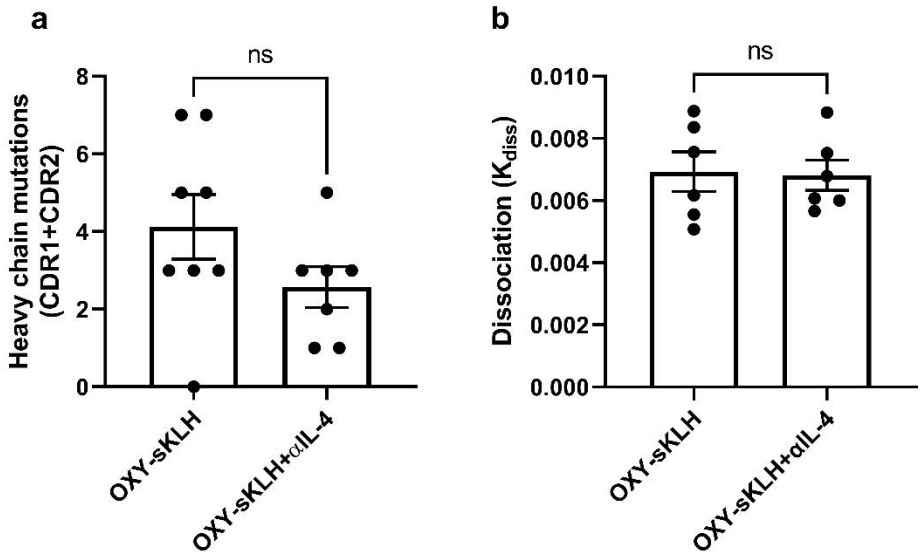

Figure 9. IL-4 depletion does not influence somatic hypermutation or affinity maturation after anti-opioid immunization. The heavy chain B cell receptor sequence from hybridoma's generated by immunization with OXY-sKLH or OXY-sKLH with IL-4 depletion were analyzed against germline heavy chain sequences using IgBlast. A) Comparison of heavy chain CDR1 and CDR2 mutations after OXY-sKLH immunization with or without IL-4 depletion. B) Sera from OXY-sKLH and OXY-sKLH+αIL-4 immunized mice were analyzed for avidity via biolayer interferometry. Data are mean±SEM. Sample size: (A) n=7-8/group, (B) n=6/group. Statistical analysis performed via Mann Whitney U test.

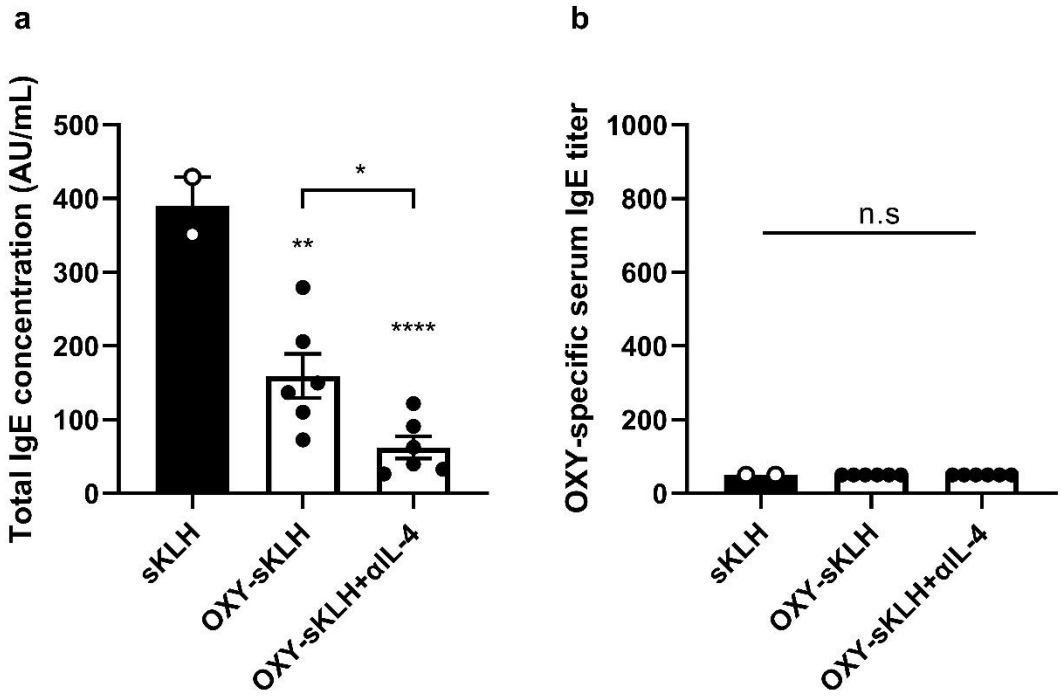

Figure 10. No oxycodone-specific IgE was detected in OXY-sKLH immunized mice. Mice were immunized on days 0, 14, and 28 with sKLH control or OXY-sKLH with or without IL-4 depletion. On day 34, blood was collected for detection of A) total IgE and B) oxycodone-specific IgE via ELISA. Data are mean±SEM. Sample size: n=6/group. Statistical analysis performed via one way ANOVA with Tukey's multiple comparison's post hoc test. Statistical symbols: * $p<0.05$, ** $p<0.01$, **** $p<0.0001$ compared to control, or brackets to indicate differences between groups.

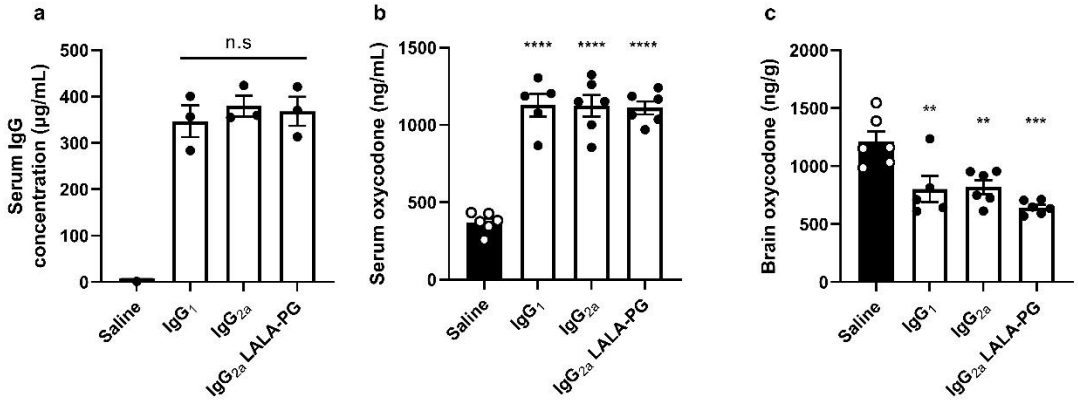

Figure 11. IgG subclass and antibody mediated effector functions do not influence vaccine efficacy. Mice were passively immunized with recombinant antibodies with identical antigen binding regions and a IgG_1, IgG_{2a}, or IgG_{2a} LALA-PG Fc region. One day later, serum was collected to measure A) antibody concentration via biolayer interferometry. Mice were then challenged with 2.25 mg/kg oxycodone and B) blood and C) brain were collected 30 minutes later to determine opioid concentration by LC-MS. Data are mean±SEM. Sample size: n=5-6/group. Statistical analysis performed via one-way ANOVA with Tukey's multiple comparisons post hoc test. Statistical symbols: ** $p<0.01$, *** $p<0.001$, **** $p<0.0001$ compared to control.

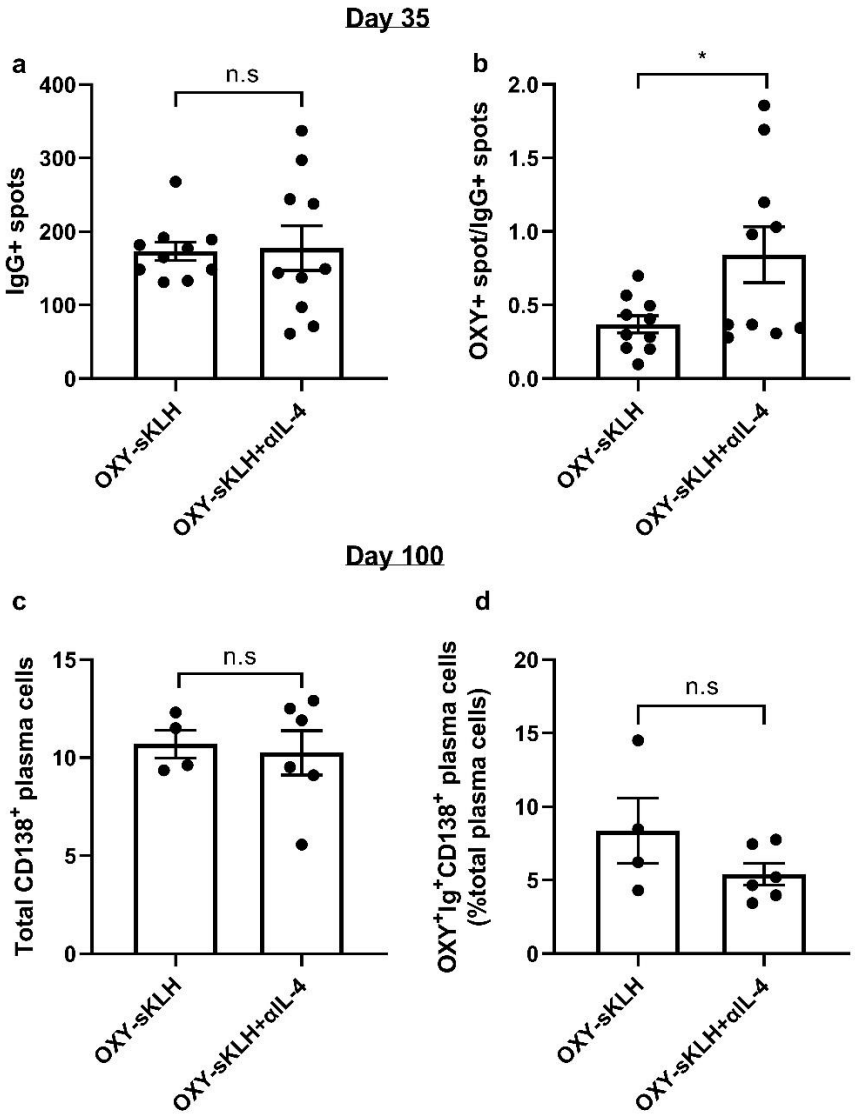

Figure 12. IL-4 depletion increases early oxycodone-specific antibody secreting B cells. Mice were immunized with OXY-sKLH with or without IL-4 depletion. After 3 immunizations, spleens and lymph nodes were collected and processed into a single cell suspension. Total and oxycodone-specific antibody secreting cells (ASCs) were measured via ELISPOT. A) Number of total IgG ASCs and B) oxycodone-specific ASCs normalized to total IgG ASCs. A second cohort of mice was similarly immunized, and bone

marrow was collected day 100. C) Total plasma cells in the bone marrow and D) oxycodone-specific plasma cells as a percentage of total plasma cells were identified via flow cytometry. Data are mean±SEM. Statistical analysis performed via Student's t test. Statistical symbols: * $p<0.05$.

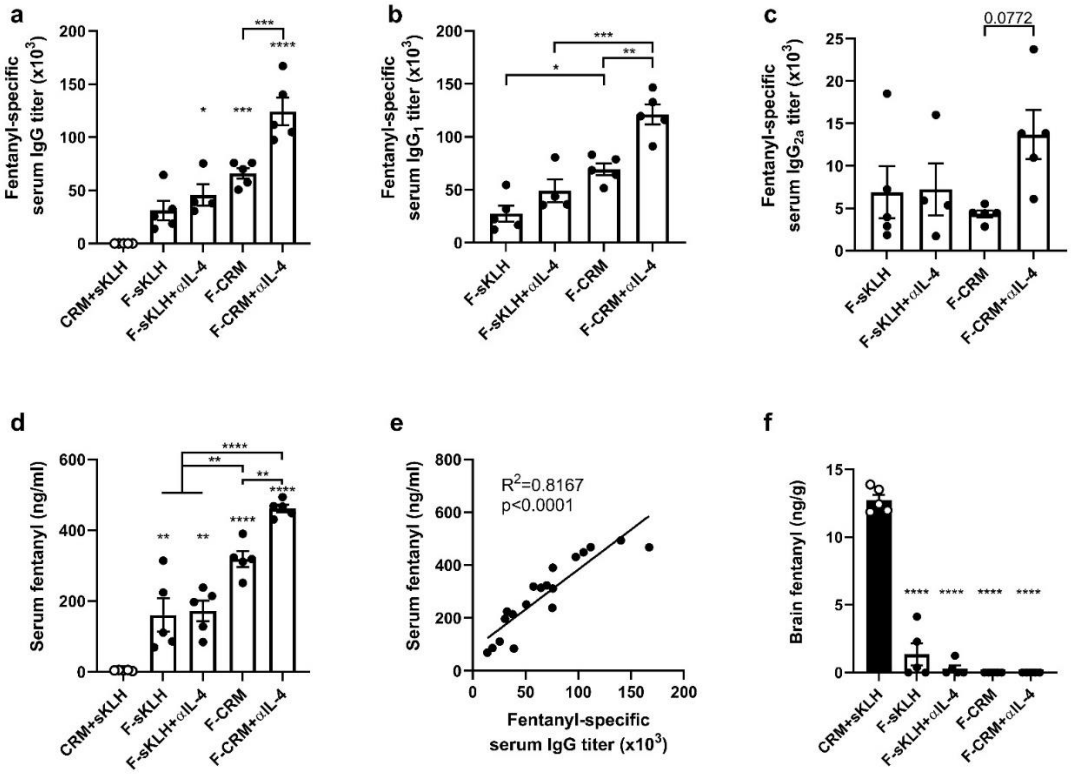

Figure 13. Depletion of IL-4 increases efficacy of anti-fentanyl vaccines. Balb/c mice were immunized with either F-sKLH or F-CRM, alone or in combination with αIL-4, and then challenged s.c. with 0.05 mg/kg fentanyl. Fentanyl-specific A) IgG, B) IgG_1, and C) IgG_{2a} subclass titers at one week after the last immunization. D) Concentration of fentanyl in serum at 30 minutes post-drug challenge. E) Linear regression of fentanyl-specific IgG titers versus serum fentanyl concentration. E) Concentration of fentanyl in the brain at 30 minutes post-drug challenge. Data are mean±SEM. Sample size: n=5 per group. Statistical analysis conducted by one-way ANOVA with Tukey's multiple comparisons post hoc test. Symbols: * $p \leq 0.05$, ** $p \leq 0.01$, *** $p \leq 0.001$, **** $p \leq 0.0001$ compared to control, or brackets to indicate differences between groups.

Chapter 3: Identification and characterization of adjuvants suitable for clinical translation

Chapter 2 established that a balanced Th_1/Th_2 response and stimulation of T_{fh} cells to increase GC formation is important for OUD vaccine efficacy. This chapter focuses on the characterization of anti-opioid vaccines combined with TLR-targeting adjuvants suitable for clinical translation. These adjuvants have been shown to promote a balanced Th_1/Th_2 response when combined with alum, and activation of the specific TLRs have been shown to stimulate T_{fh} cells or GC formation in other vaccine contexts. These studies test the efficacy, safety, and pharmacology of the lead vaccine formulation in rodent and porcine models of fentanyl misuse and overdose and test the adjuvant's applicability to other OUD vaccine formulations.

The following data were published or are currently under review:

Crouse B, Miller SM, Muelken P, Hicks L, Marker C, Guedes GPA, Pentel PT, Evans JT, LeSage MG, Pravetoni M. Novel TLR7/8 agonist increases efficacy of anti-fentanyl vaccines in rat and porcine models of fentanyl misuse and overdose. *Npj vaccines*, (2022).

Miller SM, Crouse B, Hicks L, Amin H, Bazin HG, Burkhart DJ, Pravetoni M, Evans JT. A novel lipidated TLR7/8 adjuvant enhances the efficacy of a vaccine against fentanyl in mice. *Npj Vaccines*, (2022).

Author Contributions: BC planned and executed experiments and analyzed data, SM planned and executed experiments and analyzed data, PM, LH, and GPAG executed experiments, CM and PTP provided research support, JTE planned experiments and analyzed data, MGL planned experiments and analyzed data, MP assisted with interpretation of data and editing, HA, HGB and DJB provided key reagents.

INTRODUCTION

Opioid use disorders (OUD) and overdose are currently at epidemic levels in the United States, with over 2 million people meeting the diagnostic criteria for OUD (177) and over 136 people dying every day from opioid overdose (178). In 2019, 72.9% of opioid overdoses were due to synthetic opioids such as the highly potent fentanyl (178). The rate of overdose due to synthetic opioids increased 15% from 2018 to 2019 (179), and it is estimated that the COVID-19 pandemic has further increased opioid overdose deaths by over 30% in 2020 (180). While there are FDA-approved medication-assisted therapies (MAT) for OUD, such as the mu opioid receptor (MOR) agonist methadone, MOR partial agonist buprenorphine, and MOR antagonist naltrexone, these therapies are hard to access, have limited efficacy, cause unwanted side effects, or have an intrinsic abuse liability (138, 181). The MOR antagonist naloxone, approved for the reversal of overdose, has a relatively short duration of action and must be administered after an overdose occurs, limiting its use against highly potent or longer-lasting synthetic opioids or in situations where it is not immediately accessible (182). Furthermore, as a MOR antagonist, naloxone does not reverse opioid-induced effects mediated by cholinergic and α-adrenergic receptors such as “wooden chest syndrome”, a stiffening of the chest wall muscles which further decreases lung function and complicates the performance of CPR (21). For these reasons, novel treatments for OUD and overdose are urgently needed to prevent deaths due to opioid misuse.

One such novel therapeutic is active immunization with an anti-opioid conjugate vaccine. These vaccines consist of opioid-based small molecule haptens conjugated to larger immunogenic carriers, which are often formulated with an adjuvant such as aluminum hydroxide (alum) to increase the generation of opioid-specific antibodies (142). Anti-drug antibodies selectively bind to the target opioid in serum and reduce its

distribution to the brain, attenuating opioid-induced effects such as analgesia, respiratory depression, bradycardia, and potential lethality (27, 30, 32-34, 38, 39, 41, 42, 54, 55, 65, 67, 183). Given their selectivity for the target opioid, vaccines can be used in conjunction with current treatments for OUD or overdose and could be administered prophylactically to prevent overdose in high-risk populations (27, 30, 32-34, 38, 39, 41, 42, 54, 55, 65, 67, 183). These vaccines have been extensively tested in preclinical models for efficacy and safety (27, 30, 32-34, 38, 39, 41, 42, 54, 55, 65, 67, 183), and a candidate anti-oxycodone vaccine is currently being tested in a Phase Ia/Ib clinical trial (NCT04458545).

One major barrier to the translation of vaccines for OUD and other substance use disorders (SUD) is the production of drug-specific antibodies at a concentration high enough to result in a significant reduction in drug use or adverse effects. Phase II and III trials of vaccines against cocaine and nicotine showed that a significant reduction in drug use occurred in a subset of patients that had the highest anti-drug antibody concentrations, however most patients were not such “high responders” (i.e., did not achieve high enough antibody levels for efficacy) (83, 84). To improve translation from preclinical models to clinical use, strategies are needed to increase the number of high responders to drug-based conjugate vaccines. This requires understanding the basic immunology behind conjugate vaccine response to choose appropriate delivery platforms and/or adjuvants to optimize the immune response.

The production of high affinity opioid-specific antibodies after immunization relies on $CD4^+$ T cell dependent B cell activation and the formation of germinal centers in the lymph nodes and spleen (27, 94, 160). Additionally, data suggest that a balanced Th_1/Th_2 response and the production of a combination of IgG_1 and IgG_{2a} antibodies in mice leads to higher efficacy against opioid challenge after immunization (94, 160). To facilitate

clinical translation, most anti-opioid vaccine formulations are adsorbed on aluminum hydroxide (alum) (55, 142); however this adjuvant has been shown to induce a strong Th_2 response and the production of almost exclusively IgG_1 (184). Beyond alum, pre-clinical studies have tested anti-opioid vaccines in combination with a variety of adjuvants and immunomodulators including the TLR4 agonist MPLA (31), TLR9 agonist CpG ODN 1826 (73), dsRNA (39), Advax (37), army liposome formulation (ALF) (42), anti-IL-4 monoclonal antibodies (mAbs) (94, 160), anti-IL-13 mAbs(160), anti-IL-2R mAbs (94), anti-IL-7R mAbs (160), Freund's (31), dmLT (99), LTA1 (99), and MF59 (97) with varying degrees of success in increasing anti-opioid antibody titers and inducing the production of IgG_{2a}. While potentially effective, many of these adjuvants are not feasible for clinical translation due to toxicity, side effects, cost, or availability due to intellectual property rights. In order to optimize the antibody response to a lead anti-fentanyl vaccine (F_1-CRM), our group tested the addition of two novel adjuvants targeting either TLR4 (INI-2002) or TLR7/8 (INI-4001) as adjuvants for a fentanyl vaccine in mice and rats. Both TLR4 and TLR7/8 adjuvants have been shown to induce Th_1 cell responses and the production of IgG_{2a} antibodies when combined with protein-based or protein-conjugate vaccines (185-188). Additionally, unlike other TLRs, activation of TLR7/8 has been shown to stimulate expansion of T_{fh} cells (189), which have previously been shown to be an important target for increasing OUD vaccine efficacy (94, 160). Consistent with these observations, these studies found that stimulation of TLR7/8, but not TLR4, increased antibody titers and vaccine efficacy after fentanyl challenge. We then extended these findings by testing this formulation in a rat model of fentanyl challenge, drug overdose, and fentanyl self-administration. Additionally, we tested whether the addition of INI-4001 would expand epitope recognition and increase cross-reactivity to off target molecules. Finally, since rodent models do not fully recapitulate the human immune response after TLR7/8

activation (190-192), we developed a porcine model of fentanyl challenge and overdose to provide preliminary evidence that this lead adjuvanted vaccine formulation is effective in large animal models that better mimic TLR7/8-mediated immune responses in humans. In these studies, INI-4001 adjuvanted fentanyl vaccines increased immunogenicity and efficacy in rodent models of drug-challenge, overdose, and self-administration, as well as in porcine models of fentanyl overdose. This supports the use of INI-4001 as an adjuvant in clinical studies of the F_1-CRM vaccine for treatment of OUD and prevention of opioid overdose.

MATERIALS AND METHODS

Hapten synthesis and conjugate vaccines. The fentanyl-based hapten containing a tetraglycine linker at the C6 position (F_1) was synthesized as previously described (54, 55) and conjugated to GMP grade diphtheria cross reactive material (Pfenex, San Diego, CA or FinaBio, Rockville MD) using carbodiimide chemistry as previously described (54, 55). F_1 hapten was conjugated to bovine serum albumin (BSA) as a coating antigen for titer ELISA. For competitive ELISA, a different fentanyl based hapten (F_3) conjugated to BSA was used as a coating antigen, the synthesis of which has been previously described (55). Morphine (M) conjugate was synthesized as previously described (41, 183) and conjugated to sKLH or CRM using carbodiimide chemistry and previously described (41, 183, 193). The unconjugated carrier protein or the conjugate vaccines were adsorbed on aluminum adjuvant (Alhydrogel ‘85’, 2%, Brenntag Biosector, Denmark) and TLR agonists as described in each experimental section.

Adjuvants. INI-2002 (2-[(R)-3-decanoyloxytetradecanoylamino]ethyl 2,3-di-[(R)-3-decanoyloxytetradecanoylamino]-2,3-dideoxy-4-O-sulfoxy-β-D-allopyranoside) was synthesized as previously described (194). INI-4001 was synthesized by

phospholipidation of 6-amino-2-butoxy-9-[(1-hydroxyethyl-4-piperidinyl)-methyl]-7, 9-dihydro-8H-purin-8-one (195) using the published phosphoramidite method (196).

Drugs. Fentanyl citrate, sufentanil citrate, carfentanil HCl, methadone HCl, remifentanil HCl, heroin HCl, and buprenorphine HCl were obtained from either Boynton Pharmacy (Minneapolis, MN), Hennepin County Medical Center pharmacy (Minneapolis, MN), or Sigma Aldrich (St. Louis, MO). Acetylfentanyl HCl was obtained from RTI International. Drugs doses are expressed as weight of free base.

Ethics Statement. Studies were performed according to the Guide for the Care and Use of Laboratory Animals and the National Institute of Health. Animal protocols were approved by both the University of Minnesota and the Hennepin Healthcare Research Institute Animal Care and Use Committees. Animals were euthanized by AAALAC approved CO_2 chambers (mice and rats) or IV pentobarbital sodium (pigs), and all efforts were made to minimize suffering.

Animals. For drug challenge studies, 6-8 week old male Balb/c mice were obtained from Jackson Laboratories (Bar Harbor, ME), and 8-10 week old male Sprague-Dawley rats were obtained from Charles River Laboratories (Wilmington, MA). Rodents were grouped housed under a standard 14/10 hour light/dark cycle and were given food and water *ad libitum*. For fentanyl self-administration, male and female Sprague-Dawley rats (65-75 day old on arrival; Envigo, Madison, WI) had ad lib access to water and restricted access to food (18–20 g/day) in a temperature- and humidity-controlled colony room under a reversed 12-hr light/dark cycle (experimental sessions ran during the dark phase). For mini pig studies, two-month-old Hanford miniature pigs were obtained from Sinclair Bio Resources (Auxvasse, MO). Pigs were housed 1-3 per pen under a 14/10 hour light/dark

cycle and fed 1 cup of Envigo Teklad miniswine diet # 8753 daily. All testing occurred during the light phase.

Experimental Design. Drug challenge studies in rodents: Anti-fentanyl vaccines were administered i.m. in the hind thigh on days 0, 14, and 28 (mice) or 0, 21, and 42 (rats). Animals received 5 µg unconjugated carrier protein (CRM) adsorbed on alum as a control, 5 µg F_1-CRM with no adjuvant, 5 µg F_1-CRM adsorbed on alum or 5 µg F_1-CRM adsorbed on alum with 1 µg INI-2002 or 10 µg INI-4001 as described in each experimental section. Blood was collected via facial vein (mice) or tail vein (rats) for antibody analysis. Some rats were euthanized at 49 days for trunk blood collection to run *in vitro* binding assays. Rodents were challenged starting on day 35 (mice) or 56 (rats). Mice were challenged once, while rats were challenged with one drug weekly until the end of the study. Challenge drugs included fentanyl (0.05 mg/kg-0.45 mg/kg), sufentanil (0.008 mg/kg), carfentanil (0.01 mg/kg), heroin (0.5-4 mg/kg) or methadone (4.5 mg/kg), all administered subcutaneously (s.c). Rats were boosted with vaccine every three weeks to maintain antibody titer levels. Vaccine efficacy in reducing opioid-induced behavioral effects were measured via hot plate test of centrally-mediated antinociception as described (55) or in reducing opioid-induced respiratory depression and bradycardia using a pulse oximeter (Starr Life Sciences, Oakmont, PA) (55) at 30 minutes (mice) or every 15 minutes after drug challenge for one hour (rats). In some studies, naloxone (0.1 mg/kg) was given 1 hour after drug challenge to reverse opioid-induced effects. In terminal studies, rodents were euthanized after the final time point, and blood and brain were collected for analysis by liquid chromatography/tandem mass spectrometry (LC-MS/MS).

Fentanyl self-administration (FSA) in rats: Rats were implanted with a jugular catheter under ketamine (75–90 mg/kg) and dexmedetomidine (0.25 mg/kg) anesthesia.

The opposite end of the catheter exited the body between the scapulae and attached to a vascular-access harness (VAH95AB, Instech Inc., Plymouth Meeting, PA). Rats recovered from surgery for at least three days, during which catheters were flushed daily with a heparinized (30 units/ml) saline/glycerol (25%) solution and ceftriaxone (5.25 mg), and a s.c. injection of buprenorphine (0.05 mg/kg; first two days only) was given for analgesia. Over the course of the experiment, daily infusions of heparinized saline/glycerol continued and infusions of methohexital (0.1 ml of 10 mg/ml, i.v.) were given on Fridays after the session to determine catheter patency (indicated by anesthesia within 5 sec).

After recovery from surgery, rats were trained to self-administer fentanyl (1 µg/kg/infusion) under a fixed-ratio (FR) 1 schedule during daily 120-min sessions (five days/week) using standard two-lever operant conditioning chambers (Med Associates, St. Albans, VT) as previously described (55). After at least 10 sessions and when robust fentanyl intake was established, the FR was gradually increased to 3 over several sessions. The unit dose was then increased to 2.5 µg/kg/infusion. Initial training at the lower unit dose was intended to minimize side effects of high fentanyl intake that we have observed in some rats (e.g. pica, paw licking/chewing). After at least 10 sessions at the 2.5 µg/kg unit dose and once FSA stabilized, rats were immunized i.m. with 5 µg CRM, 5 µg F_1-CRM adsorbed on 24 µg alum, or 5 µg F_1-CRM and 10 µg INI-4001 adsorbed on 24 µg alum. Rats were vaccinated every 2 weeks on Fridays after their FSA session to maintain high antibody titers during the remainder of the study. The first 8 weeks (4 vaccinations) was a maintenance phase, during which FSA continued at the 2.5 µg/kg training dose. A blood sample was collected from the tail vein 1-2 weeks after the 4th vaccination to measure antibody titers. The following 6 weeks (3 vaccinations) was a dose-response phase, during which the effects of vaccination on the FSA dose-response curve were determined. During this phase, the fentanyl unit dose was changed weekly on

Mondays (initially increased to 5.0 µg/kg/infusion and then reduced each week to 1.0, 0.75, 0.50. 0.25, and 0 µg/kg/infusion) as rats continued to be vaccinated. Following the dose-response determination, vaccination ceased, and rats were given access to 2.5 µg/kg unit dose to allow reacquisition of FSA.

If a catheter lost patency or was otherwise compromised (e.g. the rat pulled out its catheter), data from that week were excluded from analysis and another catheter was implanted in a femoral vein. The majority of these reimplants occurred during training before vaccination began. If a rat required a reimplant during the FSA maintenance phase of vaccination, rats continued being vaccinated until FSA was reacquired before beginning FSA dose-response phase. This resulted in one additional vaccination (five total) in one CRM control rat, two additional vaccinations (six total) in two F_1-CRM+alum rats, and one additional vaccination (five total) in three F_1-CRM+alum+INI-4001 rats during this phase. If a rat required a reimplant during the fentanyl dose-response phase of vaccination, vaccinations continued until baseline self-administration was recovered at the 2.5 µg/kg unit dose after the reimplant and the dose-response determinations were completed, resulting in one or two additional vaccinations in three CRM control rats, two F_1-CRM+alum rats, and three F_1-CRM+alum+INI-4001 rats. Another F_1-CRM+alum+INI-4001 rat received six additional vaccinations during the dose-response phase because it took several weeks to reacquire FSA before completing the dose-response assessment.

Mini-Pig studies: 9 pigs (n=3/group) were treated as follows: 1) non-vaccinated control group, 2) F_1-CRM (125 µg) formulated in alum (562.5 µg), and 3) F_1-CRM (125 µg) formulated in 4001 (250 µg), and alum (562.5 µg). Active vaccination groups received a total of three immunizations on days 0, 21, and 42, which were administered i.m. in a volume of 0.6 mL. Serum was collected on days 7, 28, and 49 ± 3 days to determine

antibody titers. On Day 49 ± 3 days, each mini-pig was anesthetized with isoflurane delivered in pure oxygen, then orotracheally intubated with a cuffed endotracheal tube and breathed spontaneously under a light plane of isoflurane anesthesia. Intravenous and intra-arterial catheters were placed for drug administration and blood sampling. After instrumentation and stable plane of anesthesia were achieved, mini-pigs were challenged with a continuous IV infusion of fentanyl until they reached the study endpoint which was defined as two continuous minutes of apnea. Fentanyl was infused at a rate of 30 µg/kg/hr for 1 hour (0 – 60 minutes), increasing to 60 µg/kg/hr for the second hour (60 – 120 minutes), and then increasing to 120 µg/kg/hr for the third hour (120 – 180 minutes) for a total possible dose of 210 µg/kg. Various respiratory endpoints (time to apnea, respiratory rate, end-tidal CO_2, tidal volume, and minute volume) were monitored using a Datex Ohmeda Compact S5 monitor (Clearwater, FL). Blood was collected prior to fentanyl infusion (baseline) and at multiple timepoints during fentanyl administration for serum fentanyl analysis. After animals were apneic for two continuous minutes, they were administered naloxone (10 µg/kg, IV) and monitored for respiratory recovery.

Antibody analysis. Opioid-specific IgG and IgG subclass titers were measured via titer ELISA as previously described (94). Briefly, 96-well ELISA plates (Costar 9018 EIA/RIA, Jackson ImmunoResearch Laboratories Inc., West Grove, PA) were coated overnight with 5 ng/well of unconjugated BSA or F_1 hapten conjugated to BSA and blocked the next day. Rat or pig serum was serial diluted in the appropriate wells starting at either a 1:200 or 1:50 dilution. Plates were then incubated with the following secondary antibodies: goat-anti-mouse IgG HRP (1:30,000; Jackson ImmunoResearch, West Grove, PA), goat-anti-mouse IgG_1 (1:35,000; Alpha Diagnostic International, Inc., Cat. No. 40126-GAF-BLK) or goat-anti-mouse IgG_{2a} (1:7500; Alpha Diagnostic International, Cat. No. 40127-GAF-BLK) goat-anti-rat IgG-HRP (1:50,000; Jackson ImmunoResearch, West Grove, PA), mouse

anti-Porcine IgG (1:1000; BD Biosciences, Franklin Lakes, NJ), or mouse anti-Porcine IgG_2 (1:1000; Bio-Rad, Hercules, CA). For pig ELISAs, plates were incubated with a goat anti-mouse IgG Total HRP tertiary antibody (1:1000, Southern Biotech, Birmingham AL).

In vitro binding of fentanyl analogues and off-target drugs was measured using competitive ELISA as previously described (33, 55). Briefly, 96-well ELISA plates (Costar 9018 EIA/RIA, Jackson ImmunoResearch Laboratories Inc., West Grove, PA) were coated with 0.5 ng/well of a different fentanyl based conjugate (F_3-BSA) in carbonate buffer at pH 9.6 overnight. The following day, plates were blocked with 1% gelatin. The appropriate drugs were then serially diluted on the plate with the following ranges: Fentanyl: 1.48 μM-2.79 pM; Carfentanil: 126 μM-238 pM; Alfentanil: 600 μM-1.12 nM; Remifentanil: 664 μM-1.2 nM; Acetylfentanyl: 150 μM-0.15 pM; Sufentanil: 0.9 mM-0.9 pM; Naltrexone: 5 mM-5 pM; Buprenorphine: 50 μM-0.05 pM; Naloxone: 5 mM-5 pM. A fixed dilution of serum (determined by titer ELISA) was added to each well of the plate and incubated for 2 hours. Plates were then incubated overnight with goat-anti-rat IgG-HRP (1:50,000; Jackson ImmunoResearch, West Grove, PA). Plates were developed using SIGMAFAST OPD substrate (Sigma-Aldrich, St. Louis, MO). If antibodies did not bind to drugs within the concentration range tested, results were reported as the highest concentration tested.

LC-MS analysis of fentanyl concentration. Rodent serum, rodent brains, and pig serum were processed and analyzed as previously described (55). For bound/unbound serum analysis, serum samples were centrifuged at RT for 1 hour at 10,000 x g in a Nanosep filter unit (Pall Life Sciences, Port Washington, NY) with a 10 kDa cutoff to separate free drug from antibody-bound fentanyl. Filter units were previously treated with 5% Tween-20 in distilled water for 2 hours at room temperature to minimize hydrophobic interactions and then rinsed with sterile distilled water. Filtrate (free drug) and whole serum samples were

then processed and analyzed on LC-MS as previously described (55). Protein-bound fentanyl was calculated as (total fentanyl - unbound fentanyl) and expressed as a percentage of total fentanyl.

BioLayer interferometry antibody avidity and kinetic assays. Antibody avidity assays were performed on an Octet Red 96e instrument (Fortebio). *In vivo* serum samples (analyte) and biotinylated antigen, F_1-Bio, (ligand) were diluted in 10x Kinetic Buffer (Fortebio). Assays were performed by loading F_1-Bio onto pre-hydrated streptavidin sensors at 0.1ug/ml (loading step 120s) followed by 180s baseline at 30°C with shaking at 1000rpm. Sensors were then moved into analyte for 120s for association, followed by a 600s dissociation step. Serum samples were run at three different dilutions determined by anti-fentanyl total IgG titers. Dissociation rate constants (K_{diss}) were calculated by processing raw data using ForteBio HT analysis software version 11.1.3.50. All data was inspected for quality of fit to the calculated curve (R^2>0.95), response between 0.25-3, and residual value <10% of the maximum response fitted to the curve.

Data Analysis: Statistical analyses were performed using Prism version 9.1.2 (GraphPad, LaJolla, CA). Mean antibody titers, drug concentrations, MPE% on the hotplate, heart rate, oxygen saturation, K_{diss} measurements, total fentanyl dose, and time to apnea were analyzed by one-way ANOVA followed by Tukey's multiple comparisons *post hoc* test. The relationship between opioid-specific antibodies, total fentanyl administration, and time to apnea were analyzed via two-tailed Pearson correlation after determination of normality using D'Agostino-Pearson's test. Latency to respond, heart rate, and oxygen saturation data taken over multiple time points was analyzed via two-way ANOVA with the Geisser-Greenhouse correction and Tukey's multiple comparisons *post hoc* test. Survival curve pairwise comparisons were analyzed via Mantel-Cox test.

For the FSA study, the mean number of infusions during the last three sessions at baseline and two weeks after each of the first four vaccine injections was used to assess vaccine effects on maintenance of FSA. To assess vaccine effects on the FSA dose-response curve, the mean number of infusions during the last three sessions at each unit dose was used. The data were analyzed using mixed-model or one-way ANOVA followed by Holm-Sidak multiple comparison tests. To specifically assess the effects of vaccination on fentanyl's reinforcing efficacy (i.e., motivation to consume fentanyl), exponential demand curve analysis was performed on fentanyl intake in each subject during FSA unit dose assessment as previously described (77, 197). The mean of the α (elasticity of demand), Q_0 (intensity of demand), P_{max} (unit price at maximal responding), and O_{max} (maximal level of responding) parameters of the exponential curve fits to individual subject data were compared between groups via Brown-Forsythe ANOVA followed by Dunnett's T3 tests for multiple comparisons. The α, Q_0, and O_{max} values were log transformed prior to analysis due to nonnormality of the data. Mean antibody titers were similarly compared between groups. All statistics were performed using Prism (version 9.1; GraphPad, San Diego, CA).

RESULTS

Activation of TLR7/8, but not TLR4, increases the efficacy of F_1-CRM against fentanyl in mice. *(Note: these data are featured in Miller et al 2022)* To determine whether an agonist of TLR4 (INI-2002) or TLR7/8 (INI-4001) increased fentanyl-specific antibody responses, mice were vaccinated with CRM carrier protein, F_1-CRM, F_1-CRM+alum, F_1-CRM+alum+INI-2002, F_1-CRM+alum+INI-4001, or F_1-CRM in combination with all three adjuvants at doses noted in **Figure 1**. Blood was collected prior to challenge and F_1-specific IgG titers and IgG_{2a}:IgG_1 ratio were measured in serum (**Figure 1A, B**). There was a significant increase in titers and IgG_{2a} subclass switching with the addition of INI-4001, but not with INI-2002. Mice were then challenged with 0.05 mg/kg fentanyl, and reductions in bradycardia (**Figure 1C**) and antinociception (**Figure 1D**) were measured 30 minutes post-challenge as indicators of response to fentanyl. Additionally, serum (**Figure 1E**) and brain (**Figure 1F**) were collected after 30 minutes to measure concentrations of fentanyl to determine the ability of vaccine-induced antibodies to prevent fentanyl from crossing the blood-brain barrier. After three vaccinations, all groups, including F_1-CRM alone, demonstrated significantly reduced fentanyl-induced antinociception (**Figure 1C**) and bradycardia (**Figure 1D**) compared to CRM vaccinated mice. The addition of INI-4001 to F_1-CRM+alum further reduced bradycardia compared to F_1-CRM alone, as did the triple adjuvant combination. These data demonstrate that while three vaccinations with 5 µg F_1-CRM alone is sufficient to protect against fentanyl-induced antinociception, the addition of alum+INI-4001 further increases protection against bradycardia. In addition, the TLR4 adjuvant, INI-2002, did not reduce bradycardia in comparison to F_1-CRM or F_1-CRM+alum, consistent with the lower F_1-specific IgG titers (**Figure 1A**). Finally, pharmacokinetic analysis shows that mice treated with F_1-CRM+alum+INI-4001 or with the triple adjuvant combination displayed a significant increase in serum fentanyl

concentrations (**Figure 1D**), with an associated significant decrease in brain fentanyl concentrations (**Figure 1E**) when compared to F_1-CRM only. The addition of INI-2002 to alum+INI-4001 did not further increase serum fentanyl or decrease brain fentanyl, suggesting that the protective effect arose from the use of alum+INI-4001 as a combination adjuvant with F_1-CRM (**Figure 1D, E**). Overall, these data demonstrate that adjuvanting F_1-CRM with alum+INI-4001 (TLR7/8 agonist) significantly increased the efficacy of F_1-CRM to protect against fentanyl challenge, while the addition of INI-2002 (TLR4 agonist) did not confer any further protective effects.

Activation of TLR7/8, but not TLR4, increases the efficacy of F_1-CRM against fentanyl in rats. We showed that INI-4001 (TLR7/8 agonist), but not INI-2002 (TLR4 agonist), was effective at increasing fentanyl-specific antibody titers and increasing vaccine efficacy against fentanyl challenge in mice. To determine whether this effect was consistent between species, we immunized rats on days 0, 21, and 42 with F_1-CRM alone, F_1-CRM adsorbed on different doses of alum, F_1-CRM and INI-2002 adsorbed on alum, F_1-CRM and INI-4001 adsorbed on alum, or F_1-CRM with a combination of all three adjuvants. Analysis of fentanyl-specific serum IgG titers showed that groups given INI-4001 containing vaccines had significantly higher antibody titers than groups immunized with F_1-CRM and alum alone and had trending higher antibody titers compared to groups immunized with F_1-CRM+alum+INI-2002 (**Figure 2A**). Notably, the group immunized with all three adjuvants did not have increased titers compared to F_1-CRM+alum+INI-4001, indicating that TLR7/8 agonist activity was driving the increased antibody response. After immunization, rats were challenged with 0.05 mg/kg fentanyl. Latency to respond on a hot plate (**Figure 2D**), heart rate (**Figure 2E**) and oxygen saturation (**Figure 2F**) were measured at baseline, 15 minutes, and 30 minutes after drug challenge. All actively immunized groups had significantly decreased antinociception, bradycardia, and

respiratory depression compared to the CRM immunized control in all parameters tested at 15 minutes, and antinociception and bradycardia were significantly decreased compared to control at 30 minutes. After the final measurement was taken, rats were euthanized and blood and brain were collected for analysis of opioid concentration by LC-MS. Groups adjuvanted with INI-4001 had significantly increased serum fentanyl concentration compared to the control, F_1-CRM alone or F_1-CRM with 9 μg alum, and trending increases in serum fentanyl compared to F_1-CRM+24 μg alum or F_1-CRM+alum+INI-2002 (**Figure 2B**). Again, groups given all three adjuvants did not have significantly different serum fentanyl concentration compared to the F_1-CRM+alum+INI-4001 group, suggesting that INI-4001 is responsible for the increase in efficacy. Similar trends were found in brain fentanyl concentration (**Figure 2C**), where groups adjuvanted with INI-4001 had decreased brain fentanyl concentration compared to all other groups, however this was only significant compared to the CRM control and F_1-CRM alone. Overall, this suggests that INI-4001, but not INI-2002, increases the efficacy of a lead fentanyl vaccine in rats.

Fentanyl vaccines adjuvanted with TLR7/8 agonist showed increased protection against fatal levels of respiratory depression after fentanyl challenge. Since INI-4001, but not INI-2002, increased efficacy of a lead fentanyl vaccine, a follow-up experiment was performed where rats were immunized CRM control, F_1-CRM alone, F_1-CRM adsorbed on alum, or F_1-CRM with INI-4001 adsorbed on alum. After three immunizations, rats immunized with the INI-4001 adjuvanted vaccine had significantly higher fentanyl-specific antibody titers compared to all other groups, as expected (**Figure 3A**). Rats were then challenged with repeating doses of 0.05 mg/kg fentanyl every 15 minutes, up to 0.45 mg/kg cumulative dose. The rats' oxygen saturation was monitored via pulse oximetry 15 minutes after each dose before immediately receiving the next dose.

As prolonged periods of 50% oxygen saturation would likely be considered fatal in a human (198), any rat whose oxygen saturation dropped below 50% was given naloxone and removed from the rest of the study. When assessing the number of rats that fell below 50% oxygen saturation using a Kaplan-Meier survival curve, rats immunized with F_1-CRM+alum+INI-4001 had significantly increased survival from fatal levels of respiratory depression when compared to CRM or F_1-CRM alone (**Figure 3B**) and trended towards increased survival compared to F_1-CRM+alum ($p=0.0813$). Notably, the group receiving the INI-4001 adjuvanted vaccine was the only group where none of the rats reached 50% oxygen saturation. When analyzing the change in oxygen saturation as a percent maximum possible response (baseline = 0% response and 50% oxygen saturation =100% response), the group receiving INI-4001 displayed a midpoint value that was shifted 9.3x, 6.9x, and 2.9x compared to CRM control, F_1-CRM alone, and F_1-CRM+alum, respectively (**Figure 3C**). The following week, the same rats were challenged with 0.1 mg/kg fentanyl, and antinociceptive response (**Figure 3D**), heart rate (**Figure 3E**), and oxygen saturation (**Figure 3F**) were measured after drug challenge. Rats receiving INI-4001 adjuvanted vaccine had significantly decreased antinociceptive response, bradycardia, and respiratory depression compared to CRM control and F_1-CRM alone, and trending differences when compared to F_1-CRM+alum. Immediately after the last measurement, rats were euthanized and blood and brain were collected to measure fentanyl concentration. Rats immunized with F_1-CRM+alum+INI-4001 had significantly increased serum fentanyl concentration (**Figure 3G**) and significantly decreased brain fentanyl concentration when compared to all other groups (**Figure 3H**). Together, these data indicate that the F_1-CRM+INI-4001+alum vaccine formulation produces a rightward shift in fentanyl's dose-response curve, increasing protection from respiratory depression, bradycardia, and potential lethality from high doses of fentanyl.

INI-4001 does not change IgG antibody specificity of a lead fentanyl vaccine. One hypothesis regarding how adjuvants increase vaccine efficacy is that they can broaden the resultant vaccine-induced antibody diversity, expanding epitope recognition to protein antigens. To test whether this hypothesis also applied to INI-4001 adjuvanted vaccines against small molecule targets such as fentanyl, rats were immunized with F_1-CRM+alum or F_1-CRM+alum+INI-4001 to determine whether addition of INI-4001 would increase epitope diversity within the F_1-specific antibody and B cell repertoire that could either 1) expand cross-reactivity to additional fentanyl analogues or 2) increase cross-reactivity with off target molecules such as naloxone, naltrexone, or methadone. Rats were first challenged with fentanyl *in vivo* after antibody titers were assessed via ELISA to ensure the adjuvant was effective at increasing anti-fentanyl vaccine efficacy (data not shown). Afterward, rats were challenged with carfentanil followed by naloxone reversal (**Figure 4A-C**), sufentanil (**Figure 4D-F**), or methadone (**Figure 3G-I**) on consecutive weeks. Antinociceptive response, oxygen saturation, and heart rate were monitored every 15 minutes for an hour after drug challenge. The addition of INI-4001 did not change the *in vivo* efficacy of F_1-CRM to any of the drugs tested, and notably did not interfere with naloxone reversal of carfentanil-induced respiratory depression. Serum samples were also tested for *in vitro* cross-reactivity to various fentanyl analogues, off-target medications, and endogenous opioids (**Table 1**). While the specificity of the antibodies for fentanyl is high in both groups (IC_{50}<15 nM), the addition of INI-4001 did not significantly change the affinity of the antibodies for any of the drugs tested. These data suggest that addition of INI-4001 to an anti-fentanyl vaccine does not significantly change fentanyl epitope diversity and antibody binding which would lead to interference with other medications used to treat pain or OUD.

Fentanyl vaccine adjuvanted with INI-4001 and alum attenuates the reinforcing effects of fentanyl to a greater degree than vaccine with alum alone in intravenous self-administration models. Previous studies reported that vaccines are effective in attenuating the reinforcing properties of fentanyl in operant self-administration models involving lever pressing in rats and non-human primates (55, 67, 78). Here, we investigated whether addition of INI-4001 to the lead F_1-CRM vaccine increased its efficacy in attenuating fentanyl's reinforcing effects in rats. Using a fentanyl self-administration (FSA) model, the mean number of infusions was assessed in rats self-administering fentanyl (2.5 µg/kg/infusion, i.v.) under a fixed ratio (FR) 3 schedule at two weeks following each vaccination during the initial course of 4 vaccine injections. Data were analyzed as absolute values (**Figure 5A**) and as a percentage of baseline (**Figure 5B**) to better represent the within-subject effects of vaccination. During this phase, there was a main effect of injection number ($F = 27.85$, $p < 0.0001$) and an injection number x vaccine group interaction ($F = 6.73$, $p < 0.0001$), but no effect of vaccine group on absolute number of infusions. Multiple comparisons indicated that only the F_1-CRM+alum+INI-4001 group showed a significant increase in absolute infusions after the fourth injection ($t = 3.01$, $p < 0.05$; panel A), and the increase in this group approached significance after the third injection ($t = 2.35$, $p = 0.08$). There was a significant main effect of injection number ($F = 25.0$, $p < 0.0001$), group ($F = 14.15$, $p < 0.001$), and an injection number x group interaction ($F = 6.03$, $p < 0.001$) on the number of infusions as a percentage of baseline. Both vaccine groups, but not the control group, exhibited a significant percent increase in mean infusions over the initial course of four injections, but this increase was significantly greater in F_1-CRM+alum+INI-4001 group than F_1-CRM+alum group after the third injection ($t = 2.08$, $p < 0.05$; panel B) and approached significance after the fourth injection ($t = 1.97$, $p = 0.06$).

The mean number of self-administered fentanyl infusions was then assessed across a range of unit doses, with each dose available for five sessions. Data were examined as absolute values (**Figure 6A**) and a percentage of baseline (**Figure 6B**). The baseline for calculating data in **Figure 6B** is the self-administration rate at the 2.5 µg/kg fentanyl unit dose prior to vaccination. There was a main effect of vaccine group ($F = 6.07$, $p < 0.01$) and fentanyl dose ($F = 26.63$, $p < 0.0001$), and a significant vaccine group × fentanyl dose interaction ($F = 9.54$, $p < 0.0001$) on absolute mean infusions. There was also a main effect of vaccine group ($F = 4.21$, $p < 0.05$) and fentanyl dose ($F = 28.58$, $p < 0.0001$), and a significant vaccine group × fentanyl dose interaction ($F = 9.78$, $p < 0.0001$) on the percent change in mean infusions. Overall, the FSA dose-response curve was shifted to the right in the vaccinated groups compared to controls, as indicated by higher infusion rates at the highest fentanyl doses and lower infusion rates at low fentanyl doses. However, this shift was much more apparent in the F_1-CRM+alum+INI-4001 group than the F_1-CRM+alum group. FSA was significantly decreased compared to controls in the F_1-CRM+alum+INI-4001 group at all doses below 1.0 µg/kg, whereas a decrease was only apparent at the lowest fentanyl dose in the F_1-CRM+alum group. In addition, although FSA was increased at the two highest fentanyl doses in both vaccinated groups, the increase was greater in F_1-CRM+alum+INI-4001 rats than F_1-CRM+alum rats at the 2.5 µg/kg dose (**Figure 6B**), consistent with the greater increase in FSA in this group during the initial course of vaccination (**Figure 5**).

To directly examine the effect of vaccination on the reinforcing efficacy of fentanyl, behavioral economic demand curves were compared between groups (**Figure 7A**). In this analysis, an exponential curve is fit to the data to describe the relationship between fentanyl consumption and unit price (FR / unit dose). This yields several parameters of demand (Table 2), including the rate of decline in consumption as unit price increases (i.e.

elasticity of demand (α)), where a faster decline (greater elasticity, higher α) indicates lower reinforcing efficacy; the estimated level of consumption at zero price (i.e. intensity of demand (Q_0)); the unit price at which consumption changed from relatively inelastic to relatively elastic (P_{max}, lower values indicate lower reinforcing efficacy); and the maximum level of responding for fentanyl (O_{max}, lower values indicate lower reinforcing efficacy). The change in fentanyl consumption in each group with increases in unit price was well described by the exponential demand function (mean r^2 did not differ between groups). Overall, F_1-CRM+alum+INI-4001 reduced the reinforcing efficacy of fentanyl to a greater degree than F_1-CRM+alum. Elasticity of demand (α) was significantly higher (i.e. reinforcing efficacy was lower) than CRM in the F_1-CRM+alum+INI-4001 group ($t = 2.45$, $p < 0.05$), but not the F_1-CRM+alum group. Consistent with the vaccine effects on maintenance of FSA (**Figure 5**), intensity of demand (Q_0), was significantly higher compared to CRM in both the F_1-CRM+alum group ($t = 3.51$, $p <0.01$) and F_1-CRM+alum+INI-4001 ($t = 4.51$, $p < 0.001$) groups, but the vaccines did not differ from each other. P_{max}, was significantly lower than controls in both F_1-CRM+alum ($t = 4.10$, $p < 0.01$) and F_1-CRM+alum+INI-4001 rats ($t = 6.48$, $p < 0.001$), but this effect was greater in F_1-CRM+alum+INI-4001 rats ($t = 2.93$, $p < 0.05$). O_{max} was significantly lower than CRM in the F_1-CRM+alum+INI-4001 group ($t = 2.61$, $p < 0.05$), but not the F_1-CRM+alum group.

Differences in FSA measures between groups were consistent with differences in mean fentanyl-specific antibody titers between groups measured following the 4th immunization (**Figure 7B**). Titers were significantly higher than control in F_1-CRM+alum and F_1-CRM+alum+INI-4001 rats ($t = 4.00$, $p < 0.01$ and $t= 12.52$, $p < 0.0001$, respectively), and titers in the F_1-CRM+alum+INI-4001 rats were significantly higher than those in F_1-CRM+alum rats ($t = 3.94$, $p < 0.01$).

INI-4001 increases anti-fentanyl vaccine efficacy in a porcine model of fentanyl overdose. While rodent models are more common and convenient for vaccination and drug challenge studies, both mice and rats have differentially functioning TLR8 signaling compared to humans (191, 199), making it necessary to test this lead fentanyl vaccine formulation in a model that more closely simulates the human immune system. The immune system of Hanford mini-pigs is 80% similar to humans (compared to 10% similarity between humans and rodents) (200), and their immune cells express both TLR7 and TLR8 which have a similar function as in humans (191, 200). Therefore, we developed a porcine model of vaccination and opioid-induced respiratory depression to test the effects of INI-4001 on anti-fentanyl vaccination. In a pilot study, pigs were immunized with F_1-CRM adsorbed on alum or F_1-CRM and INI-4001 adsorbed on alum on days 0, 21, and 42. Serum was collected 7 days after each vaccination for titer determination. On day 49, pigs receiving INI-4001 adjuvanted vaccine had trending higher titers of total fentanyl-specific IgG (**Figure 8A,** p=0.1145 compared to control, p=0.2318 compared to F_1-CRM+alum) and fentanyl-specific IgG_2 (**Figure 8B,** p=0.1512 compared to control, p=0.1873 compared to F_1-CRM+alum)—an antibody subclass that may be similar to IgG_{2a} in rodents (201, 202). After immunization, pigs were anesthetized with isoflurane and challenged with a continuous IV infusion of fentanyl until two minutes of continuous apnea was reached. Serum samples were collected at multiple timepoints to measure fentanyl pharmacokinetics. Total fentanyl dose (**Figure 8C**), time to apnea (**Figure 8D**), and serum fentanyl concentration at time of apnea (**Figure 8E**) were measured as parameters for vaccine efficacy. Groups immunized with F_1-CRM+alum+INI-4001 had trended towards a higher tolerated fentanyl dose (p=0.0590 compared to control, p=0.2107 compared to F_1-CRM+alum), time to apnea (p=0.0620 compared to control, p=0.2757 compared to F_1-CRM+alum), and serum fentanyl concentrations (p=0.1250 compared to control, p=0.2555

compared to F_1-CRM+alum), indicating that INI-4001 may be effective at increasing efficacy of the fentanyl vaccine. Serum collected at time the of apnea (or at the final challenge timepoint, if the pig never became apneic) was also analyzed for the ratio of protein-bound fentanyl compared to free fentanyl (**Figure 8F**). The mean protein-bound serum fentanyl was 67.2% in naïve pigs at time of apnea, which is generally consistent with literature describing fentanyl plasma protein binding in humans (203). Conversely, the F_1-CRM+alum and F_1-CRM+alum+INI-4001 groups had 97.6% and 99.2% protein-bound fentanyl, respectively, indicating that the increase in serum fentanyl seen after challenge represents almost entirely antibody-bound drug (compared to control, p=0.0364 for F_1-CRM+alum, p=0.0297 for F_1-CRM+alum+INI-4001).

The serum fentanyl-specific total IgG and IgG_2 antibodies were further analyzed by plotting them against parameters of vaccine efficacy. Higher titers of both total IgG and IgG_2 were significantly associated with greater vaccine efficacy, including a longer time to apnea and greater total fentanyl administration (**Figure 9A-D**). Additionally, the avidity of these antibodies was measured via biolayer interferometry at each time point after vaccination. The addition of INI-4001 increased early antibody avidity compared to F_1-CRM+alum, but the K_{diss} between groups was similar at both day 28 and day 49 (**Figure 9E**). Overall, these data suggest that mini-pigs can be used as a model for fentanyl-induced respiratory depression and anti-opioid vaccination, and that INI-4001 may increase the efficacy of a lead anti-fentanyl vaccine in this model.

INI-4001 increases the efficacy of conjugate vaccines with different haptens and carrier proteins. *(Note: These data are an addendum in that they were not included in the original manuscript, but belong within the context of this specific line of investigation).* We have shown that the TLR7/8 agonist INI-4001 increased the production of opioid-

specific antibody titers after fentanyl administration in mice, rats, and Hanford miniature pigs. This increase in antibody titers leads to a decrease in the pharmacological effects of fentanyl, including respiratory depression, bradycardia, apnea, and it's reinforcing properties. To extend these findings to additional conjugate vaccine formulations containing differing haptens and carrier proteins, INI-4001 was administered with a lead heroin vaccine formulation (M-sKLH+alum) in rats. The addition of INI-4001 significantly increased opioid-specific antibody titers (**Figure 10A**), which led to a ~2x shift in the heroin-induced antinociception dose-response curve after drug challenge (**Figure 10B**). Additionally, groups adjuvanted with INI-4001 had significantly increased serum:brain opioid concentration compared to the vaccine alone (**Figure 10C**). These data support the use of INI-4001 as a broadly effective adjuvant for OUD vaccines with structurally different haptens and conjugated to different carrier proteins.

DISCUSSION

Active immunization with vaccines targeting fentanyl and its analogs is a potentially safe, long-lasting, and prophylactic treatment to combat OUD and overdose in addition to the existing treatment repertoire. While anti-opioid vaccines have shown significant preclinical efficacy at reducing drug self-administration and preventing symptoms associated with fatal opioid overdose such as bradycardia and respiratory depression (27, 30, 32-34, 38, 39, 41, 42, 54, 55, 65, 67, 183), clinical evaluation of these vaccines has only recently been initiated with one Phase Ia/Ib clinical trial currently being conducted (NCT04458545). Lessons learned from clinical trials of other anti-drug conjugate vaccines reveal that high concentrations of high affinity antibodies are needed to achieve significant efficacy (83, 84). As such, efforts have focused on increasing the immune response to opioid-specific vaccines through optimization of conjugation chemistry, linker length, hapten design, formulation with adjuvant, delivery platforms, immunization schedule, and

identification of biomarkers associated with better antibody responses (27, 31, 34, 39, 42, 73, 94, 97, 133, 145, 146, 160, 161, 163, 204-206).

Aluminum hydroxide (alum) is the most widely used adjuvant in FDA-approved vaccines (98, 184). While it has been used for decades to improve immune responses to many vaccines (98), it's exact mechanism of action is unclear (184). Alum has been used in most studies involving anti-opioid vaccines (142) due to the ease of translation into clinical settings because of its known safety and efficacy profile; however, alum drives a Th_2 skewed response and elicits the production of IgG_1 antibodies in mice (184). Published literature suggests that optimal anti-opioid immune response in mice may consist of a balanced Th_1/Th_2 response and production of both IgG_1 and IgG_{2a} antibodies (94, 160). While alternative adjuvants have been tested with anti-opioid vaccines (31, 37, 39, 42, 73, 94, 97, 99, 155, 160), many of these adjuvants are not well tolerated, exhibited minimal efficacy, or have limited availability due to cost or patent considerations. Therefore, we initially tested the addition of novel synthetic TLR4 (INI-2002) and TLR7/8 (INI-4001) adjuvants adsorbed on alum to produce a safe and balanced Th_1/Th_2 response with the goal of increasing vaccine immunogenicity and efficacy. We found that the TLR7/8 agonist increased total IgG and IgG_{2a} subclass titers, which led to increased vaccine efficacy after fentanyl challenge in mice. Additionally, we found that there was a significant antigen dose sparing effect, with antigen dose being reduced over 10x compared to previous formulations containing alum alone. To extend these findings, we then tested the same adjuvanted vaccines in rats and found that vaccines adjuvanted with INI-4001 (TLR7/8 agonist), but not INI-2002 (TLR4 agonist), significantly increased rat serum IgG titers, which increased serum fentanyl concentration and decreased brain fentanyl concentration after drug challenge. This is consistent with our previous studies indicating that TLR4

agonists, such as MPLA, do not improve efficacy of oxycodone conjugate vaccines when used as vaccine adjuvants (31).

Moving forward with INI-4001 as our lead fentanyl vaccine adjuvant, we further tested its ability to protect against high dose fentanyl challenges simulating overdose situations by assessing resistance to fatal levels of respiratory depression and determining dose-response curves after repeated doses of fentanyl. The absolute EC_{50} values determined from the dose-response curves would likely be inaccurate since the study was performed using a cumulative dosing paradigm. Since doses were scheduled every 15 minutes, free fentanyl was being actively metabolized throughout the duration of the study, leading to the reported cumulative dose likely being higher than the active physiological dose. Nonetheless, comparing the magnitude of shift in the midpoint of the dose-response curve between groups is informative. We found that the addition of INI-4001 to F_1-CRM+alum shifted fentanyl's dose-response curve almost 3-fold compared to formulations containing alum alone and elicited greater protection against respiratory depression after drug challenge.

The increase in antibody titers and protection against fentanyl found when animals were immunized with INI-4001 adjuvanted F_1-CRM does not appear to be at the expense of specificity towards the target drug, as the present study found that there were no significant changes in cross-reactivity between F_1-CRM formulations containing INI-4001 adsorbed on alum or with just alum alone. Some cross-protection against additional fentanyl analogues has been previously reported (55), and the current study suggests that this cross-protection will not be affected by the inclusion of INI-4001 as a vaccine adjuvant. Importantly, we also found that there was negligible cross-reactivity to medications for OUD management such as methadone, buprenorphine, and naltrexone, medications for

overdose reversal such as naloxone, or endogenous opioids such as β-endorphin or endomorphin-1. This is critical for future translation of fentanyl vaccines into clinical settings, as these vaccines will likely be utilized in tandem with other OUD or overdose medications.

In the FSA study, fentanyl intake increased in F_1-CRM+alum and F_1-CRM+alum+INI-4001 vaccinated rats during maintenance at the 2.5 µg/kg dose relative to pre-vaccination intake and at the 5.0 µg/kg dose during the fentanyl dose-response determination. In contrast, intake was decreased at lower unit doses during the dose-response determination, and the reduction was greater in F_1-CRM+alum+INI-4001 compared to F_1-CRM+alum vaccinated rats. This rightward shift in the unit dose-response curve indicates that the F_1-CRM immunogen reduced the potency of fentanyl (i.e. effectively lowering the fentanyl dose), and that addition of the TLR7/8 agonist INI-4001 significantly enhanced this effect. We have reported similar shifts in potency produced by analogous oxycodone and heroin vaccines in oxycodone and heroin self-administration models (32, 77), and others have shown a similar reduction in potency in fentanyl self-administration models (56, 78). In addition, behavioral economic demand analysis showed F_1-CRM+alum+INI-4001 was more effective at increasing elasticity of demand (i.e., increasing α and decreasing P_{max}) and decreasing maximal responding for fentanyl, indicating a greater decrease in the reinforcing efficacy of fentanyl and rats' motivation to consume it. However, it is important to note that our demand curve analysis involved manipulation of the unit price by changing the unit dose rather than the more conventional approach of changing the FR (response cost). It is possible that demand curve parameters and vaccine effects under changing FR requirements may differ somewhat from the present study. Our approach nonetheless provides a valid and precise method for comparing fentanyl consumption between groups. To our knowledge, this is the first direct

demonstration of a TLR agonist adjuvant enhancing the efficacy of any drug abuse vaccine in attenuating the reinforcing effects of a drug. These data suggest that F_1-CRM+alum+INI-4001 may be effective at facilitating abstinence from fentanyl in humans by blocking its reinforcing effects. They also suggest that adjuvants targeting TLR 7/8 receptors enhance this effect, which may generalize to vaccines against other drugs of abuse.

The increase in fentanyl intake observed at higher unit doses in vaccinated rats has important clinical implications. The FSA maintenance model in the present study was intended to model vaccination in early clinical trials, where participants may be users of fentanyl who continue using the drug while they are being vaccinated. As such, the increase in FSA during vaccination in the present study suggests that a compensatory increase in fentanyl use might also occur in humans during immunization. It has been shown that precipitating withdrawal with an opioid antagonist can motivate increases in opioid self-administration in rats (207). Indeed, withdrawal has long been thought to play a key role in motivating drug use in humans (208-210). This raises the question of whether the increase in FSA observed in the present study was precipitated by a vaccine-induced withdrawal state. To the extent that it was, this would suggest that adjunct treatments (e.g. methadone, buprenorphine) might be needed to minimize this potential side effect of vaccination and avoid treatment noncompliance in clinical trials (i.e. not showing up for vaccinations). However, the gradual rise in antibody levels during vaccination differs from the relatively rapid blockade of opioid receptors by an opioid antagonist and may therefore be too slow to precipitate withdrawal. Accordingly, precipitated withdrawal has not been reported in preclinical studies with other drug abuse vaccines or anti-drug monoclonal antibodies (211, 212). Moreover, the level of access to fentanyl (only 2 hrs/day, 5 days/week) may not have been sufficient to induce dependence on fentanyl (207).

Nonetheless, research is needed to further assess the extent to which opioid vaccines might precipitate withdrawal.

Potentially clinically relevant differences in TLR7/8 expression and functionality have been described between rodents and humans. TLR8 is expressed and functional in human monocytes and conventional dendritic cells (cDCs) with little to no expression in plasmacytoid dendritic cells (pDCs) and B cells (190, 191, 213). TLR7 is expressed by pDCs and B cells in humans, and in contrast by pDCs, B cells, monocytes, and cDCs in mice (214, 215). While both mouse and human TLR7 respond to the same structures and compounds, compounds specific to human TLR8 instead activate mouse TLR7. While mouse TLR8 was initially thought to be non-functional, more recent studies show that it responds to different structures and compounds compared to human TLR8 (190-192, 213, 216). Pigs have been used as an alternative species for the evaluation of TLR7/8 ligands based on literature reports demonstrating more human-like responsiveness to TLR7 and TLR8 ligands (192). Thus, the lead vaccine formulation containing INI-4001 was tested in Hanford mini-pigs, which provided a relevant animal model to recapitulate human TLR7/8 vaccine efficacy and tolerability. To demonstrate vaccine efficacy in this species, we developed a model of respiratory depression after fentanyl challenge. While there have been reports of porcine models of pharmacokinetics of opioids such as morphine (217), and models of brain tissue hypoxia after opioid overdose (218), to our knowledge this is the first report of a porcine model of fentanyl induced respiratory depression and overdose after anti-fentanyl vaccination. After immunization of Hanford minipigs with F_1-CRM adsorbed on alum or F_1-CRM and INI-4001 adsorbed on alum, we saw trending increases in total IgG and IgG_2 subclass titers. No vaccine related adverse events or injection site reactogenicity was noted in any vaccinated pigs. Furthermore, we found that pigs immunized with INI-4001 adjuvanted F_1-CRM tolerated a higher fentanyl dose and were

more resistant to becoming apneic compared to naïve or F_1-CRM+alum vaccinated pigs. Indeed, two out of three pigs immunized with the INI-4001 adjuvanted vaccine did not become apneic even at the highest fentanyl dose. Similarly, we found that there was a trend toward higher levels of serum fentanyl at the time of apnea, of which almost all is protein bound, suggesting that more fentanyl was retained in the serum and not crossing through the blood brain barrier. Although these parameters did not show significant changes, this pilot study had a small sample size (n=3/group) and future studies will investigate this model with larger sample sizes to confirm the efficacy and safety of our lead F_1-CRM+alum+INI-4001 vaccine in this species.

Finally, despite a small sample size, we still found significant correlations between opioid-specific antibodies and parameters of vaccine efficacy in the porcine model. We also found that there was no difference in avidity of these antibodies between groups, except at the earliest time point. This suggests that efficacy in prevention of fentanyl-induced overdose is primarily dependent on high antibody titers, which is consistent with previous literature in mice, rats, and human clinical trials of other conjugate vaccines (27, 41, 83, 84, 99, 133, 160). Additionally, there was a significant early increase in avidity in INI-4001 adjuvanted groups despite almost indetectable titers of serum IgG at the same time point (data not shown). This suggests that there may be a more robust early IgM response after INI-4001 administration, which may lead to earlier onset of protection after vaccination compared to a vaccine adjuvanted with alum alone. Studies investigating vaccine efficacy over multiple early timepoints will be of interest for future clinical evaluation to determine onset of efficacy in human patients.

Overall, as clinical testing of anti-opioid vaccines begins, it is imperative that vaccines are optimized for safety and produce high anti-opioid antibody titers to ensure

clinical efficacy. The addition of the novel synthetic TLR7/8 agonist INI-4001 to our lead anti-fentanyl vaccine significantly increased antigen-specific antibody titers, which led to increases in vaccine efficacy after drug challenge in multiple animal species, drug doses, and administration paradigms. This supports the translation of INI-4001 as an adjuvant for clinical studies of F_1-CRM, other anti-opioid conjugate vaccines, and potentially vaccines directed against other drug targets.

FIGURES

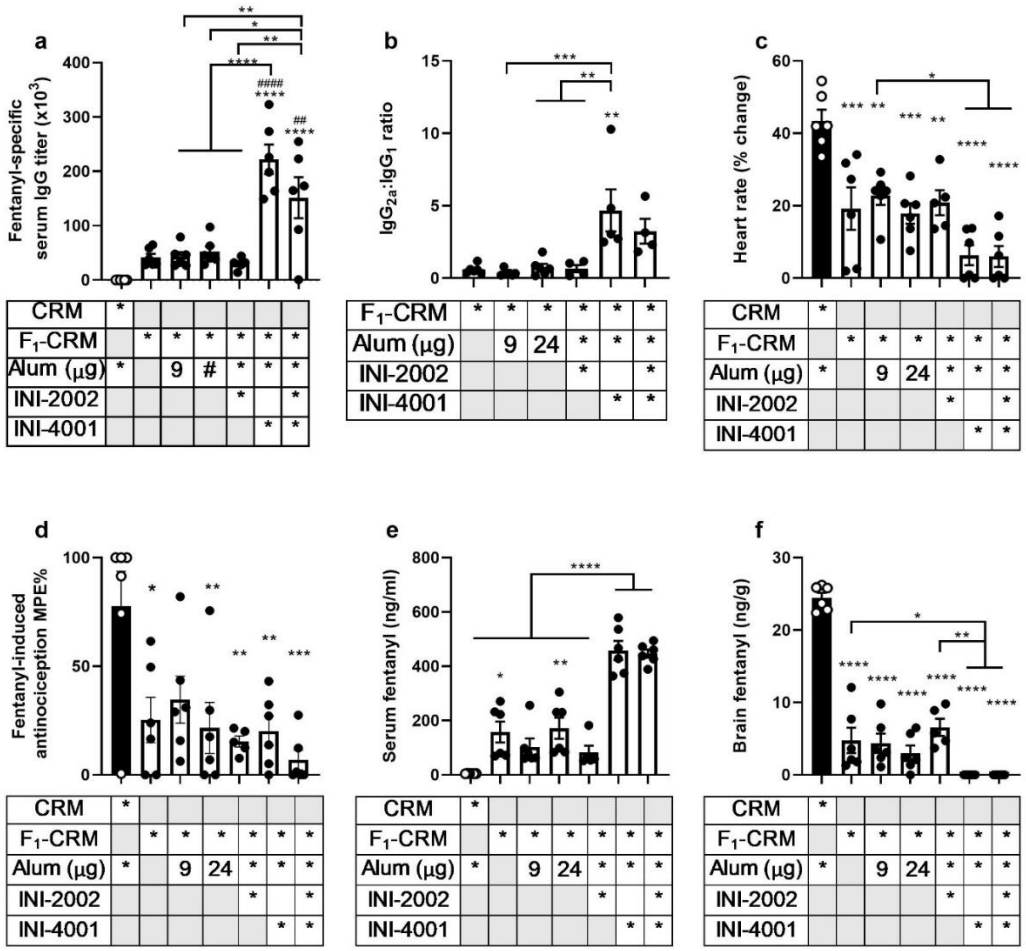

Figure 1. A novel TLR7/8 agonist, but not TLR4 agonist, increases efficacy of an anti-fentanyl vaccine in mice. Mice (n=6/group) were immunized on day 0, 14, and 28. Blood was collected on day 34 for titer measurements. On day 35, mice were challenged with fentanyl (0.05 mg/kg) and parameters of vaccine efficacy were measured at 30 minutes. Immediately after, blood and brain were collected to measure fentanyl concentration. Fentanyl-specific A) IgG titers and B) IgG_{2a}:IgG_1 ratio on day 34. C) Heart rate expressed as % change from baseline at 30 minutes post challenge. D) Antinociception measured as a % maximum possible effect (MPE%) on a hot plate. E)

Serum fentanyl concentration and F) brain fentanyl concentration after drug challenge. Data are mean±SEM. Statistical analysis run via one-way ANOVA with Tukey's multiple comparisons *post hoc* test. * directly over columns indicate significance compared to the control or as indicated by brackets. # directly over columns indicate significance to F_1-CRM alone. Statistical symbols: * P<0.05, ** or ## P<0.01, *** P<0.001, **** or #### P<0.0001.

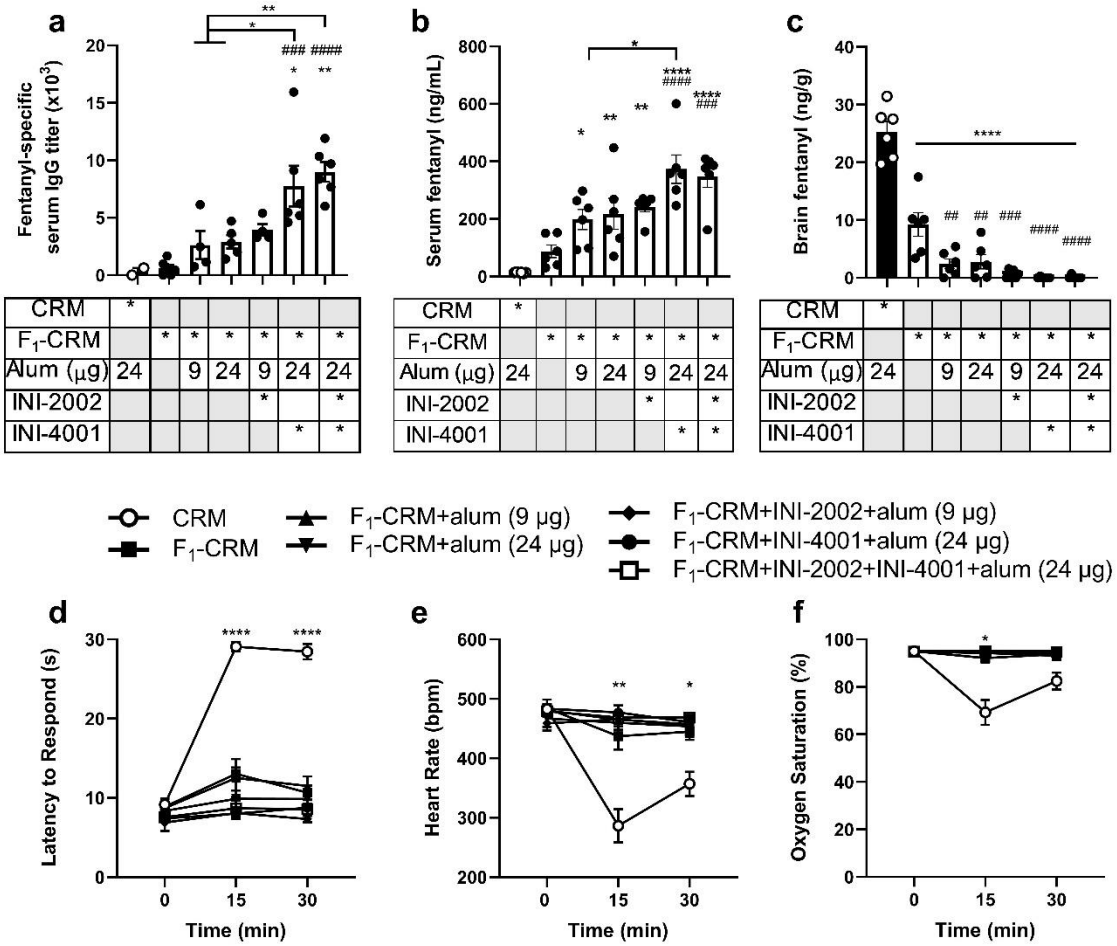

Figure 2: A novel TLR7/8 agonist, but not TLR4 agonist, increases efficacy of an anti-fentanyl vaccine in rats. Rats (n=6/group) were immunized on day 0, 21, and 42. Blood was collected on day 49 for titer measurements. On day 56, rats were challenged with fentanyl (0.05 mg/kg) and parameters of vaccine efficacy were measured at 15 and 30 minutes. Following final measurement, blood and brain were collected to measure fentanyl concentration. A) Fentanyl-specific antibody titers on day 49. B) Serum fentanyl concentration and C) brain fentanyl concentration after drug challenge. D) Latency to respond, E) heart rate, and F) oxygen saturation measured at two time points after drug challenge. Data are mean±SEM. Statistical analysis run via one-way (A-C) or two-way (D-

F) ANOVA with Tukey's multiple comparisons *post hoc* test. * directly over columns indicate significance compared to the control, or as indicated by brackets. # directly over columns indicate significance to F_1-CRM alone. Statistical symbols: * P<0.05, ** or ## P<0.01, ### P<0.001, **** or #### P<0.0001.

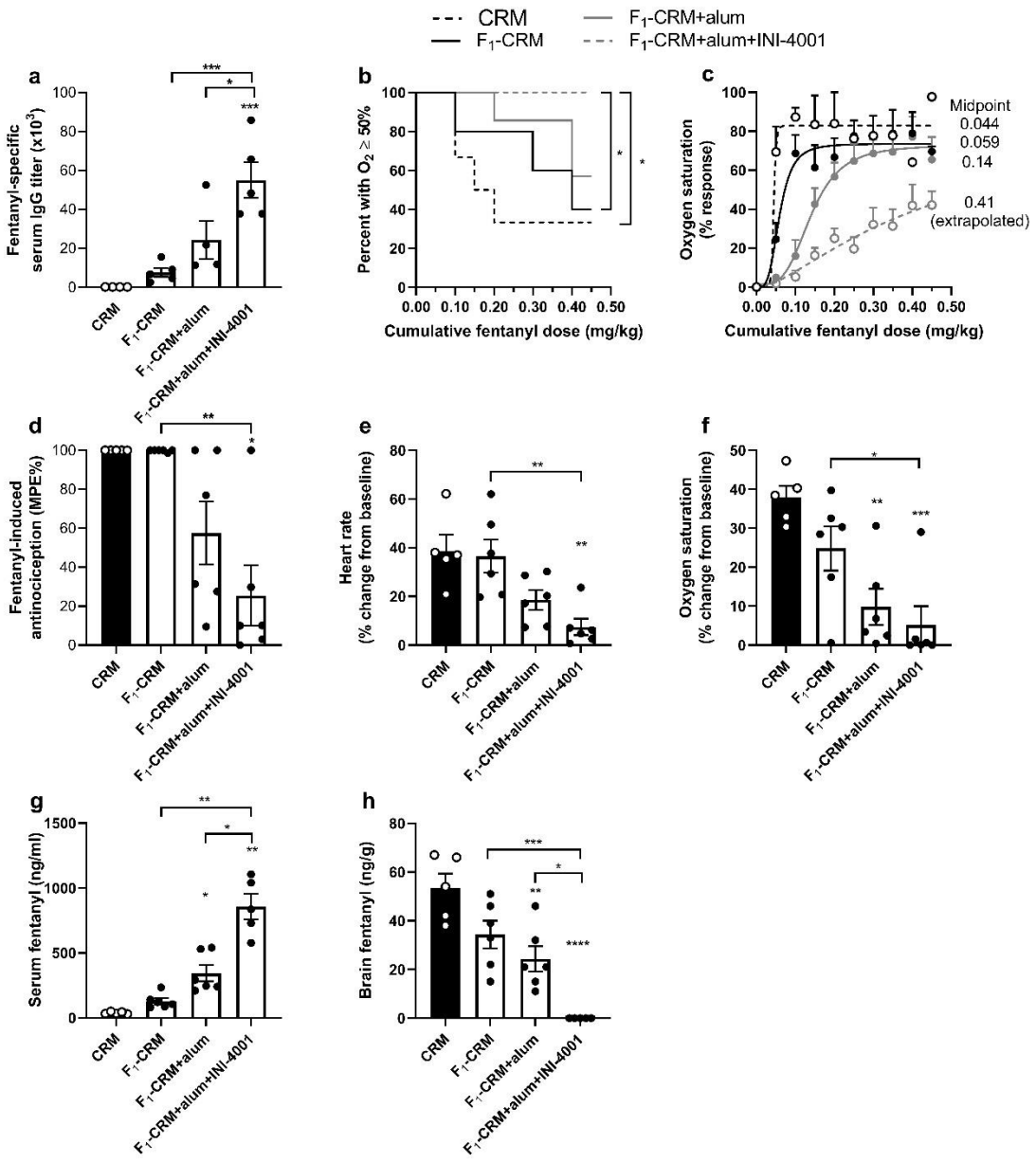

Figure 3: TLR7/8 adjuvanted vaccine protects against fatal levels of respiratory depression and high dose fentanyl challenge. Rats (n=6/group) were immunized on days 0, 21, and 42. On day 49, blood was collected to measure A) fentanyl-specific IgG titers via ELISA. Starting on day 56, rats were challenged with a cumulative dose of fentanyl (0.45 mg/kg). Oxygen saturation was measured every 15 minutes. B) Kaplan-

Meier survival curve of rats who did not fall below 50% oxygen saturation as measured by pulse oximetry. C) Dose-response curve of fentanyl-induced respiratory depression calculated as percent maximum possible response. The following week, rats were challenged with a bolus dose of fentanyl (0.1 mg/kg). 15 minutes post-challenge, D) antinociception as a percent maximum possible effect (MPE%), E) heart rate as a percent change from baseline, and F) oxygen saturation as a percent change from baseline were measured. After final measurement blood and brain were collected to determine G) serum fentanyl concentration and H) brain fentanyl concentration via LC-MS. Data are mean±SEM. Statistical analysis was run via one-way ANOVA with Tukey's multiple comparison's *post-hoc* test (A, D-G). Kaplan-Meier statistical analysis run via Mantel-Cox test between groups (B). * directly over columns indicate significance compared to the control. Statistical symbols: * $P<0.05$, ** $P<0.01$, *** $P<0.001$, **** $P<0.0001$.

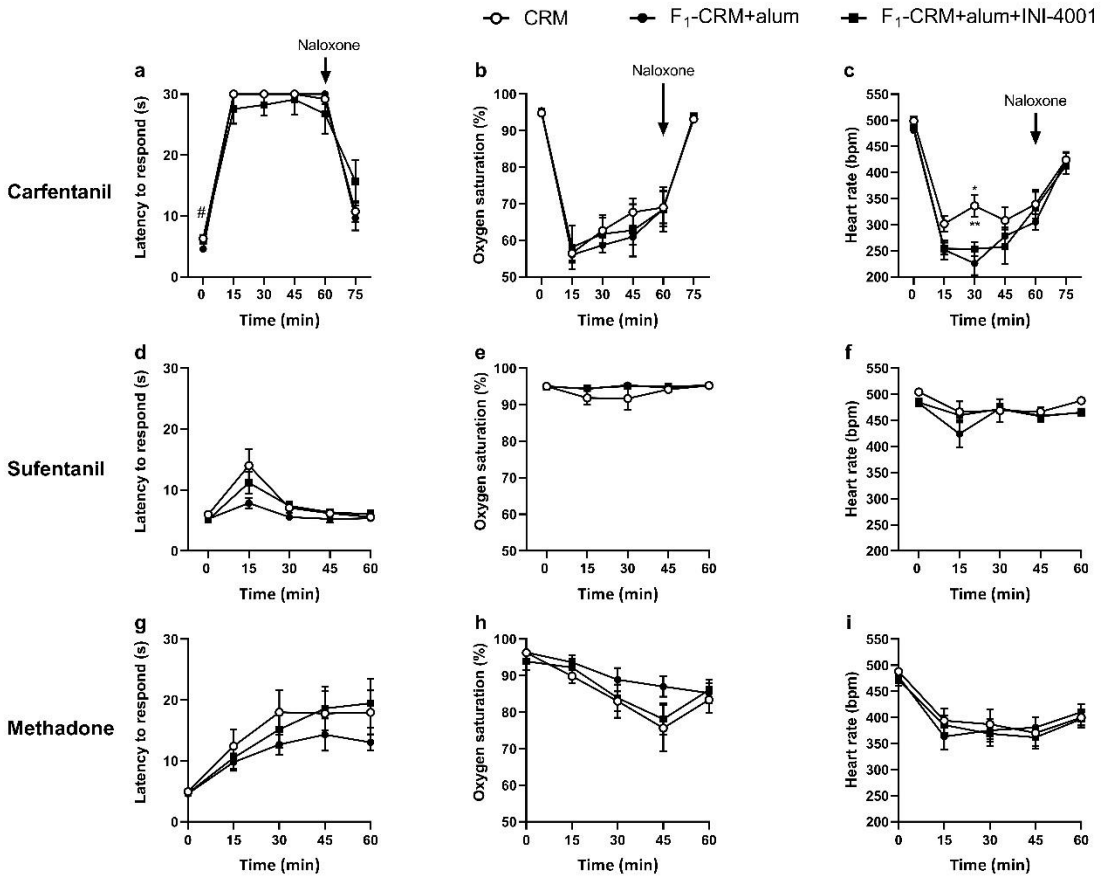

Figure 4: Addition of INI-4001 does not significantly alter *in vivo* efficacy of off-target molecules. Rats (n=8/group) were immunized on days 0, 21, and 42. Starting on day 56, rats were challenged with one drug per week. A) Latency to respond on a hot plate, B) oxygen saturation and C) heart rate after challenge with carfentanil (0.01 mg/kg). 60 minutes post-challenge, rats were given naloxone (0.1 mg/kg) to reverse carfentanil-induced effects. D) Latency to respond on a hot plate, E) oxygen saturation, and F) heart rate after challenge with sufentanil (0.008 mg/kg). G) Latency to respond on a hot plate, H) oxygen saturation, and I) heart rate after challenge with methadone (4.5 mg/kg). Data are mean±SEM. Statistical analysis run via two-way ANOVA with Tukey's multiple comparisons *post hoc* test. * directly over columns indicate significance compared to the

control. # directly over columns indicate significance to F_1-CRM alone. Statistical symbols: * or # P<0.05, ** P<0.01.

Table 1. *In vitro* cross-reactivity to off-target molecules.

	F-CRM+alum		F-CRM+alum+INI-4001	
Competitor	**IC_{50} (uM)**	**Relative Affinity**	**IC_{50} (uM)**	**Relative Affinity**
Fentanyl	0.014±0.015	100%	0.0075±0.0099	100%
Acetylfentanyl	0.200±0.243	6.71%	0.100±0.073	7.51%
Carfentanil	19.77±22.12	0.068%	8.48±3.49	0.089%
Alfentanil	91.29±63.89	0.015%	207.57±127.98	0.0036%
Remifentanil	121.45±90.62	0.011%	384.59±323.29	0.0020%
Sufentanil	319.16±297.82	0.0042%	185.11±286.9	0.0041%
Naltrexone	344.67±201.67	0.0039%	821.00± 309.44	0.00092%
Naloxone	1877.37±1788.03	0.00071%	3005.25±1556.88	0.00025%
Buprenorphine	32.61±22.07	0.04%	>50	<0.015%
Beta-endorphin	>600	<0.0022%	>600	<0.0013%
Endomorphin-1	522.3±261.1	0.0026%	770.9±385.5	0.00098%

Values are IC_{50} of off-target compounds measured by competitive binding ELISA of serum antibodies after immunization against fentanyl.

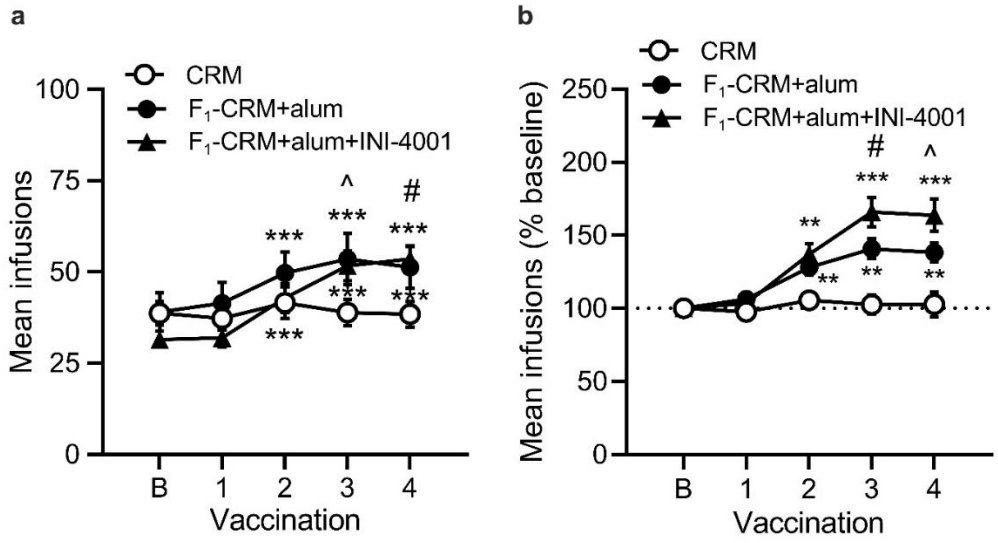

Figure 5. Effect INI-4001 adjuvanted anti-fentanyl vaccine on maintenance of fentanyl self-administration. Mean (±SEM) fentanyl infusions in rats at baseline (B) and two weeks after each of the first four vaccinations with CRM (n=11), F_1-CRM+alum (n=15), or F_1-CRM+alum+INI-4001 (n=16) as self-administration of the fentanyl training dose (2.5 µg/kg/infusion) continued. A) Absolute infusion data (Statistical symbols: different from baseline, ***p<0.01; F_1-CRM+alum+INI-4001 vs CRM, #p<0.05, ^p<0.1). B) Data expressed as a percentage of baseline (Statistical symbols: different from CRM, **p<0.01, ***p<0.001; F-CRM+alum vs F-CRM+alum+INI-4001, #p<0.05, ^p<0.1).

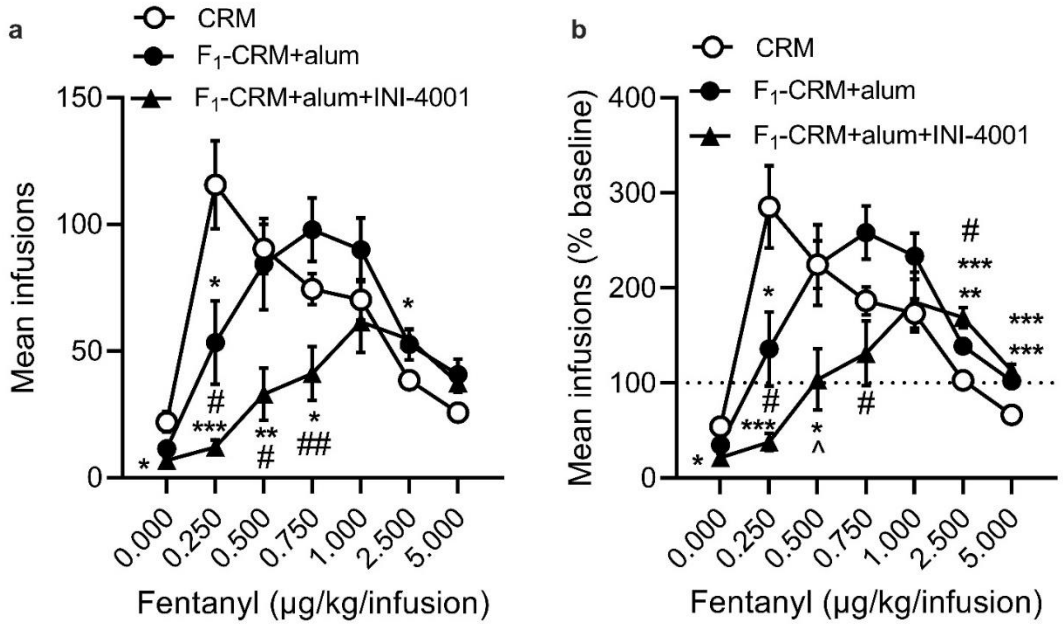

Figure 6. Effect of INI-4001 adjuvanted anti-fentanyl vaccine on the FSA dose-response curve. Mean (±SEM) fentanyl infusions during the last three sessions at each fentanyl unit dose and saline (0 µg/kg) in rats given CRM (n=11), F_1-CRM+alum (n=13), or F_1-CRM+alum+INI-4001 (n=12). A) absolute values of infusion data. B) Infusions expressed as a percentage of baseline (i.e. pre-vaccination). Statistical symbols: different from CRM, *p<0.05, **p<0.01, ***p<0.001. Different from F-CRM-alum, #p<0.05, ##p<0.01, ^p<0.1.

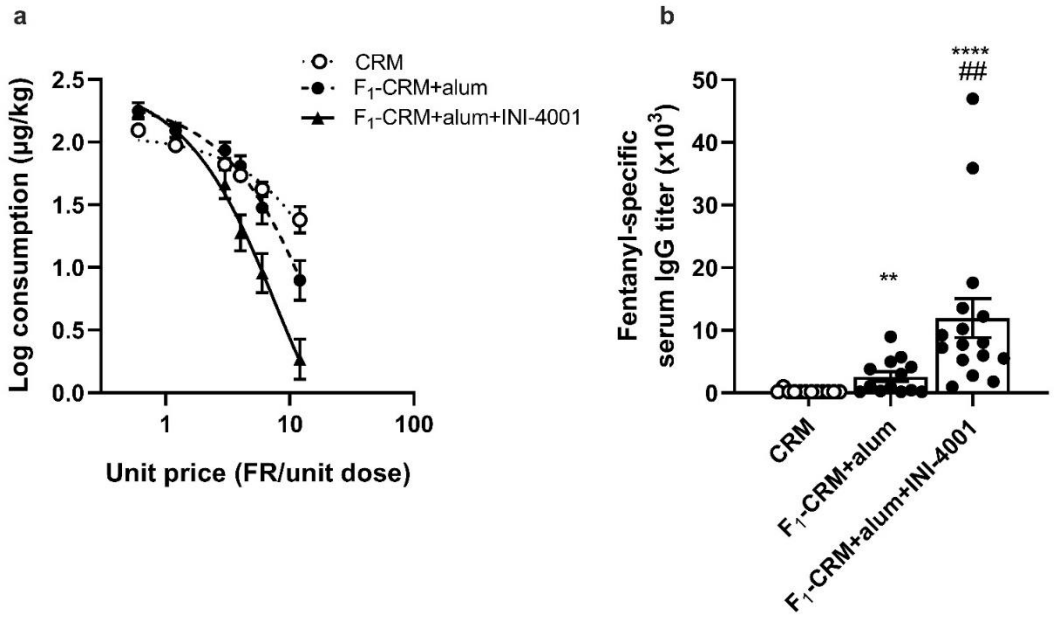

Figure 7. Effect of INI-4001 adjuvanted anti-fentanyl vaccine on elasticity of demand (α) for fentanyl and antibody titers. A) Mean (±SEM) fentanyl consumption (µg/kg) as a function unit price in rats given CRM, F_1-CRM+alum, or F_1-CRM+alum+INI-4001. Curves are fit to the data using an exponential function. Demand curve parameters are presented in Table 2. B) Mean (±SEM) antibody titers in rats given CRM, F_1-CRM+alum, or F_1-CRM+alum+INI-4001 during the FSA study. Samples were acquired 7-14 days after the fourth immunization. Statistical symbols: different from CRM, **$p < 0.01$, ****$p < 0.0001$; different from F_1-CRM+alum, $^{\#}p < 0.01$.

Table 2

Mean (±SEM) exponential demand curve parameter estimates from individual rat curve fits (group fits in Figure 6). Range constant k = 3.63.

Parameter	CRM	F_1-CRM+alum	F_1-CRM+alum+INI-4001
α	0.000170 (0.000028)	0.000218 (0.000046)	**0.000291 (0.000043)***
Q_0	118.1 (12.3)	**250.8 (51.7)****	**301.9 (52.5)****
P_{max}	8.65 (0.99)	**3.90 (0.60)****	**1.95 (0.31)****, #
O_{max}	329.1 (36.5)	290.6 (41.9)	**203.5 (31.2)***
R^2	0.88 (0.04)	0.94 (0.02)	0.93 (0.02)

Different from CRM *p < 0.05, **p < 0.01, ***p < 0.001. Different from F_1-CRM+alum, #p < 0.05.

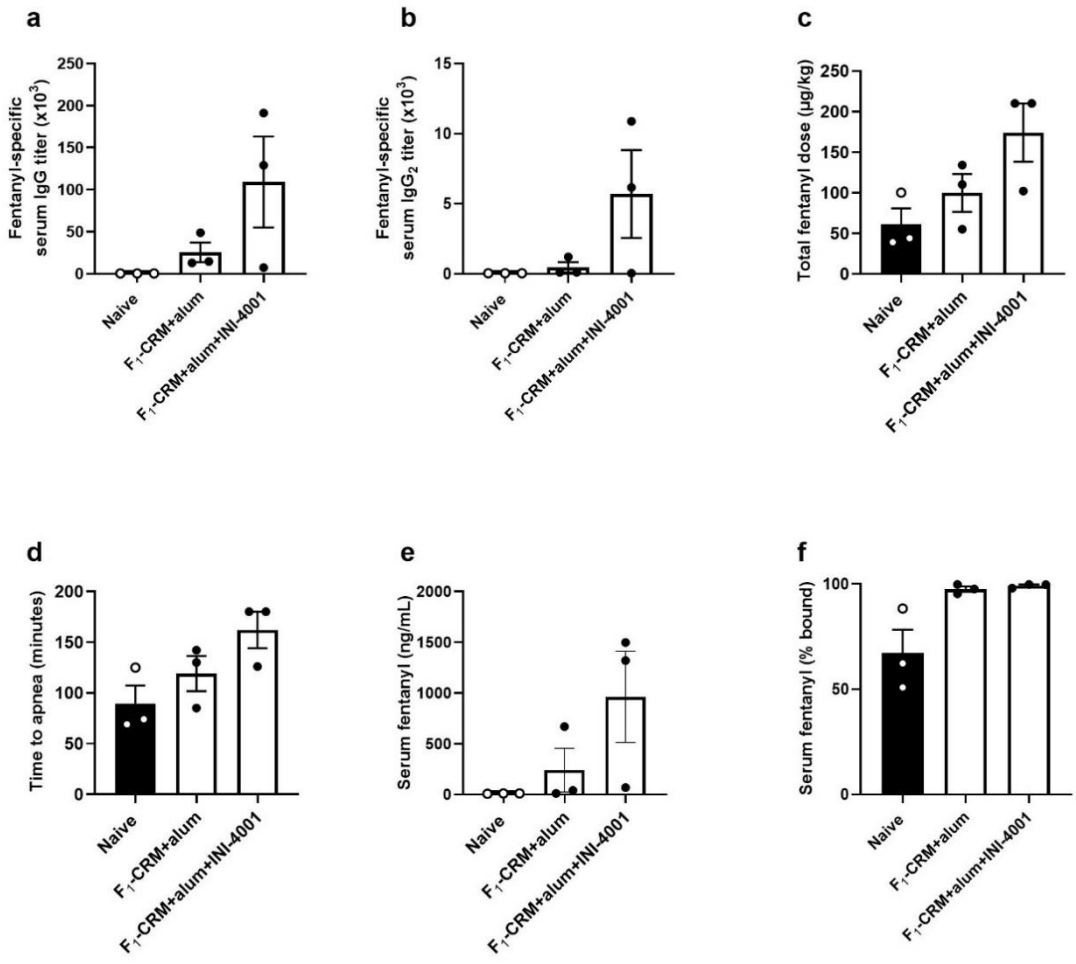

Figure 8. INI-4001 increases efficacy of an anti-fentanyl vaccine in a porcine model of fentanyl-induced respiratory depression. Pigs (n=3/group) were immunized on days 0, 21, and 42. Blood was collected on day 49±3 to measure A) fentanyl-specific serum total IgG titers and B) IgG_2 subclass titers via ELISA. Starting on day 49±3, pigs were challenged with a continuous IV infusion of fentanyl that increased over time until two minutes of continuous apnea was reached. C) Total fentanyl dose received before apnea was achieved. D) Time until apnea was achieved. E) Total serum fentanyl concentration

at time of apnea, measured via LC-MS. F) Serum fentanyl expressed as percent (%) protein bound. Data are mean±SEM.

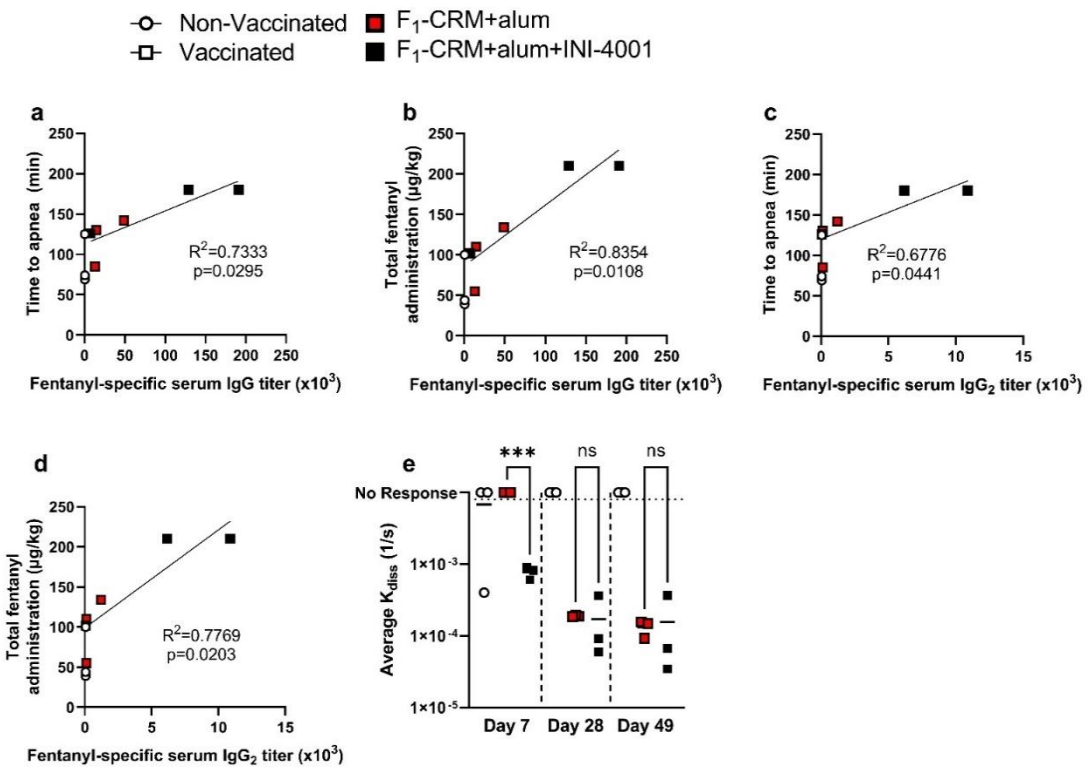

Figure 9. Porcine serum antibody titers are associated with increased vaccine efficacy. Pig total serum IgG titers were plotted against A) time to apnea and B) total fentanyl administration at time of apnea. Pig total serum IgG_2 subclass titers were plotted against C) time to apnea and D) total fentanyl administration at time of apnea. E) Polyclonal antibody avidity was measured in all groups at 3 time points using biolayer interferometry. Statistical analysis was run via Pearson correlation after determining data normality using D'Agostino-Pearson's test (A-D). Statistical analysis via one-way ANOVA followed by Tukey's multiple comparison's *post hoc* test (E). Statistical symbols: *** P<0.001.

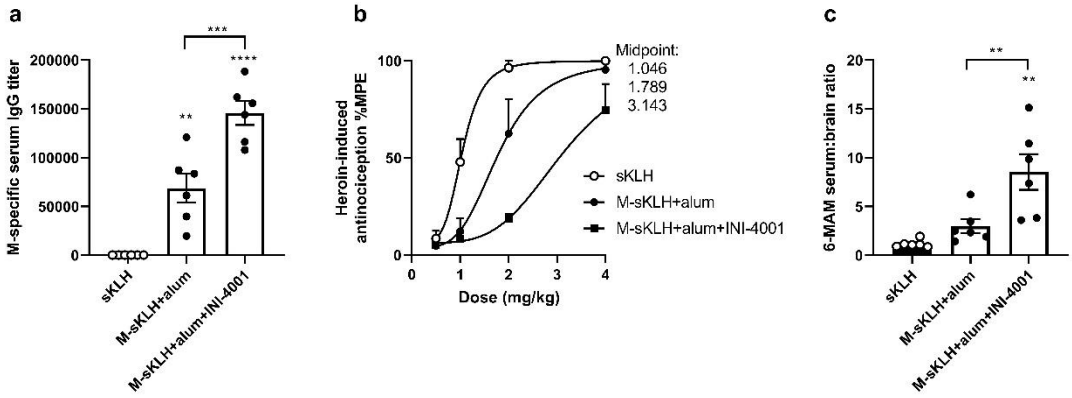

Figure 10. INI-4001 increases the efficacy of a vaccine targeting heroin (M-sKLH). Rats (n=6/group) were immunized on days 0, 21, and 42 with 5 µg M-sKLH+24 µg alum with or without 10 µg INI-4001, or 5 µg sKLH as a negative control. On day 49, serum was collected to assess A) M-specific serum IgG titers via ELISA. On day 56, rats were challenged with a 4 mg/kg cumulative dose of heroin s.c. over 60 minutes, and B) heroin -induced antinociception was measured on a hot plate. After 60 minutes, blood and brain were collected to measure concentration of 6-monoacetylmorphine (6-MAM), heroin's primary metabolite. C) Serum:brain 6-MAM concentration ratio. Data are mean±SEM. Statistical analysis performed via one-way ANOVA followed by Tukey's multiple comparisons post hoc test. Stars over columns indicate significance compared to the control or as indicated by brackets. Statistical symbols: ** P<0.01, ***P<0.001, ****P<0.0001.

Chapter 4: Improving anti-opioid vaccine efficacy through manipulation of linker length and testing bivalent immunization strategies to target multiple antigens

Vaccine efficacy can be improved through modification of hapten design, choice of carrier protein, or immunization schedule. The goal of this study was to optimize efficacy of novel carfentanil-based vaccines through manipulation of the hapten linker length. The lead vaccine was then combined with a lead fentanyl vaccine to test bivalent immunization strategies to increase vaccine efficacy to multiple target antigens.

The following data were reprinted with permission from:

Crouse B*, Wu MM*, Gradinati V, Kassick AJ, Song D, Jahan R, Averick S, Runyon S, Comer SD, Pravetoni M. Efficacy and selectivity of monovalent and bivalent vaccination strategies to protect against exposure to carfentanil, fentanyl and their mixtures in rats. *ACS Pharmacol & Transl. Sci.,* (2022).

* denotes co-first authorship

Author Contributions: BC designed and executed studies and analyzed data, MMW designed and executed studies and analyzed data, VG synthesized materials for experiments, AJK synthesized materials for experiments, DS executed studies and analyzed data, SA synthesized materials for experiments, RJ synthesized materials for the experiments, SR synthesized materials for experiments, SDC provided scientific support, MP assisted with method development, interpretation of data and editing.

INTRODUCTION

The widespread accessibility of synthetic opioids coupled with high rates of relapse has demonstrated the need for new interventional strategies to treat and manage opioid use disorders (OUD) and overdose. In the 12 months ending in April 2021, there were 75,673 opioid-related deaths, representing a large proportion of the 100,306 fatal drug overdoses (6). Fentanyl and other potent synthetic opioids accounted for the majority of these deaths (6), which continued the previously reported trend of increasing incidence of fentanyl-related mortalities from June 2019 to May 2020 (>38.4%) (7). The COVID-19 pandemic further complicated and exacerbated the opioid public health crisis as shown by increased rate of fatal and non-fatal overdoses attributed to synthetic opioids alone or in combination with other drugs (8-11). Carfentanil is a synthetic opioid that is 80-100x more potent than its parent compound fentanyl and 10,000x more potent than morphine (219). Both fentanyl and carfentanil were placed in Schedule II of the Controlled Substances Act, meaning that they have “high potential for abuse” and are “considered dangerous” (220). Carfentanil-induced toxicity is reported in non-human primates at a dose of 0.8 μg/kg (221), which would translate to a dose of only 56 μg (approximately the mass of a grain of salt) in an average-sized human. Carfentanil’s only approved clinical use is in veterinary medicine as a large animal tranquilizer (219); however, illicitly manufactured carfentanil has been found in street mixtures intended for recreational use by humans. While the exact number of deaths due to carfentanil is unknown given its extremely high potency and low tissue concentration which complicates detection by most currently available testing methods (219), it has been speculated to contribute significantly to the increased incidence of fatal opioid-related overdoses (222).

Fentanyl and carfentanil have been found as adulterants in street drug mixtures of heroin, cocaine, benzodiazepines, and methamphetamine (134, 219, 223), which can lead to unintentional consumption and accidental overdose in individuals diagnosed with a substance use disorder (SUD) and occasional drug users. While it has often been hypothesized that first responders, law enforcement, paramedics, and custom agents may be accidentally exposed to fentanyl and its analogues as an occupational hazard (224), the risk of overdose is largely anecdotical and thought to be low with the proper precautions (224). Nevertheless, due to carfentanil's extremely high potency, the possibility of symptoms may be greater after exposure compared to other synthetic opioids. Carfentanil may also be of concern to civilian and military personnel exposed to chemical attacks or deliberate poisoning. In 2002, Russian Special Forces introduced aerosolized carfentanil and remifentanil through the ventilation system of a Moscow theatre to subdue Chechen terrorists who were holding hostages. Of the 800 people who were exposed, 127 died and over 650 were hospitalized (223). This has led to increased concerns that carfentanil may be used as a chemical weapon during wartime or in terrorist attacks.

While the mu-opioid receptor (MOR) antagonist naloxone is an approved treatment for opioid overdose, its relatively short duration of action can lead to a return of opioid overdose symptoms several hours after apparent recovery, a phenomenon known as renarcotization (20, 219, 223). Additionally, naloxone is only useful if it is administered soon after the overdose occurs, requiring an individual to have access to the medication and someone available to deliver it. Respiratory deficits are further complicated by the propensity of fentanyl-like drugs to induce airway closure and muscle rigidity in the chest, known as wooden chest syndrome, which are mediated by α_1-adrenergic and cholinergic signaling and therefore partially refractory to naloxone (21-23). Despite the availability of

effective medications for treating OUD (MOUDs), including methadone, buprenorphine, and naltrexone, opioid-related overdoses continue to increase, which highlights the need for novel, long-lasting, and more selective strategies against OUD and overdose from highly potent fentanyl analogues.

One such treatment modality is active immunization via conjugate vaccines to stimulate the production of opioid-specific polyclonal IgG antibodies. Antibodies bind to the target drug in circulation and prevent the distribution of unbound (free) drug to the brain, which prevents drug-induced rewarding effects as well as lethal symptoms such as bradycardia and respiratory depression (29, 33, 34, 37, 38, 54, 55, 65). Vaccine-induced polyclonal antibodies have significantly longer half-lives compared to traditional MOUDs or overdose reversal agents (225), reducing the risk of renarcotization after opioid exposure. Additionally, because antibodies selectively neutralize the target opioid itself, without interfering with MOR's activity, this treatment strategy may be effective at preventing the pharmacological effects of target opioids regardless of the underlying signaling mechanism. Finally, vaccines can be administered both therapeutically and prophylactically, making them a desirable choice for individuals at high risk of opioid overdose and/or developing OUD.

In this study, two novel carfentanil-based haptens, F_{11} and F_{13}, were synthesized, conjugated to a carrier protein, and tested in rats in comparison to a previously described vaccine containing a fentanyl-based (F_1) hapten (55). Vaccines composed of F_1 conjugated to diphtheria cross-reactive material-197 (CRM) were previously shown to be effective in preventing fentanyl-induced antinociception, respiratory depression, bradycardia, and intravenous self-administration (55). Evaluation of F_1-CRM alongside other conjugates containing a series of next-generation haptens ($F_{2\text{-}6}$, and $F_{7\text{-}10}$) provided

further evidence for this approach against fentanyl and selected analogues such as sufentanil, alfentanil, and acetylfentanyl (55, 58). In this series, the fentanyl-based hapten F_{12} was synthesized but discarded early on from further screening (*unpublished data*). The F_{11} and F_{13} haptens are structurally different than other carfentanil-targeting haptens reported in the literature (59, 225) as the pendant phenethyl substituent has been replaced with linear amide-based linkers of different lengths (**Figure 1**). Compounds F_{11} and F_{13} retain the characteristic 4-anilidopiperidine core structure of both fentanyl and carfentanil, but also possess the sterically crowded methyl ester-bearing quaternary carbon center of the latter. This strategy was designed with the goal of preserving antibody affinity for fentanyl while also extending cross-reactivity to carfentanil. Haptens F_{11} and F_{13} were conjugated to the CRM carrier protein and tested for their efficacy in blocking the effects of carfentanil, fentanyl, or their mixture in rats. To achieve protection against both target drugs, the efficacy of bivalent vaccination strategies to target both fentanyl and carfentanil was also assessed. Previous studies reported use of bivalent vaccines against fentanyl and its analogues consisting of either divalent presentation of two haptens sharing the same linker conjugated to the same carrier or co-administration of individual conjugates (38, 40, 67). Similar studies reported the possibility of co-administration of individual conjugate vaccines to target heroin and oxycodone mixtures (34, 183), or heroin and fentanyl mixtures (38, 40, 53, 66, 67). The current study further extended the concept of bivalent vaccination by testing co-administration of individual conjugate vaccines in comparison to a heterologous prime/boost immunization regimen commonly used in vaccines for infectious diseases (reviewed in (226)). Results support further development of multivalent vaccine formulations to protect against the potentially lethal effects of structurally related and distinct drug substances in both mono- or poly-drug use or overdose scenarios.

MATERIALS AND METHODS

Synthesis of fentanyl- and carfentanil-based haptens.

General Information. N-benzylnorcarfentanil oxalate **1** was prepared according to published procedures (227). All other reagents and solvents were obtained from commercial sources and used according to manufacturer's instructions. ^{1}H and ^{13}C NMR spectra were measured in chloroform-d ($CDCl_3$), dimethylsulfoxide-d_6 (DMSO-d_6), or methanol-d_4 (CD3OD) on a Bruker Avance 500 MHz spectrometer. Chemical shifts are reported in ppm employing the residual solvent resonance as the internal standard. Liquid chromatography paired with mass spectrometry (LC-MS) was performed using a Dionex Ultimate 3000 Ultra-High-Performance Liquid Chromatography (UHPLC) system coupled to a Thermo Scientific TSQ Quantum Access MAX triple quadrupole mass spectrometer. Reverse-phase chromatographic separation was accomplished on an Agilent ZORBAX Eclipse Plus C18 column (3.5 µm, 100 × 4.6 mm) with acetonitrile (CH_3CN) and water (H_2O), modified with 0.1% formic acid, as the mobile phase solvents. Standard HPLC method consisted of a linear gradient from 20-95% CH_3CN over 5 min followed by a hold at 95% CH_3CN for 1 min and then a re-equilibration at 20% CH_3CN for 2.5 min. Total run time was 10 min, flow rate was 0.400 mL/min, and the injection volume was 10 µL.

Fentanyl-based hapten (F_1). The fentanyl-based hapten containing a tetraglycine linker (F_1, or $F(Gly)_4$) was synthesized as previously described (54), and belongs to a series of haptens F_n currently under development (55, 58).

Carfentanil-based hapten (F_{11}). The synthesis of F_{11} initiated with the preparation of norcarfentanil from the previously described compound, *N*-benzylnorcarfentanil oxalate, **1** (227). Michael addition of norcarfentanil and *tert*-butyl acrylate in CH_3CN solvent at room temperature provided *tert*-butyl ester intermediate **2**. Treatment of the resulting 1, 4-addition product **2** with neat trifluoroacetic acid (TFA) then afforded the corresponding carboxylic acid TFA salt **3** in excellent yield. Acid **3** was then converted to amide **4** following a standard EDC-coupling with *N*-Boc-ethylenediamine and excess diisopropylethylamine. Subsequent acid-mediated deprotection of Boc-carbamate **4** with 85% H_3PO_4 then furnished the amino-functionalized carfentanil hapten (**F_{11}**) for conjugation to the CRM carrier protein. The detailed synthesis scheme for F_{11} is below.

Methyl 1-(3-(tert-butoxy)-3-oxopropyl)-4-(N-phenylpropionamido)piperidine-4-carboxylate **(2)**

To a mixture of *N*-benzylnorcarfentanil oxalate **1** (0.700 g, 1.49 mmol, 1.0 equiv) and $HCOONH_4$ (0.469 g, 7.44 mmol, 5.0 equiv) under N_2 was added anhydrous MeOH (18 mL). The resulting white suspension was degassed for 1 h. Palladium on carbon (Pd/C) was added and the mixture was heated at reflux for 3 h. The reaction was removed from the heat and maintained overnight at room temperature. The crude reaction mixture was filtered through Celite to remove the catalyst. The Celite pad was washed with MeOH (100 mL) and the filtrate was concentrated. The residue was dissolved in CH_2Cl_2 (60 mL) and diluted with saturated aqueous $NaHCO_3$ (50 mL), transferred to a separatory funnel, and separated the layers. The aqueous layer was further extracted with CH_2Cl_2 (2 x 25 mL). The combined organics were then dried over $MgSO_4$, filtered, and concentrated to afford 385 mg (89%) of norcarfentanil as a viscous, pale-yellow oil that was used in the next step

without further purification. MS (ESI) *m/z*: calculated for $C_{16}H_{22}N_2O_3$ 290.16, found 291.02 $[M + H]^+$, 313.01 $[M + Na]^+$. Norcarfentanil (0.380 g, 1.31 mmol, 1.0 equiv) was dissolved in 2 mL of anhydrous CH_3CN and treated with *tert*-butyl acrylate (0.250 mL, 1.71 mmol, 1.25 equiv) via syringe at room temperature. The reaction was maintained for 20 h. The crude reaction mixture was concentrated under reduced pressure to afford a yellow oil. Purification by flash chromatography on SiO_2 (42 g, 80:20 EtOAc/hexanes) afforded 425 mg (77%) of the desired product as a viscous, pale-yellow oil. ^{1}H NMR (500 MHz, DMSO-d_6) δ 7.52–7.42 (m, 3H), 7.36–7.30 (m, 2H), 3.64 (s, 3H), 2.54–2.46 (m, 2H), 2.46–2.39 (m, 2H), 2.31–2.17 (m, 4H), 2.06 (d, J = 13.0 Hz, 2H), 1.77 (q, *J* = 7.4 Hz, 2H), 1.53–1.41 (m, 2H), 1.33 (s, 9H), 0.81 (t, *J* = 7.4 Hz, 3H); ^{13}C NMR (125 MHz, DMSO-d_6) δ 173.0, 172.8, 171.3, 139.1, 130.5 (2C), 129.4 (2C), 128.7, 79.4, 61.8, 53.1, 51.8, 48.9 (2C), 33.2, 32.9 (2C), 28.4, 27.7 (3C), 9.2; MS (ESI) *m/z*: calculated for $C_{23}H_{34}N_2O_5$ 418.25, found 419.08 $[M + H]^+$, 441.09 $[M + Na]^+$.

3-(4-(Methoxycarbonyl)-4-(*N*-phenylpropionamido)piperidin-1-yl)propanoic acid TFA salt **(3)**

tert-Butyl ester **2** (0.410 g, 0.980 mmol, 1.0 equiv) was treated with TFA (4.5 mL, 58.8 mmol, 60 equiv) at room temperature then maintained for 90 min. The reaction was then concentrated to furnish a viscous, yellow oil that was subsequently triturated with dry Et_2O to yield a white precipitate. The material was filtered and dried to obtain 398 mg (85%) of the desired product as a white solid. ^{1}H NMR (500 MHz, DMSO- d_6) δ 12.6 (br s, 1H), 9.43 (br s, 1H), 7.58–7.46 (m, 3H), 7.38 (br s, 2H), 3.71 (s, 3H), 3.37 (m, 2H), 3.24 (t, *J* = 7.4 Hz, 2H), 3.18–3.02 (m, 2H), 2.66 (t, *J* = 7.4 Hz, 2H), 2.30 (d, *J* = 14.2 Hz, 2H), 1.90–1.63 (m, 4H), 0.83 (t, *J* = 7.4 Hz, 3H); ^{13}C NMR (125 MHz, DMSO-d_6) δ 173.3, 172.2, 171.5, 138.2, 130.4 (2C), 129.7 (2C), 129.1, 59.6, 52.4, 51.4, 49.1 (2C), 30.1 (2C), 28.7, 28.2,

9.0; MS (ESI) *m/z*: calculated for $C_{19}H_{26}N_2O_5$ 362.18, found 363.01 $[M + H]^+$, 385.01 $[M + Na]^+$.

Methyl 1-(3-((2-((tert-butoxycarbonyl)amino)ethyl)amino)-3-oxopropyl)-4-(N-phenylpropionamido)-piperidine -4-carboxylate **(4)**

To a 0 °C suspension of acid **3** (0.391 g, 0.821 mmol, 1.0 equiv) in anhydrous CH_2Cl_2 (8 mL) was added *N*-Boc-ethylenediamine (0.195 mL, 1.23 mmol, 1.5 equiv) via pipette. The suspension became a solution. EDC 0.393 g, 2.05 mmol, 2.5 equiv) and DMAP (10 mg, 0.082 mmol, 10 mol%) were added and the reaction mixture was maintained at room temperature for 20 h. The reaction was diluted with CH_2Cl_2 (80 mL) and washed with saturated aqueous $NaHCO_3$, H_2O, and brine. The organics were dried over anhydrous $MgSO_4$, filtered and concentrated. Purification by flash chromatography on SiO_2 (45 g, 6% MeOH/CH_2Cl_2) afforded 389 mg (94%) of the desired product as a white foam. ^{1}H NMR (500 MHz, DMSO- d_6) δ 7.83 (br s, 1H), 7.57–7.40 (m, 3H), 7.35 (d, J = 7.3 Hz, 2H), 6.80–6.65 (m, 1H), 3.65 (s, 3H), 3.08–2.96 (m, 2H), 2.95–2.83 (m, 2H), 2.56–2.46 (m, 2H), 2.46–2.36 (m, 2H), 2.32–2.17 (m, 2H), 2.16–2.00 (m, 4H), 177 (q, J = 7.4 Hz, 2H), 1.58–1.42 (m, 2H), 1.36 (s, 9H), 0.82 (t, *J* = 7.4 Hz, 3H); ^{13}C NMR (125 MHz, DMSO-d_6) δ 173.1, 172.8, 171.2, 155.6, 139.1, 130.5 (2C), 129.4 (2C), 128.7, 77.6, 61.9, 53.7, 51.8, 48.9 (2C), 38.5, 33.3, 32.9 (2C), 28.3, 28.2 (4C), 9.1; MS (ESI) *m/z*: calculated for $C_{26}H_{40}N_4O_6$ 504.29, found 505.12 $[M + H]^+$, 527.10 $[M + Na]^+$.

Methyl 1-(3-((2-aminoethyl)amino)-3-oxopropyl)-4-(*N*-phenylpropionamido)piperidine-4-carboxylate **(F_{11})**

To a solution of *N*-Boc amine (0.380 g, 0.753 mmol, 1.0 equiv) in anhydrous CH_2Cl_2 (1.0 mL) at room temperature was added 85% H_3PO_4 (0.5 mL) dropwise via syringe. The

reaction mixture was maintained for 1 h with vigorous stirring. An oily whitish residue formed. The reaction was diluted with H_2O (3 mL) after 80 min of total reaction time, then cooled to 0 °C. 5 N NaOH (~2 mL) was added to bring to pH ~8-9, then the product was extracted with CH_2Cl_2 (5 x 10 mL). The combined organics were dried over anhydrous $MgSO_4$, filtered, and concentrated to afford 189 mg (62%) of a white foam (**F_{11}**). ^{1}H NMR (500 MHz, DMSO- *d_6*) δ 7.80 (t, *J* = 5.4 Hz, 1H), 7.54–7.47 (m, 2H), 7.47–7.41(m, 1H), 7.39–7.32 (m, 2H), 3.64 (s, 3H), 2.99 (q, *J* = 6.2 Hz, 2H), 2.55–2.48 (m, 2H), 2.42 (t, *J* = 7.2 Hz, 2H), 2.28–2.18 (m, 2H), 2.12 (t, *J* = 7.1 Hz, 2H), 2.06 (br d, *J* = 13.3 Hz, 2H), 1.77 (q, *J* = 7.4 Hz, 2H), 1.55–1.43 (m, 2H), 0.82 (t, *J* = 7.4 Hz, 3H). ^{13}C NMR (125 MHz, DMSO-*d_6*) δ 173.1, 172.8, 171.1, 139.1, 130.5, 129.4, 128.7, 61.9, 53.8, 51.7, 48.9 (2C), 41.9, 41.3, 33.3, 32.9 (2C), 28.3, 9.2; MS (ESI) *m/z*: calculated for $C_{21}H_{32}N_4O_4$ 404.24, found 405.08 $[M + H]^+$, 427.06 $[M + Na]^+$.

Scheme 1

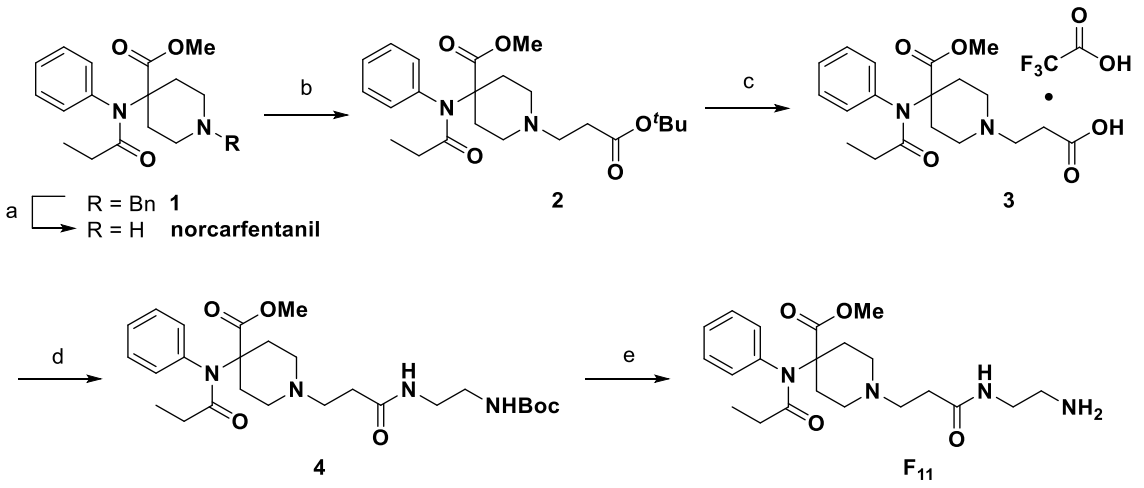

Reagents and conditions: a) $HCOONH_4$, 10% Pd/C, MeOH, reflux, 3 h; b) *tert*-Butyl acrylate, CH_3CN, room temperature (RT), 20 h; c) TFA, RT, 1.5 h; d) N-Boc-ethylenediamine, EDC, DMAP, CH_2Cl_2, 0 °C→RT; 20 h; e) 85% H_3PO_4, CH_2Cl_2, RT, 1 h.

Carfentanil-based hapten (F_{13}). Synthesis of F_{13} was initiated by a previously reported aniline-based Bargellini reaction to arrive at the sterically hindered carboxylic acid **5** (228). A one-pot transformation of compound **5** involving *N*-acylation with propionic anhydride and subsequent acid to ester interconversion then furnished *N*-Boc norcarfentanil **6** in good yield. Standard acidic hydrolysis of carbamate **6** revealed amine **7** which was then treated with *N*-Boc-2-aminoacetaldehyde in the presence of $Na(OAc)_3BH$ to yield the corresponding reductive amination product **8**. TFA-mediated Boc-deprotection of carbamate **8** followed by *N*-acylation of the resultant primary amine **9** with 5-(benzyloxy)-5-oxopentanoyl chloride **11** afforded benzyl ester **12** in moderate yield. Compound **12** was subsequently converted into the corresponding carboxylic acid **13** via palladium-catalyzed hydrogenolysis. The remainder of the peptide linker was installed with a benzotriazole-mediated amide coupling protocol employing gly_4Cbz arriving at ester intermediate **14**. Benzyl ester hydrogenation with 10% palladium on carbon at atmospheric pressure then arrived at the desired carfentanil-targeting hapten **F_{13}**. The detailed synthesis scheme for F_{13} is below.

1-(*tert*-Butoxycarbonyl)-4-(phenylamino)piperidine-4-carboxylic acid (**5**)

To a solution of aniline (2.0 g, 21.48 mmol) in THF (60 ml), NaOH (fine powder, 4.29 g, 107.38 mmol) and *N*-Boc-4-piperidone (8.56 g, 42.95 mmol) were added at 0 ^{o}C. $CHCl_3$ (8.6 mL, 107.38 mmol) was added dropwise via a syringe and the reaction mixture was stirred at 0^{o} C for 1 h and at room temperature overnight. The reaction was filtered, and the filter cake was dissolved in water (50 mL). The aqueous solution was extracted with Et_2O (3 x 50 mL) to retain non-polar impurities. The aqueous layer was cooled to 0 ^{o}C and acidified to ~pH 3 with HCl (2 N) and extracted with EtOAc (2 x 50 mL). The combined organic layers were washed with brine (3 x 30 mL), dried (Na_2SO_4), and concentrated *in vacuo* to furnish the carboxylic acid **5** (5.36 g, 78%) as a yellow solid. This material was used for the next transformation without any purification. ^{1}H NMR (300 MHz, $CDCl_3$) δ 7.15 (t, *J* = 7.8 Hz, 2H), 6.79 (t, *J* = 7.3 Hz, 1H), 6.64 (d, *J* = 7.9 Hz, 2H), 3.78–3.62 (m, 2H), 3.37–3.19 (m, 2H), 2.16–2.09 (m, 1H), 2.03 (s, 1H), 2.02–1.91 (m, 2H), 1.44 (s, 9H); ^{13}C NMR (75 MHz, $CDCl_3$) δ 179.0, 155.0, 144.3, 129.2, 119.6, 116.3, 80.2, 58.6, 39.2, 32.4, 28.4; MS (ESI) *m/z*: calculated for $C_{17}H_{24}N_2O_4$ 320.38, found 321.2 $[M + H]^+$.

1-*tert*-Butyl 4-methyl 4-(*N*-phenylpropionamido)piperidine-1,4-dicarboxylate (**6**)

To a stirred suspension of acid **5** (3.83 g, 11.94 mmol) and propionic anhydride (10.67 mL, 83.59 mmol) in EtOAc (50 mL) at reflux, TEA (5.0 mL, 35.83 mmol) was added slowly and the resulting reaction was heated at reflux for 2 h. The reaction mixture was cooled to 70 ^{o}C and MeOH (6 mL, excess) was added; the heating was continued for additional 3 h. After that, the reaction was cooled to room temperature and basified with aq. NaOH (3 M). The organic layer was separated, and the aqueous layer was extracted with EtOAc (2 x 50 mL). The combined organic layers were washed with brine (3 x 30 mL), dried (Na_2SO_4), and concentrated under reduced pressure. The residue was subjected to chromatography

on silica gel using 0–50% CMA80 in EtOAc to furnish amido ester **6** (3.60 g, 77%) as a pale yellow solid. ^{1}H NMR (300 MHz, $CDCl_3$) δ 7.50–7.39 (m, 3H), 7.34–7.24 (m, 2H), 3.87–3.69 (m, 5H), 3.17 (br s, 2H), 2.31–2.13 (m, 2H), 1.89 (q, *J* = 7.4 Hz, 2H), 1.54–1.38 (m, 11H), 0.96 (t, *J* = 7.4 Hz, 3H); ^{13}C NMR (75 MHz, $CDCl_3$) δ 174.2, 173.6, 154.7, 139.2, 130.5, 129.4, 128.9, 79.6, 62.9, 52.2, 40.4, 33.1, 28.9, 28.3, 9.1; MS (ESI) *m/z*: calculated for $C_{21}H_{30}N_2O_5Na$ 413.46, found 413.4 $[M + Na]^+$.

Methyl 4-(*N*-phenylpropionamido) piperidine-4-carboxylate (**7**)

To an ice-cold solution of carbamate **6** (3.60 g, 9.22 mmol) in dry DCM (30 mL), HCl (11.5 mL, 4 M solution in dioxane) was added. The reaction, which resulted, was stirred at room temperature for 20 h. The solvent was removed under reduced pressure and the residue was subjected to chromatography on silica gel using 0–100% CMA80 in DCM to furnish amine **7** (2.32 g, 87%) as a white solid. ^{1}H NMR (300 MHz, $CDCl_3$) δ 7.50–7.38 (m, 3H), 7.37–7.30 (m, 2H), 3.81 (s, 3H), 3.50–3.43 (m, 1H), 3.26–3.07 (m, 4H), 2.46–2.30 (m, 2H), 1.99–1.80 (m, 4H), 0.95 (t, *J* = 7.4 Hz, 3H); ^{13}C NMR (75 MHz, $CDCl_3$) δ 174.4, 173.1, 138.6, 130.5, 129.7, 129.2, 61.3, 52.6, 41.4, 31.1, 29.0, 9.1; MS (ESI) *m/z*: calculated for $C_{16}H_{22}N_2O_3$ 290.36, found 291.4 $[M + H]^+$.

Methyl 1-(2-((*tert*-butoxycarbonyl)amino)ethyl)-4-(*N*-phenylpropionamido)piperidine-4-carboxylate (**8**)

To a solution of amine **7** (1.76 g, 6.06 mmol) in 1,2-DCE (30 mL), *N*-Boc-2-aminoacetaldehyde (1.16 g, 7.27 mmol, dissolved in 5 mL DCE) was added dropwise at 0 ^{o}C. Sodium triacetoxyborohydride (1.93 g, 9.09 mmol) was added to the above reaction

in two portions at 0 °C and the reaction, which resulted, was stirred at room temperature for 20 h. Upon completion, the reaction was quenched with saturated aq. $NaHCO_3$ (20 mL). The organic layer was separated, and the aqueous layer was extracted with DCM (3 x 30 mL). The combined organic layers were washed with brine (3 x 30 mL), and dried (Na_2SO_4). The solvent was removed under reduced pressure and the residue was subjected to chromatography on silica gel using 0–50% CMA80 in DCM to furnish compound **8** (1.93 g, 73%) as a white solid. ^{1}H NMR (300 MHz, $CDCl_3$) δ 7.50–7.38 (m, 3H), 7.37–7.28 (m, 2H), 5.14–5.03 (m, 1H), 3.79 (s, 3H), 3.22–3.08 (m, 2H), 2.71–2.54 (m, 2H), 2.47–2.35 (m, 4H), 2.27 (d, *J* = 13.2 Hz, 2H), 1.88 (q, *J* = 7.4 Hz, 2H), 1.70–1.52 (m, 2H), 1.42 (s, 9H), 0.95 (t, *J* = 7.4 Hz, 3H); ^{13}C NMR (75 MHz, $CDCl_3$) δ 174.0, 173.8, 155.8, 139.3, 130.5, 129.3, 128.7, 78.9, 62.7, 57.0, 52.0, 49.6, 37.2, 33.3, 28.9, 28.3, 9.1; MS (ESI) *m/z*: calculated for $C_{23}H_{35}N_3O_5$ 433.54, found 434.4 $[M + H]^+$.

Methyl 1-(2-aminoethyl)-4-(*N*-phenylpropionamido)piperidine-4-carboxylate (**9**)

To a solution of carbamate **8** (1.93 g, 4.45 mmol) in DCM (20 mL), TFA (1.36 mL, 17.81 mmol) was added at 0 °C and the reaction, which resulted, was stirred at room temperature overnight. The solvent was removed with nitrogen flow. The residue was subjected to chromatography on silica gel using 0–100% CMA80 in DCM to furnish amine **9** (1.28 g, 87%) as a white solid. ^{1}H NMR (300 MHz, CD_3OD) δ 7.57–7.45 (m, 3H), 7.44–7.33 (m, 2H), 3.80 (s, 3H), 3.26–3.10 (m, 4H), 3.10–2.90 (m, 4H), 2.40 (d, *J* = 14.0 Hz, 2H), 1.99–1.80 (m, 4H), 0.93 (t, *J* = 7.4 Hz, 3H); ^{13}C NMR (75 MHz, CD_3OD) δ 176.7, 174.6, 139.8, 131.5, 130.9, 130.5, 62.7, 54.9, 53.1, 51.1, 50.0, 48.3, 36.3, 32.8, 29.9, 9.7; MS (ESI) *m/z*: calculated for $C_{18}H_{27}N_3O_3$ 333.43, found 334.4 $[M + H]^+$.

Methyl 1-(2-(5-(benzyloxy)-5-oxopentanamido)ethyl)-4-(*N*-phenylpropionamido)piperidine-4-carboxylate (**12**)

To a solution of 5-(benzyloxy)-5-oxopentanoic acid (1.27 g, 5.71 mmol) in DCM (20 mL) at 0 ^{o}C, oxalyl chloride (2.4 mL, 5 eq) was added, followed by DMF (cat.). The resulting reaction was stirred at room temperature for 3 h. The solvent was removed under reduced pressure to furnish *benzyl 5-chloro-5-oxopentanoate* **11** (1.37 g, quant.) as a yellowish residue, which was used directly for the next transformation. To a solution of the acid chloride **11** (1.37 g, 5.71 mmol) in dry DCM, TEA (3.2 mL, 22.85 mmol) was added at 0 ^{o}C, followed by amine **9** (1.52 g, 4.57 mmol). The reaction was stirred overnight at room temperature. The solvent was removed under reduced pressure, and the residue was subjected to chromatography on silica gel using 0–100% CMA80 in DCM to furnish amide **12** (1.33 g, 54%) as a white solid. ^{1}H NMR (300 MHz, $CDCl_3$) δ 7.49–7.28 (m, 10H), 6.16–6.06 (m, 1H), 5.10 (s, 2H), 3.78 (s, 3H), 3.25 (dd, *J* = 11.3, 5.7 Hz, 2H), 2.66–2.52 (m, 2H), 2.48–2.35 (m, 6H), 2.33–2.13 (m, 4H), 2.01–1.82 (m, 4H), 1.69–1.53 (m, 2H), 0.95 (t, *J* = 7.4 Hz, 3H); ^{13}C NMR (75 MHz, $CDCl_3$) δ 174.1, 173.8, 173.0, 172.0, 139.3, 135.9, 130.6, 129.3, 128.7, 128.5, 128.2, 128.1, 66.1, 62.7, 56.5, 52.1, 49.6, 36.1, 35.2, 33.3, 33.3, 29.0, 20.8, 9.1; MS (ESI) *m/z*: calculated for $C_{30}H_{39}N_3O_6$ 537.65, found 538.6 $[M + H]^+$.

5-((2-(4-(methoxycarbonyl)-4-(*N*-phenylpropionamido)piperidin-1-yl)ethyl)amino)-5-oxopenta-noic acid (**13**)

To a solution of benzyl ester **12** (0.65 g, 1.21 mmol) in MeOH (20 mL), Pd (0.26 g, 0.24 mmol, 10% on C) was added and the mixture was hydrogenated overnight (40 psi) at room

temperature. The reaction mixture was filtered through Celite, and the filtrate was concentrated to dryness to provide acid **13** (0.47 g, 86%) as a white solid. ^{1}H NMR (300 MHz, CD_3OD) δ 7.45–7.34 (m, 3H), 7.31–7.25 (m, 2H), 3.68 (s, 3H), 3.32–3.19 (m, 2H, merged with solvent peak), 3.07–2.89 (m, 2H), 2.78–2.57 (m, 4H), 2.32–2.18 (m, 2H), 2.08 (q, *J* = 7.1 Hz, 4H), 1.88–1.68 (m, 6H), 0.83 (t, *J* = 7.4 Hz, 3H); ^{13}C NMR (75 MHz, CD_3OD) δ 180.4, 176.6, 176.1, 174.7, 140.1, 131.7, 130.8, 130.4, 63.2, 57.7, 52.9, 50.8, 37.2, 36.7, 36.4, 32.9, 29.9, 23.1, 9.6; MS (ESI) *m/z*: calculated for $C_{23}H_{33}N_3O_6$ 447.52, found 448.4 $[M + H]^+$.

Methyl 1-(3,6,9,12,15,19-hexaoxo-1-phenyl-2-oxa-5,8,11,14,20-pentaazadocosan-22-yl)-4-(*N*-phenylpropionamido)piperidine-4-carboxylate (**14**)

To a solution of acid **13** (0.10 g, 0.22 mmol) in DMF (5 mL), BOP (0.15 g, 0.34 mmol) was added at 0 °C. After that, a solution of TEA (0.1 mL, 0.67 mmol) and gly_4Cbz tosylate salt (0.12 g, 0.25 mmol) in DMF was added dropwise to the above reaction at 0°C. The reaction was stirred at room temperature for 16 h. The solvent was removed under nitrogen flow and the residue was subjected to chromatography on silica gel using 0–100% CMA80 in DCM to furnish amide **14** (62.8 mg, 37%) as a white solid. ^{1}H NMR (300 MHz, DMSO-d_6) δ 8.30 (t, *J* = 5.9 Hz, 1H), 8.22–8.07 (m, 3H), 7.70 (t, *J* = 5.4 Hz, 1H), 7.54–7.43 (m, 3H), 7.41–7.29 (m, 7H), 5.13 (s, 2H), 3.91 (d, *J* = 5.9 Hz, 2H), 3.79–3.68 (m, 6H), 3.65 (s, 3H), 3.07 (dd, *J* = 12.2, 6.3 Hz, 2H), 2.60–2.44 (m, 2H, merged with solvent peak), 2.30–2.17 (m, 4H), 2.14–1.95 (m, 6H), 1.84–1.60 (m, 4H), 1.59–1.42 (m, 2H), 0.82 (t, *J* = 7.4 Hz, 3H); ^{13}C NMR (75 MHz, DMSO-d_6) δ 173.0, 172.7, 172.3, 171.5, 169.6, 169.6, 169.3, 169.0, 139.1, 135.9, 130.5, 129.3, 128.6, 128.4, 128.0, 127.8, 65.8, 61.9, 56.8, 54.8, 51.7,

49.2, 42.0, 41.7, 40.6, 36.0, 34.6, 34.4, 32.8, 28.3, 21.4, 9.1; MS (ESI) *m/z*: calculated for $C_{38}H_{51}N_7O_{10}$ 765.85, found 766.8 $[M + H]^+$. HPLC (220 nm) t_R = 11.62 min.

20-(4-(methoxycarbonyl)-4-(*N*-phenylpropionamido)piperidin-1-yl)-4,7,10,13,17-pentaoxo-3,6,9,12,18-pentaazaicosan-1-oic acid (**F_{13}**)

To a solution of ester **14** (34 mg, 0.04 mmol) in MeOH (10 mL), Pd (9.0 mg, 0.01 mmol, 10% on C) was added and the mixture was hydrogenated (1 atm) overnight at room temperature. The reaction mixture was filtered through Celite, and the filtrate was concentrated to dryness under nitrogen flow to provide acid **F_{13}** (28 mg, 93%) as a white solid. ^{1}H NMR (300 MHz, DMSO-d_6) δ 8.23–8.09 (m, 3H), 7.97 (t, *J* = 5.4 Hz, 1H), 7.76 (t, *J* = 5.3 Hz, 1H), 7.54–7.41 (m, 3H), 7.38–7.30 (m, 2H), 3.77–3.62 (m, 11H), 3.13–3.03 (m, 2H), 2.63–2.53 (m, 2H), 2.34–2.21 (m, 4H), 2.13–1.96 (m, 6H), 1.84–1.60 (m, 4H), 1.59–1.42 (m, 2H), 0.82 (t, *J* = 7.4 Hz, 3H); ^{13}C NMR (75 MHz, DMSO-d_6) δ 173.0, 172.8, 172.3, 171.6, 171.0, 169.6, 169.0, 168.7, 139.0, 130.4, 129.3, 128.7, 61.8, 56.7, 51.7, 49.2, 42.1, 42.0, 41.8, 41.1, 35.9, 34.6, 34.4, 32.6, 28.3, 21.3, 9.1; MS (ESI) *m/z*: calculated for $C_{31}H_{45}N_7O_{10}$ 675.7, found 676.60 $[M + H]^+$. HPLC (220 nm) t_R = 9.62 min.

Scheme 2

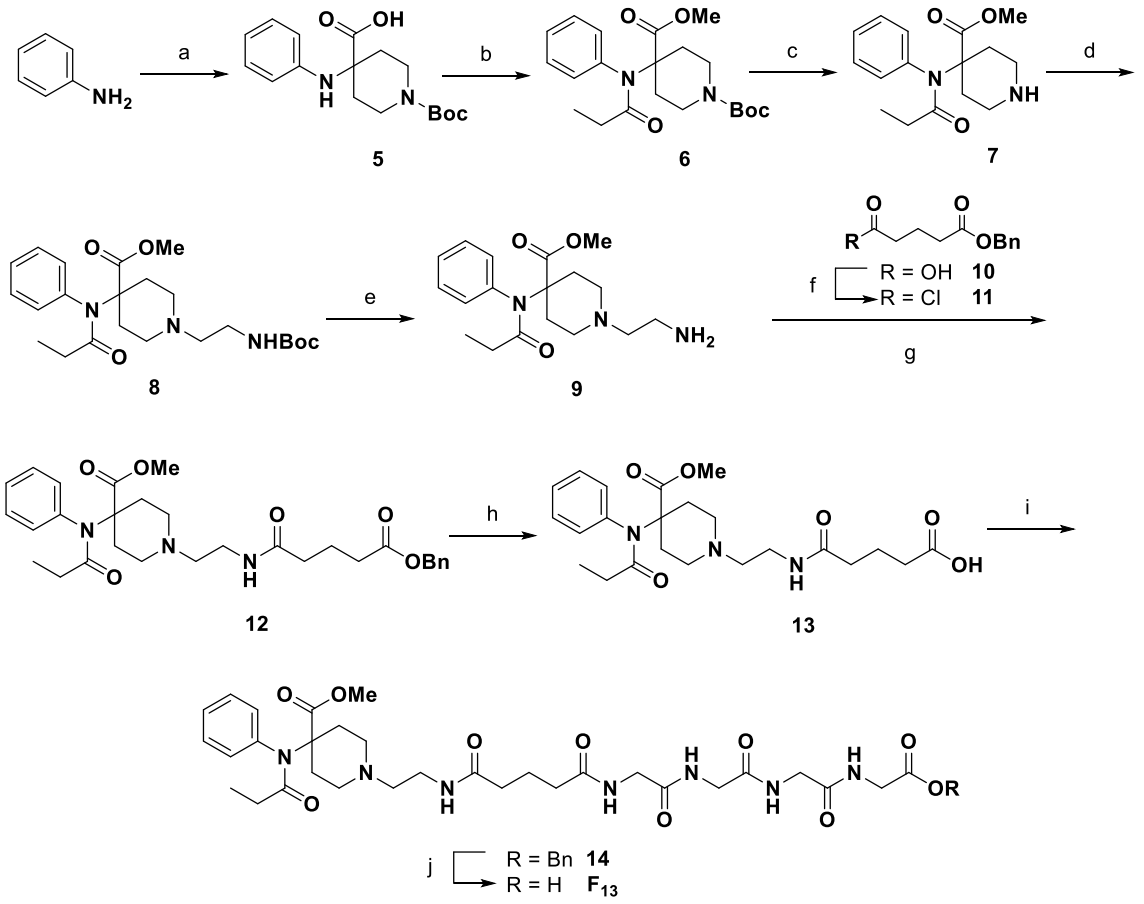

Reagents and conditions: a) *N*-Boc-4-piperidone, NaOH, $CHCl_3$, THF, 0 $^oC \rightarrow$RT, overnight; b) propionic anhydride, TEA, EtOAc, MeOH, reflux, 5 h; c) HCl (4 M in dioxane), DCM, 0 $^oC \rightarrow$RT, 20 h; d) *N*-Boc-2-aminoacetaldehyde, $Na(OAc)_3BH$, 1,2-DCE, 0 $^oC \rightarrow$RT, 20 h; e) TFA, DCM, 0 $^oC \rightarrow$RT, overnight; f) 5-(benzyloxy)-5-oxopentanoic acid, oxalyl chloride, DCM, DMF (cat.), 0 $^oC \rightarrow$RT, 3 h; g) benzyl 5-chloro-5-oxopentanoate **11**, TEA, DCM, 0 $^oC \rightarrow$RT, overnight; h) Pd (10% on C), H_2 (40 psi), MeOH, RT, overnight; i) gly_4Cbz, BOP, TEA, DMF, 0 $^oC \rightarrow$RT, 16 h; j) Pd (10% on C), H_2 (1 atm), MeOH, RT, overnight.

Conjugation and formulation of vaccines. All haptens were conjugated to either the CRM (Pfenex, San Diego, CA) carrier protein for immunization studies or bovine serum albumin (BSA) for antibody analysis by ELISA. The F_1 hapten was conjugated to proteins via carbodiimide chemistry as described before (55). The novel F_{11} and F_{13} haptens were conjugated following procedures previously described for other haptens in the F_n series (55). Briefly, haptens were dissolved at a concentration of 5.2 mM and activated with 208 mM N-ethyl-N′-(3 dimethylaminopropyl) carbodiimide hydrochloride (EDAC, Sigma-Aldrich, St. Louis, MO) in 0.1 M 2-(N-morpholino)ethanesulfonic acid (MES) buffer pH 5.0 containing 10% DMSO (final). The reaction mixture was stirred for 10 min at room temperature, and then CRM or BSA were added to a final concentration of 2.8 mg/mL and stirred for 3 hr at room temperature. To terminate the reaction, MES buffer was exchanged with PBS buffer pH 7.2 using an Amicon filter unit (MilliporeSigma, Merck, Burlington, MA) with 50 kDa molecular weight cutoff, and resuspended to a final concentration of 2.5 mg/mL prior to storage at 4°C. A final concentration of 250 mM sucrose was added to the MES and PBS buffers for CRM stabilization during the conjugation reaction. The haptenation ratios of CRM conjugates were measured by MALDI-TOF (AB SCIEX 5800, Foster City, CA) and estimated accordingly to the following formula: $\frac{MW_{conjugated\ protein} - MW_{carrier\ protein}}{MW_{hapten}}$ as previously described (55). The unconjugated protein and the conjugate vaccines were formulated with aluminum hydroxide adjuvant (Alhydrogel ‘85’, 2%, Brenntag Biosector, Denmark) prior to *in vivo* immunization studies as described in the experimental section.

Drugs. Fentanyl citrate was obtained from the University of Minnesota Boynton Pharmacy, and carfentanil hydrochloride was obtained from the NIDA Drug Supply at RTI International (Research Triangle Park, NC). Naloxone hydrochloride was obtained through Sigma-Aldrich (St. Louis, MO). Drug doses are expressed as concentration of the free base.

Animal subjects. All animal studies were approved by the University of Minnesota Animal Care and Use Committee and conducted in AAALAC-approved facilities. Male Balb/c mice or Sprague Dawley rats (Envigo, Indianapolis, IN) were 6-8 weeks old at arrival. Rodents were housed under standard conditions with a 14/10 light/dark cycle and provided with food and water *ad libitum*.

***In vivo* efficacy: antinociception, respiratory depression, and bradycardia.** Opioid-induced behavioral and pharmacological effects were measured via the hot plate test and pulse oximetry as previously described (55). Briefly, antinociception was assessed by placing rats on a hot plate set to 54^{o}C (Columbus Instruments, Columbus, OH) at baseline and at 15 min intervals up to 60 min post-drug challenge. Rats were removed from the hot plate when a lift or flick of the hind paw was observed, or by reaching the maximal cutoff of 30 sec to avoid thermal tissue damage. Data are displayed as latency to respond. To assess the effects of opioids on respiratory depression and bradycardia, a MouseOx Plus pulse oximeter (Starr Life Sciencies, Oakmont, PA) was used to measure oxygen saturation (SaO_2) and heart rate (bpm, beats per minute) on the same schedule. Drug doses for *in vivo* challenges were chosen based on previous studies (55, 59).

Antibody analysis. Serum hapten-specific IgG antibody titers were analyzed via indirect ELISA using blood collected from tail veins (55). Determination of hapten-specific IgG antibody titers in lung and heart tissue was performed on supernatant obtained after

centrifuging homogenized tissue for 20 min at 10,000xg at 4°C. Ninety-six-well plates were coated with 5 ng/well of the corresponding $F_{1/11/13}$-BSA conjugate, or unconjugated BSA as a control, diluted in 50 mM Na_2CO_3, pH 9.6 (Sigma-Aldrich, St. Louis, MO). Plates were blocked with 1% porcine gelatin for 1 hr at room temperature. Plates were then incubated with diluted serum samples for 90 min at room temperature with shaking, then an additional 30 min at room temperature without shaking. Plates were washed and incubated with an HRP-conjugated goat anti-rat IgG overnight at 4°C (1:50,000, Jackson ImmunoResearch Laboratories). The following day, plates were developed with enzyme substrate *o*-phenylenediamine (OPD; SIGMA*FAST*™ tablet set, Sigma-Aldrich, St. Louis, MO). After 30 min of incubation with OPD, 2% oxalic acid was added to stop the enzymatic reaction. Plates were read at 492 nm on a Tecan Infinite M1000 PRO microplate reader. Titers are reported as the dilution producing 50% maximal binding (EC_{50}).

Analysis of antibody-bound and -unbound (free) fentanyl and carfentanil concentration in serum and tissue. After the last drug challenge**,** mice or rats were euthanized for collection of serum, brain, heart and/or lungs for *post mortem* analysis of carfentanil or fentanyl concentrations. To obtain drug concentrations (total, bound and unbound), tissue extraction and analysis by LCMS/MS were performed as described previously (55). Additional steps were performed to obtain unbound (free) drug concentrations in lung and heart tissue. Nanosep filter units (10 kDa cutoff, Pall Life Sciences, Port Washington, NY) were pre-treated with 5% Tween-20 in distilled water for 1 hr at room temperature and then rinsed with distilled water to minimize hydrophobic interactions. Lung or heart homogenate samples were then centrifuged in the filter units at 10,000 x g at room temperature for 1 hr. Unfiltered samples (total opioid) and flow

through from the filter unit (unbound opioid) were analyzed via LCMS/MS. Drug concentrations were determined using an Agilent G6470A triple quadrupole LCMS/MS system consisting of an Infinity II 1290 G7116B Multicolumn Thermostat, G7120A High Speed Quad Pumps, and a G7267B Multisampler. Data acquisition and peak integration were analyzed using Mass Hunter software (Tokyo, Japan). Percent unbound was calculated as (unbound opioid/total opioid)*100%.

Statistical analysis. Mean latency to respond on the hotplate, oxygen saturation, respiratory rate, and heart rate were analyzed by two-way ANOVA with Geisser-Greenhouse correction followed by Dunnett's or Bonferroni's multiple comparisons *post-hoc* test. Drug concentration in tissue, antibody bound/unbound analysis, and antibody titers were analyzed by one-way ANOVA paired with Tukey's multiple comparisons *post-hoc* test. Statistical analyses were performed using Prism v.9 (GraphPad, La Jolla, CA).

RESULTS

A carfentanil-based hapten protects against carfentanil-induced respiratory depression. To assess the efficacy of vaccine formulations containing the novel carfentanil-based haptens F_{11} and F_{13} (**Figure 1**), rats were immunized intramuscularly (i.m.) on days 0, 21, and 42 with CRM, F_1-CRM, F_{11}-CRM, or F_{13}-CRM adsorbed on alum. All active vaccine formulations induced detectable serum IgG antibody titers for the cognate hapten (**Figure 6**). A week after the third immunization, rats were challenged s.c. with carfentanil (0.02 mg/kg) and assessed for drug-induced antinociception, respiratory depression, and bradycardia. Rats immunized with F_{13}-CRM were the only group to show any attenuation of antinociception after carfentanil challenge, although this difference is not statistically significant (**Figure 2A**). All other immunized groups were identical to the control. When assessing protection against other opioid-induced pharmacological effects, F_{13}-CRM prevented carfentanil-induced respiratory depression relative to control at most time points (**Figure 2B**). In contrast, rats immunized with F_{11}-CRM attained significantly attenuated respiratory depression only at 30 min post-challenge. No differences were seen between any groups when assessing carfentanil-induced bradycardia (**Figure 2C**). While F_1-CRM has been previously shown to protect against fentanyl and sufentanil (55), it did not protect against carfentanil. These data suggest that the F_{13}-CRM conjugate vaccine protects against selected pharmacological and behavioral effects of carfentanil.

A carfentanil-based hapten may cross-protect against fentanyl. Because of the increasing involvement of fentanyl analogues in drug-related overdoses, it is important to identify possible cross-reactivity of lead haptens within the fentanyl-like chemical family to assess the potential of individual vaccines for cross-protection. Previous studies have

demonstrated the feasibility of targeting both fentanyl and carfentanil with the same hapten structure (59). Here, the same rats were challenged s.c. with 0.1 mg/kg fentanyl, and immunization with F_1-CRM protected against fentanyl-induced antinociception, respiratory depression, and bradycardia (**Figure 2D-F**). Rats immunized with F_{13}-CRM also showed significant protection against fentanyl-induced respiratory depression at 15 min post-drug challenge (**Figure 2E**). These results indicate that the F_{13} hapten may target both carfentanil and fentanyl, warranting further investigation.

Vaccine efficacy against a mixture of fentanyl and carfentanil. Because of the potential efficacy of F_{13} against both fentanyl and carfentanil, rats were then re-challenged s.c. with a mixture of fentanyl (0.05 mg/kg) and carfentanil (0.01 mg/kg) delivered as a single bolus. While no groups were significantly protected against the behavioral effects of the fentanyl/carfentanil mixture, rats immunized with F_{13}-CRM trended towards protection as reported by the hot plate test ($p=0.0612$ at t=45 min; $p=0.1090$ at t=60 min) and oximetry measures ($p=0.0544$ at t=45 min and $p=0.0453$ at t=60 min) relative to all other groups (**Figure 2G, 2H**). Significant differences in heart rate were found only at 60 min post-challenge (**Figure 2I**). After 60 min, rats were rescued with naloxone (0.1 mg/kg, s.c), and all immunized groups returned to baseline in all parameters tested, indicating that fentanyl- and carfentanil-specific antibodies do not interfere with naloxone rescue of opioid-induced effects.

Anti-carfentanil vaccines prevent distribution of carfentanil to the brain. To assess the dose-response relationship of carfentanil and its effects on antinociception and respiratory depression, rats were administered carfentanil (0.005 mg/kg, s.c.) every 15

min up to a cumulative dose of 0.02 mg/kg. Antinociception and pulse oximetry were measured at each time point before the subsequent injection. Both F_{11}- and F_{13}-CRM offered protection against carfentanil-induced antinociception at 0.005 mg/kg carfentanil when compared to CRM immunized controls, with F_{13}-CRM also protecting against doses up to 0.015 mg/kg (**Figure 3A**). At 0.015 mg/kg, groups immunized with either F_{11}-CRM or F_{13}-CRM had significantly higher oxygen saturation compared to control (**Figure 3B**), and F_{13}-CRM immunized animals also displayed significantly higher heart rate (**Figure 3C**). Fifteen minutes after the final carfentanil dose, animals were euthanized and serum, brain, heart and lungs were collected to determine the concentration of carfentanil in each organ. All immunized groups showed a significantly lower brain:serum carfentanil ratio compared to control, indicating that antibodies produced from active immunization retained the drug in the serum and prevented its distribution to the brain. Groups immunized with F_{11} and F_{13} displayed significantly lower brain:serum ratios of carfentanil compared to the F_1-CRM group. The group immunized with F_{13}-CRM displayed an increased carfentanil concentration in the heart and lungs compared to control or F_1-CRM immunized groups, likely due to an increase in the antibody-bound fraction of drug in either serum, extracellular fluids, or parenchyma. Together, these data show that active immunization alters the distribution of carfentanil to the brain, and possibly other target organs such as the heart and lungs, which attenuates carfentanil-induced pharmacological effects.

Comparison of bivalent vaccination strategies in protecting against the behavioral and pharmacological effects of carfentanil, fentanyl, and their mixture. An independent follow-up study conducted in a second cohort of rats tested the hypothesis

that bivalent vaccination with F_1-CRM and F_{13}-CRM would protect against carfentanil, fentanyl, and their mixture to a greater degree than each individual vaccine. In this study, rats were immunized on days 0, 14, 28, and 42 with either individual F_1-CRM or F_{13}-CRM conjugates (monovalent), or both F_1- and F_{13}-CRM co-administered as individual vaccinations on either hind leg (bivalent co-administration, or Co). The co-administration strategy consisted of immunization with half doses of each individual vaccine to equal the total conjugate and alum dose used in monovalent vaccination. An additional treatment group tested whether a heterologous vaccination strategy, consisting of alternating full doses of either F_1-CRM or F_{13}-CRM every two weeks (bivalent heterologous, or Het), would enhance protection against the pharmacological effects of carfentanil, fentanyl, or their mixture. The monovalent, co-administered, and heterologous vaccinations strategies provided rats with an equal total dose of protein. Antibody titers against both F_1 and F_{13} were detected on day 49 (**Figure 6**) and showed that co-administration did not interfere with the generation of antibodies to either hapten. Rats were then challenged with multiple drugs over the next three weeks, with drugs administered each week randomized among groups to reduce the potential confounding effects of tolerance. As expected, rats vaccinated with F_1-CRM were significantly protected against the antinociceptive effects of fentanyl (0.1 mg/kg, s.c.). Interestingly, rats that received the co-administered immunization with both F_1- and F_{13}-CRM were protected against fentanyl-induced antinociception at 30-, 45-, and 60- min post-drug challenge, and trended toward protection ($p=0.0798$) at 15 min (**Figure 4A**). Rats immunized with F_1- and F_{13}-CRM on a heterologous immunization schedule were only protected against the antinociceptive effects of fentanyl at 45- and 60- min post-exposure. When assessing fentanyl-induced respiratory depression (**Figure 4B)** and bradycardia (**Figure 4C**), co-administered vaccination afforded protection against fentanyl-induced respiratory depression at 30- min

post-drug exposure, similar to rats that received F_1-CRM. However, both bivalent immunization strategies trended towards protection at all time points [At t=15, p=0.0567 (Het) and p=0.0570 (Co); At t=45, p=0.0684 (Het) and p=0.0634 (Co); At t=60, p=0.1010 (Het) and p=0.1634 (Co)]. Following a carfentanil challenge (0.02 mg/kg, s.c), rats immunized with F_{13}-CRM were protected against carfentanil-induced respiratory depression, as expected (**Figure 4E**). While not statistically significant, the co-administered immunized group displayed early trends in protection (p=0.1513 at t=15 min) against carfentanil-induced respiratory depression (**Figure 4E**). No differences in carfentanil-induced antinociception (**Figure 4D**) or bradycardia were detected (**Figure 4F**).

After challenge with fentanyl (0.05 mg/kg, s.c) combined with carfentanil (0.01 mg/kg, s.c), only the co-administered bivalent group was significantly protected against drug-induced antinociception at all time points post-exposure (**Figure 4G).** When assessing respiratory depression, rats immunized with F_{13}-CRM or the co-administered bivalent regimen were significantly protected from respiratory depression at most time points, while the heterologous immunized group trended towards protection (p=0.0804 at t=15 min) at early timepoints (**Figure 4H**). Similar to the carfentanil challenge, no differences were found between any group when measuring heart rate, except for the latest timepoint (**Figure 4I**). These data suggest that bivalent immunization strategies can protect against the pharmacological effects of carfentanil, fentanyl, or their mixture, and that co-administration may be more effective than heterologous immunization.

Bivalent immunization strategies alter the distribution of higher doses of fentanyl and carfentanil to key organs. Rats were challenged with a final mixture of 0.1 mg/kg

fentanyl and 0.02 mg/kg carfentanil (2x dose from the original dual challenge). Oxygen saturation and heart rate were measured at 30-min post-challenge, and then blood, brain, lungs, and heart were collected to measure opioid concentrations in each compartment. At this higher dose, no differences in respiratory depression and bradycardia were detected across groups (data not shown), but there was a significant reduction in brain:serum ratio of carfentanil or fentanyl in all groups immunized with either the F_{13} hapten or the F_1 hapten, respectively (**Figure 5A, B**). Carfentanil and fentanyl concentrations were also increased in the heart (**Figure 5C, D)** and lungs **(Figure 5G, H**) in groups immunized with either the F_{13} or F_1 haptens. In these organs, there was a significant decrease in unbound (free circulating) fentanyl in the F_1 monovalent and bivalent immunized groups and a decrease in unbound carfentanil in the F_{13} monovalent and bivalent immunized groups, indicating that most of the drug circulating in these organs is antibody-bound (**Figure 5E, F, I, J**). While it is not clear whether antibody-bound complexes would reside in blood, extracellular fluids, or parenchyma, these data are consistent with previous reports of nicotine bound in the heart, lungs, and other tissues (229, 230). These results indicate that a bivalent vaccination strategy that combines fentanyl- and carfentanil-based haptens may enhance cross-protection against both drugs alone and in combination when compared to monovalent vaccination strategies.

INI-4001 increases the efficacy of a lead carfentanil vaccine. *(Note: These data are an addendum in that they were not included in the original manuscript, but belong within the context of this specific line of investigation).* Because we have previously reported an increase in vaccine efficacy with the addition of a novel TLR7/8 adjuvant in combination with a lead fentanyl (F_1-CRM) or heroin (M-sKLH) vaccine, we tested whether addition of

INI-4001 would similarly increase the efficacy of the newly identified lead carfentanil vaccine, F_{13}-CRM. Immunized mice displayed significantly increased F_{13}-specific antibody titers with the addition of INI-4001 compared to alum alone (**Figure 7A**). Additionally, after challenge with 0.02 mg/kg s.c. carfentanil, there was a significantly increased serum:brain ratio of carfentanil in groups given the INI-4001 adjuvanted F_{13}-CRM (**Figure 7B**), indicating that the vaccine is decreasing distribution of carfentanil to the brain. Taken together, these data suggest that INI-4001 does increase the efficacy of a lead carfentanil vaccine, and further supports our data indicating that INI-4001 is a broadly effective adjuvant for increasing the efficacy of anti-opioid vaccines.

DISCUSSION

Vaccines may offer a viable approach to prevent overdose related to carfentanil, fentanyl, and their mixtures. Previous studies showed that vaccines containing carfentanil-based haptens are effective at reducing antinociception, respiratory depression, and distribution of carfentanil to the brain after drug challenge (59). This study reports the development of vaccines containing two novel carfentanil-based F_{11} and F_{13} hapten structures with varying linker lengths (**Figure 1**), which were conjugated to CRM, a carrier protein suitable for further product development (231), and adsorbed to a commercially available aluminum adjuvant commonly used in marketed vaccine formulations. Similar to F_1, both F_{11} and F_{13} haptens lack the *N*-phenethyl substituent, and thus are considered unscheduled by the Drug Enforcement Agency (*Pravetoni, personal communication*). F_{11} contains a 5-atom linker displaying an amino terminal group suited for conjugation to aspartic and glutamic acid residues on the carrier protein, while F_{13} contains an 18-atom long tetraglycine linker displaying a carboxyl group suitable for lysine-reactive

conjugations (**Figure 1**). Both haptens were conjugated to CRM by carbodiimide chemistry, which yielded similar haptenation ratios (F_{11}-CRM=10; F_{13}-CRM=12), minimizing concerns for direct comparison due to their similar molecular weight, number of haptens displayed on the carrier, or relative conjugation efficiency. Given that F_{13} outperformed F_{11} *in vivo*, it is likely that the longer linker length enabled the accessibility of the carfentanil moiety and the carrier structure to be recognized by hapten-specific B and cognate carrier-specific $CD4^+$ T cell lymphocytes after immunization. The importance of the linker length has been noted with other vaccines against OUD and substance use disorders (26, 133, 232), and may inform design of future haptens derived from other opioids, psychostimulants, or designer drugs.

Antibodies elicited by F_{13} had significant cross-reactivity with the F_1 hapten, while the F_1 hapten had almost no cross-reactivity to the F_{13} hapten, which is consistent with the *in vivo* efficacy data for F_1-CRM and F_{13}-CRM. The F_{13} hapten produced significantly higher antibody titers than F_1 when each was tested against its cognate coating antigen (**Figure 6**). While comparisons of ELISA data resulting from different coating antigens should be interpreted with caution, this may suggest that the F_{13} hapten is generally more immunogenic than F_1, perhaps due to the increased number of polar residues within the hapten itself, which could potentially result in greater engagement of hapten-specific B cell receptors (BCR). Although in the context of carfentanil, F_{13} proved superior to F_1, F_1 was still the more effective hapten against fentanyl, and possibly other analogues (55). Hence, in an attempt to target fentanyl and carfentanil simultaneously, this study tested the efficacy of bivalent vaccine formulations that combine F_1-CRM and F_{13}-CRM.

Multivalent immunization is an appealing strategy to address multiple drug targets simultaneously, bypassing a limitation of current pharmacotherapies for SUDs. To date,

bivalent or trivalent immunization strategies have shown proof of principle against nicotine (233, 234), heroin/fentanyl (38, 53, 67), and heroin/oxycodone (28, 183), but our understanding of how to best deploy multivalent vaccines in the context of OUD and other SUDs is still limited. For instance, it is not clear if divalent presentation of structurally unrelated haptens on the same carrier protein is a viable strategy to circumvent the need for admixing two individual conjugate vaccines in the same formulation (40, 66). The current study showed that when comparing antibody titers from bivalent vaccination strategies, co-administration produced significantly higher F_{13}-specific antibody titers compared to heterologous immunization, while F_1-specific titers were similar between the two groups. This discrepancy may be because a bivalent co-administration strategy simultaneously engages both overlapping and non-overlapping B cell populations specific for one antigen or the other, while a heterologous prime/boost strategy introduces one antigen at a time, which may refine the antibody specificity towards those that are specific for both fentanyl and carfentanil at the expense of higher titers. While F_1 was used for the initial antigen followed by an F_{13} boost in the heterologous immunization strategy, it would be of interest to test whether priming with an antigen of potentially higher immunogenicity (e.g., F_{13}) would further increase the antibody concentration or narrow the selectivity of the polyclonal antibody responses towards an immunodominant epitope or antigen. Despite the differences seen in antibody titers, *in vivo* results suggest that either strategy could be effective at reducing carfentanil's centrally mediated effects. Future studies will determine whether multiple individual vaccines could be co-administered in the same vehicle without interfering with their respective properties.

The *in vivo* pharmacokinetics of carfentanil are relatively understudied. One published study showed that administration of high doses of carfentanil (>0.01mg/kg) cause non-linear accumulation and impaired clearance in rats (235). The authors

postulated this to be one of the main causes of the toxicity and life-threatening effects associated with carfentanil. Consistently, the behavioral effects of carfentanil were longer-lasting than fentanyl in non-human primate models of self-administration (236), which provides additional evidence of the longer half-life of fentanyl analogues. The carfentanil doses used for the current study ranged from 0.01-0.02 mg/kg in most cases, exceeding the limit needed for non-linear accumulation. Despite this, rats immunized with the carfentanil-based hapten F_{13} showed attenuation of respiratory depression after carfentanil challenge, indicating that immunization and subsequent neutralization of carfentanil in the serum via antibody binding may prevent the toxic effects associated with non-linear accumulation. Published literature shows that opioids in immunized animals persist in the serum for much longer than controls (29), suggesting that antibody-bound opioid is protected from metabolism. In this case, antibody-bound carfentanil may prevent impaired clearance by neutralizing a portion of the serum carfentanil and allowing for linear accumulation and clearance similar to what is observed at lower carfentanil doses. As the potentially unusual pharmacokinetics of carfentanil are studied in further detail, it will also be necessary to determine how the addition of carfentanil-specific antibodies through active or passive immunization change these pharmacokinetic properties. For instance, we have previously reported that immunization with OUD vaccines increases antibody-bound opioid in the serum, reducing the free circulating opioid (34, 35, 41). This study extended these findings by showing that vaccination resulted in a decrease in free circulating fentanyl and carfentanil in the heart and lungs, which may contribute to protection against drug-induced effects on respiratory and cardiovascular functions. Previous reports showed that nicotine vaccines elicit functional drug-specific antibody IgG and IgA responses in various organs including the lungs (229, 230). Consistently, the current results suggest that vaccine-induced antibodies may be effective in decreasing the

unbound fentanyl and carfentanil circulating within the lungs and heart vasculature or parenchyma.

Despite showing considerable efficacy at attenuating carfentanil-induced antinociception and respiratory depression, the vaccines tested remained largely ineffective at reducing carfentanil-induced bradycardia. While most opioids have been shown to induce some level of bradycardia after administration, published literature shows that the relative doses needed to induce bradycardia can vary between opioids (237). There are few papers investigating the dose-response relationships of different pharmacological effects of carfentanil (235, 238), but our current data may suggest that bradycardia is induced preferentially and/or at lower doses as compared to analgesia or respiratory depression, making it resistant to attenuation by active immunization. Comprehensive studies detailing carfentanil's dose-dependent pharmacological effects, including its reinforcing effects, will be needed in order to fully understand and develop effective medications against this extremely potent opioid.

As the illicit use of carfentanil and other highly potent opioids increases, development of effective therapeutics is needed to prevent toxicity or overdose due to accidental or deliberate exposure in drug users, medical workers, first responders, or military personnel. While the approval of naloxone for reversal of opioid overdose has saved countless lives, naloxone may not be as effective in reversing the effects of highly potent opioids. Development of vaccines that can induce the production of antibodies that prevent opioids from entering the brain is a novel strategy that may be more effective with highly potent opioids due to the favorable molar ratio of drug molecules to antibody binding sites. Here, the development and testing of a pair of novel anti-carfentanil conjugate vaccines are described. We found that F_{13}-CRM was more effective than F_{11}-CRM at

attenuating the effects of carfentanil, fentanyl, or their mixture. We then tested the effectiveness of F_{13}-CRM to be administered in tandem with a lead fentanyl vaccine (F_1-CRM) and found that either co-administered or heterologous immunization strategies further increased cross-protection against both drugs, with co-administration being more effective than heterologous immunization. Additionally, we found that F_{13}-CRM can be combined with a lead TLR7/8 agonist adjuvant, INI-4001, to increase vaccine efficacy against carfentanil. These studies inform and justify further development and clinical testing of F_{13}-CRM as a lead anti-carfentanil vaccine in single and multivalent formulations to reduce the incidence of carfentanil overdose in subjects at risk of exposure.

FIGURES

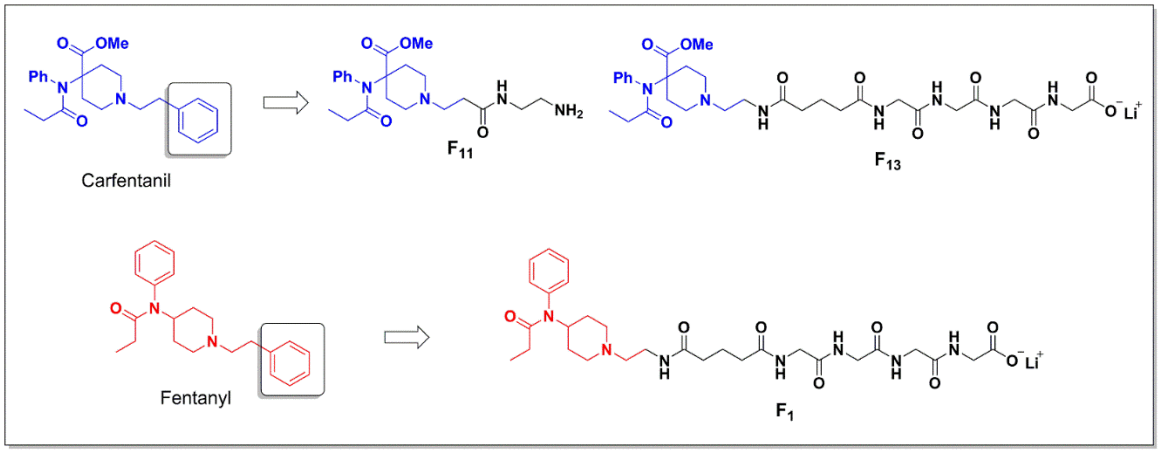

Figure 1. Haptens targeting fentanyl (F_1) and carfentanil (F_{11} and F_{13}).

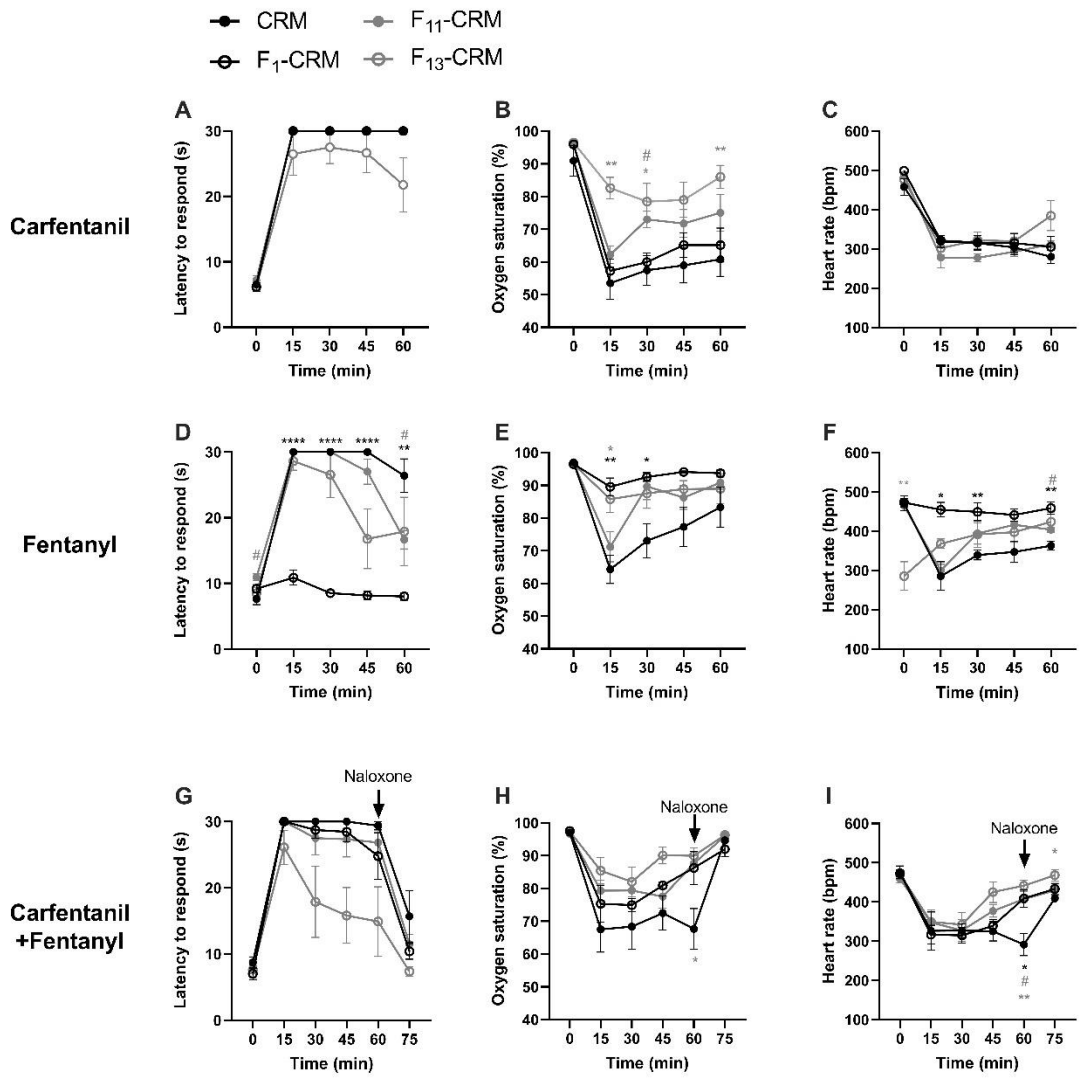

Figure 2. Immunization with F_{13}-CRM protected against carfentanil- and fentanyl-induced respiratory depression. Following a baseline measurement, immunized male Sprague Dawley rats (n=6 per group) were challenged s.c. with 0.02 mg/kg carfentanil and tested every 15 min for (A) antinociception via latency to respond on a hot plate, (B) respiratory depression reported as the percent (%) oxygen saturation measured by pulse oximetry, and (C) bradycardia reported as heart rate (beats per minute, bpm). The same cohort was challenged s.c. with 0.1 mg/kg fentanyl and tested every 15 min for (D)

antinociception, (E) respiratory depression, and (F) bradycardia. Finally, rats were challenged s.c. with a mixture of 0.05 mg/kg fentanyl and 0.01 mg/kg carfentanil delivered as a single bolus and tested every 15 min for (G) antinociception, (H) respiratory depression, and (I) bradycardia. Naloxone (0.1 mg/kg) was administered at 60 min and its effects were assessed 15 min later. Data are presented as mean ± SEM. Statistical analysis was performed via two-way ANOVA paired with Dunnett's (B, C, E, F, G-I) or Bonferroni's (A, D) multiple comparisons *post hoc* tests. Statistical symbols: ****p<0.0001 ** or ** (gray) p<0.01, * or * (gray) or # (gray) p<0.05. Placement of * indicate significance between F_1-CRM and CRM, # (gray) indicate significance between F_{11}-CRM and CRM, and * (gray) indicate significance between F_{13}-CRM and CRM.

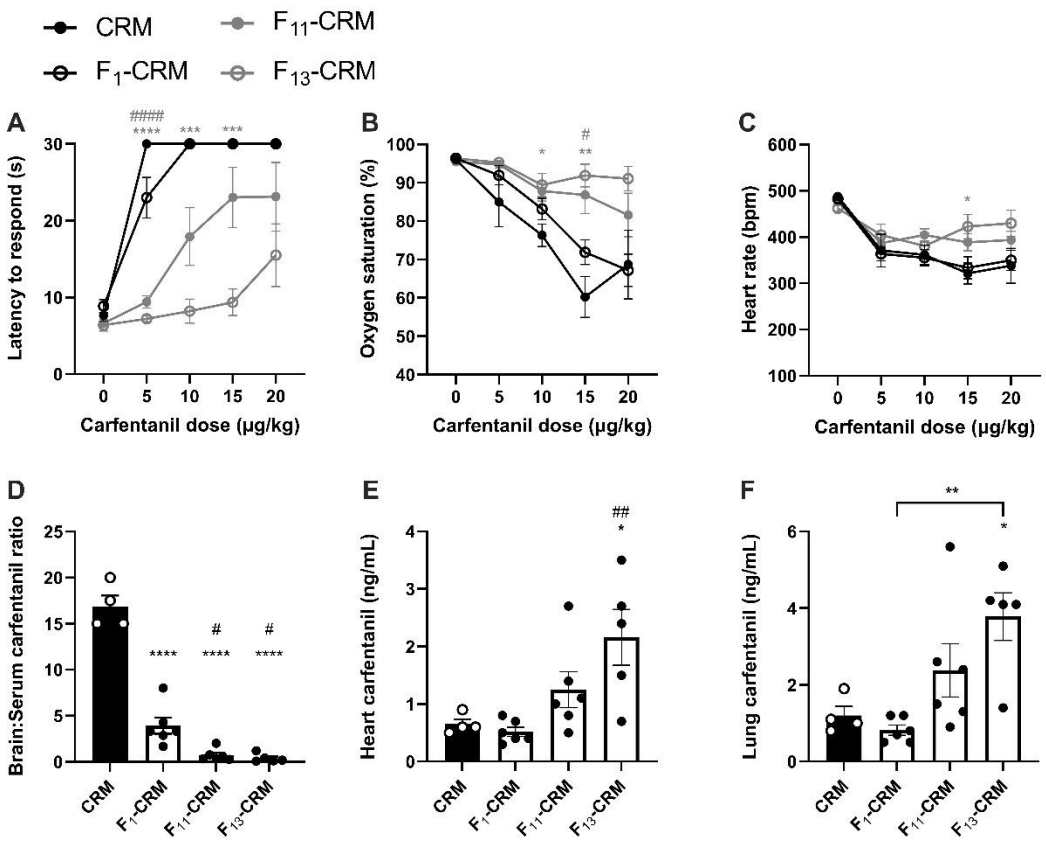

Figure 3. Vaccination alters the distribution of carfentanil to key organs. Following a baseline measurement, immunized male Sprague Dawley rats (n=4-6 per group) were repeatedly challenged s.c. with 5 µg/kg carfentanil every 15 min and tested every 15 min for (A) antinociception, (B) oxygen saturation (%), and (C) heart rate (bpm). At 15 min after the final dose, rats were euthanized, and organs were collected to analyze the distribution of carfentanil. (D) Ratio of carfentanil in the brain versus the serum, and concentration of carfentanil in the (E) heart, and (F) lungs. Data are presented as mean ± SEM. Statistical analysis was performed via one- or two-way ANOVA paired with Tukey's (D-F) Dunnett's (B,C), or Bonferroni's (A) multiple comparisons post hoc test. Statistical symbols: **** or **** (gray) or #### (gray) p<0.0001, *** or *** (gray) p<0.001 ## or ** (gray) p<0.01, # or * (gray) or # p<0.05. Placement of * above columns indicate significance compared to

control. # above columns indicate significance compared to F_1-CRM. # (gray) indicates significance between F_{11}-CRM and CRM, while * (gray) indicate significance between F_{13}-CRM and CRM.

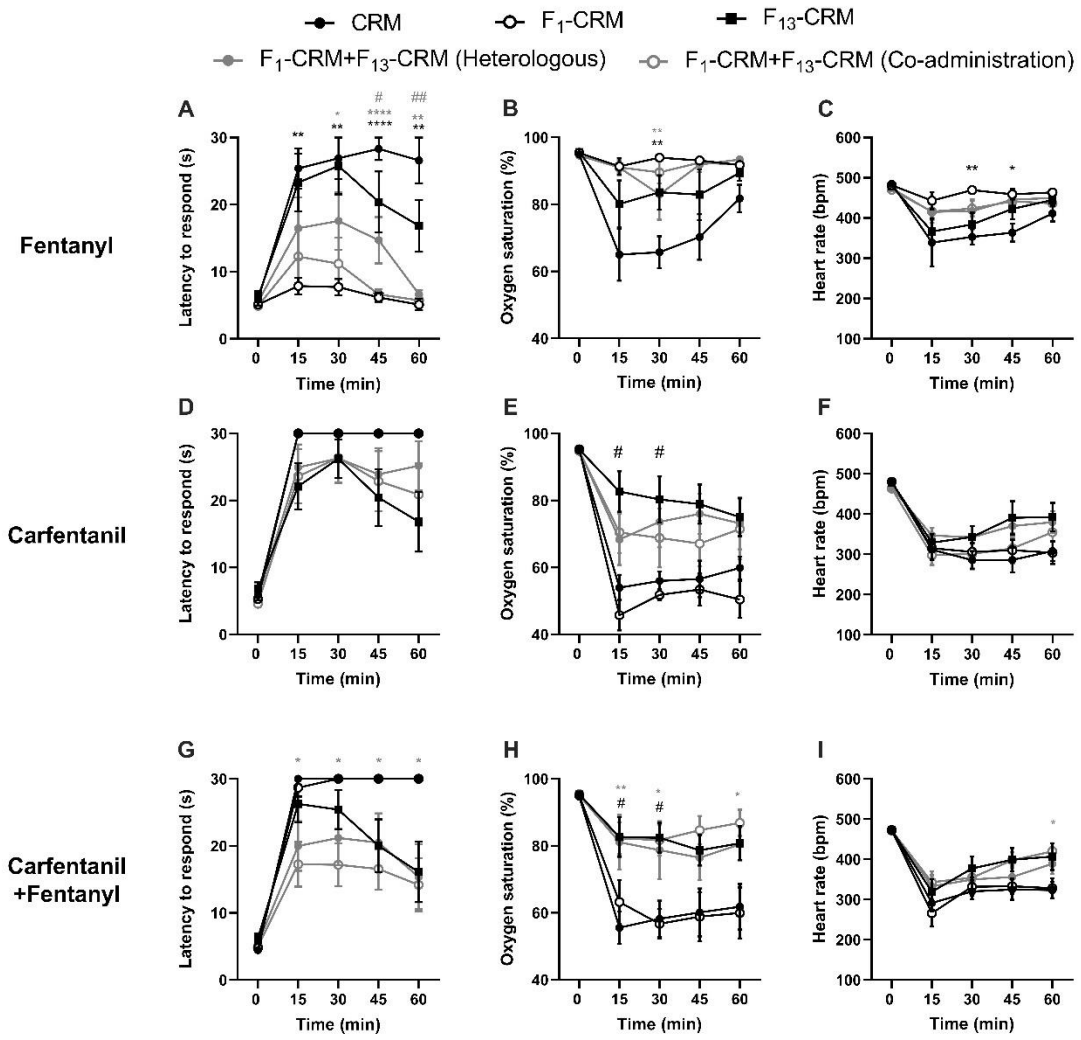

Figure 4. Bivalent vaccination strategies may enhance protection against the pharmacological effects of both carfentanil and fentanyl. Rats were vaccinated with F_1-CRM, F_{13}-CRM, or both in either a co-administered (Co) or heterologous (Het) vaccination schedule every 2 weeks for a total of 4 vaccinations. Following a baseline measurement, rats (n=4-6 per group) were challenged s.c. with 0.1 mg/kg fentanyl and tested every 15 min for (A) antinociception, (B) oxygen saturation (%), and (C) heart rate (bpm). The same cohort of rats was challenged s.c. with 0.02 mg/kg carfentanil and tested every 15 min for (D) antinociception, (E) respiratory depression and (F) bradycardia.

Finally, rats were challenged with a combined s.c. bolus dose of fentanyl (0.05 mg/kg) and carfentanil (0.01 mg/kg). Every 15 min, rats were tested for (G) antinociception, (H) respiratory depression and (I) bradycardia. Data are presented as mean ± SEM. Statistical analysis was performed via two-way ANOVA paired with Dunnett's (A-C, E, F, H, I) or Bonferroni's (D, G) multiple comparisons post hoc test. Statistical symbols: **** (gray) or ****p<0.0001, ## (gray) or ** (gray) or **p<0.01, # or # (gray) or * (gray) or *p<0.05. Placement of * indicates significance between F_1-CRM and CRM, # indicates significance between F_{13}-CRM and CRM, # (gray) indicates significance between heterologous and CRM, and * (gray) indicates significance between co-administration and CRM.

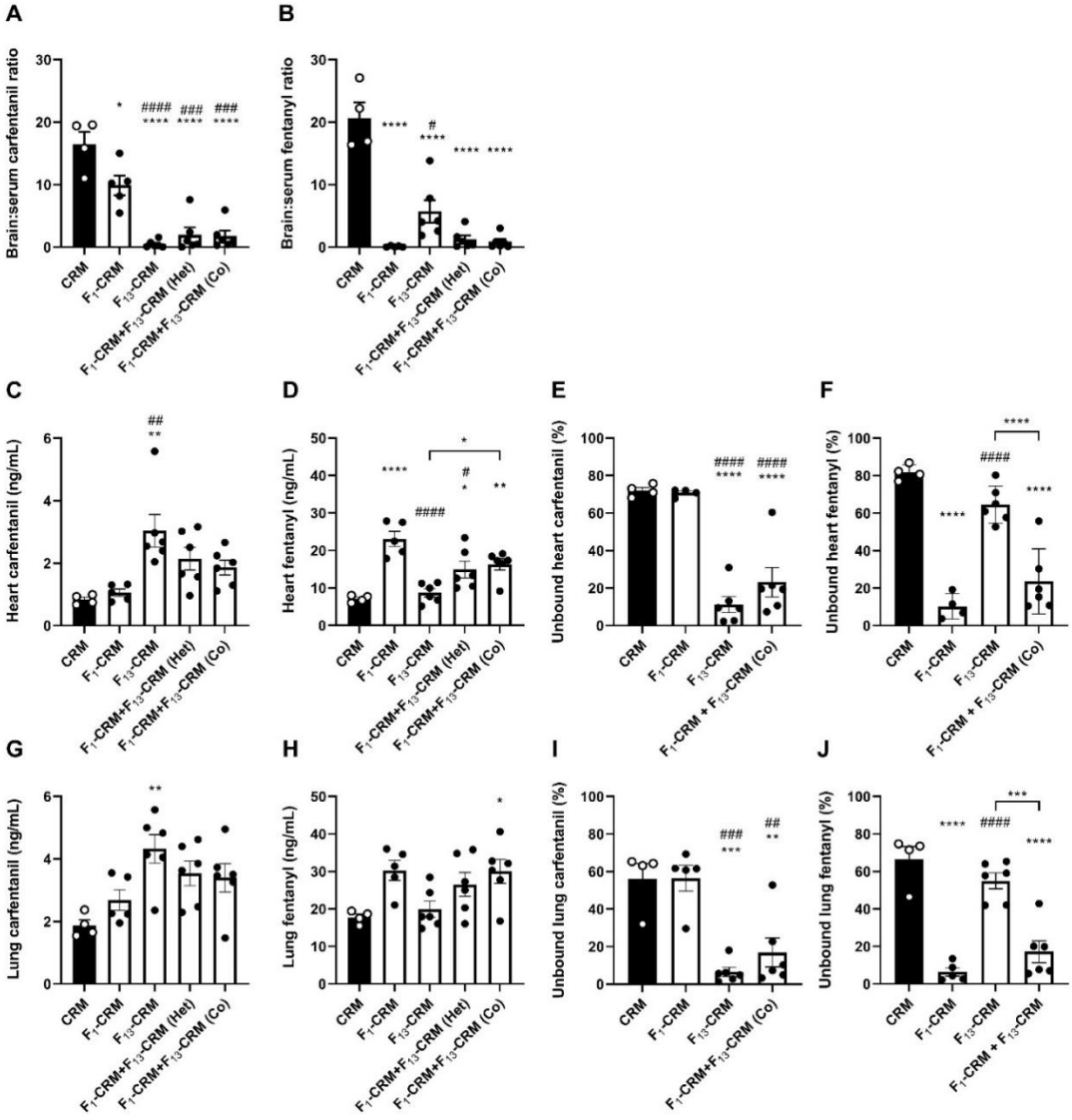

Figure 5. Bivalent immunization strategies alter the distribution of carfentanil and fentanyl to key organs. Immunized rats (n=4-6 per group) were challenged with a combined s.c. bolus dose of 0.1 mg/kg fentanyl and 0.02 mg/kg carfentanil. After 30 min, serum, brain, lungs, and heart were collected. Shown: (A) brain:serum ratio of carfentanil and (B) brain:serum ratio of fentanyl. Hearts were analyzed for (C) total carfentanil concentration (bound + unbound), (D) total fentanyl concentration (bound + unbound), (E) unbound (free circulating) carfentanil as a percent of total carfentanil, and (F) unbound

fentanyl as a percent of total fentanyl. Lungs were analyzed for (G) total carfentanil concentration (H) total fentanyl concentration, (I) unbound carfentanil as a percent of total carfentanil, and (J) unbound fentanyl as a percent of total fentanyl. Data are presented as mean±SEM. Statistical analysis was performed via one-way ANOVA paired with Tukey's multiple comparisons post hoc test. Symbols: #### or **** p<0.0001, ### *p*<0.001, ## or **p<0.01, # or * p<0.05. Placement of * above columns indicate significance compared to control or as indicated by brackets, # indicates significance compared to F_1-CRM.

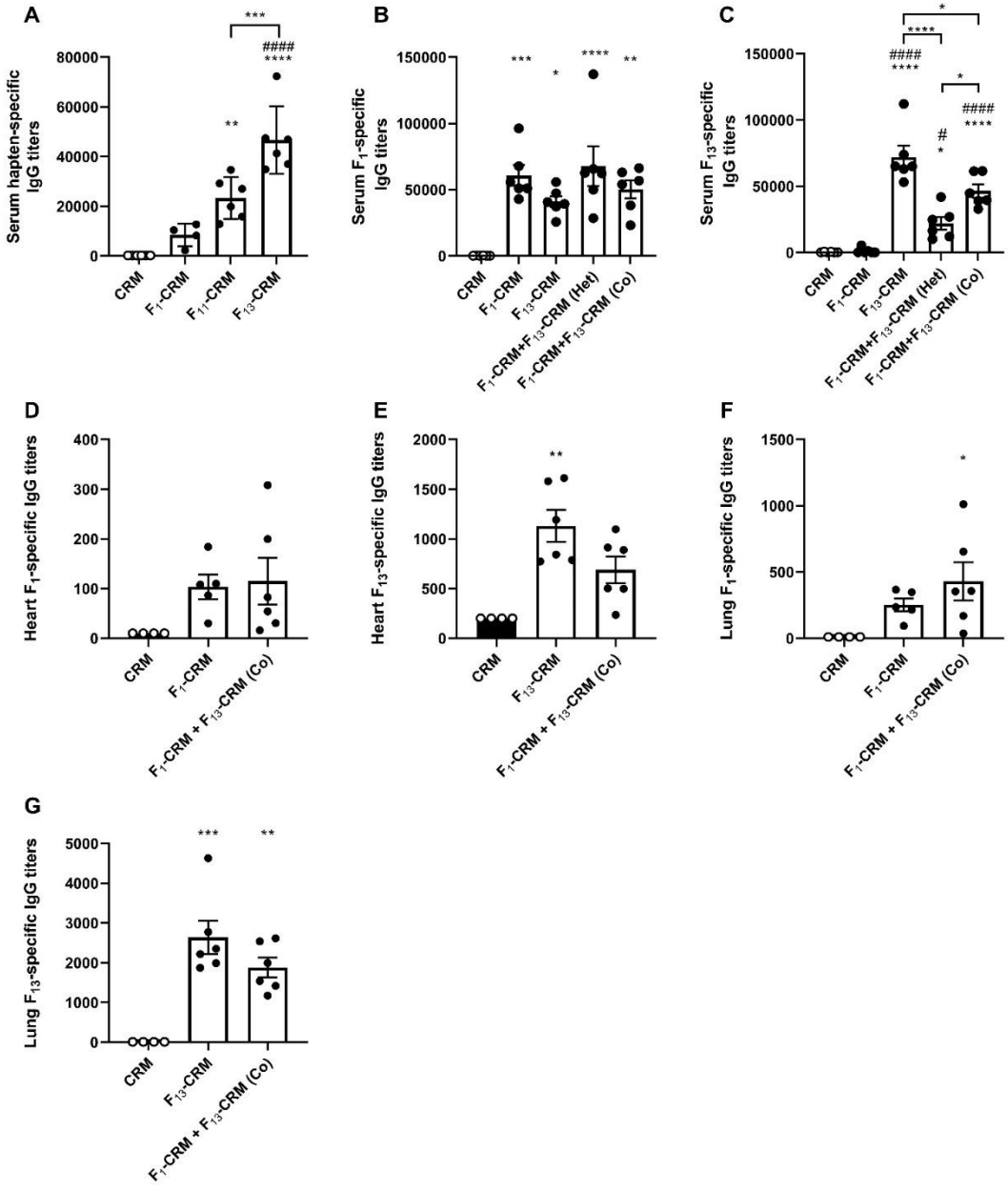

Figure 6. Hapten-specific IgG antibody titers in serum, heart, and lungs of vaccinated rats. One week after the final immunization, tail blood was collected from rats (n=4-6/group) to measure hapten-specific IgG titers via ELISA. (A) Serum hapten-specific IgG titers in each vaccination group in the first study were measured using the cognate F_1-, F_{11}-, F_{13}-BSA conjugates as coating antigens. Serum hapten-specific IgG titers from

the second study were measured using (B) an F_1-BSA coating antigen to measure fentanyl-specific IgG titers or (C) F_{13}-BSA coating antigen to measure carfentanil-specific IgG titers. Individual heart and lung homogenates from the second study were analyzed for IgG titers specific for either the (D, F) F_1 or (E, G) F_{13}-haptens. Data are presented as mean±SEM. Statistical analysis was performed via one way ANOVA paired with Tukey's multiple comparisons *post hoc* test. * over columns indicate significance compared to control or as indicated with brackets. # over columns indicate significance compared to F_1-CRM. Statistical symbols: **** or #### $p<0.0001$, ***$p<0.001$, **$p<0.01$, *$p<0.05$.

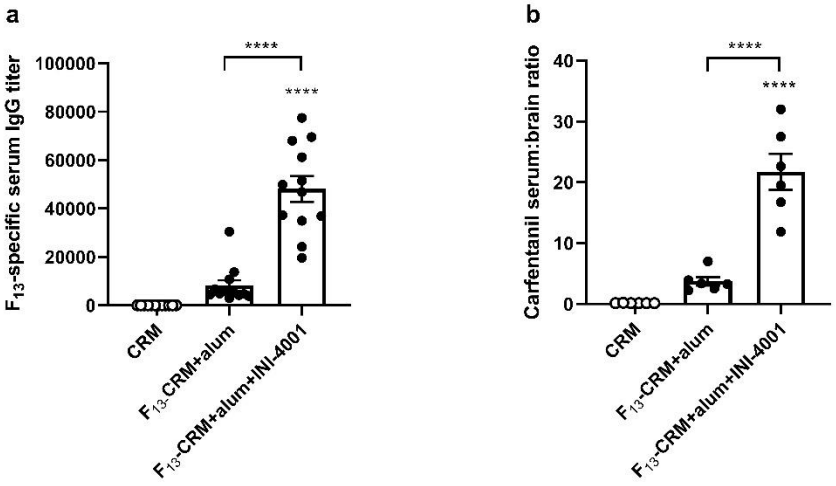

Figure 7. INI-4001 increases the efficacy of a lead carfentanil vaccine. Mice (n=6/group) were immunized on days 0, 14, and 28 with 5 µg F_{13}-CRM+24 µg alum with or without 10 µg INI-4001, or 5 µg CRM as a negative control. On day 34, serum was collected to assess A) F_{13}-specific serum IgG titers via ELISA. On day 35, mice were challenged with 0.02 mg/kg carfentanil s.c., and brain and serum were collected 30 minutes post challenge. B) Serum:brain carfentanil concentration ratio after drug challenge. Statistical analysis was performed via one way ANOVA paired with Tukey's multiple comparisons *post hoc* test. * over columns indicate significance compared to control or as indicated with brackets.

Chapter 5: Environmental factors contributing to anti-opioid vaccine efficacy

The goal of this study was to assess whether changes in the gastrointestinal (GI) microbiome would affect efficacy of vaccines against oxycodone or fentanyl. As opioid users often have gut dysbiosis due to their drug use, these results are an important step to determine whether microbiome changes may affect clinical efficacy of OUD vaccines. Additionally, if specific changes in the gut microbiome could be associated with vaccine efficacy, these would represent putative biomarkers in OUD vaccine clinical studies.

This is an 'Accepted/Original Manuscript' of an article published by Taylor & Francis Group in Human Vaccines & Immunotherapeutics on Nov. 2, 2021, available online: https://www.tandfonline.com/doi/full/10.1080/21645515.2021.1954442.

Crouse B, Zhang L, Robinson C, Ban Y, Vigliaturo JR, Roy S, Pravetoni M. Housing conditions and microbial environment do not affect the efficacy of vaccines for treatment of opioid use disorders in mice and rats. *Hum Vaccin Immunother*, (2021).

Author Contributions: BC designed and executed studies and analyzed data, ZL executed and analyzed studies looking at GI microbiome, CR designed and executed studies, YB executed and analyzed studies looking at GI microbiome, JRV analyzed data relating to serum and brain opioid concentrations, SR executed and analyzed studies looking at GI microbiome, MP assisted with method development, interpretation of data and editing.

INTRODUCTION

The epidemic of opioid-related fatal overdoses constitutes a significant public health burden. An estimated 2 million people in the US suffer from opioid use disorder (OUD) (239) and two out of three drug overdoses in 2018 involved opioids (240). Synthetic opioids such as fentanyl and its analogues are increasingly prevalent in the community and have proven especially deadly. Synthetic opioids were responsible for 67% of opioid-related deaths in 2018 (240). During the SARS-CoV-2 epidemic, opioid-related fatal overdoses further increased, highlighting the complex interplay of OUD and other public health threats (241). Current treatments for OUD include medication-assisted therapy with drugs such as methadone, buprenorphine, or naltrexone, as well as overdose reversal using naloxone. However, these medications have an associated abuse liability and can complicate necessary pain management. Vaccines have been explored as a viable addition to the OUD-treatment repertoire and have displayed efficacy against several opioids in mice, rats, dogs, and nonhuman primates (36, 49, 74, 142, 144, 242-245). Vaccine efficacy varies between individuals and is dependent on the ability of the subject's immune system to generate high levels of drug-specific antibodies (26). Pre-clinical studies in mice have shown that sex and strain differences may have an impact on the efficacy of vaccines against heroin (72), oxycodone (160), and cocaine (246). Outside of the laboratory, there are many factors that may impact translation such as age, sex, genetics, and environmental influences. While some of these factors have been explored in the context of OUD vaccines, many others have not.

One such factor is the link between the gut microbiome and the body's immune response. Our knowledge of the relationship between the gut microbiome and our health continues to grow as more studies investigate this connection. In the context of vaccines,

gut microbiota has been shown to affect vaccine efficacy (247-249). Given that opioid use is linked to an altered gut microbiome (250-254), the potential for gut dysbiosis in the target population to receive OUD vaccines is high. Currently, most studies involving OUD vaccine efficacy involve immunization of sterile laboratory animals; however, previous literature indicates that the abnormally hygienic environment of laboratory mice may impact their immune systems. This was demonstrated by studies on “dirty mice”, which were raised outside of the sterile environment of most research animals, which resulted in more robust immune responses to infection (255). Therefore, to assess if changes in environmental microflora will affect anti-opioid vaccine efficacy, it is essential to directly compare the effect of different housing conditions on OUD vaccine efficacy. Such information will also be helpful to interpret preclinical data across laboratories using mice and rats housed under different conditions, and to ensure validity of findings across academic labs and contract research organizations (CROs) conducting GLP studies to support IND filing. Additionally, understanding the contribution that housing or the microbiome may have on therapeutic outcomes will inform clinical management of OUD patients, who may have altered flora based upon the effects of opioids on the GI tract. Finally, if specific changes in microbiota can be linked to variability in efficacy of OUD vaccines, these may be of use as predictive biomarkers of vaccine efficacy in future clinical studies.

In this study, we tested the hypothesis that sterile housing conditions would alter response to OUD vaccines due to changes in the gut microbiome. Mice and rats were housed in either specified pathogen-free (SPF) conditions (wherein a sterile barrier is kept throughout the study) or conventional housing, where no such barrier is maintained. We then assessed the effect of these housing conditions on the efficacy of oxycodone and fentanyl vaccines through examination of parameters such as the generation of drug-

specific antibodies, inhibition of antinociception, and blockage of drug distribution to the brain. Finally, we tested mice housed under different conditions for changes in the microbiome that may be related to differential housing or administration of vaccines.

MATERIALS AND METHODS

Drugs and Reagents. Oxycodone and fentanyl were obtained from the University of Minnesota Pharmacy. Drug doses and concentrations are expressed as weight of the free base. Subunit keyhole limpet hemocyanin (sKLH) was obtained as GMP-grade source (Biosyn, Carlsbad, CA).

Animals. Male BALB/c mice (Jackson Laboratories, Bar Harbor, ME) and male Sprague-Dawley rats (Envigo, Madison, WI) were housed in 14/10 hours light/dark cycle and fed *ad libitum*. Mice were 6 weeks old on arrival, while rats were 2 months old on arrival. Specified pathogen-free (SPF) animals were handled in a laminar flow hood under sterile conditions for the duration of the experiment. Conventionally housed animals were housed in a separate facility where no sterile barrier was maintained. Mice and rats were tested in the same room for vaccine efficacy against drug-induced behavioral effects. All testing occurred in the light cycle.

Vaccine formulation. The anti-oxycodone conjugate vaccine consists of an oxycodone-based hapten (OXY) conjugated to the subunit keyhole limpet hemocyanin carrier protein (sKLH) through a tetraglycine linker. The OXY-sKLH has been extensively described in mice and rats, and it has shown efficacy against oxycodone-induced behavioral, pharmacological, and toxic effects (26, 31, 33, 36). The anti-fentanyl conjugate vaccine consists of a fentanyl-based hapten (F) conjugated to the sKLH through a tetraglycine linker, which has been previously tested in both mice and rats (54, 55).

Immunization. Mice were immunized intramuscularly (i.m.) with 60 µg of F-sKLH or unconjugated sKLH carrier protein as control. Conjugates were adsorbed on 300 µg of aluminum adjuvant (Alhydrogel85, Brenntag) and delivered in a final volume of 30 µl in each hindleg for a total of 60 µl. Mice were immunized on days 0, 14, and 28. Rats were immunized i.m. with 60 µg of either OXY-sKLH or sKLH. Conjugates were adsorbed on 90 µg of aluminum to a final volume of 150 µl and delivered into one hind leg. Rats were immunized on days 0, 21, and 42.

Antibody Analysis. Serum antibody analysis was performed via indirect ELISA on blood sampled from facial veins in mice (days 14 and 34) and from tail veins in rats (day 49). 96-well plates were coated with 5 ng/well of F-BSA conjugate or OXY-OVA conjugate (for mice and rats, respectively) or unconjugated BSA or OVA as a control. Conjugates were diluted in 50mM Na_2CO_3, pH 9.6 (Sigma) and blocked with 1% porcine gelatin. Serum was incubated on the plate and then washed and incubated with an HRP-conjugated goat anti-mouse IgG (1:30,000, Jackson ImmunoResearch Laboratories), IgG_1 (1:35,000, Alpha Diagnostic International), IgG_{2a} (1:7500, Alpha Diagnostic International), or goat anti-rat IgG (1:50,000, Jackson ImmunoResearch Laboratories) to assess hapten-specific serum IgG antibody levels using statistical analysis previously described (26, 133).

Effect of vaccine on opioid-induced antinociception. To determine the efficacy of the vaccine to block opioid-induced analgesia, a hot plate test was performed to establish whether vaccines protect against centrally-mediated effects of opioids. Rodents were acclimated to the testing environment for 1 hour prior to measuring baseline. Rodents were placed on a hot plate (Columbus Instruments, OH) set to 54ºC and removed after displaying a lift or flick of the hind paw or jumping. In mice, baselines were measured on

day 35 (7 days after last immunization), followed by administration of 0.05 mg/kg fentanyl, s.c. Hotplate response was measured again 30 minutes after injection. In rats, baselines were measured on day 56 (14 days after last immunization), and rats were given 2.25 mg/kg of oxycodone, delivered subcutaneously at 0 and again at 17 minutes (cumulative dose of 4.5 mg/kg oxycodone). Hotplate response was measured at 15 and 30 minutes. Data is displayed as percent maximum possible effect (MPE) calculated as: (postdrug latency − baseline latency)/(maximal cutoff − baseline latency) × 100.

Effect of vaccine on opioid-induced respiratory depression and bradycardia. Oxygen saturation, heart rate (BPM), and breath rate (BRPM) were measured by oximetry before and after drug administration in rats. Oximetry was measured using a MouseOx Plus (Starr Life Sciences, Oakmont, PA). Rats were acclimated to the testing environment for 1 hour prior to measuring baseline. After baseline rats were given two doses of 2.25mg/kg oxycodone, delivered subcutaneously at time 0- and 17-minutes. Oximetry measurements were taken at baseline and post-challenge at 15 and 30 minutes.

Analysis of oxycodone and fentanyl concentration in serum and brain. After the final oximetry and hot plate measurements, animals were anesthetized, decapitated, and trunk blood and brain were collected for analysis. For fentanyl samples, material was processed using liquid chromatography coupled to mass spectrometry (LC-MS) as previously described (54). Oxycodone samples were processed using gas chromatography coupled to mass spectrometry (GC-MS) as previously described (36).

Analysis of microbiome in vaccinated mice. Mouse fecal samples were collected pre-challenge on day 35 and flash frozen in liquid nitrogen. The fecal content was processed using DNeasy PowerSoil® kits (Qiagen, Germantown, Maryland) modified to include a bead-beating step where fecal pellets were lysed using glass beads by a MagnaLyser tissue disruptor (250). Sequencing and bioinformatics were performed by the University of Minnesota Genomic Center, MN, United States. At University of Minnesota, after DNA isolation, 16S ribosomal DNA hypervariable regions V5 and V6 were PCR amplified using primers with the V5F RGGATTAGATACCC and V6R CGACRRCCATGCANCACCT gene-specific sequences, Illumina adaptors, and molecular barcodes as described to produce 427 base pair (bp) amplicons. Samples were sequenced on an Illumina MiSeq (Illumina, San Diego, California) using MiSeq 600 cycle v3 kit (256).

16S rRNA sequencing data analysis. Primer sequences were removed from raw sequencing reads and low-quality bases (Phred score<20) were trimmed from 3' end using Cutadapt (257). Microbial taxonomy assignment abundance quantification was analyzed with Greengenes database (ver.08/13) using dada2 pipeline (258). Microbial diversity was quantified by Shannon's index (α-diversity), and Bray-Curtis dissimilarity (β-diversity) using R package "vegan" (259). The dissimilarity between pairs of treatment groups was assessed using permutation multivariate analysis of ANOVA (PERMANOVA), and the significance of pair-wise comparison was adjusted for multiple comparison using Bonferroni correction. Individual differential taxa were identified using DESeq2 with significance determined based on a false discovery rate (FDR) of 0.05 (260). Relative abundance of functional content of microbial communities was obtained using PICRUSt (261).

RESULTS

Housing conditions do not affect vaccine efficacy against fentanyl in mice. To determine the effects of housing conditions on vaccine efficacy, mice housed in either SPF or conventional conditions were immunized on days 0, 14 and 28 with F-sKLH or unconjugated sKLH. After a primary immunization, F-sKLH elicited significantly lower antibody titers in SPF mice compared to conventionally housed mice (**Figure 1A**). However, on day 34, no significant differences in antibody response were detected between SPF and conventionally housed mice (**Figure 1B**). To further assess whether housing conditions would affect the quality of the humoral response, IgG_1 and IgG_{2a} subclasses were measured on day 34. Vaccinated groups in both SPF and conventional housing showed equivalent levels and distribution of IgG_1 (**Figure 1C**) and IgG_{2a} titers (**Figure 1D**).

After immunization, the ability of F-sKLH to block drug distribution to the brain was assessed by a hot plate test of centrally mediated analgesia. Animals were challenged with 0.05 mg/kg s.c. fentanyl and the hot plate response was measured 30 minutes post-challenge and compared to baseline as a percent of maximum possible effect (MPE%). Both SPF and conventionally housed vaccinated mice showed a significant reduction in fentanyl-induced analgesia ($p<0.05$) at 30 minutes post-challenge, with no significant difference seen between housing conditions in vaccinated groups (**Figure 1E**). Fentanyl distribution to the brain was also directly analyzed via LC-MS (**Figure 1F**). Across both conditions, the F-sKLH vaccine was able to effectively block fentanyl distribution to the brain as compared to control animals. All together, these data indicate that housing conditions do not have a significant effect on fentanyl vaccine efficacy in mice.

Housing conditions do not affect vaccine efficacy against oxycodone in rats. An anti-oxycodone conjugate vaccine was used to assess vaccine efficacy in rats housed in either SPF or conventional conditions (**Figure 2**). Rats were immunized on days 0, 21, and 42 with an oxycodone conjugate (OXY-sKLH) vaccine or unconjugated carrier protein as a control. Blood was collected on day 49 to assess oxycodone-specific antibodies in serum via ELISA (**Figure 2A**). While the vaccine did produce high anti-oxycodone serum IgG titers, there was no significant differences between housing conditions.

On day 56 (14 days after final immunization), rats were challenged with 2.25 mg/kg dose of s.c. oxycodone at time 0 and a second dose 17 minutes later. Vaccine efficacy was assessed by hot plate analgesia (**Figure 2B, C**) measured prior to drug delivery and at 15- and 30-minutes post-challenge. After each dose, rats in both housing conditions showed trends towards significantly lowered MPE%, but these trends were only statistically significant for conventional housing after the first dose, and for SPF after the second dose.

As another measure of vaccine efficacy, a pulse oximeter was used to assess oxycodone-induced respiratory depression and bradycardia, which are both commonly associated with opioid use (262). Baseline oximetry was measured prior to drug challenge in each rat. Oximetry readings were then taken at 15- and 30-minutes post-challenge to measure oxygen saturation (**Figure 2D**), heart rate (**Figure 2E**) and breath rate (**Figure 2F**). At 15 minutes post-challenge (2.25 mg/kg oxycodone), only SPF-housed control animals showed a significant decrease in oxygen saturation as compared to vaccine groups. However, at 30 minutes post-challenge (total cumulative dose of 4.5mg/kg oxycodone) both conventional and SPF vaccine and control groups showed significant differences in oxygen saturation. The oxycodone conjugate vaccine was able to effectively

protect animals against this opioid-induced respiratory depression under both housing conditions.

The heart rate of control animals decreased in both SPF and conventionally housed rats after oxycodone administration. At 15 minutes, this drop was statistically significant only between vaccine and control groups housed under SPF conditions. Interestingly, at 30 minutes, the SPF animals did not show a significant difference in heart rate between vaccine and control groups, while conventionally housed animals showed a strongly significant change in heart rate between vaccine and control groups. Breath rates of animals in all housing conditions and vaccine groups trended downwards as the dose of oxycodone increased, but none were statistically significant. After 30 minutes post-drug challenge, blood and brain were collected and tested to determine distribution of oxycodone in each compartment. In both SPF and conventionally housed animals, vaccination with OXY-sKLH led to a significant decrease in brain oxycodone concentration and an increase in serum oxycodone concentration.

Magnitude of change in metrics of vaccine efficacy do not differ between SPF and conventionally housed animals. While there was no significant difference between vaccine response in SPF and conventionally housed rodents, the percent change in response from control was calculated in each group to ensure the magnitude of response was similar between groups. Mean of the control was calculated and compared between SPF and conventional housing. Next, the percent change in efficacy between the immunized animals and the mean of the control was determined and compared between housing conditions (**Table 1**). There was no change in magnitude of the response in any of the metrics tested, with the exception of the rat serum oxycodone concentration. Of

note, the mean control values were significantly different between both rat serum and brain oxycodone concentrations when comparing housing conditions.

Effect of housing condition and vaccine on microbiome in mice. To evaluate whether housing condition or vaccination is responsible for microbiota changes, gut microbial composition was evaluated by 16S rRNA gene sequencing of fecal pellets from each group. The alpha diversity was quantified by the Shannon diversity index, which accounts for both OTU richness and evenness. The Shannon diversity was significantly decreased in SPF groups compared with conventionally raised groups, regardless of vaccination status (**Figure 3A**).

Nonmetric multidimensional scaling (NMDS) analysis of the Bray-Curtis distance plot was also performed among the fecal samples from different groups. There is a clear separation between conventional and SPF sKLH controls (PERMANOVA test, FDR q=0.007; **Figure 3B**) and conventional and SPF F-sKLH (PERMANOVA test, FDR q=0.007; **Figure 3B**). This suggests the changes in microbiota are influenced more by environmental conditions than vaccination status.

SPF mice receiving sKLH had a decreased relative abundance of *Proteobacteria* at phylum level, *Rikenellaceae*, *Gemellaceae* and *Clostridiaceae* at family level and *Candidatus Arthromitus*, *Gemella* and *Nelumbo* at genus level compared to conventional sKLH controls. The relative abundance of *Dehalobacteriacea* and *Ruminococcaceae* at family level and *Marvinbryantia* and *Oscillospira* at genus levels were increased (**Figure 3C**).

Additionally, the overlap between F-sKLH and control groups in SPF condition (PERMANOVA test, FDR q=0.114) represents resilience to modulation by vaccination (**Figure 3B**). Interestingly, there was significant and distinct clustering of F-sKLH comparing to control animals in conventional housing groups (PERMANOVA test, FDR q=0.046; **Figure 3C**). There was a reduction of *Rikenellaceae* at family level and *Anaerostipes* and *Candidatus Arthromitus* at genus level and expansion of *Marvinbryantia* at genus level in conventional F-sKLH treatment group (**Figure 3C**).

The functional profiles of the microbial communities were analyzed in each group using PICRUSt. Of 42 KEGG pathways tested, 8 non-human-gene pathways differed in abundance between SPF and conventional raised controls (FDR q<0.05). These include pathways relating to cell growth and death, transcription, cancers, infectious diseases, carbohydrate metabolism, energy metabolism, metabolism of cofactors and vitamins, and metabolism of terpenoids and polyketides. There were no significant changes in functional composition related to vaccination in either conventional groups or SPF groups (**Figure 3D**). However, when comparing SPF and conventional sKLH controls, KEGG pathways related with cell growth and death, cancers, energy metabolism, metabolism of cofactors and vitamins, and metabolism of terpenoids and polyketides were found down-regulated while KEGG pathways related with carbohydrate metabolism, transcription, and infectious disease up-regulated in SPF controls. This suggests that environmental factors have a more important impact on microbial changes compared to vaccination.

DISCUSSION

The effect of the microbiome on health and disease has been of increasing interest in recent years. Changes in the microbiome have been associated with cardiovascular

disease, autoimmune conditions, cancer, obesity, diabetes, and potentially even mental health disorders (263, 264). Studies have suggested that the microbiome plays a role in the immune response to vaccination (247-249), making it critical that vaccine efficacy is tested in conditions that closely mimic the human microbiome. Since opioid use is also correlated to gut dysbiosis, it is even more imperative that vaccines for OUD are tested in a variety of contexts (250-254) to ensure vaccines will translate into a clinical setting. In this study, we sought to determine if changes in animal housing conditions affected the efficacy of fentanyl and oxycodone vaccines in mice and rats. We found that while there were some differences in microbiota diversity between the two housing conditions, there was no major differences in the efficacy of either vaccine.

Differences in housing conditions and subsequent effects on behavior and disease have been noted in the literature in both mice and rats. Published studies show that housing conditions can affect the development of experimental autoimmune encephalitis in mice (265), and rats housed in conventional vs. SPF conditions showed varying response to surgical trauma and anesthesia (266). Studies exploring the differences between wild and laboratory mice also show that immune composition varies greatly between environmental conditions. Wild mice have more robust numbers and heterogeneity of circulating IgG, as well as significantly greater numbers of T cells, with less NK cells and dendritic cells (267). In this study we found that there was a significant increase in diversity in the gut microbiota when comparing mice in conventional vs. SPF conditions, regardless of vaccination status. Since alterations in gut microbiota has been closely tied to many pathologies and alterations in metabolism, this study supports the need for careful consideration of mouse models when testing new therapies, and the requirement for comparisons between housing conditions to ensure microbiota differences do not affect treatment outcomes.

When analyzing the microbiome via sequencing, a distinct change in bacterial species was observed between conventionally housed control and immunized mice. Interestingly, these changes in microflora mirrored the changes observed in SPF mice when compared to conventionally housed mice. This suggests that the administration of the F hapten may influence the GI microbiome. While the F hapten was has been shown to be inactive at the mu-opioid receptor (55), formal GLP toxicology studies of conjugate vaccines containing fentanyl-based haptens are warranted. Histopathology and blood chemistry analysis in mice injected with OXY-KLH (94), as well as GLP toxicology studies of OXY-sKLH in rats (Pravetoni, personal communication), did not show any sign of toxicity. There have been reports that opioids modulate toll-like receptor (TLR) 4 (268), a TLR involved in regulation of the GI microbiome, and that OXY-KLH responses were altered in TLR4KO mice (31). Follow-up studies will be needed to explore any potential interaction between anti-opioid vaccination, immunity, and microbiome.

Despite these differences in gut microbiota, we found no major significant differences in the efficacy of vaccines targeting fentanyl or oxycodone when examining opioid-specific antibody titers, pharmacokinetic parameters, and physiological and behavior responses. This outcome was unexpected, as there have been several studies noting the effects of the microbiome on immune response after vaccination (247-249). These results help validate previous data of preclinical studies of OUD vaccines in SPF conditions. This also suggests anti-opioid vaccination is not significantly changed by housing condition, making interpretation of data from different laboratories more consistent. Additionally, these data suggest that OUD patients with opioid-induced dysbiosis may equally benefit from anti-opioid vaccination. Finally, since immunization was equally effective despite differences in the microbiome, our results did not point to any bacterial species that could be utilized as a predictive biomarker.

One point of interest is that in control rats, serum and brain oxycodone levels were significantly increased in SPF housing conditions compared to conventional conditions. This would suggest that the metabolism of oxycodone is decreased in SPF conditions, which may be linked to differences in the microbiota. Published literature has established a link between diversity of gut microbiota and the dysregulation of metabolism of morphine (251). While few studies have addressed the potential of the microbiome to affect the metabolism of other opioid molecules, such as oxycodone or fentanyl, it is possible that decreased microbial diversity in SPF rats would lead to decreased oxycodone metabolism, resulting in increased oxycodone concentrations in the serum and brain. This would be consistent with the findings that the functional differences in microbiome between SPF and conventional mice (**Figure 3D**) resulted in differences in metabolism of carbohydrates, vitamins, cofactors, terpenoids, and polyketides. These potential differences in metabolism and microbiome conditions will need to be further evaluated, although they may be of note for future experimental design and when comparing studies of animals housed under different conditions.

Future follow-up experiments will address some of the limitations of the current study to further explore the interplay between the microbiome and vaccination against OUD. One limitation is that current studies were only performed in male mice and rats. Significant differences in titers between male and female mice after anti-opioid vaccination were previously reported (72), and there have been noted sex differences in microbiome composition (269). Future studies will compare male and female animals to determine whether the GI microbiome affects the efficacy of anti-opioid vaccines in a sex-dependent fashion. Another limitation of this study was that the SPF condition likely does not fully capture the changes in microbiome that are found in chronic opioid users. For example, previous literature indicates that active opioid users have an increase in abundance in

Bifidobacterium and decreases in *Baceterodacea, Clostridiales XI*, and *Ruminococcaceae*, which were not recapitulated in the current study (253). However, there was a decrease in overall alpha diversity and in *Rikenellaceae*, which are consistent with previous literature using mice chronically treated with morphine (251). While it has been shown that rats chronically treated with opioid agonists and antagonists still mount an anti-opioid antibody response after vaccination (33, 54, 55), the relationship between chronic opioid treatment and microbiome composition has not yet been explored in the context of vaccines for OUD. This will be critical in future studies to determine whether opioid users will respond to anti-opioid vaccination.

As testing of OUD vaccines in clinical settings becomes imminent, the impact of vaccination on gut microbiota and vice versa will help to inform clinicians on therapeutic management of OUD patients. Pre-clinical studies are often conducted in sterile environments, which may be masking or changing pathologies and/or outcomes related to disease treatment. In the case of OUD, looking at the impact of the GI microbiome on potential therapeutic efficacy becomes even more crucial when the target population may have a higher incidence of abnormal microbiome function. These studies support the use of OUD vaccines as a treatment strategy for individuals that may have deficits or abnormal microbiomes, as well as otherwise healthy individuals.

FIGURE LEGENDS

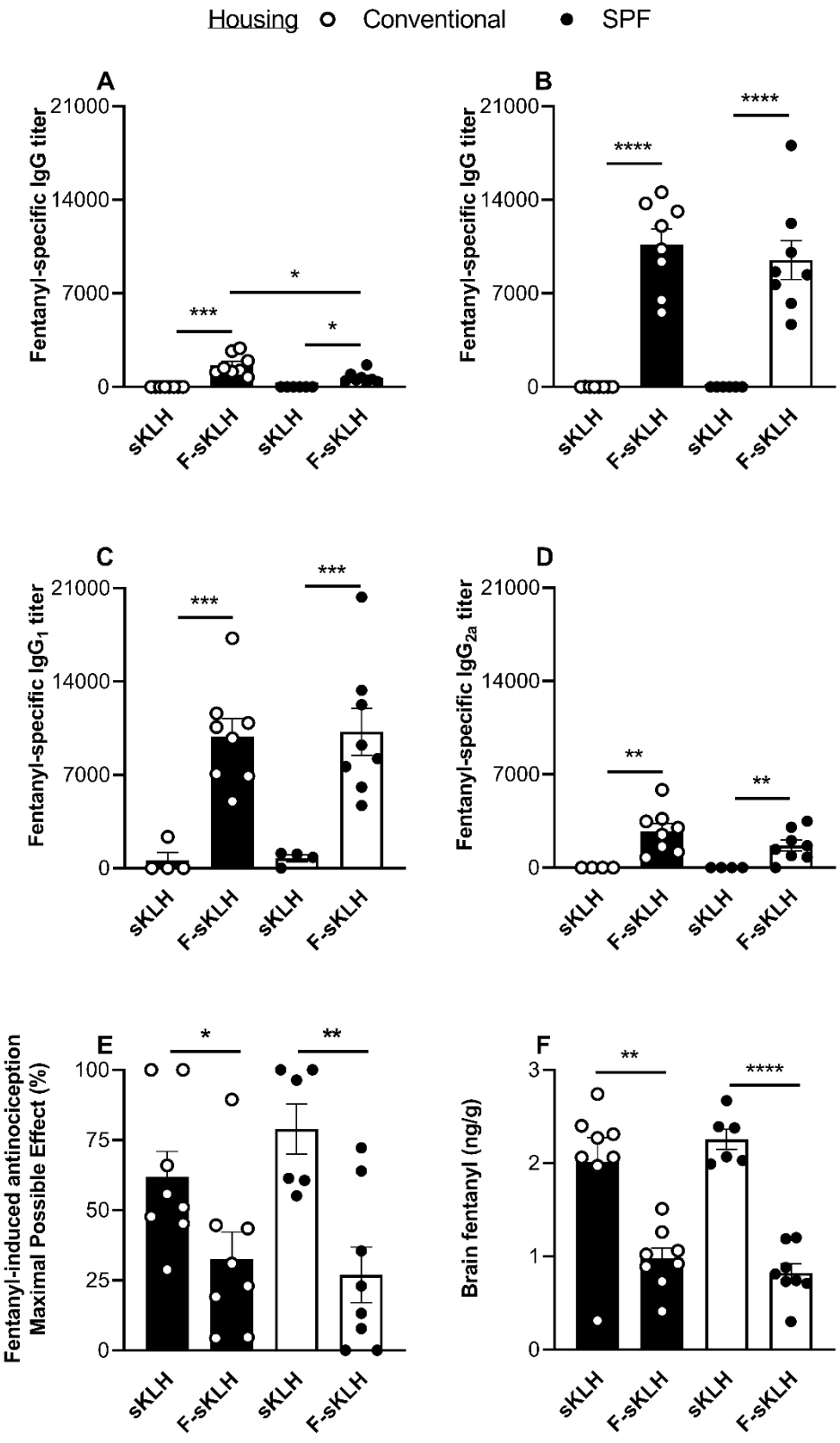

Figure 1. *In vivo* comparison of SPF and conventional vaccine response in mice. F-sKLH vaccine was tested in male BALB/c mice in either SPF or conventional housing. Conjugate was adsorbed on alum adjuvant and injected in mice i.m. on days 0, 14 and 28. Blood was collected via facial vein at days 14 and 34 to test for fentanyl-specific serum antibody titers via ELISA. IgG titers are shown for A) 14 days post immunization and B) 34 post-immunization. Serum from 34 days post immunization was tested for C) IgG_1 subclass titers and D) IgG_{2a} subclass titers. On day 35, all mice were challenged with 0.05 mg/kg fentanyl, s.c. E) F_1-sKLH effect in blocking fentanyl-induced antinociception in the hot plate test at 30-minutes post-challenge. After being tested on the hot plate, mice were euthanized and brains were collected. F) Brain fentanyl concentration in mice measured via LC-MS. Statistical analysis run via Welch's T-test between control and immunized mice in different housing conditions, after establishing no statistical difference in the control mean between housing conditions via T-test. * $p \leq 0.05$, ** $p \leq 0.01$, *** $p \leq 0.001$, **** $p \leq 0.0001$.

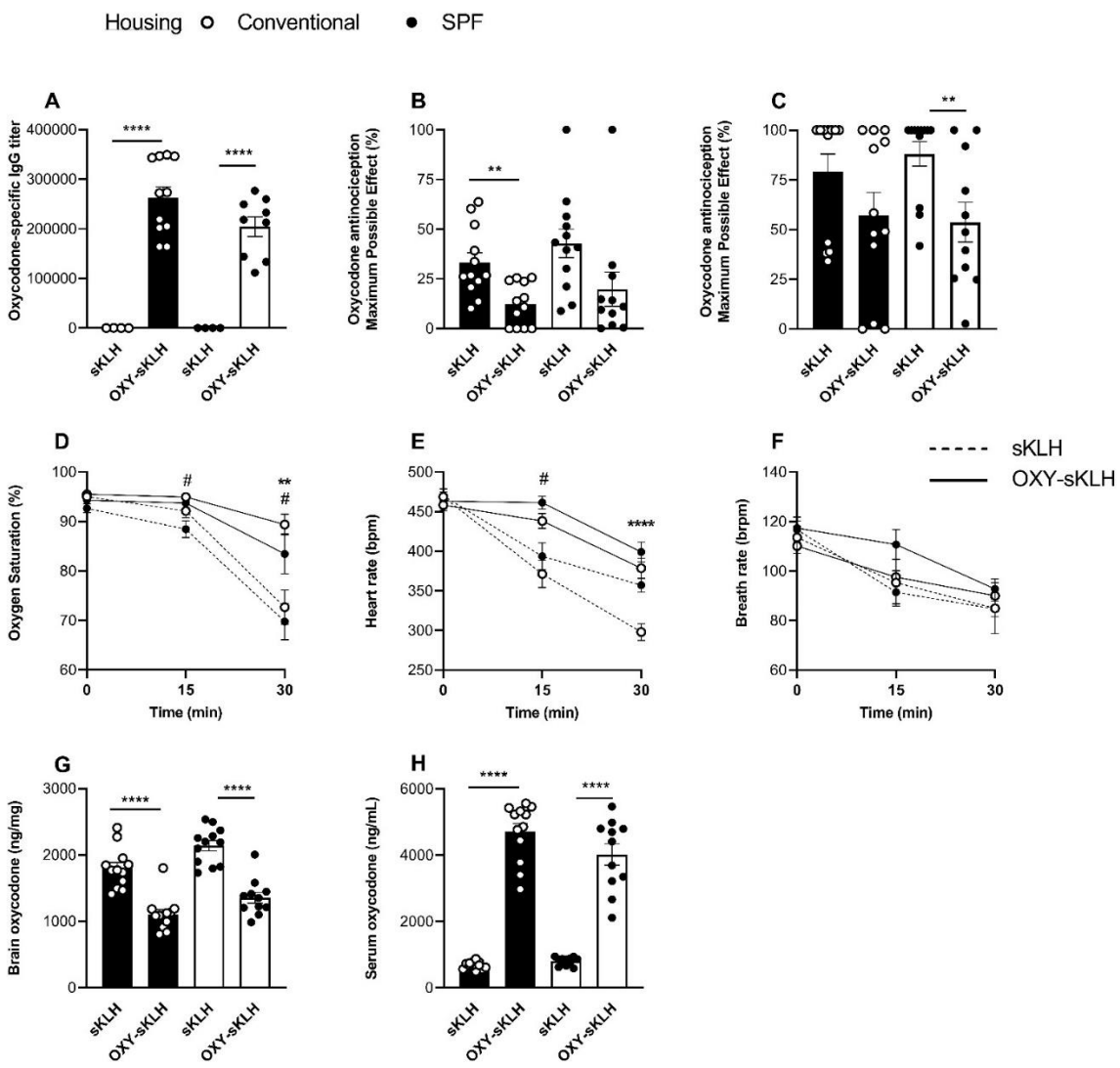

Figure 2. *In vivo* comparison of SPF and conventional vaccine response in rats. OXY-sKLH vaccine was tested in male Sprague-Dawley rats in either SPF or conventional housing. Conjugate was adsorbed on alum adjuvant and injected i.m. on days 0, 21 and 42. Blood was collected via tail vein at day 49 to measure A) oxycodone-specific IgG tiers via ELISA. On day 56, all rats were challenged with two doses of 2.25 mg/kg oxycodone s.c. at 0 min and again at 17 min. Hotplate response was measured at baseline, 15 mins and 30 mins, and maximum possible effect (MPE%) was calculated for B) 2.25 mg/kg and

C) 4.5 mg/kg cumulative dose. Efficacy of OXY-sKLH was further assessed by measuring D) oxygen saturation, E) heart rate and F) breath rate at baseline, 15 minutes, and 30 minutes post-drug challenge. After 30 minutes, rats were euthanized for blood and brain collection to measure oxycodone distribution in the G) brain and H) serum, measured via GC-MS. Statistical analysis run via Welch's T-test between control and immunized mice in different housing conditions. Symbols: * represents significance between conventionally housed animals or as indicated by lines between groups, # represents significance between SPF-housed animals. * or # $p \leq 0.05$, ** $p \leq 0.01$, *** $p \leq 0.001$, **** $p \leq 0.0001$.

Table 1. Statistical analysis of metrics of vaccine efficacy between housing conditions in control groups and change from percent change from mean control value in immunized groups.

	Control					Immunized Change from Mean Control Value (%)				
	Conventional		SPF			Conventional		SPF		
Metric	Mean	SEM	Mean	SEM	Signficance?	Mean	SEM	Mean	SEM	Signficance?
Mouse Brain Fentanyl Concentration (ng/g)	2.015	0.242	2.255	0.100	ns	51.613	5.430	63.636	4.229	ns
Mouse Hotplate Latency (s)	42.063	4.366	50.717	3.512	ns	21.426	9.885	45.3582	8.560	ns
Rat Brain Oxycodone Concentration (ng/g)	1799.000	87.957	2139.917	78.975	*	38.697	4.091	36.659	3.854	ns
Rat Serum Oxycodone Concentration (ng/ml)	679.500	31.826	798.917	35.109	*	692.544	37.092	503.049	38.788	**
Rat Hotplate Latency (15 min)	15.150	1.290	16.592	1.739	ns	27.833	5.773	31.599	12.446	ns
Rat Hotplate Latency (30 min)	25.175	2.035	27.150	1.471	ns	17.411	9.806	28.579	8.595	ns

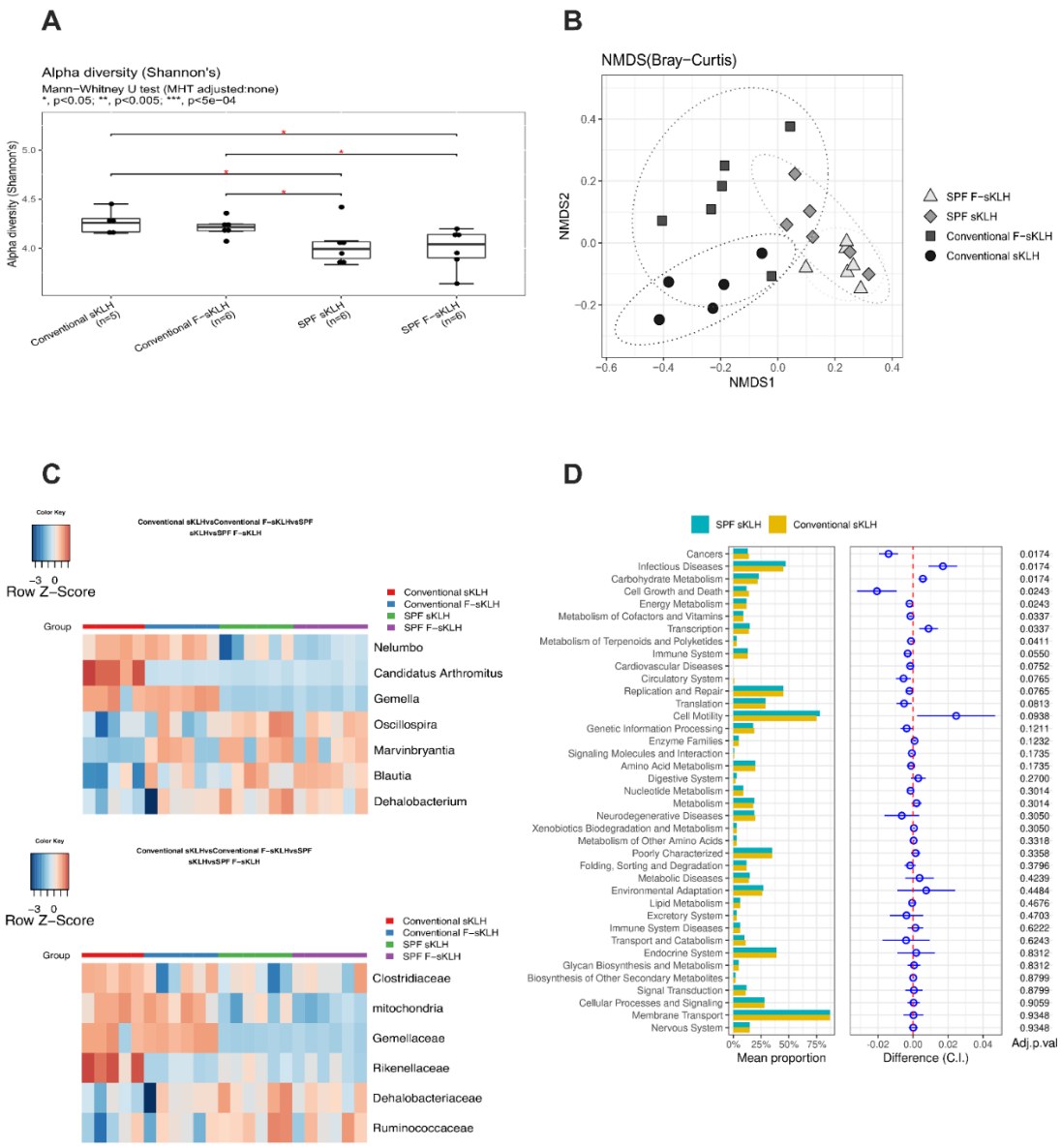

Figure 3. The impact of environment and vaccination on mouse gut microbiome. After immunization, mouse fecal matter was collected for analysis of microbiome via 16s rRNA sequencing. (a) Box plots show that conventionally housed mice exhibited a significant increase in α-diversity (calculated by Shannon's index) compared with SPF mice. (b) Non-metric multidimensional scaling (NMDS) plot was used to visualize the unweighted UniFrac distances of each group (calculated by Bray-Curtis distance). (c)

Changes in abundance of bacteria by environment or vaccination at family and genus levels were displayed in the heatmaps. Bacteria were selected from the comparison SPF and conventionally housed sKLH controls with FDR<0.1. (d) In control mice housed in either SPF or conventional conditions, bacterial gene functions were predicted from 16S rRNA gene-based microbial compositions using the PICRUSt.

Chapter 6: Exploratory predictive biomarker identification for an anti-oxycodone vaccine in Phase I clinical trial

The goal of this exploratory study was to identify putative predictive biomarkers of vaccine efficacy that could be used in future OUD vaccine clinical trials. Utilizing information learned from preclinical studies, we determined whether IL-4 could be used as a predictive biomarker in genetically diverse preclinical models. Furthermore, we conducted immunoprofiling of naïve individuals and those with OUD to determine whether there were differences that could be leveraged for clinical biomarker identification.

The presented data is unpublished. The following people contributed to this work:

Crouse B, Hicks D, Baehr C, Huseby Kelcher A, Holt T, Guevara Lopez M, Conn J, Persano S, Marker C, Comer SD, Pravetoni M.

Author Contribution: BC planned and conducted experiments and analyzed data. AHK conducted experiments and analyzed data. TH conducted experiments and analyzed data. MGL conducted experiments and analyzed data. JC conducted experiments and analyzed data. SP conducted experiments and analyzed data. CM provided support in acquiring human samples. SDC provided the clinical site for acquiring human samples. MP assisted in experiment planning, data interpretation, and editing.

INTRODUCTION

Anti-opioid vaccines are a novel therapeutic for the treatment of opioid use disorders (OUD), which affect over 40 million people worldwide (5). Active immunization with a drug-carrier protein conjugate stimulates the production of opioid-specific antibodies, which bind to the drug in the blood and prevent distribution to the brain. This, in turn, reduces opioid-induced effects such as analgesia, respiratory depression, and bradycardia [reviewed in (142)]. These vaccines have several advantages over current medications for OUD, which include the mu-opioid receptor (MOR) agonist methadone, partial agonist buprenorphine, and antagonist naltrexone (14). Anti-opioid vaccines are not controlled substances and are long lasting, potentially increasing patient compliance compared to methadone or buprenorphine, which are strictly regulated and need to be taken daily. Since they do not activate the MOR, vaccines also do not carry the risk of respiratory depression or diversion like methadone or buprenorphine. Unlike naltrexone, anti-opioid vaccines do not induce withdrawal (12) and its associated unpleasant adverse effects. Because of this potentially enhanced safety and efficacy profile, anti-opioid vaccines, including an anti-oxycodone vaccine (OXY-sKLH), have been extensively tested for preclinical safety and efficacy which has resulted in the first anti-opioid vaccine clinical trial in the United States (NCT04458545).

Clinical trials have been conducted for other drug-conjugate vaccines for substance use disorders (SUD) with variable results. In studies of vaccines for nicotine (83) and cocaine (84), primary efficacy endpoints were not met; however, significant efficacy was seen in a subset of patients who produced high concentrations of high affinity drug-specific antibodies, indicating that anti-drug vaccines can be clinically efficacious if sufficient antibody titers are produced. In order to increase vaccine efficacy, many groups have attempted to add adjuvants to their SUD vaccine formulations to stimulate the

immune system to produce antibodies (31, 37, 39, 42, 68, 70, 73, 77, 97, 99, 124, 163, 270). While these adjuvants are effective in animal models, many have never been tested in humans, highlighting concerns about safety and making it difficult to obtain approval for clinical studies.

A complementary approach to increase vaccine efficacy is to identify pre-immunization biomarkers predictive of drug-specific antibody production. If predictive biomarkers can be identified, a simple blood or saliva test could be performed in the office of a primary care physician to determine whether immunization would be the best treatment strategy, or whether the patient would more likely benefit from traditional pharmacotherapies. Biomarkers of efficacy of an anti-cocaine vaccine have been identified and include single nucleotide polymorphisms (SNPs) in the dopamine β-hydroxylase (DBH) (205) and κ-opioid receptor (OPRK1) (206). Protective alleles of these genes were associated with increased abstinence from cocaine after immunization, but it was thought that this was due to altered pharmacokinetics and pharmacodynamics of cocaine, not necessarily due to increased immune response. Nevertheless, these were among the first identified biomarkers for SUD vaccine efficacy in a human population.

For OUD vaccines, preclinical studies have shown that post-immunization antibody titers were correlated with pre-immunization number of naïve opioid-specific B cells. Mice that had higher pre-immunization opioid-specific B cells generally produced higher titers than those with lower B cell numbers (94). To date, this is the only preclinical biomarker for anti-opioid vaccines. With anti-opioid vaccine clinical studies beginning, identification of additional biomarkers is imperative so they may be validated in these ongoing studies. To this end, both preclinical studies in relevant animal models and exploratory clinical studies on the target population for anti-opioid vaccines (i.e., current

opioid users) may be useful to reveal additional putative biomarkers to be tested in anti-opioid vaccine trials. In this study, we identify IL-4 as a preclinical predictive biomarker of vaccine efficacy for OXY-sKLH in genetically diverse outbred mice. This biomarker was identified based on previous preclinical studies indicating that IL-4 depletion increases opioid-specific antibody titers in mice (94). In addition, serum samples from naïve healthy individuals and individuals with OUD were assayed in an exploratory study to identify differences in the immune environment that may be leveraged for predictive biomarker identification in clinical studies. We found that individuals with OUD have increased opioid-specific naïve and memory B cells, indicating they may produce better antibody responses after immunization. Serum analysis also revealed that several cytokines and opioid-specific antibody titers correlated with opioid-specific B cells, which may also be of interest in future clinical studies to enhance OUD vaccine clinical success.

MATERIALS AND METHODS

Hapten synthesis and conjugate vaccines. The oxycodone-based hapten containing a tetraglycine linker at the C6 position (OXY) was synthesized as previously described (26, 27) and conjugated to GMP grade subunit KLH (sKLH, Biosyn, Carlsbad, CA) using carbodiimide chemistry as previously described (26, 27). For use as a coating antigen in ELISA, OXY hapten was conjugated to chicken ovalbumin (OVA) or dextran. Briefly, 5 mM OXY was activated with 104 mM EDAC in 0.1 M MES buffer pH 5. The reaction mixture was stirred for 10 minutes at room temperature (RT). Carrier was then added to a final concentration of 2.8 mg/mL and stirred for 3 hours at RT. MES buffer was exchanged with PBS buffer pH 7.2 using an Amicon filter unit (MilliporeSigma, Merck, Burlington, MA) with 100 kDa molecular cutoff, and resuspended to a final concentration of 2.5 mg/mL before storage at 4°C. Haptenation ratio of OVA conjugate was measured by MALDI-TOF

analysis (AB SCIEX 5800, Foster City, CA), while sKLH conjugate formation was confirmed by Dynamic Light Scattering (DLS) as described (27). The unconjugated carrier protein and the conjugate vaccines were adsorbed to 300 μg aluminum adjuvant (Alhydrogel '85', 2%, Brenntag Biosector, Denmark).

Decoy and tetramer reagents for flow cytometry. OXY hapten containing a biotinylated tetraglycine linker was conjugated to streptavidin (SA)-phycoerythrin (PE) (Prozyme, Hayward, CA) through incubation in PBS buffer (0.01M pH 7.2) for 1 hour at room temperature with magnetic stirring while protected from light. For decoy preparation, SA-PE was conjugated to Alexa Fluor 647 (AF647) using a protein labeling kit (Life Technologies, Grand Island, NY) following the manufacturer's instructions. After preparation, decoy and tetramer reagents were purified and concentrated by ultrafiltration with PBS buffer using Amicon Ultra-4 centrifugal filter tubes with a 30 KDa molecular weight cutoff. Concentrations of the reagents were determined by measuring the absorbance at 565 nm (ε=1.96x106cm-1M-1) using a NanoDrop 2000c spectrophotometer.

Drugs. Oxycodone HCl was obtained from Boynton Pharmacy (Minneapolis, MN). Drugs doses are expressed as weight of free base.

Ethics Statement. Animal studies were performed according to the Guide for the Care and Use of Laboratory Animals and the National Institute of Health. Animal protocols were approved by the University of Minnesota Institute Animal Care and Use Committee. Animals were euthanized by AAALAC approved CO_2 chambers and all efforts were made to minimize suffering. All human studies were approved by the Institutional Review Board of the University of Minnesota (IRB#6130).

Animals. Six- to ten-week old male J:DO diversity outbred mice (strain #009376) were obtained from Jackson Laboratory (Bar Harbor, ME). Mice were group housed under a 14/10 hour standard light/dark cycle and fed standard mouse chow *ad libitum*. Testing occurred during the light phase.

Preclinical study experimental design: Mice were bled via facial vein on days -28, and -14 prior to immunization for *in vitro* stimulation of whole blood. Mice were also bled on day 34 for oxycodone-specific IgG analysis. Mice were immunized on days 0, 14, and 28 with 60 µg OXY-sKLH formulated with 300 µg aluminum hydroxide in 60 µL total volume. Immunizations were performed intramuscularly (i.m) in two sites (opposite legs) in the gastrocnemius muscle. On day 35, mice were challenged with 2.25 mg/kg oxycodone delivered subcutaneously (s.c). Thirty minutes after injection, mice were euthanized and decapitated to collect brain and blood samples for LC-MS analysis as previously described (55).

***In vitro* stimulation of whole blood in mice:** Facial blood samples were collected in EDTA coated tubes. Blood was mixed with 200 µL of RPMI and plated in 96 well plates. Phytohemagglutinin (PHA, Invivogen, San Diego, CA) was added to a final concentration of 10 µg/mL, or lipopolysaccharide (LPS, Sigma-Aldrich, St. Louis, MO) was added to a final concentration of 1 ng/mL. Samples were incubated at 37ºC with 5% CO_2 overnight. The following day, supernatants were collected and quantified using an IL-4 ELISA (Biolegend, San Diego, CA) using the manufacturer's instructions. Quantification was normalized to the volume of blood collected.

Antibody analysis. Opioid-specific IgG titers were measured by ELISA as described (55). Briefly, 96-well ELISA plates (Costar 9018 EIA/RIA, Jackson ImmunoResearch Laboratories Inc., West Grove, PA) were coated with 5 ng/well of unconjugated chicken

ovalbumin (OVA) or OXY hapten conjugated to OVA in carbonate buffer at pH 9.6 overnight. For human antibody analysis, 50 ng/well oxycodone (OXY-) or morphine (M-) haptens conjugated to dextran were used as a coating reagent. The following day, plates were blocked with 1% gelatin. Serum was added to wells starting at a 1:200 dilution and serially diluted, and plate were incubated for 2 hours. Chimeric oxycodone- or morphine-specific monoclonal antibodies were used to determine a concentration curve. Primary antibodies were then incubated overnight with 1:30,000 goat-anti-mouse IgG (Jackson ImmunoResearch, Cat. No. 115-035-008) or 1:10,000 goat-anti-human IgG (Alpha Diagnostic Cat. No. 10320) conjugated to horseradish peroxidase to measure concentration of oxycodone- or morphine-specific total IgG. SIGMAFAST OPD substrate (Sigma-Aldrich, St. Louis, MO) was used to develop plates.

Human blood sample collection: Normal healthy volunteers that did not use drugs recreationally (n=25) and opioid-using volunteers (n=23) were recruited at the laboratory of Dr. Sandra Comer at the Columbia University and New York Psychiatric Institute (NYSPI), New York, NY. The inclusion criteria for this study included male and non-pregnant female adults (18+) weighing at least 110 pounds. All subjects signed informed consent and were compensated $20 for participation. Each subject was requested to answer a questionnaire outlining their demographic information and current and past opioid use. Blood and urine samples were collected from each subject. Urine samples were tested for drugs. Blood samples were used for titers, B cell, and cytokine analysis.

Human PBMC preparation and flow cytometry. Blood samples were collected in 10 ml heparin coated tubes and shipped overnight at room temperature. Peripheral blood mononuclear cells (PBMCs) were separated by density gradient centrifugation over Ficoll PLUS medium immediately upon receipt of the blood samples. PBMCs were harvested

and incubated in ACK lysis buffer to remove residual red blood cells. Plasma was also harvested to measure antibody titers and for cytokine analysis in separate tubes and frozen at -80ºC until use. The isolated PBMCs were blocked with Human TruStain FcX™ for 5 minutes at room temperature. Afterward, PBMCs were incubated for 10 minutes at room temperature with PE-SA-AF647 decoy reagent at a final concentration of 80nM, and then 30 minutes on ice with OXY-SA-PE at a final concentration of 80 nM. Tetramer-positive cells were enriched from PBMCs by incubation with anti-PE beads followed by magnetic separation on LS MACS columns (Miltenyi Biotec). After magnetic enrichment, cells were stained for 30 minutes on ice with a cocktail of fluorescently labelled antibodies. Samples were fixed with 4% paraformaldehyde and analyzed with a LSRII flow cytometer (BD Biosciences). Fluorophores used were: IgD FITC, CD27 PE-Cy7, CD19 V500, CD3 APC-eF780, CD14 APC-eF780, CD16 APC-eF780, IgG BV421.

Multiplex cytokine analysis: Cytokines in human plasma samples were measured with MILLIPLEX Map Human Cytokine/Chemokine/Growth Factor Panel A 48 Plex Premixed Magnetic Bead Panel (Cat. # HCTYA-60K-PX48) from EMD Millipore (St. Charles MO), Q-Plex Human Cytokine High Sensitivity 15-Plex (Cat. # 112433HU) from Quansys Biosciences (Logan, UT), or Q-Plex Human Chemokine 9-Plex (Cat. # 120233HU) from Quansys Biosciences (Logan, UT). Three sets of data were collected from identical patient samples, with 1 and 2 being from MILLIPLEX kits, while data set 3 was collected using Q-Plex kits. Data using the MILLIPLEX kits were tested by the Cytokine Reference Laboratory (CRL, University of Minnesota), which is a CLIA'88 licensed facility (license #24D0931212). Samples were run on a Luminex-based platform according to manufacturer's instructions. Briefly, fluorescent color-coded beads coated with a specific capture antibody were added to each sample. After incubation and washing, biotinylated detection antibody was added followed by phycoerythrin-conjugated streptavidin. The

beads were read on a Bioplex 200, which is a dual-laser fluidics-based Luminex instrument. One laser determines the analyte being detected via the color coding while the other measures the magnitude of the PE signal from the detection antibody which is proportional to the amount of analyte bound to the bead. Samples were tested in duplicate and values were interpolated from 5-parameter fitted standard curves. Data using Q-Plex kits were measured in Dr. Michael Y. Tsai's Research Laboratory (University of Minnesota). Kits were run according to manufacturer's instructions and quantified using a Q-View Imager and software (Quansys BioSciences, Logan, UT). All samples were run in duplicate.

Statistical Analysis: Statistical analyses were performed using Prism version 9.1.2 (GraphPad, LaJolla, CA). Differences in B cell populations were analyzed via Student's T test. For cytokine analysis, all data points that were below baseline or had a pixel intensity of 0 were considered 0 pg/mL, and data was averaged between duplicates. For comparison between Naïve (NHV) samples to opioid use disorder (OUD) patient samples, data were analyzed for normality using D'Agostino-Pearson's test. If either group was non-normal, Mann-Whitney U-test was used to determine differences between groups. If both groups had a normal distribution, an unpaired t-test was performed with or without Welch's correction, depending on whether groups had equal variances. For correlations, serum cytokine concentrations and antibody concentrations were matched with self-reported heroin use data or oxycodone-specific B cell data and analyzed for both linear and monotonic relationships using Pearson correlations or Spearman correlations, respectively.

RESULTS

T-cell secreted IL-4 is a predictive biomarker of oxycodone vaccine efficacy in mice. Our group has previously shown that depletion of IL-4 during anti-opioid immunization increases opioid-specific antibody titers and subsequently increases vaccine efficacy after drug challenge (94). As a result, we hypothesized that pre-immunization production of IL-4 could be used as a predictive biomarker of post-immunization antibody titers and vaccine efficacy. To assess IL-4 as a predictive biomarker, blood was collected from genetically diverse outbred mice and plated for *in vitro* stimulation with either lipopolysaccharide (LPS, for innate immune cell stimulation) or phytohemagglutinin (PHA, for T cell stimulation). After 24 hours, supernatant was collected and analyzed for IL-4. Mice were then immunized with an anti-oxycodone vaccine on days 0, 14, and 28, and blood was collected again on day 34 to assess oxycodone-specific antibody titers. The next day, mice were challenged with 2.25 mg/kg oxycodone and blood and brain were collected 30 minutes post-challenge to analyze the pharmacokinetics of oxycodone. Pre-immunization concentration of IL-4 produced from T cells through non-specific PHA stimulation was significantly negatively correlated with oxycodone-specific antibody concentration (**Figure 1A**), positively correlated with serum oxycodone concentration after challenge (**Figure 1B**), and negatively correlated with brain oxycodone concentration after challenge (**Figure 1C**). On the other hand, these metrics did not correlate with pre-immunization IL-4 produced by innate immune cells through stimulation with LPS (**Figure 1D-F**). These data suggest that pre-immunization T cell derived IL-4 can be used as a biomarker to predict anti-oxycodone vaccine efficacy.

Individuals with opioid use disorder have a higher frequency of oxycodone-specific B cells than naïve healthy controls. We previously reported finding oxycodone-specific B cells in naïve mice using magnetic enrichment paired with flow cytometry, and that a higher frequency of pre-immunization opioid-specific naive B cells correlates with increased antibody titers and vaccine efficacy after immunization (133). Here, we extended these findings by collected blood samples from naïve healthy controls (NHV) or individuals with opioid use disorder (OUD) and assessing whether 1) humans have detectable opioid-specific cells in their B cell repertoire and 2) individuals with OUD have a higher frequency of opioid-specific B cells due to ongoing opioid use. Demographics for patient samples can be found in **Table 1**. After magnetically enriching for antigen-specific B cells using an oxycodone-specific bait reagent, cells were analyzed via flow cytometry (gating strategy in **Figure 2A**) to determine number of oxycodone-specific B cells in each sample. We found that there was an increased number of oxycodone-specific B cells in individuals with OUD compared to NHV (**Figure 2B**), most of which were naïve (**Figure 2C**). These data suggest ongoing opioid use may stimulate the expansion of opioid-specific B cells, and we hypothesize that individuals with OUD may have an increased response to anti-opioid immunization due to this increased proportion of naïve opioid-specific B cells.

Individuals with OUD may have differing plasma cytokine expression compared to healthy controls. To further characterize immune system differences between healthy controls and individuals with OUD, plasma samples were analyzed for 53 unique cytokines, chemokines, and growth factors in an exploratory study to determine if there are differences in cytokine expression in these two populations. Cytokines from identical

patient samples were analyzed twice using a Luminex bead-based multiplex kit (MILLIPLEX) to determine variability between plates, and a third time using antibody-based chemiluminescent kits (Q-Plex) to assess variability between quantification methods. A complete list of the cytokine comparisons between naïve and OUD participants can be found in **Table 2.** The concentration of interleukin (IL)-1RA, IL-18, IL-8 (CXCL8), interferon-γ induced protein-10 (IP-10, or CXCL10), monocyte chemoattractant protein (MCP)-1, monokine induced by interferon-γ (MIG, or CXCL9), macrophage inflammatory protein (MIP)-1β, platelet-derived growth factor (PDGF)-AB/BB and sCD40L were significantly different between naïve and OUD individuals in at least one of the kits tested (**Figure 3**). Concentrations of fractalkine, interferon (IFN)-α2, IL-12p40, IL-15, IL-1α, IL-1β, IL-22, and macrophage colony stimulating factor (M-CSF) also differed, but should be interpreted with caution because the group means were below the lowest point on the standard curve, potentially affecting the accuracy of the quantification.

Select plasma cytokines correlate with frequency of opioid-specific B cells in opioid users. Cytokines were analyzed for linear or monotonic correlations with the number of oxycodone-specific B cells (**Table 3**). Plasma concentrations of thymus- and activation-regulated chemokine (TARC, or CCL17), VEGF-A, and MCP-2 were positively associated with number of oxycodone-specific B cells, while IL-1RA, IL-27, growth regulated oncogene alpha (GROα, or CXCL1), and FLT-3L were negatively associated (**Figure 4**). Additional associations were found between oxycodone-specific B cells and FGF-2, IL-12p40, IL-17A, IL-1α, IL-6, IL-8, MCP-3, M-CSF, MIG/CXCL9, TNFα, and TNFβ, but should be interpreted with caution because group means were below the lowest point on the standard curve. As these cytokines correlated with oxycodone-specific B cells, and

pre-immunization opioid-specific B cells correlate with vaccine efficacy in mice, these cytokines may be of interest as future biomarkers in clinical studies with anti-opioid vaccines.

Select plasma cytokines correlate with self-reported heroin use in individuals with opioid use disorder. Cytokines were analyzed for linear or monotonic correlations between self-reported drug use to determine whether there was a relationship between these two variables (**Table 3**). Concentrations of epidermal growth factor (EGF), FMS-like tyrosine kinase 3 ligand (FLT-3L), IL-9, IL-5, vascular endothelial growth factor A (VEGF-A) were positively correlated with number of bags of heroin used per day. Concentrations of IP-10 correlated positively with years of heroin use, while IL-9, EGF, and RANTES (CCL5) correlated negatively with years of heroin use (**Figure 5**). Concentrations of fibroblast growth factor (FGF)-2, fractalkine, granulocyte colony stimulating factor (G-CSF), IFNα2, IFNγ, IL-10, IL-12p40, IL-12p70, IL-13, IL-15, IL-17A, IL-17E/IL-25, IL-17F, IL-1α, IL-1β, IL-23, IL-4, IL-5, IL-6, MCP-3, MIG/CXCL9, and transforming growth factor (TGF)-α were also associated with drug use, but should be interpreted with caution because group means were below the lowest point on the standard curve. Concentrations of MIG/CXCL9, IL-13, IFNα2, IL-1α, IL-1β, TGFα, IL-17A, and IL-4 were also significantly associated with age (*data not shown*), and because length of time using drugs is dependent on age, these cytokines may not be associated with drug use itself.

Number of oxycodone-specific B cells does not correlate with self-reported heroin use in individuals with opioid use disorder. Since the number of oxycodone-specific B cells was significantly higher in opioid users, we hypothesized that the number of

oxycodone-specific B cells was directly dependent on the quantity or frequency of drug use. To this end, number of oxycodone-specific B cells was plotted against either self-reported number of bags of heroin (equal to $10 worth) used per day or self-reported years of heroin use. There was no significant correlation between heroin use and oxycodone-specific B cells, indicating that frequency of oxycodone-specific B cells is not associated with heroin use (**Figure 6**). Of note, we could not perform this analysis with frequency of oxycodone use, as most individuals in this study did not report consistent ongoing oxycodone use. Future studies will focus on recruitment of higher number of subjects so that analyses could be performed within and across population subsets (e.g., methadone treated vs untreated, heroin vs prescription opioid users, etc).

Oxycodone-specific B cells subsets correlate with morphine-specific serum IgG concentration in individuals with opioid use disorder. As an additional putative biomarker for opioid use, we tested whether opioid-specific B cell subsets correlated with opioid-specific serum IgG concentration measured via ELISA. We found that oxycodone-specific serum IgG concentration trended towards monotonic correlation with oxycodone-specific switched and unswitched memory B cells (**Figure 7A, B**). Additionally, there was a significant linear correlation between morphine-specific serum IgG concentration and oxycodone-specific switched memory B cells. Since pre-immunization oxycodone-specific B cell subsets were correlated with vaccine efficacy in mice (133), oxycodone- or morphine-specific serum IgG titers may represent another predictive biomarker for vaccine efficacy.

DISCUSSION

Published literature suggests that while clinical endpoints in human trials of previous SUD vaccines were not met, the subset of patients that achieved the highest antibody response benefitted from immunization and attained abstinence from either nicotine or cocaine (83, 84). As clinical evaluation of anti-opioid vaccines begins, the identification of putative biomarkers that are indicative of higher titers will be critical for stratification of patients to determine who would most likely benefit from anti-opioid immunization to enhance clinical success. To this end, this exploratory study sought to identify putative cytokines and other biological or behavioral markers that may be of interest as predictive biomarkers of anti-opioid vaccine efficacy. In mice, *in vitro* stimulation of whole blood with the non-specific T cell stimulator PHA can induce IL-4 production that negatively correlates with opioid-specific IgG response after immunization with an anti-oxycodone vaccine. This effect was not replicated when using the TLR4 agonist and innate immune cell stimulator LPS. These data are consistent with our previous work in mice suggesting that IL-4 depletion increases opioid-specific IgG titers in mice, and that this IL-4 depletion results in changes in the number of germinal center T follicular helper cells and the T cell transcription program.

In humans, we sought to identify differences in the immune environment between naïve healthy individuals and opioid users that may be leveraged for putative biomarker identification in future clinical vaccine studies. Using antigen-specific magnetic enrichment and flow cytometry, we found that individuals with OUD have a higher frequency of oxycodone-specific B cells than naïve individuals. As we have previously reported that the frequency of naïve opioid-specific B cells positively correlated with vaccine efficacy in mice (133), we would hypothesize that individuals with OUD may have greater responses to

anti-opioid vaccines compared to opioid-naïve individuals. Interestingly, this increase in oxycodone-specific B cells did not correlate with increased drug use; however, it is notable that since the majority of participants were not oxycodone users, the relationship was examined between oxycodone-specific B cells and heroin use rather than oxycodone use. It will be of interest in future studies to determine whether frequency of opioid-specific B cells correlates with the increased use of the cognate opioid, as this could be used as putative behavioral biomarker in lieu of measuring B cell responses.

We then sought to assess the differences in cytokines and chemokines between the two populations and to determine whether any of these metrics correlated with oxycodone-specific B cells and could also be of interest as putative biomarkers in future clinical studies. From a practical standpoint, cytokines may be superior biomarkers due to ease of testing in clinical settings, as a small quantity of blood and no specialized machinery would be needed to assess cytokine levels compared to a rare B cell population which would need specialized reagents and equipment to identify. We found that there were significant decreases in many chemokines and cytokines related to innate immunity, which is consistent with reports suggesting use of opioids may be immunosuppressive to innate immune signaling, including monocytes and NK cells [reviewed in (271)]. We also found that several cytokines correlated with the number of oxycodone-specific B cells, including TARC, VEGF-A, MCP-2, IL-1RA, IL-27, GRO-α, and FLT-3L. Results were not fully consistent between the three different multiplex cytokine assays performed, and these cytokines will be evaluated more closely using single-plex cytokine analysis in future studies for enhanced accuracy. One further caveat to this study is that the sample size was too small to perform effective multivariate analysis on these cytokines in relation to additional variables, including drug use, age, or sex, so analyses were performed separately to determine relationships between cytokines and each variable. While

separate analyses may not fully capture the complex relationship between variables that may influence cytokine and chemokine production, this preliminary study is nevertheless informative to narrow down some potential cytokines of interest for future clinical studies.

Like cytokines, assessing oxycodone- or morphine-specific antibody concentration as an indirect measure of opioid-specific B cells may be easier in clinical settings. To this end, IgG concentrations were tested as correlates of B cell responses to assess their potential as putative biomarkers. We found that oxycodone-specific serum IgG concentration was associated with oxycodone-specific switched and unswitched memory cells, although these differences only approached statistical significance. Similarly, morphine-specific serum IgG concentration correlated significantly with oxycodone-specific switched memory B cells. While previous preclinical studies did not directly assess associations between pre-immunization levels of opioid-specific memory B cells and vaccine efficacy, one would hypothesize that pre-existing memory B cell populations would rapidly expand in response to vaccination with their cognate antigen. This could lead to increased immune responses compared to individuals who do not possess the same memory B cell populations. Therefore, pre-immunization oxycodone- and morphine-specific IgG concentrations may be valuable as additional predictive biomarkers to be tested in ongoing clinical studies.

To leverage predictive biomarker identification in future clinical OUD vaccine studies, a pipeline of sample collection has been developed to explore biomarkers related to cytokine expression, single-nucleotide polymorphisms (SNPs), mRNA expression, microRNA expression, immune cell populations, and B cell receptor (BCR) sequences (**Figure 8**). Many of these putative biomarkers are identified based on exploratory studies such as the data reported above, while additional putative biomarkers are being identified

through literature searches of biomarkers that were of interest in other vaccine clinical trials. A complete list of SNPs of interest are listed in **Table 4,** and notably includes SNPs from the IL-4 pathway and in the TLR7 and TLR8 receptors. Utilization of this predictive biomarker pipeline to identify correlates of protection for OUD vaccine efficacy in our ongoing OXY-sKLH clinical trial will be critical for enhancing clinical success and allowing a personalized medicine approach to ensure individuals with OUD receive the most effective treatment to manage their disease. Beyond the OXY-sKLH trial, these biomarkers could be applied to other vaccines against OUD, SUD, and potentially other chemical threats.

FIGURES

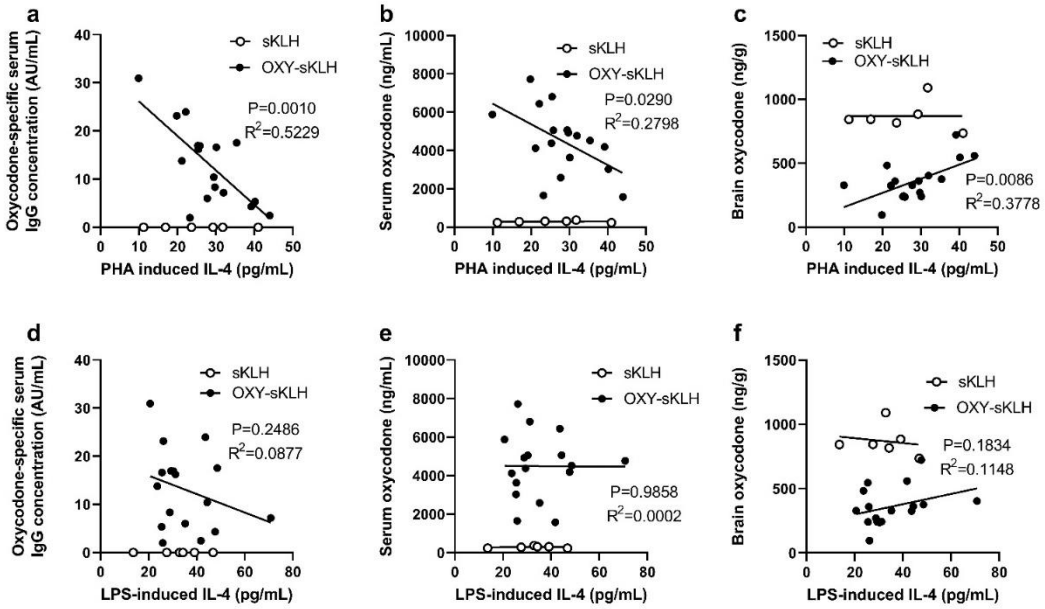

Figure 1. Pre-immunization IL-4 concentration correlates with vaccine efficacy in mice. Jackson outbred diversity (J:DO) mice were bled pre-immunization, and whole blood was plated for *in vitro* stimulation with either PHA (to stimulate T cells) or LPS (to stimulate innate immune cells). After 24 hours, supernatant was collected, and IL-4 was measured via ELISA. Mice were then immunized 3 times and blood was collected 7 days after the final immunization. Oxycodone-specific IgG concentration was measured via ELISA. Mice were subsequently challenged with oxycodone (2.25 mg/kg, s.c.), and blood and brain were collected thirty minutes post-challenge to measure concentration of oxycodone via LCMS/MS. Linear correlation between A) oxycodone-specific IgG concentration and PHA-induced IL-4, B) post-challenge serum oxycodone concentration and PHA-induced IL-4, and C) post-challenge brain oxycodone concentration and PHA-induced IL-4. There was no linear correlation between D) oxycodone-specific IgG concentration and LPS-induced IL-4, E) post-challenge serum oxycodone concentration

and LPS-induced IL-4, or F) post-challenge brain oxycodone concentration and LPS-induced IL-4. Linear associations determined via Pearson correlation.

Table 1. Demographics and drug use information for naïve and OUD subjects (self-reported).

	Naïve (*N*= 25)	**OUD (*N* = 23)**
Age, *M* (SD)	48.2 (8.9)	49.4 (8.1)
Sex		
Male, *N* (%)	20 (80)	21 (91)
Female, *N* (%)	5 (20)	2 (9)
Tetanus vaccination in past 10 years, *N* (%)	7 (28)	6 (26)
Heroin use, *N* (%)	0 (0)	19 (83)
Lifetime heroin use in years, *M* (SD)	-	20.2 (14.3)
Current use: days/week, *M* (SD)	-	6.2 (2.8)
Current use: bags/day, *M* (SD)	-	6.2 (3.6)
Current use: $ spent on heroin/day, *M* (SD)	-	55.00 (31.30)
Current route of administration		
Intranasal	-	14 (61)
Intravenous	-	2 (9)
Intranasal & Intravenous	-	3 (13)
Current or past prescription opioid use, *N* (%)	0 (0)	19 (83)
Current methadone use, *N* (%)	0 (0)	8 (35)
Current buprenorphine use, *N* (%)	0 (0)	3 (13)

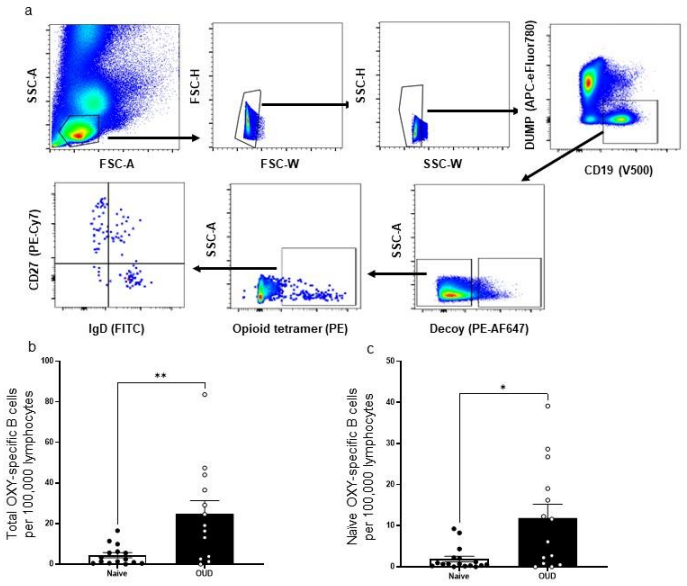

Figure 2. Individuals with OUD have higher frequency of oxycodone-specific total and naïve B cells compared to naïve controls. PBMCs from naïve controls (n=17) or individuals with OUD (n=15) were processed for flow cytometry using antigen-based magnetic enrichment with an oxycodone-specific tetramer (Tet). Both the enriched (bound) sample and the flow through were analyzed via flow cytometry. A) Gating strategy for oxycodone-specific B cells. B) Total oxycodone-specific B cells ($CD19^{+}Tet^{+}Decoy^{-}$) expressed per 100,000 total lymphocytes from bound and flow through samples. C) Oxycodone-specific naïve B cells ($CD19^{+}Tet^{+}Decoy^{-}IgD^{+}CD27^{-}$) expressed per 100,000 total lymphocytes. Data are mean±SEM. Statistical analysis performed via Student's T test.

Table 2. Comparison of cytokine expression means between naïve controls and individuals with OUD. Colors designate difference in OUD compared to control. Kit type: M=Milliplex, Q= Q-plex

Cytokine	Kit	Naïve Mean (pg/mL)	Naïve SEM (pg/mL)	OUD Mean (pg/mL)	OUD SEM (pg/mL)	P-value
EGF	M	5.631	1.167	2.569	0.687	0.0656
	M	1.957	0.6316	0.7573	0.1838	0.2193
Eotaxin	M	20.89	2.687	20.23	1.884	0.9946
	M	14.89	2.12	17.43	1.73	0.1632
	Q	39.31	4.042	46.37	5.163	0.4429
FGF-2	M	8.791	1.855	5.706	0.4844	0.1236
	M	6.827	0.9103	5.98	0.7084	0.2952
FLT-3L	M	1.904	0.473	2.166	0.7056	0.0961
	M	0.9928	0.08898	1.085	0.1341	0.8666
Fractalkine	M	26.39	3.861	21.08	3.758	0.0216
	M	18.84	1.273	19.28	1.27	0.8114
G-CSF	M	5.646	2.065	1.566	0.7566	0.2537
	M	1.437	0.6187	0.4241	0.244	0.2889
GM-CSF	M	0	0	0	0	NA
	M	0	0	0	0	NA
GROα	M	0.9461	0.1771	1.556	0.4586	0.9946
	M	0.7372	0.1334	1.703	0.6502	0.1781
	Q	5.657	0.7434	16.97	6.489	0.0605
I-309	Q	2.606	0.2847	2.762	0.3122	0.7162
IFNα2	M	0.7472	0.1597	0.3359	0.08678	0.0089
	M	1.355	0.1996	1.092	0.1166	0.2825
IFNγ	M	0.065	0.05259	0	0	0.1962
	M	0	0	0	0	NA
	Q	0.6417	0.1337	0.7512	0.1236	0.4899
IL-10	M	4.858	1.597	2.028	0.6404	0.2902
	M	1.673	0.4393	1.175	0.2148	0.9839
	Q	2.333	0.2661	2.802	0.299	0.5817
IL-12p40	M	7.461	0.9181	4.983	0.8105	0.0496
	M	4.588	0.3566	4.416	0.3621	0.7401

IL-12p70	M	0.105	0.05314	0.02227	0.01351	0.0969
	M	0.1911	0.111	0.3745	0.1311	0.288
	Q	0.1622	0.088	0.1362	0.09931	0.587
IL-13	M	1.469	0.6088	1.224	0.4813	0.2854
	M	1.53	0.2177	1.531	0.2529	0.9968
	Q	0.2575	0.06575	0.2214	0.05152	0.7384
IL-15	M	0.5172	0.1322	0.5023	0.177	0.0288
	M	0.4656	0.04848	0.56	0.04601	0.1678
	Q	1.054	0.3453	2.184	0.7471	0.2027
IL-17	Q	0.275	0.1887	0.9043	0.5063	0.4062
IL-17A	M	0.2944	0.1342	0.2068	0.1139	0.6726
	M	0	0	0	0	NA
IL-17E/IL-25	M	8.933	1.452	5.753	0.7299	0.0615
	M	5.819	0.6145	5.811	0.7432	0.6424
IL-17F	M	4.033	3.013	2.975	1.115	0.718
	M	1.553	0.6675	2.61	0.9319	0.3278
IL-18	M	26.59	5.365	10.09	3.656	0.0002
	M	18.7	3.477	7.812	2.276	0.0002
IL-1RA	M	9.179	1.527	3.966	1.56	0.0001
	M	3.286	0.5742	1.581	0.3724	0.0001
IL-1α	M	0.1267	0.08024	0.165	0.08708	0.817
	M	0.09389	0.02916	0.1068	0.01734	0.6936
	Q	1.263	0.1671	2.265	1.131	0.0387
IL-1β	M	0.8322	0.339	0.8218	0.3922	0.347
	M	0.9133	0.1405	0.6568	0.1338	0.1963
	Q	2.304	0.3688	0.9119	0.3249	0.0177
IL-2	M	0	0	0	0	NA
	M	0	0	0	0	NA
	Q	0.1703	0.01881	0.2024	0.01729	0.1574
IL-22	M	2.822	1.283	0	0	0.013
	M	0	0	0	0	NA
IL-23	Q	103.6	84.56	16.28	3.166	0.7006
IL-27	M	76.33	11.47	74.91	14.09	0.8825
	M	56.58	5.786	85.06	17.13	0.2188
IL-3	M	0	0	0	0	NA

	M	0	0	0	0	NA
IL-4	M	0.4772	0.194	0.115	0.051	0.1066
	M	0.01944	0.01364	0.000909	0.000909	0.1926
	Q	0.00475	0.001815	0.005381	0.001349	0.5586
IL-5	M	0.9861	0.4675	1.209	0.4854	0.4463
	M	0.3033	0.06029	0.3359	0.07467	0.762
	Q	0.05167	0.02545	0.3531	0.2034	0.0981
IL-6	M	0.04611	0.01469	0.06909	0.02455	0.938
	M	0.01056	0.007518	0.08591	0.04732	0.4005
	Q	0.525	0.08253	1.012	0.2743	0.0953
IL-7	M	0	0	0	0	NA
	M	0	0	0	0	NA
IL-8	M	0.6956	0.1307	0.6205	0.2069	0.0192
	M	0.655	0.1212	0.6114	0.1386	0.392
	Q	2.358	0.417	2.564	0.7654	0.5347
IL-9	M	6.156	2.12	6.584	2.44	0.5585
	M	2.858	0.7802	2.598	0.6556	0.7408
IP-10	M	18.77	1.566	12.99	2.689	0.0054
	M	12.21	1.141	14.94	4.267	0.251
	Q	9.073	0.8911	16.33	3.267	0.2024
MCP-1	M	19.42	3.825	22.52	3.003	0.2989
	M	15.47	3.132	22.19	2.967	0.1292
	Q	29.93	3.682	50.81	8.942	0.03
MCP-2	Q	4.081	0.6382	5.636	0.8949	0.2121
MCP-3	M	0.065	0.04947	0.1741	0.1741	0.5791
	M	1.751	0.3141	1.783	0.2269	0.7014
M-CSF	M	10.91	1.213	7.475	0.9024	0.001
	M	9.092	1.118	8.278	0.8413	0.505
MDC	M	23.69	2.106	20.66	2.407	0.3606
	M	27.03	2.342	32	3.181	0.234
MIG/ CXCL9	M	42.63	6.816	39.33	12.83	0.0419
	M	38.09	5.956	63.83	25.44	0.7778
MIP-1α	M	0	0	0	0	NA
	M	0	0	0	0	NA
MIP-1β	M	2.313	0.2886	1.431	0.1406	0.0015

	M	1.953	0.1916	1.533	0.1937	0.1361
PDGF-AA	M	187.8	31.71	128	22.03	0.1397
	M	107.4	15.76	82.69	12.28	0.2159
PDGF-AB/BB	M	1141	135.6	769.6	101.8	0.0295
	M	881.7	94.4	773.9	75.31	0.3717
RANTES	M	1002	66.38	942.8	80.77	0.9678
	M	782.1	43.15	782.5	53.35	0.6768
	Q	2008	210.4	2421	317.7	0.286
sCD40L	M	140	24.47	84.7	21.29	0.0077
	M	64.42	9.105	52.44	7.258	0.3665
TARC	Q	20.26	2.064	25.16	2.241	0.121
TGFα	M	2.164	1.215	1.131	0.4017	0.1088
	M	1.027	0.345	0.7005	0.1312	0.8453
TNFα	M	1.82	0.3027	1.441	0.1893	0.2369
	M	1.679	0.1216	1.855	0.1955	0.6714
	Q	1.21	0.1198	1.878	0.3347	0.1329
TNFβ	M	1.424	0.6227	0.65	0.2867	0.171
	M	0.5772	0.1393	0.9068	0.3221	0.9082
	Q	0.6569	0.09525	0.83	0.1717	0.7852
VEGF-A	M	11.35	2.532	5.563	1.249	0.0618
	M	6.302	1.124	5.609	0.8075	0.6112

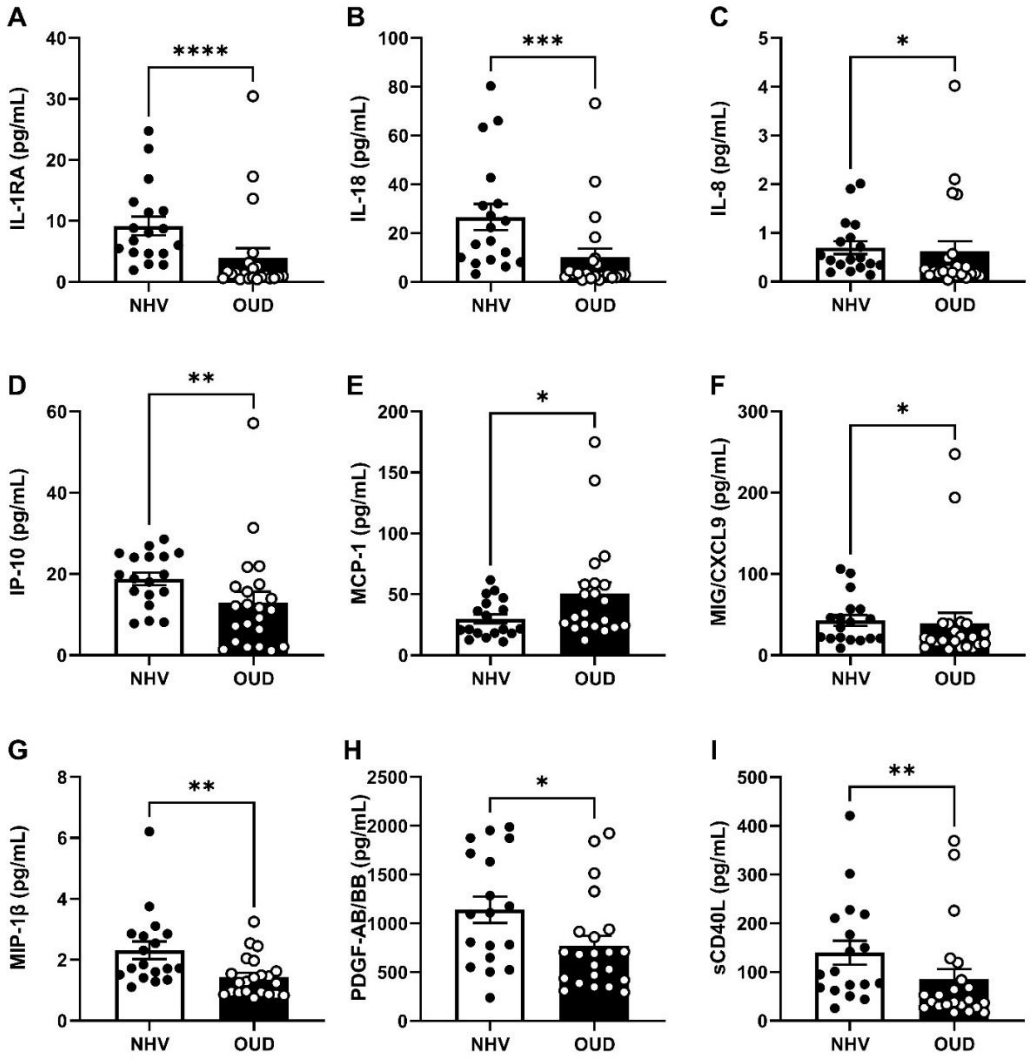

Figure 3. Individuals with opioid use disorder have a differing plasma cytokine expression compared to naïve healthy controls. Plasma samples from naïve healthy controls (NHV, n=18) or individuals with opioid use disorder (OUD, n=21-22) were assessed using multiplex cytokine kits. Differences were seen in expression of several plasma cytokines, including A) IL-1RA, B) IL-18, C) IL-8, D) IP-10, E) MCP-1, F) MIG/CXCL9, G) MIP-1β, H) PDGF-AB/BB, and I) sCD40L. A full list of tested cytokines and expression levels can be found in **Table 2**. Data are mean±SEM. Data was tested for normality using D'Agostino-Pearson's test. If normal, data was analyzed using an unpaired

T-test (G, H). If non-normal, data was analyzed using Mann-Whitney U-test (A-F, I). Statistical symbols: * $p<0.01$, ** $p<0.01$, *** $p<0.001$, **** $p<0.0001$.

Table 3. Correlations between cytokines and self-reported heroin use or oxycodone-specific B cells in individuals with OUD. Spearman correlations designated by reporting an r value while Pearson correlations designated by reporting an R^2 value.

Cytokine	Kit Type	Correlation to Heroin Use (years)	Correlation to Heroin Use (bags/day)	Correlation to OXY+ B cells/100,000 lymphocytes
EGF	MILLIPLEX	Negative (P=0.0447, r=-0.4423)	Positive (P=0.0066, R^2=0.3434)	None (P=0.1775)
	MILLIPLEX	None (P=0.2216)	None (P=0.1805)	None (P=0.8564)
Eotaxin	MILLIPLEX	None (P=0.4502)	None (P=0.7189)	None (P=0.4502)
	MILLIPLEX	None (P=0.8802)	None (P=0.3601)	None (P=0.6904)
	Q-Plex	None (P=0.4833)	None (P=0.1024)	None (P=0.0901)
FGF-2	MILLIPLEX	None (P=0.6800)	None (P=0.2630)	None (P=0.4502)
	MILLIPLEX	Negative (P=0.0027, R^2=0.3849)	Negative (P=0.0171, R^2=0.2913)	Positive (P=0.0261, R^2=0.2730)
FLT-3L	MILLIPLEX	None (P=0.2170)	Positive (P=0.0145, R^2=0.2891)	Negative (P=0.0185, r=-0.5483)
	MILLIPLEX	None (P=0.2398)	None (P=0.1217)	None (P=0.1170)
Fractalkine	MILLIPLEX	None (P=0.4443)	Positive (P=0.0144, R^2=0.2895)	None (P=0.1251)
	MILLIPLEX	None (P=0.3349)	None (P=0.2144)	Positive (P=0.0248, r=0.5266)
G-CSF	MILLIPLEX	None (P=0.0913)	Positive (P=0.0172, R^2=0.2768)	None (P=0.5601)
	MILLIPLEX	None (P=0.3576)	None (P=0.1637)	None (P=0.8190)
GM-CSF	MILLIPLEX	None (NA)	None (NA)	None (NA)
	MILLIPLEX	None (NA)	None (NA)	None (NA)
GROα	MILLIPLEX	None (P=0.9461)	None (P=0.7216)	Negative (P=0.0106, r=-0.5857)
	MILLIPLEX	None (P=0.9898)	None (P=0.9341)	None (P=0.6011)
	Q-Plex	None (P=0.7298)	None (P=0.3133)	None (P=0.3731)
I-309	Q-Plex	None (P=0.3012)	None (P=0.7723)	None (P=0.8673)
IFNα2	MILLIPLEX	None (P=0.1058)	None (P=0.2445)	None (P=0.7577)
	MILLIPLEX	Negative (P=0.0020, R^2=0.4014)	None (P=0.1467)	None (P=0.1670)

IFNγ	MILLIPLEX	None (NA)	None (NA)	None (NA)
	MILLIPLEX	None (NA)	None (NA)	None (NA)
	Q-Plex	None (P=0.8995)	Negative (P=0.0415, R^2=0.2349)	None (P=0.7255)
IL-10	MILLIPLEX	None (P=0.0655)	Positive (P=0.0403, R^2=0.2135)	None (P=0.4321)
	MILLIPLEX	None (P=0.0963)	None (P=0.6004)	None (P=0.4746)
	Q-Plex	None (P=0.6952)	None (P=0.5067)	None (P=0.1188)
IL-12p40	MILLIPLEX	None (P=0.6232)	Positive (P=0.0168, R^2=0.2786)	Negative (P=0.0329, R^2=0.2543)
	MILLIPLEX	None (P=0.6614)	None (P=0.4865)	None (P=0.5717)
IL-12p70	MILLIPLEX	None (P=0.5113)	None (P=0.0664)	None (P=0.2107)
	MILLIPLEX	None (P=0.9274)	Negative (P=0.0453, R^2=0.2154)	None (P=0.7090)
	Q-Plex	None (P=0.3449)	Positive (p=0.0004, R^2=0.5579)	None (P=0.6229)
IL-13	MILLIPLEX	None (P=0.3140)	Positive (P=0.0084, R^2=0.3276)	None (P=0.1503)
	MILLIPLEX	Negative (P=0.0069, R^2=0.3253)	None (P=0.5074)	None (P=0.0552)
	Q-Plex	None (P=0.2411)	Positive (P=0.0015, R^2=0.4768)	None (P=0.08704)
IL-15	MILLIPLEX	None (P=0.1989)	Positive (P=0.0229, R^2=0.2557)	None (P=0.1806)
	MILLIPLEX	Negative (P=0.0355, R^2=0.2123)	None (P=0.4782)	None (P=0.3473)
	Q-Plex	None (P=0.8389)	None (P=0.2996)	None (P=0.2355)
IL-17	Q-Plex	None (P=0.4541)	None (P=0.6415)	None (P=0.9656)
IL-17A	MILLIPLEX	None (P=0.3265)	Positive (P=0.0377, R^2=0.4917)	None (P=0.1724)
	MILLIPLEX	None (P=0.1920)	None (P=0.1518)	Positive (P=0.0008, R^2=0.5170)
IL-17E/IL-25	MILLIPLEX	Negative (P=0.0161, R^2=0.2687)	None (P=0.2918)	None (P=0.4093)

	MILLIPLEX	Negative (P=0.0027, r=-0.6205)	None (P=0.4132)	None (P=0.5718)
IL-17F	MILLIPLEX	Negative (P=0.0141, r=-0.5271)	None (P=0.3946)	None (P=0.4765)
	MILLIPLEX	Negative (P=0.0429, R^2=0.1986)	None (P=0.2898)	None (P=0.5512)
IL-18	MILLIPLEX	None (P=0.7334)	None (P=0.2582)	None (P=0.2045)
	MILLIPLEX	None (P=0.5429)	None (P=0.2918)	None (P=0.2243)
IL-1RA	MILLIPLEX	None (P=0.9016)	None (P=0.2173)	Negative (P=0.0051, r=-0.6302)
	MILLIPLEX	None (P=0.6557)	None (P=0.3311)	None (P=0.3433)
IL-1α	MILLIPLEX	None (P=0.2536)	Positive (P=0.0263, R^2=0.2456)	None (P=0.1732)
	MILLIPLEX	Negative (P=0.0010, R^2=0.4407)	None (P=0.4486)	None (P=0.4420)
	Q-Plex	None (P=0.1001)	None (P=0.6968)	Positive (P=0.0369, r=0.5140)
IL-1β	MILLIPLEX	None (P=0.3074)	Positive (P=0.0211, R^2=0.2618)	None (P=0.1644)
	MILLIPLEX	Negative (P=0.0040, R^2=0.3610)	None (P=0.9838)	None (P=0.1884)
	Q-Plex	None (P=0.6254)	None (p=0.8979)	None (P=0.3291)
IL-2	MILLIPLEX	None (NA)	None (NA)	None (NA)
	MILLIPLEX	None (NA)	None (NA)	None (NA)
	Q-Plex	None (P=0.6157)	None (P=0.3359)	None (P=0.2595)
IL-22	MILLIPLEX	None (NA)	None (NA)	None (NA)
	MILLIPLEX	None (NA)	None (NA)	None (NA)
IL-23	Q-Plex	None (P=0.0961)	Positive (P=0.0141, R^2=0.3217)	None (P=0.8266)
IL-27	MILLIPLEX	None (P=0.4207)	None (P=0.3727)	Negative (P=0.0170, r=-0.5542)
	MILLIPLEX	None (P=0.4366)	None (P=0.8241)	None (P=0.5258)
IL-3	MILLIPLEX	None (NA)	None (NA)	None (NA)
	MILLIPLEX	None (NA)	None (NA)	None (NA)

IL-4	MILLIPLEX	None (P=0.1048)	Positive (P=0.0049, R^2=0.3640)	None (P=0.3201)
	MILLIPLEX	None (P=0.3485)	None (P=0.0861)	None (P=0.9769)
	Q-Plex	None (P=0.1631)	None (P=0.2836)	None (P=0.6217)
IL-5	MILLIPLEX	None (P=0.2386)	Positive (P=0.0142, R^2=0.2903)	None (P=0.2367)
	MILLIPLEX	None (P=0.2575)	None (P=0.1737)	None (P=0.9158)
	Q-Plex	None (P=0.8179)	None (P=0.5439)	None (P=0.0517)
IL-6	MILLIPLEX	Positive (P=0.0134, R^2=0.2812)	None (P=0.7429)	Negative (P=0.0211, r=-0.5385)
	MILLIPLEX	Positive (P=0.0120, R^2=0.2888)	None (P=0.2134)	None (P=0.8415)
	Q-Plex	None (P=0.4878)	None (P=0.1020)	None (P=0.8543)
IL-7	MILLIPLEX	None (NA)	None (NA)	None (NA)
	MILLIPLEX	None (NA)	None (NA)	None (NA)
IL-8	MILLIPLEX	None (P=0.7954)	None (P=0.1036)	Negative (P=0.0238, r=-0.5297)
	MILLIPLEX	None (P=0.1333)	None (P=0.8322)	None (P=0.3956)
	Q-Plex	None (P=0.0964)	None (P=0.2039)	None (P=0.8452)
IL-9	MILLIPLEX	None (P=0.1662)	Positive (P=0.0089, R^2=0.3237)	None (P=0.1963)
	MILLIPLEX	Negative (P=0.0292, r=-0.4759)	None (P=0.0700)	None (P=0.5447)
IP-10	MILLIPLEX	Positive (P=0.0157, R^2=0.2701)	None (P=0.5613)	None (P=0.1004)
	MILLIPLEX	Positive (P=0.0042, R^2=0.3571)	None (P=0.6201)	None (P=0.3889)
	Q-Plex	None (P=0.0562)	None (P=0.2539)	None (P=0.7375)
MCP-1	MILLIPLEX	None (P=0.1556)	None (P=0.5125)	None (P=0.3955)
	MILLIPLEX	None (P=0.1964)	None (P=0.2088)	None (P=0.7037)
	Q-Plex	None (P=0.2427)	None (P=0.0712)	None (P=0.1179)
MCP-2	Q-Plex	None (P=0.8722)	None (P=0.2059)	Positive (P=0.0442, r=0.4975)
MCP-3	MILLIPLEX	None (P=0.3707)	None (P=0.7722)	None (NA)

	MILLIPLEX	Negative (P=0.0436, R^2=0.1975)	None (P=0.2553)	Positive (P=0.0076, r=0.6067)
M-CSF	MILLIPLEX	None (P=0.4206)	None (P=0.1499)	Negative (P=0.0303, r=-0.5109)
	MILLIPLEX	None (P=0.2557)	None (P=0.2758)	None (P=0.6811)
MDC	MILLIPLEX	None (P=0.7576)	None (P=0.2237)	None (P=0.2499)
	MILLIPLEX	None (P=0.2921)	None (P=0.9856)	None (P=0.3115)
MIG/CXCL9	MILLIPLEX	Positive (P=0.0020, R^2=0.4015)	None (P=0.9507)	Negative (P=0.0004, r=-0.7420)
	MILLIPLEX	Positive (P=0.0039, R^2=0.3621)	None (P=0.5893)	None (P=0.3855)
MIP-1α	MILLIPLEX	None (NA)	None (NA)	None (NA)
	MILLIPLEX	None (NA)	None (NA)	None (NA)
MIP-1β	MILLIPLEX	None (P=0.3418)	None (P=0.0809)	None (P=0.0901)
	MILLIPLEX	None (P=0.7258)	None (P=0.4585)	None (P=0.8053)
PDGF-AA	MILLIPLEX	None (P=0.1921)	None (P=0.3622)	None (P=0.5710)
	MILLIPLEX	None (P=0.0886)	None (P=0.9891)	None (P=0.9517)
PDGF-AB/BB	MILLIPLEX	None (P=0.3035)	None (P=0.5304)	None (P=0.6257)
	MILLIPLEX	None (P=0.1162)	None (P=0.3618)	None (P=0.2797)
RANTES	MILLIPLEX	None (P=0.4387)	None (P=0.8187)	None (P=0.4147)
	MILLIPLEX	Negative (P=0.0209, r=-0.5002)	None (P=0.9879)	None (P=0.4157)
	Q-Plex	None (P=0.7917)	None (P=0.8247)	None (P=0.5824)
sCD40L	MILLIPLEX	None (P=0.9131)	None (P=0.2091)	None (P=0.1603)
	MILLIPLEX	None (P=0.6010)	None (P=0.8865)	None (P=0.7745)
TARC	Q-Plex	None (P=0.2471)	None (P=0.3146)	Positive (P=0.0244, r=0.0244)
TGFα	MILLIPLEX	None (P=0.2219)	Positive (P=0.0289, R^2=0.2385)	None (P=0.1761)
	MILLIPLEX	Negative (P=0.0080, R^2=0.3159)	None (P=0.9355)	None (P=0.4254)
TNFα	MILLIPLEX	None (P=0.5129)	None (P=0.3994)	Negative (P=0.0170, R^2=0.3070)
	MILLIPLEX	None (P=0.3330)	None (P=0.1552)	None (P=0.7852)

	Q-Plex	None (P=0.1097)	None (P=0.4224)	None (P=0.7136)
TNFβ	MILLIPLEX	None (P=0.9035)	None (P=0.1526)	None (P=0.3670)
	MILLIPLEX	None (P=0.1128)	None (P=0.2217)	Positive (P=0.0305, R^2=0.2603)
	Q-Plex	None (P=0.2076)	None (P=0.5019)	None (P=0.8639)
VEGF-A	MILLIPLEX	None (P=0.4259)	Positive (P=0.0183, r=0.5216)	None (P=0.3375)
	MILLIPLEX	None (P=0.3504)	None (P=0.8266)	Positive (P=0.0225, r=0.5338)

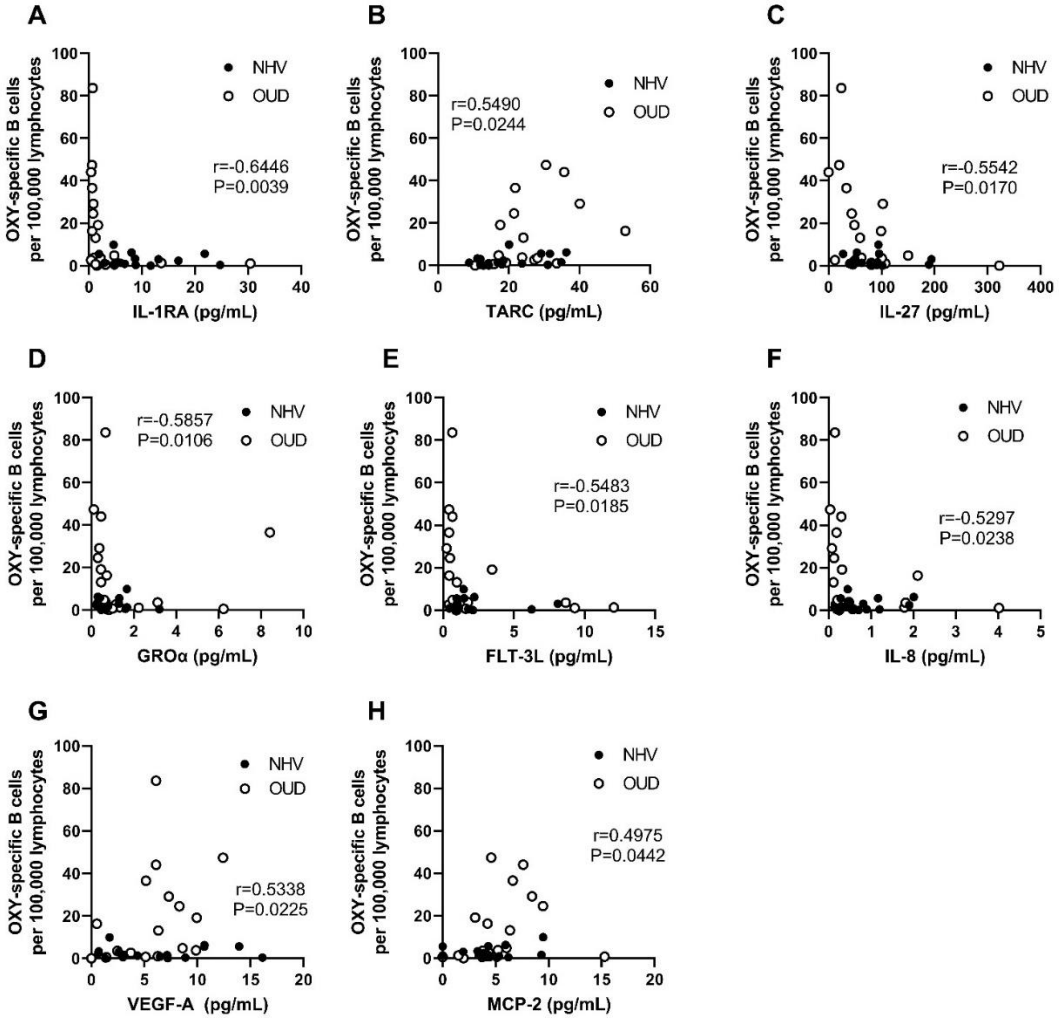

Figure 4. Number of oxycodone-specific B cells correlate with cytokine expression in individuals with opioid use disorder. Number of oxycodone-specific B cells per 100,000 lymphocytes was assessed for linear or monotonic relationships with cytokine expression from multiplex cytokine analysis. Significant associations were found between oxycodone-specific B cells and A) IL-1RA, B) TARC, C) IL-27, D) GROα, E) FLT-3L, F) IL-8, G) VEGF-A and H) MCP-2. A full list of cytokines and associations can be found in **Table 3**. Data were analyzed for linear relationships using Pearson correlation and for monotonic relationships using Spearman correlation. Monotonic relationships are designated by reporting an r value.

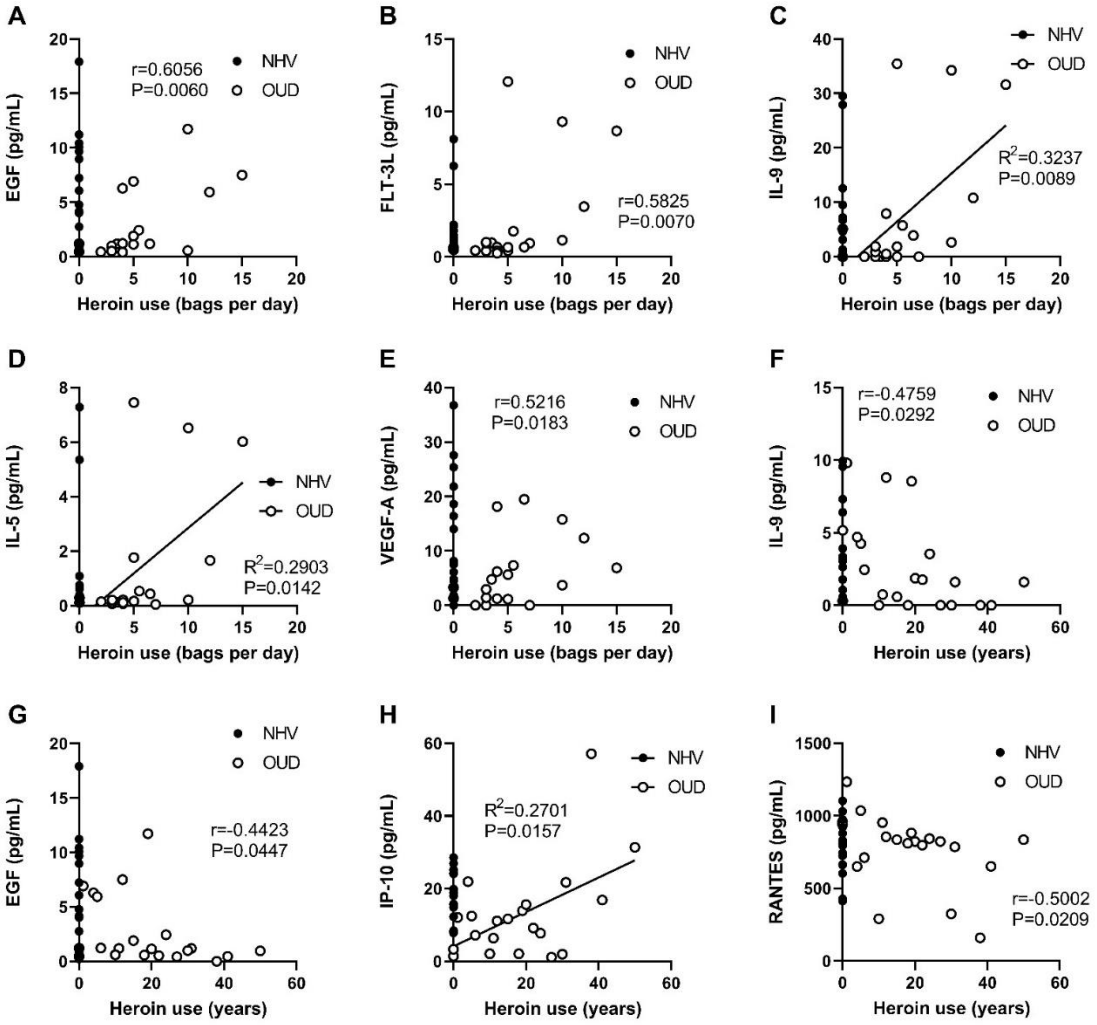

Figure 5. Plasma cytokine expression significantly correlates with self-reported heroin use in individuals with OUD. Plasma cytokine expression was assessed for linear and monotonic relationships with self-reported drug use including number of bags of heroin used per day and total years of heroin use. Heroin use significantly correlated with A) EGF, B) FLT-3L, C) IL-9, D) IL-5, E) VEGF-A, F) IL-9, G) EGF, H) IP-10, and I) RANTES. A full list of cytokines and associations can be found in **Table 3**. Data were analyzed for linear relationships using Pearson correlation and for monotonic relationships using Spearman correlation. Linear correlations are designated by reporting an R^2 value, while monotonic relationships are designated by reporting an r value.

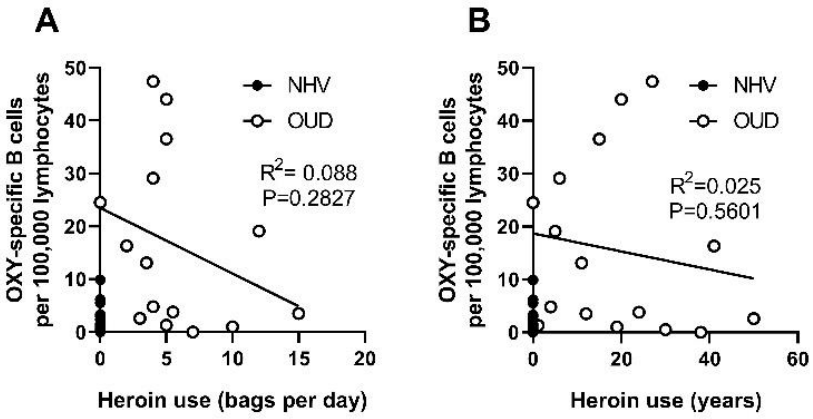

Figure 6. Number of oxycodone-specific B cells does not correlate with self-reported heroin use in individuals with OUD. Number of oxycodone-specific B cells per 100,000 lymphocytes was analyzed for linear and monotonic relationships with A) self-heroin use including number of bags of heroin used per day and B) total years of heroin use. No correlation was seen between these variables in individuals with OUD. Data were analyzed for linear relationships using Pearson correlation and for monotonic relationships using Spearman correlations.

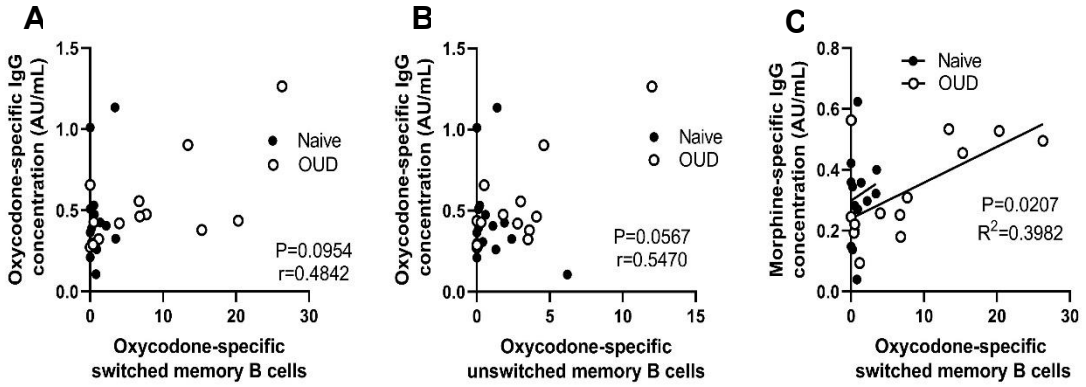

Figure 7. Oxycodone-specific B cell subsets have trending or significant correlations with oxycodone or morphine-specific IgG concentrations in individuals with OUD. Oxycodone-specific B cell subsets per 100,000 lymphocytes were analyzed for linear and monotonic relationships with opioid-specific antibody concentrations measured via ELISA. A) Near significant monotonic correlation between oxycodone-specific IgG titers and oxycodone-specific switched memory B cells. B) Near significant monotonic correlation between oxycodone-specific IgG concentration and oxycodone-specific unswitched memory B cells. C) Significant linear correlation between morphine-specific IgG concentration and oxycodone-specific switched memory B cells. Data were analyzed for linear relationships using Pearson correlation and for monotonic relationships using Spearman correlations.

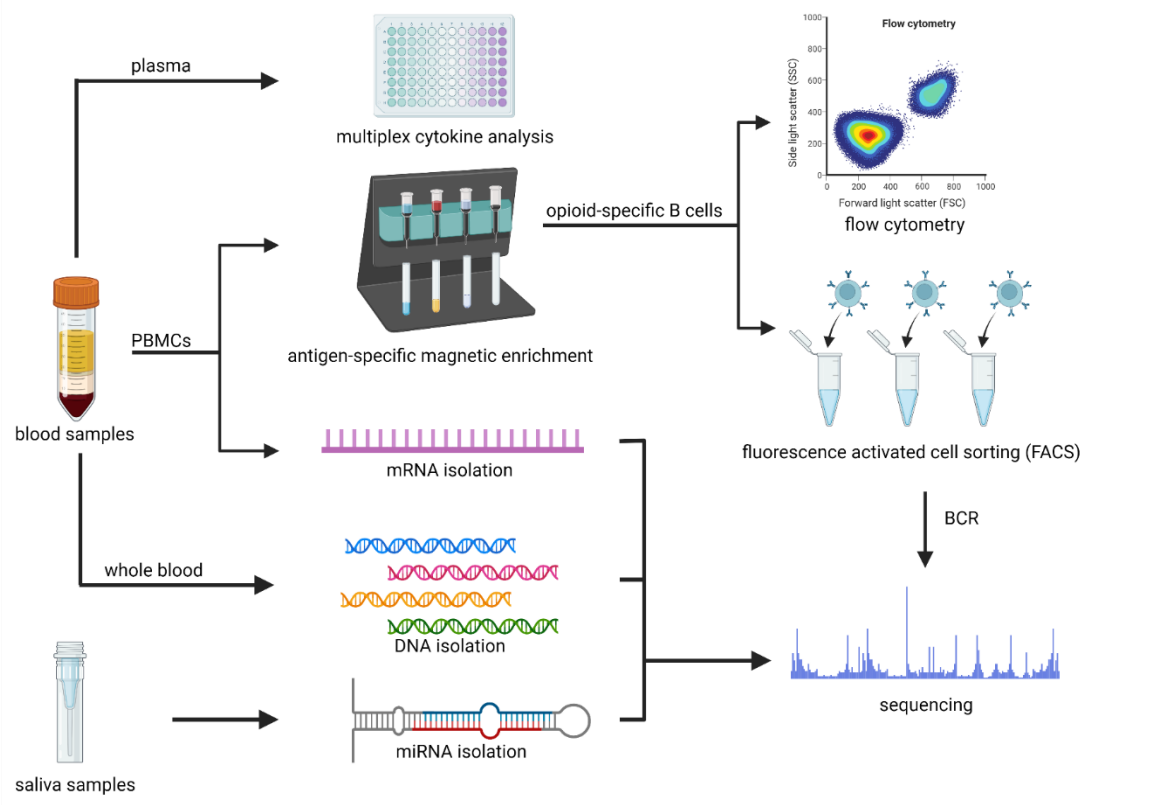

Figure 8. Biomarker discovery pipeline for ongoing and future anti-opioid vaccine clinical trials.

Table 4. Single nucleotide polymorphisms identified as putative biomarkers for an anti-oxycodone vaccine

Target	rs number	Minor Allele Frequency	Target	rs number	Minor Allele Frequency
IL-4	rs2227284	44-49%	TLR8	rs5744078	2-7%
	rs2243250	14-67%		rs5744080	41%
	rs2070874	13-45%		rs3747414	29%
	rs2243248	7-18%	TLR9	rs5743836	25%
	rs2243268	13-27%		rs187084	47%
	rs2243291	38-45%	IL-13	rs20541	18-23%
IL-4R	rs1801275	21-66%	IL-28B	rs8099917	14-19%
	rs1805010	44-46%	IL-12B	rs3213094	22-36%
	rs1805015	16-39%		rs17860508	-
	rs2057768	24-31%		rs3212227	22-27%
	rs2243290	13-36%	IFNL3	rs8099917	14-19%
	rs1805011	10-53%	IFNG	rs2069727	34-44%
	rs1805016	5-43%	MAPK8	rs3827680	40%
	rs8832	43-77%		rs10857565	6%
	rs1029489	40%	ITGAL	rs4243232	37-43%
	rs3024585	43%		rs2230433	31-32%
	rs3024622	31-35%	IL-6	rs1800796	10-22%
STAT6	rs1059513	7-10%		rs2069861	2-6%
	rs324013	48-49%	TNFRSF1A	rs4149621	4-16%
	rs324011	25-38%	IL1R1	rs3732131	10-13%
	rs324015	24-25%	IL1RN	rs315952	28-37%
IL-10	rs1800896	28-52%		rs315951	27-37%
	rs1800871	23-44%	IL2RA	rs2228150	4-8%
	rs1800872	31-32%		rs12722605	6-10%
IL-10RA	rs2508450	43-48%	IFNB1	rs1364613	10-13%
	rs2229113	24-30%	DDX58	rs10813831	21-23%
	rs4252249	11-12%		rs669260	15-16%
	rs4252243	11-16%	RARB	rs6793694	37.70%
IL-10RB	rs3171425	33%		rs1153600	32-34%
TLR2	rs5743708	5-14%	TRIM5	rs3824949	44%
	rs3804100	7-8%		rs3740996	11%
TLR4	rs4986790	6-10%	TRIM22	rs2179	30%
	rs4986791	6-10%	SIRPB3P	rs6135736	16-22%
TLR7	rs179008	17-18%	SIRPG	rs3818168	19%
	rs179016	16-48%	SIRPG-AS1	rs17770331	19%
	rs864058	24%		rs4813191	25-26%

TLR8	rs3764880	36%	ADGRB3	rs551216	31-33%
	rs4830805	24-29%		rs2042086	21-28%
	rs5741883	27-30%	IFITM3	rs12252	12-15%
	rs5744077	15%	TNF-α	rs1800629	11-15%

Chapter 7: Discussion and Conclusions

SUD vaccines have historically performed poorly in clinical studies due to lack of efficacy; however, this lack of efficacy is largely due to individual variability, as those who produce sufficient antibody responses did have improved clinical outcomes. The research program presented here sought to investigate strategies to increase OUD vaccine efficacy to overcome individual variability in antibody responses using a variety of complementary approaches including the elucidation of immunological mechanisms of vaccine efficacy to inform rational vaccine design and biomarker identification, the addition of novel adjuvants to increase vaccine efficacy, assessing variations in hapten design and immunization schedule to increase efficacy of monovalent and bivalent vaccines, investigation of environmental factors that may contribute to vaccine efficacy, and the identification of predictive biomarkers of vaccine efficacy.

Chapter 2 investigated the mechanisms of anti-opioid vaccine efficacy by assaying immune cell populations and signaling mechanisms involved in a previously reported IL-4 mediated increase in vaccine efficacy (94). The goal of this chapter was to elucidate critical mechanisms of vaccine efficacy that can then be used for rational adjuvant selection to optimize the immune response and biomarker identification in clinical studies. The studies in this chapter found that IL-4 increases opioid vaccine efficacy through increasing the number and size of germinal centers in secondary lymphoid organs, likely through an expansion of T cell populations, which in turn provide help to GC B cells and increase the number of antibody secreting cells. Additionally, it was discovered the NKT cells, changes in affinity maturation, and reduced class switching to IgE did not play a role in the increased vaccine efficacy. Importantly, while the depletion of IL-4 increased subclass switching to IgG_{2a}, this IgG subclass did not directly increase vaccine efficacy after drug

challenge. This implies that it is not a strongly polarized Th_2 response that is needed, but rather a balanced Th_1/Th_2 response that engages both populations of cells. These changes appeared to be mediated through Type I IL-4 signaling, but were not mediated through downstream STAT6 or IRS2 signaling, calling into question whether IL-4 signals through a noncanonical receptor or noncanonical signaling pathway downstream of the IL-4R, such as STAT5. This also suggests that while IL-4 may be useful as a predictive biomarker in clinical studies, other signaling components such as IL-13, IL-4R, STAT6 or IRS2 may not. Future investigations into the signaling mechanisms behind this increase in efficacy are of interest, but they may need to wait until additional animal models and/or reagents are available for the targeted depletion of signaling downstream of IL-4. In addition, while the studies in this chapter focused on the effect of IL-4 depletion on lymphocyte populations such as B and T cells, future studies should address whether the changes in lymphocyte populations are due to modulation from other cell populations involved in GC formation, including conventional dendritic cells, follicular dendritic cells, or macrophages.

Using insights gained from the studies in Chapter 2, **Chapter 3** assessed the potential of novel TLR adjuvants to increase the efficacy of a lead fentanyl vaccine. While studies in Chapter 2 were focused on a lead oxycodone vaccine which is currently in a Phase I clinical trial, Chapter 3 focused on a novel fentanyl conjugate vaccine (F_1-CRM or F-CRM) still in preclinical development. Studies from Chapter 2 suggest that the identified mechanisms may be similar between the two vaccines, as IL-4 depletion similarly increased the efficacy of F-CRM. As studies from Chapter 2 suggested that a balanced Th_1/Th_2 response is necessary for vaccine efficacy, the studies in Chapter 3 investigated the utility of Th_1 polarizing novel TLR4 (INI-2002) and TLR7/8 (INI-4001) agonist adjuvants (272) combined with aluminum hydroxide, a Th_2 polarizing adjuvant (98). Unlike other

TLRs, TLR7/8 agonists have also been found to increase proliferation of T_{fh} cells (189), which was another mechanism found to be important for vaccine efficacy in Chapter 2. These studies found that when formulated with F-CRM, the TLR7/8 agonist with alum increased vaccine efficacy in both mice and rats, while the TLR4 agonist with alum did not. This was consistent with the IgG subclass titer data suggesting that the TLR7/8 agonist with alum produced a balanced IgG_1/IgG_{2a} response, while the TLR4 agonist with alum failed to produce IgG_{2a}. Further studies investigated the pharmacology of the lead F-CRM+INI-4001+alum formulation and found that addition of the adjuvants shifted the dose-response curve of the vaccine in preventing respiratory depression almost 3-fold compared to the vaccine without the adjuvants. In a model of fentanyl self-administration which mimics opioid misuse, the vaccine was found to shift the dose-response curve and attenuate lever pressing at the lower doses of fentanyl that were assessed. Studies assessing the safety of the vaccine formulation found that there was not any *in vitro* or *in vivo* cross reactivity to MOUD including methadone, buprenorphine, naltrexone, or naloxone, or to endogenous opioids such as β-endorphin or endomorphin-1. Finally, in a porcine model of overdose, immunization with the lead formulation tended to induce higher antibody titers which prevented apnea in 2 out of the 3 pigs tested. The results of the studies from this chapter were the basis for a pre-Investigational New Drug (pre-IND) submission to the Food and Drug Administration (FDA) with the intention of moving this formulation forward into a Phase I clinical trial. Ongoing and future studies involve the completion of toxicology studies and additional efficacy and safety studies in order to complete an IND application to receive approval for clinical studies.

Another strategy to increase vaccine efficacy is through manipulation of vaccine design, which could include varying hapten design, linker length, and carrier proteins [reviewed in (242)]. In **Chapter 4**, the efficacy of a novel carfentanil vaccine is investigated

by testing two identical hapten structures with varying linker lengths. In this study, longer linker length appears to be superior at eliciting antibody titers, potentially due to decreased steric hindrance to facilitate presentation to antigen-specific B and T cells. Once a lead carfentanil vaccine was identified, several bivalent immunization strategies were tested to increase the efficacy of vaccines to target multiple antigens, including fentanyl and carfentanil. Immunization using a co-administration strategy was more effective at inducing antibody titers when compared to a heterologous strategy, which was reflected in trending increases in efficacy after drug challenge. Future studies will investigate the mechanisms involved in the increase in efficacy seen after co-administration, and will directly investigate other factors related to vaccine design that may contribute to efficacy of multivalent vaccine formulations, including divalent hapten designs or choice of carrier protein.

In addition to vaccine-intrinsic factors such as chemistry, formulation, and mechanism of action, environmental factors of the indicated population for vaccination are important in determining correlates of vaccine efficacy. For example, it has been previously shown that sex, age, and strain (genetics) may influence OUD vaccine efficacy in mice (72, 97). **Chapter 5** further investigated environmental conditions that could impact vaccine efficacy by testing the influence of housing condition and microbiome on OUD vaccine efficacy in mice and rats using model vaccines for both oxycodone and fentanyl. We hypothesized that reduction in microbial diversity would lead to reduction in vaccine efficacy, and that specific changes in the microbiome may be identified to use as predictive biomarkers in clinical studies. Contrary to our hypothesis, the present data suggests that reduction in microbial diversity associated with sterile housing conditions does not affect vaccine efficacy. While this study did not identify any putative biomarkers related to

gastrointestinal microbiota, these data suggest that individuals with altered microbiomes due to opioid use may equally benefit from OUD immunization.

There is one current anti-oxycodone (OXY-sKLH) vaccine in clinical trials, and additional OUD vaccines, including F-CRM, are in late stages of preclinical development. In addition to the use of adjuvants to minimize individual variability, utilization of predictive biomarkers is a complementary strategy to identify patients that would most benefit from anti-opioid immunization. In order to test the value of predictive biomarkers in vaccinated patients, putative biomarkers can be identified through the use of preclinical and clinical models. In **Chapter 6**, a combination of preclinical and clinical studies was used to identify putative biomarkers rationally selected from knowledge of the immunological mechanisms of vaccine efficacy, or through exploratory investigations of cytokines and B cells in opioid users. In genetically diverse mice, it was found that the innate ability of T cells to produce IL-4 after non-specific stimulation correlates with OXY-sKLH titers and vaccine efficacy. This suggests that IL-4 production, or single nucleotide polymorphisms within the immune system that affect IL-4 production, may be of interest in clinical studies as a biomarker. Additionally, clinical studies of opioid-naïve and OUD populations revealed that individuals with OUD have higher frequencies of oxycodone-specific naïve B cells than non-OUD populations. Since we have previously established that higher oxycodone-specific naïve B cells are correlated with higher antibody titers after immunization with OXY-sKLH in mice (94), we predict that OUD populations may have better responses to OUD vaccines. We then used a multiplex cytokine analysis approach to identify cytokines that correlated with frequency of oxycodone-specific naïve B cell populations, as well as measuring serum opioid-specific antibody concentration. These markers may help further stratify opioid users based on their oxycodone-specific naïve B cell populations to potentially predict OUD vaccine efficacy and may establish an easier and cheaper biomarker

identification method, as quantification of serum markers such as antibodies and cytokines requires small serum volumes and no specialized equipment. These exploratory studies were critical for identifying the putative targets listed in Chapter 6, which will be further validated in vaccinated patient populations in the ongoing OXY-sKLH clinical trial and upcoming F_1-CRM clinical trial. These studies have also assisted in developing a clinical biomarker identification pipeline, so that rare patient samples may be efficiently used to assess as many putative biomarkers as possible.

Taken together, the research program presented in this dissertation furthers the goal of overcoming individual variability and increasing the efficacy of OUD vaccines through use of novel adjuvants and identification of predictive biomarkers to increase the success of OUD treatment to combat the opioid crisis.

References:

1. Breasted J. Ancient Records of Egypt. University of Chicago Oriental Institute Publications: University of Chicago Press, 1930;Vol. III, 217.
2. Presley CC, Lindsley CW. DARK Classics in Chemical Neuroscience: Opium, a Historical Perspective. ACS Chem Neurosci 2018; 9 (10), 2503-2518.
3. Trescot AM, Datta S, Lee M, Hansen H. Opioid pharmacology. Pain Physician 2008; 11 (2 Suppl), S133-153.
4. Ramirez JM, Burgraff NJ, Wei AD, Baertsch NA, Varga AG, Baghdoyan HA, Lydic R, Morris KF, Bolser DC, Levitt ES. Neuronal mechanisms underlying opioid-induced respiratory depression: our current understanding. J Neurophysiol 2021; 125 (5), 1899-1919.
5. Degenhardt L, Grebely J, Stone J, Hickman M, Vickerman P, Marshall BDL, Bruneau J, Altice FL, Henderson G, Rahimi-Movaghar A, Larney S. Global patterns of opioid use and dependence: harms to populations, interventions, and future action. Lancet 2019; 394 (10208), 1560-1579.
6. https://www.cdc.gov/nchs/pressroom/nchs_press_releases/2021/20211117.htm (accessed Dec 7, 2021 2021).
7. Control CfD. Increase in Fatal Drug Overdoses Across the United States Driven by Synthetic Opioids Before and During the COVID-19 Pandemic. 2020.
8. Burgess-Hull AJ, Smith KE, Panlilio LV, Schriefer D, Preston KL, Alter A, Yeager C, Chizmar T, Delbridge T, Zamore K, Beeson J, Epstein DH. Nonfatal opioid overdoses before and after Covid-19: Regional variation in rates of change. PLoS One 2022; 17 (3), e0263893.
9. Bolinski RS, Walters S, Salisbury-Afshar E, Ouellet LJ, Jenkins WD, Almirol E, Van Ham B, Fletcher S, Johnson C, Schneider JA, Ompad D, Pho MT. The Impact of the COVID-19 Pandemic on Drug Use Behaviors, Fentanyl Exposure, and Harm Reduction Service Support among People Who Use Drugs in Rural Settings. Int J Environ Res Public Health 2022; 19 (4).
10. Ghose R, Forati AM, Mantsch JR. Impact of the COVID-19 Pandemic on Opioid Overdose Deaths: a Spatiotemporal Analysis. J Urban Health 2022, 1-12.
11. Slavova S, Rock P, Bush HM, Quesinberry D, Walsh SL. Signal of increased opioid overdose during COVID-19 from emergency medical services data. Drug Alcohol Depend 2020; 214, 108176.
12. Volkow ND, Blanco C. The changing opioid crisis: development, challenges and opportunities. Mol Psychiatry 2021; 26 (1), 218-233.
13. Florence C, Luo F, Rice K. The economic burden of opioid use disorder and fatal opioid overdose in the United States, 2017. Drug Alcohol Depend 2021; 218, 108350.
14. Bell J, Strang J. Medication Treatment of Opioid Use Disorder. Biol Psychiatry 2020; 87 (1), 82-88.
15. Lim J, Farhat I, Douros A, Panagiotoglou D. Relative effectiveness of medications for opioid-related disorders: A systematic review and network meta-analysis of randomized controlled trials. PLoS One 2022; 17 (3), e0266142.
16. Timko C, Schultz NR, Cucciare MA, Vittorio L, Garrison-Diehn C. Retention in medication-assisted treatment for opiate dependence: A systematic review. J Addict Dis 2016; 35 (1), 22-35.
17. Morgan JR, Schackman BR, Leff JA, Linas BP, Walley AY. Injectable naltrexone, oral naltrexone, and buprenorphine utilization and discontinuation among

individuals treated for opioid use disorder in a United States commercially insured population. J Subst Abuse Treat 2018; 85, 90-96.
18. Sordo L, Barrio G, Bravo MJ, Indave BI, Degenhardt L, Wiessing L, Ferri M, Pastor-Barriuso R. Mortality risk during and after opioid substitution treatment: systematic review and meta-analysis of cohort studies. Bmj 2017; 357, j1550.
19. Wermeling DP. Review of naloxone safety for opioid overdose: practical considerations for new technology and expanded public access. Ther Adv Drug Saf 2015; 6 (1), 20-31.
20. Armenian P, Vo KT, Barr-Walker J, Lynch KL. Fentanyl, fentanyl analogs and novel synthetic opioids: A comprehensive review. Neuropharmacology 2018; 134 (Pt A), 121-132.
21. Torralva R, Janowsky A. Noradrenergic Mechanisms in Fentanyl-Mediated Rapid Death Explain Failure of Naloxone in the Opioid Crisis. J Pharmacol Exp Ther 2019; 371 (2), 453-475.
22. Kelly E, Sutcliffe K, Cavallo D, Ramos-Gonzalez N, Alhosan N, Henderson G. The anomalous pharmacology of fentanyl. Br J Pharmacol 2021.
23. Pergolizzi JV, Jr., Webster LR, Vortsman E, Ann LeQuang J, Raffa RB. Wooden Chest syndrome: The atypical pharmacology of fentanyl overdose. J Clin Pharm Ther 2021; 46 (6), 1505-1508.
24. Berkowitz B, Spector S. Evidence for active immunity to morphine in mice. Science 1972; 178 (4067), 1290-1292.
25. Bonese KF, Wainer BH, Fitch FW, Rothberg RM, Schuster CR. Changes in heroin self-administration by a rhesus monkey after morphine immunisation. Nature 1974; 252 (5485), 708-710.
26. Pravetoni M, Le Naour M, Harmon TM, Tucker AM, Portoghese PS, Pentel PR. An oxycodone conjugate vaccine elicits drug-specific antibodies that reduce oxycodone distribution to brain and hot-plate analgesia. J Pharmacol Exp Ther 2012; 341 (1), 225-232.
27. Baruffaldi F, Kelcher AH, Laudenbach M, Gradinati V, Limkar A, Roslawski M, Birnbaum A, Lees A, Hassler C, Runyon S, Pravetoni M. Preclinical Efficacy and Characterization of Candidate Vaccines for Treatment of Opioid Use Disorders Using Clinically Viable Carrier Proteins. Mol Pharm 2018; 15 (11), 4947-4962.
28. Baruffaldi F, Raleigh MD, King SJ, Roslawski MJ, Birnbaum AK, Hassler C, Carroll FI, Runyon SP, Winston S, Pentel PR, Pravetoni M. Formulation and Characterization of Conjugate Vaccines to Reduce Opioid Use Disorders Suitable for Pharmaceutical Manufacturing and Clinical Evaluation. Mol Pharm 2019; 16 (6), 2364-2375.
29. Kimishima A, Wenthur CJ, Zhou B, Janda KD. An Advance in Prescription Opioid Vaccines: Overdose Mortality Reduction and Extraordinary Alteration of Drug Half-Life. ACS Chem Biol 2017; 12 (1), 36-40.
30. Nguyen JD, Hwang CS, Grant Y, Janda KD, Taffe MA. Prophylactic vaccination protects against the development of oxycodone self-administration. Neuropharmacology 2018; 138, 292-303.
31. Pravetoni M, Vervacke JS, Distefano MD, Tucker AM, Laudenbach M, Pentel PR. Effect of currently approved carriers and adjuvants on the pre-clinical efficacy of a conjugate vaccine against oxycodone in mice and rats. PLoS One 2014; 9 (5), e96547.
32. Pravetoni M, Pentel PR, Potter DN, Chartoff EH, Tally L, LeSage MG. Effects of an oxycodone conjugate vaccine on oxycodone self-administration and

oxycodone-induced brain gene expression in rats. PLoS One 2014; 9 (7), e101807.
33. Raleigh MD, Peterson SJ, Laudenbach M, Baruffaldi F, Carroll FI, Comer SD, Navarro HA, Langston TL, Runyon SP, Winston S, Pravetoni M, Pentel PR. Safety and efficacy of an oxycodone vaccine: Addressing some of the unique considerations posed by opioid abuse. PLoS One 2017; 12 (12), e0184876.
34. Raleigh MD, Laudenbach M, Baruffaldi F, Peterson SJ, Roslawski MJ, Birnbaum AK, Carroll FI, Runyon SP, Winston S, Pentel PR, Pravetoni M. Opioid Dose- and Route-Dependent Efficacy of Oxycodone and Heroin Vaccines in Rats. J Pharmacol Exp Ther 2018; 365 (2), 346-353.
35. Raleigh MD, King SJ, Baruffaldi F, Saykao A, Hamid FA, Winston S, LeSage MG, Pentel PR, Pravetoni M. Pharmacological mechanisms underlying the efficacy of antibodies generated by a vaccine to treat oxycodone use disorder. Neuropharmacology 2021; 195, 108653.
36. Pravetoni M, Le Naour M, Tucker AM, Harmon TM, Hawley TM, Portoghese PS, Pentel PR. Reduced antinociception of opioids in rats and mice by vaccination with immunogens containing oxycodone and hydrocodone haptens. J Med Chem 2013; 56 (3), 915-923.
37. Blake S, Bremer PT, Zhou B, Petrovsky N, Smith LC, Hwang CS, Janda KD. Developing Translational Vaccines against Heroin and Fentanyl through Investigation of Adjuvants and Stability. Mol Pharm 2021; 18 (1), 228-235.
38. Hwang CS, Smith LC, Natori Y, Ellis B, Zhou B, Janda KD. Efficacious Vaccine against Heroin Contaminated with Fentanyl. ACS Chem Neurosci 2018; 9 (6), 1269-1275.
39. Hwang CS, Bremer PT, Wenthur CJ, Ho SO, Chiang S, Ellis B, Zhou B, Fujii G, Janda KD. Enhancing Efficacy and Stability of an Antiheroin Vaccine: Examination of Antinociception, Opioid Binding Profile, and Lethality. Mol Pharm 2018; 15 (3), 1062-1072.
40. Natori Y, Hwang CS, Lin L, Smith LC, Zhou B, Janda KD. A chemically contiguous hapten approach for a heroin-fentanyl vaccine. Beilstein J Org Chem 2019; 15, 1020-1031.
41. Raleigh MD, Pravetoni M, Harris AC, Birnbaum AK, Pentel PR. Selective effects of a morphine conjugate vaccine on heroin and metabolite distribution and heroin-induced behaviors in rats. J Pharmacol Exp Ther 2013; 344 (2), 397-406.
42. Sulima A, Jalah R, Antoline JFG, Torres OB, Imler GH, Deschamps JR, Beck Z, Alving CR, Jacobson AE, Rice KC, Matyas GR. A Stable Heroin Analogue That Can Serve as a Vaccine Hapten to Induce Antibodies That Block the Effects of Heroin and Its Metabolites in Rodents and That Cross-React Immunologically with Related Drugs of Abuse. J Med Chem 2018; 61 (1), 329-343.
43. Méndez SB, Matus-Ortega M, Miramontes RH, Salazar-Juárez A. Effect of the morphine/heroin vaccine on opioid and non-opioid drug-induced antinociception in mice. Eur J Pharmacol 2021; 891, 173718.
44. Bremer PT, Schlosburg JE, Banks ML, Steele FF, Zhou B, Poklis JL, Janda KD. Development of a Clinically Viable Heroin Vaccine. J Am Chem Soc 2017; 139 (25), 8601-8611.
45. Gutman ES, Irvin TC, Morgan JB, Barrientos RC, Torres OB, Beck Z, Matyas GR, Jacobson AE, Rice KC. Synthesis and immunological effects of C14-linked 4,5-epoxymorphinan analogues as novel heroin vaccine haptens. RSC Chem Biol 2021; 2 (3), 835-842.

46. Kosten TA, Shen XY, O'Malley PW, Kinsey BM, Lykissa ED, Orson FM, Kosten TR. A morphine conjugate vaccine attenuates the behavioral effects of morphine in rats. Prog Neuropsychopharmacol Biol Psychiatry 2013; 45, 223-229.
47. Li QQ, Luo YX, Sun CY, Xue YX, Zhu WL, Shi HS, Zhai HF, Shi J, Lu L. A morphine/heroin vaccine with new hapten design attenuates behavioral effects in rats. J Neurochem 2011; 119 (6), 1271-1281.
48. Farhangi A, Akbarzadeh A, Mehrabi MR, Chiani M, Saffari Z, Ghassemi S, Kheiri M, Bashar R. Safety of human therapeutic morphine vaccine employing Lohmann specific pathogen free eggs. Pak J Biol Sci 2010; 13 (21), 1047-1051.
49. Anton B, Leff P. A novel bivalent morphine/heroin vaccine that prevents relapse to heroin addiction in rodents. Vaccine 2006; 24 (16), 3232-3240.
50. Li F, Cheng K, Antoline JF, Iyer MR, Matyas GR, Torres OB, Jalah R, Beck Z, Alving CR, Parrish DA, Deschamps JR, Jacobson AE, Rice KC. Synthesis and immunological effects of heroin vaccines. Org Biomol Chem 2014; 12 (37), 7211-7232.
51. Ma LX, Zhou Q, Zheng HB, Li SB. [Preparation and characterization of anti-morphine vaccine antibody]. Xi Bao Yu Fen Zi Mian Yi Xue Za Zhi 2006; 22 (3), 368-370.
52. Sulima A, Li F, Morgan JB, Truong P, Antoline JFG, Oertel T, Barrientos RC, Torres OB, Beck Z, Imler GH, Deschamps JR, Matyas GR, Jacobson AE, Rice KC. Design, Synthesis, and In Vivo Evaluation of C1-Linked 4,5-Epoxymorphinan Haptens for Heroin Vaccines. Molecules 2022; 27 (5).
53. Barrientos RC, Whalen C, Torres OB, Sulima A, Bow EW, Komla E, Beck Z, Jacobson AE, Rice KC, Matyas GR. Bivalent Conjugate Vaccine Induces Dual Immunogenic Response That Attenuates Heroin and Fentanyl Effects in Mice. Bioconjug Chem 2021; 32 (11), 2295-2306.
54. Raleigh MD, Baruffaldi F, Peterson SJ, Le Naour M, Harmon TM, Vigliaturo JR, Pentel PR, Pravetoni M. A Fentanyl Vaccine Alters Fentanyl Distribution and Protects against Fentanyl-Induced Effects in Mice and Rats. J Pharmacol Exp Ther 2019; 368 (2), 282-291.
55. Robinson C, Gradinati V, Hamid F, Baehr C, Crouse B, Averick S, Kovaliov M, Harris D, Runyon S, Baruffaldi F, LeSage M, Comer S, Pravetoni M. Therapeutic and Prophylactic Vaccines to Counteract Fentanyl Use Disorders and Toxicity. J Med Chem 2020.
56. Townsend EA, Blake S, Faunce KE, Hwang CS, Natori Y, Zhou B, Bremer PT, Janda KD, Banks ML. Conjugate vaccine produces long-lasting attenuation of fentanyl vs. food choice and blocks expression of opioid withdrawal-induced increases in fentanyl choice in rats. Neuropsychopharmacology 2019; 44 (10), 1681-1689.
57. Barrientos RC, Bow EW, Whalen C, Torres OB, Sulima A, Beck Z, Jacobson AE, Rice KC, Matyas GR. Novel Vaccine That Blunts Fentanyl Effects and Sequesters Ultrapotent Fentanyl Analogues. Mol Pharm 2020; 17 (9), 3447-3460.
58. Baehr C, Robinson C, Kassick AJ, Jahan R, Averick S, Runyon S, Pravetoni M. Characterization and prophylactic efficacy of vaccines targeting fentanyl, alfentanil, sufentanil, and acetylfentanyl in rats. ACS Omega 2022.
59. Eubanks LM, Blake S, Natori Y, Ellis B, Bremer PT, Janda KD. A Highly Efficacious Carfentanil Vaccine That Blunts Opioid-Induced Antinociception and Respiratory Depression. ACS Chem Biol 2021; 16 (2), 277-282.
60. Bremer PT, Kimishima A, Schlosburg JE, Zhou B, Collins KC, Janda KD. Combatting Synthetic Designer Opioids: A Conjugate Vaccine Ablates Lethal

Doses of Fentanyl Class Drugs. Angew Chem Int Ed Engl 2016; 55 (11), 3772-3775.
61. Lee JC, Park H, Eubanks LM, Ellis B, Zhou B, Janda KD. A Vaccine against Benzimidazole-Derived New Psychoactive Substances That Are More Potent Than Fentanyl. J Med Chem 2022; 65 (3), 2522-2531.
62. Komla E, Torres OB, Jalah R, Sulima A, Beck Z, Alving CR, Jacobson AE, Rice KC, Matyas GR. Effect of Preexisting Immunity to Tetanus Toxoid on the Efficacy of Tetanus Toxoid-Conjugated Heroin Vaccine in Mice. Vaccines (Basel) 2021; 9 (6).
63. Barbosa-Méndez S, Matus-Ortega M, Hernández-Miramontes R, Salazar-Juárez A. The morphine/heroin vaccine decreased the heroin-induced antinociceptive and reinforcing effects in three inbred strains mouse. Int Immunopharmacol 2021; 98, 107887.
64. Li QQ, Sun CY, Luo YX, Xue YX, Meng SQ, Xu LZ, Chen N, Deng JH, Zhai HF, Kosten TR, Shi J, Lu L, Sun HQ. A conjugate vaccine attenuates morphine- and heroin-induced behavior in rats. Int J Neuropsychopharmacol 2014; 18 (5).
65. Tenney RD, Blake S, Bremer PT, Zhou B, Hwang CS, Poklis JL, Janda KD, Banks ML. Vaccine blunts fentanyl potency in male rhesus monkeys. Neuropharmacology 2019; 158, 107730.
66. Park H, Lee JC, Eubanks LM, Ellis B, Zhou B, Janda KD. Improvements on a chemically contiguous hapten for a vaccine to address fentanyl-contaminated heroin. Bioorg Med Chem 2021; 41, 116225.
67. Townsend EA, Bremer PT, Faunce KE, Negus SS, Jaster AM, Robinson HL, Janda KD, Banks ML. Evaluation of a Dual Fentanyl/Heroin Vaccine on the Antinociceptive and Reinforcing Effects of a Fentanyl/Heroin Mixture in Male and Female Rats. ACS Chem Neurosci 2020; 11 (9), 1300-1310.
68. Gradinati V, Baruffaldi F, Abbaraju S, Laudenbach M, Amin R, Gilger B, Velagaleti P, Pravetoni M. Polymer-mediated delivery of vaccines to treat opioid use disorders and to reduce opioid-induced toxicity. Vaccine 2020; 38 (30), 4704-4712.
69. Schlosburg JE, Vendruscolo LF, Bremer PT, Lockner JW, Wade CL, Nunes AA, Stowe GN, Edwards S, Janda KD, Koob GF. Dynamic vaccine blocks relapse to compulsive intake of heroin. Proc Natl Acad Sci U S A 2013; 110 (22), 9036-9041.
70. Wang J, Ellis B, Zhou B, Eubanks LM, Blake S, Janda KD. A fentanyl vaccine constructed upon opsonizing antibodies specific for the Galα1-3Gal epitope. Chem Commun (Camb) 2020; 56 (48), 6551-6554.
71. Barbosa-Mendez S, Matus-Ortega M, Hernandez-Miramontes R, Salazar-Juárez A. Synergistic immune and antinociceptive effects induced from the combination of two different vaccines against morphine/heroin in mouse. Hum Vaccin Immunother 2021; 17 (10), 3515-3528.
72. Hwang CS, Smith LC, Wenthur CJ, Ellis B, Zhou B, Janda KD. Heroin vaccine: Using titer, affinity, and antinociception as metrics when examining sex and strain differences. Vaccine 2019; 37 (30), 4155-4163.
73. Bremer PT, Schlosburg JE, Lively JM, Janda KD. Injection route and TLR9 agonist addition significantly impact heroin vaccine efficacy. Mol Pharm 2014; 11 (3), 1075-1080.
74. Stowe GN, Vendruscolo LF, Edwards S, Schlosburg JE, Misra KK, Schulteis G, Mayorov AV, Zakhari JS, Koob GF, Janda KD. A vaccine strategy that induces protective immunity against heroin. J Med Chem 2011; 54 (14), 5195-5204.
75. Matyas GR, Rice KC, Cheng K, Li F, Antoline JF, Iyer MR, Jacobson AE, Mayorov AV, Beck Z, Torres OB, Alving CR. Facial recognition of heroin vaccine opiates:

type 1 cross-reactivities of antibodies induced by hydrolytically stable haptenic surrogates of heroin, 6-acetylmorphine, and morphine. Vaccine 2014; 32 (13), 1473-1479.
76. Jalah R, Torres OB, Mayorov AV, Li F, Antoline JF, Jacobson AE, Rice KC, Deschamps JR, Beck Z, Alving CR, Matyas GR. Efficacy, but not antibody titer or affinity, of a heroin hapten conjugate vaccine correlates with increasing hapten densities on tetanus toxoid, but not on CRM197 carriers. Bioconjug Chem 2015; 26 (6), 1041-1053.
77. Raleigh MD, Pentel PR, LeSage MG. Pharmacokinetic correlates of the effects of a heroin vaccine on heroin self-administration in rats. PLoS One 2014; 9 (12), e115696.
78. Townsend EA, Bremer PT, Jacob NT, Negus SS, Janda KD, Banks ML. A synthetic opioid vaccine attenuates fentanyl-vs-food choice in male and female rhesus monkeys. Drug Alcohol Depend 2021; 218, 108348.
79. Belz TF, Bremer PT, Zhou B, Ellis B, Eubanks LM, Janda KD. Enhancement of a Heroin Vaccine through Hapten Deuteration. J Am Chem Soc 2020; 142 (31), 13294-13298.
80. Raleigh MD, Accetturo C, Pravetoni M. Combining a Candidate Vaccine for Opioid Use Disorders with Extended-Release Naltrexone Increases Protection against Oxycodone-Induced Behavioral Effects and Toxicity. J Pharmacol Exp Ther 2020; 374 (3), 392-403.
81. Schwienteck KL, Blake S, Bremer PT, Poklis JL, Townsend EA, Negus SS, Banks ML. Effectiveness and selectivity of a heroin conjugate vaccine to attenuate heroin, 6-acetylmorphine, and morphine antinociception in rats: Comparison with naltrexone. Drug Alcohol Depend 2019; 204, 107501.
82. Truong TT, Kosten TR. Current status of vaccines for substance use disorders: A brief review of human studies. J Neurol Sci 2022; 434, 120098.
83. Hatsukami DK, Jorenby DE, Gonzales D, Rigotti NA, Glover ED, Oncken CA, Tashkin DP, Reus VI, Akhavain RC, Fahim RE, Kessler PD, Niknian M, Kalnik MW, Rennard SI. Immunogenicity and smoking-cessation outcomes for a novel nicotine immunotherapeutic. Clin Pharmacol Ther 2011; 89 (3), 392-399.
84. Martell BA, Orson FM, Poling J, Mitchell E, Rossen RD, Gardner T, Kosten TR. Cocaine vaccine for the treatment of cocaine dependence in methadone-maintained patients: a randomized, double-blind, placebo-controlled efficacy trial. Arch Gen Psychiatry 2009; 66 (10), 1116-1123.
85. Hilligan KL, Ronchese F. Antigen presentation by dendritic cells and their instruction of CD4+ T helper cell responses. Cell Mol Immunol 2020; 17 (6), 587-599.
86. Vaccari M, Franchini G. T Cell Subsets in the Germinal Center: Lessons from the Macaque Model. Front Immunol 2018; 9, 348.
87. Zhu J, Yamane H, Paul WE. Differentiation of effector CD4 T cell populations (*). Annu Rev Immunol 2010; 28, 445-489.
88. Allen CD, Okada T, Cyster JG. Germinal-center organization and cellular dynamics. Immunity 2007; 27 (2), 190-202.
89. Cyster JG, Allen CDC. B Cell Responses: Cell Interaction Dynamics and Decisions. Cell 2019; 177 (3), 524-540.
90. De Silva NS, Klein U. Dynamics of B cells in germinal centres. Nat Rev Immunol 2015; 15 (3), 137-148.
91. Stebegg M, Kumar SD, Silva-Cayetano A, Fonseca VR, Linterman MA, Graca L. Regulation of the Germinal Center Response. Front Immunol 2018; 9, 2469.

92. Fagarasan S, Honjo T. T-Independent immune response: new aspects of B cell biology. Science 2000; 290 (5489), 89-92.
93. Salerno-Gonçalves R, Sztein MB. Cell-mediated immunity and the challenges for vaccine development. Trends Microbiol 2006; 14 (12), 536-542.
94. Laudenbach M, Baruffaldi F, Robinson C, Carter P, Seelig D, Baehr C, Pravetoni M. Blocking interleukin-4 enhances efficacy of vaccines for treatment of opioid abuse and prevention of opioid overdose. Sci Rep 2018; 8 (1), 5508.
95. Huseby Kelcher AM, Baehr CA, Hamid FA, Hart GT, Pravetoni M. Contribution of Antibody-Mediated Effector Functions to the Mechanism of Efficacy of Vaccines for Opioid Use Disorders. J Immunol 2021; 207 (3), 860-867.
96. Lin M, Lee JC, Blake S, Ellis B, Eubanks LM, Janda KD. Broadly Neutralizing Synthetic Cannabinoid Vaccines. JACS Au 2021; 1 (1), 31-40.
97. Robinson C, Baehr C, Schmiel SE, Accetturo C, Mueller DL, Pravetoni M. Alum adjuvant is more effective than MF59 at prompting early germinal center formation in response to peptide-protein conjugates and enhancing efficacy of a vaccine against opioid use disorders. Hum Vaccin Immunother 2019; 15 (4), 909-917.
98. Di Pasquale A, Preiss S, Tavares Da Silva F, Garcon N. Vaccine Adjuvants: from 1920 to 2015 and Beyond. Vaccines (Basel) 2015; 3 (2), 320-343.
99. Stone AE, Scheuermann SE, Haile CN, Cuny GD, Velasquez ML, Linhuber JP, Duddupudi AL, Vigliaturo JR, Pravetoni M, Kosten TA, Kosten TR, Norton EB. Fentanyl conjugate vaccine by injected or mucosal delivery with dmLT or LTA1 adjuvants implicates IgA in protection from drug challenge. NPJ Vaccines 2021; 6 (1), 69.
100. Defrance T, Vanbervliet B, Pène J, Banchereau J. Human recombinant IL-4 induces activated B lymphocytes to produce IgG and IgM. J Immunol 1988; 141 (6), 2000-2005.
101. Duan L, Liu D, Chen H, Mintz MA, Chou MY, Kotov DI, Xu Y, An J, Laidlaw BJ, Cyster JG. Follicular dendritic cells restrict interleukin-4 availability in germinal centers and foster memory B cell generation. Immunity 2021; 54 (10), 2256-2272.e2256.
102. Gaya M, Barral P, Burbage M, Aggarwal S, Montaner B, Warren Navia A, Aid M, Tsui C, Maldonado P, Nair U, Ghneim K, Fallon PG, Sekaly RP, Barouch DH, Shalek AK, Bruckbauer A, Strid J, Batista FD. Initiation of Antiviral B Cell Immunity Relies on Innate Signals from Spatially Positioned NKT Cells. Cell 2018; 172 (3), 517-533.e520.
103. Gonzalez DG, Cote CM, Patel JR, Smith CB, Zhang Y, Nickerson KM, Zhang T, Kerfoot SM, Haberman AM. Nonredundant Roles of IL-21 and IL-4 in the Phased Initiation of Germinal Center B Cells and Subsequent Self-Renewal Transitions. J Immunol 2018; 201 (12), 3569-3579.
104. Turqueti-Neves A, Otte M, Prazeres da Costa O, Hopken UE, Lipp M, Buch T, Voehringer D. B-cell-intrinsic STAT6 signaling controls germinal center formation. Eur J Immunol 2014; 44 (7), 2130-2138.
105. Weinstein JS, Herman EI, Lainez B, Licona-Limón P, Esplugues E, Flavell R, Craft J. TFH cells progressively differentiate to regulate the germinal center response. Nat Immunol 2016; 17 (10), 1197-1205.
106. Yusuf I, Kageyama R, Monticelli L, Johnston RJ, Ditoro D, Hansen K, Barnett B, Crotty S. Germinal center T follicular helper cell IL-4 production is dependent on signaling lymphocytic activation molecule receptor (CD150). J Immunol 2010; 185 (1), 190-202.

107. Yoshimoto T. The Hunt for the Source of Primary Interleukin-4: How We Discovered That Natural Killer T Cells and Basophils Determine T Helper Type 2 Cell Differentiation In Vivo. Front Immunol 2018; 9, 716.
108. Junttila IS. Tuning the Cytokine Responses: An Update on Interleukin (IL)-4 and IL-13 Receptor Complexes. Front Immunol 2018; 9, 888.
109. Mendonça MS, Peraçolli TS, Silva-Vergara ML, Ribeiro SC, Oliveira RF, Mendes RP, Rodrigues V, Jr. High interleukin-4 expression and interleukin-4 gene polymorphisms are associated with susceptibility to human paracoccidioidomycosis. Mem Inst Oswaldo Cruz 2015; 110 (6), 781-785.
110. Mountford AP, Hogg KG, Coulson PS, Brombacher F. Signaling via interleukin-4 receptor alpha chain is required for successful vaccination against schistosomiasis in BALB/c mice. Infect Immun 2001; 69 (1), 228-236.
111. Roberts MT, Stober CB, McKenzie AN, Blackwell JM. Interleukin-4 (IL-4) and IL-10 collude in vaccine failure for novel exacerbatory antigens in murine Leishmania major infection. Infect Immun 2005; 73 (11), 7620-7628.
112. Choe J, Kim HS, Armitage RJ, Choi YS. The functional role of B cell antigen receptor stimulation and IL-4 in the generation of human memory B cells from germinal center B cells. J Immunol 1997; 159 (8), 3757-3766.
113. Moon HB, Severinson E, Heusser C, Johansson SG, Moller G, Persson U. Regulation of IgG1 and IgE synthesis by interleukin 4 in mouse B cells. Scand J Immunol 1989; 30 (3), 355-361.
114. Wang N, Liang H, Zen K. Molecular mechanisms that influence the macrophage m1-m2 polarization balance. Front Immunol 2014; 5, 614.
115. Zhu J. T helper 2 (Th2) cell differentiation, type 2 innate lymphoid cell (ILC2) development and regulation of interleukin-4 (IL-4) and IL-13 production. Cytokine 2015; 75 (1), 14-24.
116. Gour N, Wills-Karp M. IL-4 and IL-13 signaling in allergic airway disease. Cytokine 2015; 75 (1), 68-78.
117. Finkelman FD, Katona IM, Urban JF, Jr., Holmes J, Ohara J, Tung AS, Sample JV, Paul WE. IL-4 is required to generate and sustain in vivo IgE responses. J Immunol 1988; 141 (7), 2335-2341.
118. Andoh A, Masuda A, Yamakawa M, Kumazawa Y, Kasajima T. Absence of interleukin-4 enhances germinal center reaction in secondary immune response. Immunol Lett 2000; 73 (1), 35-41.
119. Jackson RJ, Worley M, Trivedi S, Ranasinghe C. Novel HIV IL-4R antagonist vaccine strategy can induce both high avidity CD8 T and B cell immunity with greater protective efficacy. Vaccine 2014; 32 (43), 5703-5714.
120. Tang YW, Graham BS. Anti-IL-4 treatment at immunization modulates cytokine expression, reduces illness, and increases cytotoxic T lymphocyte activity in mice challenged with respiratory syncytial virus. J Clin Invest 1994; 94 (5), 1953-1958.
121. Lim KH, Staudt LM. Toll-like receptor signaling. Cold Spring Harb Perspect Biol 2013; 5 (1), a011247.
122. Takeda K, Akira S. Toll-like receptors. Curr Protoc Immunol 2015; 109, 14.12.11-14.12.10.
123. Hennessy EJ, Parker AE, O'Neill LA. Targeting Toll-like receptors: emerging therapeutics? Nat Rev Drug Discov 2010; 9 (4), 293-307.
124. Arora R, Haile CN, Kosten TA, Wu Y, Ramakrishnan M, Hawkins LD, Orson FM, Kosten TR. Preclinical efficacy of an anti-methamphetamine vaccine using E6020 adjuvant. Am J Addict 2019; 28 (2), 119-126.

125. Toussi DN, Massari P. Immune Adjuvant Effect of Molecularly-defined Toll-Like Receptor Ligands. Vaccines (Basel) 2014; 2 (2), 323-353.
126. Ahmed SS, Black S, Ulmer J. New developments and concepts related to biomarker application to vaccines. Microb Biotechnol 2012; 5 (2), 233-240.
127. Roh EY, Song EY, Yoon JH, Oh S, Chang JY, Park H, Seo SH, Shin S. Effects of interleukin-4 and interleukin-12B gene polymorphisms on hepatitis B virus vaccination. Ann Hepatol 2017; 16 (1), 63-70.
128. Cui W, Sun CM, Deng BC, Liu P. Association of polymorphisms in the interleukin-4 gene with response to hepatitis B vaccine and susceptibility to hepatitis B virus infection: a meta-analysis. Gene 2013; 525 (1), 35-40.
129. Yao Y, Xu X, Li Y, Wang X, Yang H, Chen J, Liu S, Deng Y, Zhao Z, Yin Q, Sun M, Shi L. Study of the association of seventeen single nucleotide polymorphisms and their haplotypes in the TNF-α, IL-2, IL-4 and IL-10 genes with the antibody response to inactivated Japanese encephalitis vaccine. Hum Vaccin Immunother 2020; 16 (10), 2449-2455.
130. Clifford HD, Hayden CM, Khoo SK, Naniche D, Mandomando IM, Zhang G, Richmond P, Le Souëf PN. Genetic Variants in the IL-4/IL-13 Pathway Influence Measles Vaccine Responses and Vaccine Failure in Children from Mozambique. Viral Immunol 2017; 30 (7), 472-478.
131. Baynam G, Zhang G, Khoo SK, Sly P, Holt P, Goldblatt J, Le Souef PN. Gender-specific effects of cytokine gene polymorphisms on childhood vaccine responses. Vaccine 2008; 26 (29-30), 3574-3579.
132. Wiertsema SP, Baynam G, Khoo SK, Veenhoven RH, van Heerbeek N, Zhang G, Laing IA, Rijkers GT, Goldblatt J, Sanders EA, Le Souef PN. Impact of genetic variants in IL-4, IL-4 RA and IL-13 on the anti-pneumococcal antibody response. Vaccine 2007; 25 (2), 306-313.
133. Laudenbach M, Baruffaldi F, Vervacke JS, Distefano MD, Titcombe PJ, Mueller DL, Tubo NJ, Griffith TS, Pravetoni M. The frequency of naive and early-activated hapten-specific B cell subsets dictates the efficacy of a therapeutic vaccine against prescription opioid abuse. J Immunol 2015; 194 (12), 5926-5936.
134. https://www.who.int/substance_abuse/information-sheet/en/ 2020).
135. Schuchat A, Houry D, Guy GP, Jr. New Data on Opioid Use and Prescribing in the United States. Jama 2017; 318 (5), 425-426.
136. Chen Q, Larochelle MR, Weaver DT, Lietz AP, Mueller PP, Mercaldo S, Wakeman SE, Freedberg KA, Raphel TJ, Knudsen AB, Pandharipande PV, Chhatwal J. Prevention of Prescription Opioid Misuse and Projected Overdose Deaths in the United States. JAMA Netw Open 2019; 2 (2), e187621.
137. Howard J, Cimineri L, Evans T, Chosewood LC, Afanuh S. Medication-Assisted Treatment for Opioid Use Disorder. *USDHHS, CDC and NIOSH*, 2019.
138. https://www.samhsa.gov/medication-assisted-treatment/statutes-regulations-guidelines.
139. Wiegand TJ, Le Lait MC, Bartelson BB, Dart RC, Green JL. Analysis of the Abuse and Diversion of the Buprenorphine Transdermal Delivery System. J Pain 2016; 17 (6), 745-752.
140. Lavonas EJ, Severtson SG, Martinez EM, Bucher-Bartelson B, Le Lait MC, Green JL, Murrelle LE, Cicero TJ, Kurtz SP, Rosenblum A, Surratt HL, Dart RC. Abuse and diversion of buprenorphine sublingual tablets and film. J Subst Abuse Treat 2014; 47 (1), 27-34.
141. Cicero TJ, Ellis MS, Surratt HL, Kurtz SP. Factors contributing to the rise of buprenorphine misuse: 2008-2013. Drug Alcohol Depend 2014; 142, 98-104.

142. Pravetoni M, Comer SD. Development of vaccines to treat opioid use disorders and reduce incidence of overdose. Neuropharmacology 2019; 158, 107662.
143. Hwang CS, Janda KD. A Vision for Vaccines: Combating the Opioid Epidemic. Biochemistry 2017; 56 (42), 5625-5627.
144. Heekin RD, Shorter D, Kosten TR. Current status and future prospects for the development of substance abuse vaccines. Expert Rev Vaccines 2017; 16 (11), 1067-1077.
145. Pentel PR, LeSage MG. New directions in nicotine vaccine design and use. Adv Pharmacol 2014; 69, 553-580.
146. Laudenbach M, Tucker AM, Runyon SP, Carroll FI, Pravetoni M. The frequency of early-activated hapten-specific B cell subsets predicts the efficacy of vaccines for nicotine dependence. Vaccine 2015; 33 (46), 6332-6339.
147. Luckheeram RV, Zhou R, Verma AD, Xia B. CD4(+)T cells: differentiation and functions. Clin Dev Immunol 2012; 2012, 925135.
148. Jacob NT, Anraku K, Kimishima A, Zhou B, Collins KC, Lockner JW, Ellis BA, Janda KD. A bioconjugate leveraging xenoreactive antibodies to alleviate cocaine-induced behavior. Chem Commun (Camb) 2017; 53 (58), 8156-8159.
149. Hart TK, Blackburn MN, Brigham-Burke M, Dede K, Al-Mahdi N, Zia-Amirhosseini P, Cook RM. Preclinical efficacy and safety of pascolizumab (SB 240683): a humanized anti-interleukin-4 antibody with therapeutic potential in asthma. Clin Exp Immunol 2002; 130 (1), 93-100.
150. Ellis J, van Maurik A, Fortunato L, Gisbert S, Chen K, Schwartz A, McHugh S, Want A, Santos Franco S, Oliveira JJ, Price J, Coles A, Brown K, Su D, Craigen JL, Yang J, Brett S, Davis B, Cheriyan J, Kousin-Ezewu O, Gray F, Thompson PW, Fernando D. Anti-IL-7 receptor alpha monoclonal antibody (GSK2618960) in healthy subjects - a randomized, double-blind, placebo-controlled study. Br J Clin Pharmacol 2019; 85 (2), 304-315.
151. Rech AJ, Vonderheide RH. Clinical use of anti-CD25 antibody daclizumab to enhance immune responses to tumor antigen vaccination by targeting regulatory T cells. Ann N Y Acad Sci 2009; 1174, 99-106.
152. Passariello M, D'Alise AM, Esposito A, Vetrei C, Froechlich G, Scarselli E, Nicosia A, De Lorenzo C. Novel Human Anti-PD-L1 mAbs Inhibit Immune-Independent Tumor Cell Growth and PD-L1 Associated Intracellular Signalling. Sci Rep 2019; 9 (1), 13125.
153. Sullivan BA, Tsuji W, Kivitz A, Peng J, Arnold GE, Boedigheimer MJ, Chiu K, Green CL, Kaliyaperumal A, Wang C, Ferbas J, Chung JB. Inducible T-cell co-stimulator ligand (ICOSL) blockade leads to selective inhibition of anti-KLH IgG responses in subjects with systemic lupus erythematosus. Lupus Sci Med 2016; 3 (1), e000146.
154. Toellner KM. Cognate interactions: extrafollicular IL-4 drives germinal-center reactions, a new role for an old cytokine. Eur J Immunol 2014; 44 (7), 1917-1920.
155. Baehr C, Kelcher AH, Khaimraj A, Reed DE, Pandit SG, AuCoin D, Averick S, Pravetoni M. Monoclonal Antibodies Counteract Opioid-Induced Behavioral and Toxic Effects in Mice and Rats. J Pharmacol Exp Ther 2020; 375 (3), 469-477.
156. Schindelin JA-C, Ignacio Frise, Erwin Kaynig, Verena Longair, Mark Pietzsch, Tobias Preibisch, Stephan Rueden, Curtis Saalfeld, Stephan Schmid, Benjamin Tinevez, Jean-Yves White, Daniel James Hartenstein, VolkerEliceiri, KevinTomancak, PavelCardona, Albert. Fiji: an open-source platform for biological-image analysis. nature methods, 2012;Vol. 9, 676-682.
157. Jassal B, Matthews L, Viteri G, Gong C, Lorente P, Fabregat A, Sidiropoulos K, Cook J, Gillespie M, Haw R, Loney F, May B, Milacic M, Rothfels K, Sevilla C,

Shamovsky V, Shorser S, Varusai T, Weiser J, Wu G, Stein L, Hermjakob H, D'Eustachio P. The reactome pathway knowledgebase. Nucleic Acids Res 2020; 48 (D1), D498-d503.
158. Ho IY, Bunker JJ, Erickson SA, Neu KE, Huang M, Cortese M, Pulendran B, Wilson PC. Refined protocol for generating monoclonal antibodies from single human and murine B cells. J Immunol Methods 2016; 438, 67-70.
159. Lo M, Kim HS, Tong RK, Bainbridge TW, Vernes JM, Zhang Y, Lin YL, Chung S, Dennis MS, Zuchero YJ, Watts RJ, Couch JA, Meng YG, Atwal JK, Brezski RJ, Spiess C, Ernst JA. Effector-attenuating Substitutions That Maintain Antibody Stability and Reduce Toxicity in Mice. J Biol Chem 2017; 292 (9), 3900-3908.
160. Crouse B, Robinson C, Huseby Kelcher A, Laudenbach M, Abrahante JE, Pravetoni M. Mechanisms of interleukin 4 mediated increase in efficacy of vaccines against opioid use disorders. NPJ Vaccines 2020; 5, 99.
161. Lofano G, Mancini F, Salvatore G, Cantisani R, Monaci E, Carrisi C, Tavarini S, Sammicheli C, Rossi Paccani S, Soldaini E, Laera D, Finco O, Nuti S, Rappuoli R, De Gregorio E, Bagnoli F, Bertholet S. Oil-in-Water Emulsion MF59 Increases Germinal Center B Cell Differentiation and Persistence in Response to Vaccination. J Immunol 2015; 195 (4), 1617-1627.
162. Reinhardt RL, Liang HE, Locksley RM. Cytokine-secreting follicular T cells shape the antibody repertoire. Nat Immunol 2009; 10 (4), 385-393.
163. Lockner JW, Eubanks LM, Choi JL, Lively JM, Schlosburg JE, Collins KC, Globisch D, Rosenfeld-Gunn RJ, Wilson IA, Janda KD. Flagellin as carrier and adjuvant in cocaine vaccine development. Mol Pharm 2015; 12 (2), 653-662.
164. Song Z, Zhang J, Zhang X, Li D, Wang H, Xu X, Xu W, Yin Y, Cao J. Interleukin 4 Deficiency Reverses Development of Secondary Pseudomonas aeruginosa Pneumonia During Sepsis-Associated Immunosuppression. J Infect Dis 2015; 211 (10), 1616-1627.
165. Mohrs M, Ledermann B, Kohler G, Dorfmuller A, Gessner A, Brombacher F. Differences between IL-4- and IL-4 receptor alpha-deficient mice in chronic leishmaniasis reveal a protective role for IL-13 receptor signaling. J Immunol 1999; 162 (12), 7302-7308.
166. Zamorano J, Wang HY, Wang LM, Pierce JH, Keegan AD. IL-4 protects cells from apoptosis via the insulin receptor substrate pathway and a second independent signaling pathway. J Immunol 1996; 157 (11), 4926-4934.
167. Vella A, Teague TK, Ihle J, Kappler J, Marrack P. Interleukin 4 (IL-4) or IL-7 prevents the death of resting T cells: stat6 is probably not required for the effect of IL-4. J Exp Med 1997; 186 (2), 325-330.
168. Lischke A, Moriggl R, Brändlein S, Berchtold S, Kammer W, Sebald W, Groner B, Liu X, Hennighausen L, Friedrich K. The interleukin-4 receptor activates STAT5 by a mechanism that relies upon common gamma-chain. J Biol Chem 1998; 273 (47), 31222-31229.
169. Lin JX, Leonard WJ. The role of Stat5a and Stat5b in signaling by IL-2 family cytokines. Oncogene 2000; 19 (21), 2566-2576.
170. Bélanger S, Crotty S. Dances with cytokines, featuring TFH cells, IL-21, IL-4 and B cells. Nat Immunol 2016; 17 (10), 1135-1136.
171. Barrington R, Zhang M, Fischer M, Carroll MC. The role of complement in inflammation and adaptive immunity. Immunol Rev 2001; 180, 5-15.
172. Kranich J, Krautler NJ. How Follicular Dendritic Cells Shape the B-Cell Antigenome. Front Immunol 2016; 7, 225.

173. Strainic MG, Liu J, Huang D, An F, Lalli PN, Muqim N, Shapiro VS, Dubyak GR, Heeger PS, Medof ME. Locally produced complement fragments C5a and C3a provide both costimulatory and survival signals to naive CD4+ T cells. Immunity 2008; 28 (3), 425-435.
174. Liszewski MK, Kolev M, Le Friec G, Leung M, Bertram PG, Fara AF, Subias M, Pickering MC, Drouet C, Meri S, Arstila TP, Pekkarinen PT, Ma M, Cope A, Reinheckel T, Rodriguez de Cordoba S, Afzali B, Atkinson JP, Kemper C. Intracellular complement activation sustains T cell homeostasis and mediates effector differentiation. Immunity 2013; 39 (6), 1143-1157.
175. Jayasekera JP, Moseman EA, Carroll MC. Natural antibody and complement mediate neutralization of influenza virus in the absence of prior immunity. J Virol 2007; 81 (7), 3487-3494.
176. Meyer K, Basu A, Przysiecki CT, Lagging LM, Di Bisceglie AM, Conley AJ, Ray R. Complement-mediated enhancement of antibody function for neutralization of pseudotype virus containing hepatitis C virus E2 chimeric glycoprotein. J Virol 2002; 76 (5), 2150-2158.
177. Chang HY, Kharrazi H, Bodycombe D, Weiner JP, Alexander GC. Healthcare costs and utilization associated with high-risk prescription opioid use: a retrospective cohort study. BMC Med 2018; 16 (1), 69.
178. Centers for Disease Control and Prevention NCfIPaC. Drug Overdose. 2021;Vol. 2021.
179. Centers for Disease Control and Prevention NCfIPaC. Opioids. 2021.
180. Ahmad F, Rossen L, Sutton P. Provisional drug overdose death counts. National Center for Health Statistics, 2021.
181. Bart G. Maintenance medication for opiate addiction: the foundation of recovery. J Addict Dis 2012; 31 (3), 207-225.
182. Rzasa Lynn R, Galinkin JL. Naloxone dosage for opioid reversal: current evidence and clinical implications. Ther Adv Drug Saf 2018; 9 (1), 63-88.
183. Pravetoni M, Raleigh MD, Le Naour M, Tucker AM, Harmon TM, Jones JM, Birnbaum AK, Portoghese PS, Pentel PR. Co-administration of morphine and oxycodone vaccines reduces the distribution of 6-monoacetylmorphine and oxycodone to brain in rats. Vaccine 2012; 30 (31), 4617-4624.
184. HogenEsch H. Mechanisms of stimulation of the immune response by aluminum adjuvants. Vaccine 2002; 20 Suppl 3, S34-39.
185. Miller SM, Cybulski V, Whitacre M, Bess LS, Livesay MT, Walsh L, Burkhart D, Bazin HG, Evans JT. Novel Lipidated Imidazoquinoline TLR7/8 Adjuvants Elicit Influenza-Specific Th1 Immune Responses and Protect Against Heterologous H3N2 Influenza Challenge in Mice. Front Immunol 2020; 11, 406.
186. Short KK, Miller SM, Walsh L, Cybulski V, Bazin H, Evans JT, Burkhart D. Co-encapsulation of synthetic lipidated TLR4 and TLR7/8 agonists in the liposomal bilayer results in a rapid, synergistic enhancement of vaccine-mediated humoral immunity. J Control Release 2019; 315, 186-196.
187. Massena CJ, Lathrop SK, Davison CJ, Schoener R, Bazin HG, Evans JT, Burkhart DJ. A tractable covalent linker strategy for the production of immunogenic antigen-TLR7/8L bioconjugates. Chem Commun (Camb) 2021; 57 (38), 4698-4701.
188. Smith AJ, Li Y, Bazin HG, St-Jean JR, Larocque D, Evans JT, Baldridge JR. Evaluation of novel synthetic TLR7/8 agonists as vaccine adjuvants. Vaccine 2016; 34 (36), 4304-4312.
189. Ugolini M, Gerhard J, Burkert S, Jensen KJ, Georg P, Ebner F, Volkers SM, Thada S, Dietert K, Bauer L, Schäfer A, Helbig ET, Opitz B, Kurth F, Sur S, Dittrich N,

Gaddam S, Conrad ML, Benn CS, Blohm U, Gruber AD, Hutloff A, Hartmann S, Boekschoten MV, Müller M, Jungersen G, Schumann RR, Suttorp N, Sander LE. Recognition of microbial viability via TLR8 drives T(FH) cell differentiation and vaccine responses. Nat Immunol 2018; 19 (4), 386-396.
190. Gorden KB, Gorski KS, Gibson SJ, Kedl RM, Kieper WC, Qiu X, Tomai MA, Alkan SS, Vasilakos JP. Synthetic TLR agonists reveal functional differences between human TLR7 and TLR8. J Immunol 2005; 174 (3), 1259-1268.
191. Heil F, Hemmi H, Hochrein H, Ampenberger F, Kirschning C, Akira S, Lipford G, Wagner H, Bauer S. Species-specific recognition of single-stranded RNA via toll-like receptor 7 and 8. Science 2004; 303 (5663), 1526-1529.
192. Liu J, Xu C, Hsu LC, Luo Y, Xiang R, Chuang TH. A five-amino-acid motif in the undefined region of the TLR8 ectodomain is required for species-specific ligand recognition. Mol Immunol 2010; 47 (5), 1083-1090.
193. Crouse B, Wu MM, Gradinati V, Kassick AJ, Song D, Jahan R, Averick S, Runyon S, Comer SD, Pravetoni M. Efficacy and Selectivity of Monovalent and Bivalent Vaccination Strategies to Protect against Exposure to Carfentanil, Fentanyl, and Their Mixtures in Rats. ACS Pharmacol Transl Sci 2022; 5 (5), 331-343.
194. Bazin-lee H, Ettenger G, Khalaf J, Ryter KT. Toll-like Receptor Ligands. 2021.
195. Evans JT, Bess LS, Mwakwari SC, Livesay MT, Li Y, Cybulski V, Johnson DA, Bazin HG. Synthetic Toll-like Receptors 7 and 8 Agonists: Structure-Activity Relationship in the Oxoadenine Series. ACS Omega 2019; 4 (13), 15665-15677.
196. Bazin HG, Bess LS, Livesay MT, Mwakwari SC, Johnson DA. Phospholipidation of TLR7/8-active imidazoquinolines using a tandem phosphoramidite method. Tetrahedron Lett 2016; 57 (19), 2063-2066.
197. Hursh SR, Roma PG. Behavioral Economics and the Analysis of Consumption and Choice. Managerial and Decision Economics 2016; 37 (4-5), 224-238.
198. Peterson BK. Vital Signs. In Physical Rehabilitation: Evidence Based Examination, Evaluation, and Intervention; Falk K., ed.; St. Louis, Missouri: Saunders Elsevier, 2007, 598-624.
199. Cocks BG, de Waal Malefyt R, Galizzi JP, de Vries JE, Aversa G. IL-13 induces proliferation and differentiation of human B cells activated by the CD40 ligand. Int Immunol 1993; 5 (6), 657-663.
200. Pabst R. The pig as a model for immunology research. Cell Tissue Res 2020; 380 (2), 287-304.
201. Butler JE, Wertz N, Deschacht N, Kacskovics I. Porcine IgG: structure, genetics, and evolution. Immunogenetics 2009; 61 (3), 209-230.
202. Kacskovics I, Sun J, Butler JE. Five putative subclasses of swine IgG identified from the cDNA sequences of a single animal. J Immunol 1994; 153 (8), 3565-3573.
203. Meuldermans WE, Hurkmans RM, Heykants JJ. Plasma protein binding and distribution of fentanyl, sufentanil, alfentanil and lofentanil in blood. Arch Int Pharmacodyn Ther 1982; 257 (1), 4-19.
204. de Jong SE, Olin A, Pulendran B. The Impact of the Microbiome on Immunity to Vaccination in Humans. Cell Host Microbe 2020; 28 (2), 169-179.
205. Kosten TR, Domingo CB, Hamon SC, Nielsen DA. DBH gene as predictor of response in a cocaine vaccine clinical trial. Neurosci Lett 2013; 541, 29-33.
206. Nielsen DA, Hamon SC, Kosten TR. The κ-opioid receptor gene as a predictor of response in a cocaine vaccine clinical trial. Psychiatr Genet 2013; 23 (6), 225-232.
207. Kenny PJ, Chen SA, Kitamura O, Markou A, Koob GF. Conditioned withdrawal drives heroin consumption and decreases reward sensitivity. J Neurosci 2006; 26 (22), 5894-5900.

208. Wikler A. Dynamics of drug dependence. Implications of a conditioning theory for research and treatment. Arch Gen Psychiatry 1973; 28 (5), 611-616.
209. Koob GF, Le Moal M. Addiction and the brain antireward system. Annu Rev Psychol 2008; 59, 29-53.
210. Robinson TE, Berridge KC. Addiction. Annu Rev Psychol 2003; 54, 25-53.
211. Lindblom N, de Villiers SH, Semenova S, Kalayanov G, Gordon S, Schilström B, Johansson AM, Markou A, Svensson TH. Active immunisation against nicotine blocks the reward facilitating effects of nicotine and partially prevents nicotine withdrawal in the rat as measured by dopamine output in the nucleus accumbens, brain reward thresholds and somatic signs. Naunyn Schmiedebergs Arch Pharmacol 2005; 372 (3), 182-194.
212. Roiko SA, Harris AC, LeSage MG, Keyler DE, Pentel PR. Passive immunization with a nicotine-specific monoclonal antibody decreases brain nicotine levels but does not precipitate withdrawal in nicotine-dependent rats. Pharmacol Biochem Behav 2009; 93 (2), 105-111.
213. Jurk M, Heil F, Vollmer J, Schetter C, Krieg AM, Wagner H, Lipford G, Bauer S. Human TLR7 or TLR8 independently confer responsiveness to the antiviral compound R-848. In Nat Immunol; United States, 2002;Vol. 3, 499.
214. Kadowaki N, Ho S, Antonenko S, Malefyt RW, Kastelein RA, Bazan F, Liu YJ. Subsets of human dendritic cell precursors express different toll-like receptors and respond to different microbial antigens. J Exp Med 2001; 194 (6), 863-869.
215. Gilliet M, Cao W, Liu YJ. Plasmacytoid dendritic cells: sensing nucleic acids in viral infection and autoimmune diseases. Nat Rev Immunol 2008; 8 (8), 594-606.
216. Gorden KK, Qiu XX, Binsfeld CC, Vasilakos JP, Alkan SS. Cutting edge: activation of murine TLR8 by a combination of imidazoquinoline immune response modifiers and polyT oligodeoxynucleotides. J Immunol 2006; 177 (10), 6584-6587.
217. Crandall CS, Kerrigan S, Aguero RL, Lavalley J, McKinney PE. The influence of collection site and methods on postmortem morphine concentrations in a porcine model. J Anal Toxicol 2006; 30 (9), 651-658.
218. Elmer J, Flickinger KL, Anderson MW, Koller AC, Sundermann ML, Dezfulian C, Okonkwo DO, Shutter LA, Salcido DD, Callaway CW, Menegazzi JJ. Effect of neuromonitor-guided titrated care on brain tissue hypoxia after opioid overdose cardiac arrest. Resuscitation 2018; 129, 121-126.
219. (WHO) WHO. Carfentanil Critical Review Report. 2017.
220. https://www.dea.gov/drug-information/drug-scheduling (accessed March 17 2022).
221. Langston JL, Moffett MC, Makar JR, Burgan BM, Myers TM. Carfentanil toxicity in the African green monkey: Therapeutic efficacy of naloxone. Toxicol Lett 2020; 325, 34-42.
222. Jalal H, Burke DS. Carfentanil and the rise and fall of overdose deaths in the United States. Addiction 2021; 116 (6), 1593-1599.
223. Leen JLS, Juurlink DN. Carfentanil: a narrative review of its pharmacology and public health concerns. Can J Anaesth 2019; 66 (4), 414-421.
224. Attaway PR, Smiley-McDonald HM, Davidson PJ, Kral AH. Perceived occupational risk of fentanyl exposure among law enforcement. Int J Drug Policy 2021; 95, 103303.
225. Smith LC, Bremer PT, Hwang CS, Zhou B, Ellis B, Hixon MS, Janda KD. Monoclonal Antibodies for Combating Synthetic Opioid Intoxication. J Am Chem Soc 2019; 141 (26), 10489-10503.

226. Lu S. Heterologous prime-boost vaccination. Curr Opin Immunol 2009; 21 (3), 346-351.
227. Walz AJ, Hsu F-L. Scaled up synthesis: salts of carfentanil and remifentanil. Aberdeen Proving Ground, MD: Edgewood Chemical Biological Center, 2017.
228. Butcher KJ, Hurst J. Aromatic amines as nucleophiles in the Bargellini reaction. Tetrahedron Letters, 2009;Vol. 50, 2497-2500.
229. Pravetoni M, Keyler DE, Raleigh MD, Harris AC, Lesage MG, Mattson CK, Pettersson S, Pentel PR. Vaccination against nicotine alters the distribution of nicotine delivered via cigarette smoke inhalation to rats. Biochem Pharmacol 2011; 81 (9), 1164-1170.
230. Satoskar SD, Keyler DE, LeSage MG, Raphael DE, Ross CA, Pentel PR. Tissue-dependent effects of immunization with a nicotine conjugate vaccine on the distribution of nicotine in rats. Int Immunopharmacol 2003; 3 (7), 957-970.
231. Pichichero ME. Protein carriers of conjugate vaccines: characteristics, development, and clinical trials. Hum Vaccin Immunother 2013; 9 (12), 2505-2523.
232. Pryde DC, Jones LH, Gervais DP, Stead DR, Blakemore DC, Selby MD, Brown AD, Coe JW, Badland M, Beal DM, Glen R, Wharton Y, Miller GJ, White P, Zhang N, Benoit M, Robertson K, Merson JR, Davis HL, McCluskie MJ. Selection of a novel anti-nicotine vaccine: influence of antigen design on antibody function in mice. PLoS One 2013; 8 (10), e76557.
233. de Villiers SH, Cornish KE, Troska AJ, Pravetoni M, Pentel PR. Increased efficacy of a trivalent nicotine vaccine compared to a dose-matched monovalent vaccine when formulated with alum. Vaccine 2013; 31 (52), 6185-6193.
234. Zeigler DF, Roque R, Clegg CH. Construction of an enantiopure bivalent nicotine vaccine using synthetic peptides. PLoS One 2017; 12 (6), e0178835.
235. Bergh MS, Bogen IL, Garibay N, Baumann MH. Evidence for nonlinear accumulation of the ultrapotent fentanyl analog, carfentanil, after systemic administration to male rats. Neuropharmacology 2019; 158, 107596.
236. Flynn SM, France CP. Discriminative stimulus effects of carfentanil in rats discriminating fentanyl: Differential antagonism by naltrexone. Drug Alcohol Depend 2021; 221, 108599.
237. Behzadi M, Joukar S, Beik A. Opioids and Cardiac Arrhythmia: A Literature Review. Med Princ Pract 2018; 27 (5), 401-414.
238. Heard DJ, Nichols WW, Buss D, Kollias GV. Comparative cardiopulmonary effects of intramuscularly administered etorphine and carfentanil in goats. Am J Vet Res 1996; 57 (1), 87-96.
239. NSDUH. 2018 National Survey of Drug Use and Health (NSDUH) Releases. https://www.samhsa.gov/data/release/2018-national-survey-drug-use-and-health-nsduh-releases, 2018.
240. CDC. Wide-ranging OnLine Data for Epidemiological Research (WONDER). http://wonder.cdc.gov, 2020.
241. Network CHA. Increase in Fatal Drug Overdoses Across the United States Driven by

Synthetic Opioids Before and During the COVID-19 Pandemic. Center for Disease Control, 2020.
242. Pravetoni M. Biologics to treat substance use disorders: Current status and new directions. Hum Vaccin Immunother 2016; 12 (12), 3005-3019.

243. Carrera MR, Ashley JA, Zhou B, Wirsching P, Koob GF, Janda KD. Cocaine vaccines: antibody protection against relapse in a rat model. Proc Natl Acad Sci U S A 2000; 97 (11), 6202-6206.
244. Evans SM, Foltin RW, Hicks MJ, Rosenberg JB, De BP, Janda KD, Kaminsky SM, Crystal RG. Efficacy of an adenovirus-based anti-cocaine vaccine to reduce cocaine self-administration and reacqusition using a choice procedure in rhesus macaques. Pharmacol Biochem Behav 2016; 150-151, 76-86.
245. Ozgen MH, Blume S. The continuing search for an addiction vaccine. Vaccine 2019; 37 (36), 5485-5490.
246. Kosten TA, Shen XY, Kinsey BM, Kosten TR, Orson FM. Attenuation of cocaine-induced locomotor activity in male and female mice by active immunization. Am J Addict 2014; 23 (6), 604-607.
247. Pulendran B. Immunology taught by vaccines. Science 2019; 366 (6469), 1074-1075.
248. Collins N, Belkaid Y. Do the Microbiota Influence Vaccines and Protective Immunity to Pathogens? Engaging Our Endogenous Adjuvants. Cold Spring Harb Perspect Biol 2018; 10 (2).
249. Praharaj I, John SM, Bandyopadhyay R, Kang G. Probiotics, antibiotics and the immune responses to vaccines. Philos Trans R Soc Lond B Biol Sci 2015; 370 (1671).
250. Banerjee S, Sindberg G, Wang F, Meng J, Sharma U, Zhang L, Dauer P, Chen C, Dalluge J, Johnson T, Roy S. Opioid-induced gut microbial disruption and bile dysregulation leads to gut barrier compromise and sustained systemic inflammation. Mucosal Immunol 2016; 9 (6), 1418-1428.
251. Wang F, Meng J, Zhang L, Johnson T, Chen C, Roy S. Morphine induces changes in the gut microbiome and metabolome in a morphine dependence model. Sci Rep 2018; 8 (1), 3596.
252. Kiraly DD, Walker DM, Calipari ES, Labonte B, Issler O, Pena CJ, Ribeiro EA, Russo SJ, Nestler EJ. Alterations of the Host Microbiome Affect Behavioral Responses to Cocaine. Sci Rep 2016; 6, 35455.
253. Meckel KR, Kiraly DD. A potential role for the gut microbiome in substance use disorders. Psychopharmacology (Berl) 2019; 236 (5), 1513-1530.
254. Lee K, Vuong HE, Nusbaum DJ, Hsiao EY, Evans CJ, Taylor AMW. The gut microbiota mediates reward and sensory responses associated with regimen-selective morphine dependence. Neuropsychopharmacology 2018; 43 (13), 2606-2614.
255. Beura LK, Hamilton SE, Bi K, Schenkel JM, Odumade OA, Casey KA, Thompson EA, Fraser KA, Rosato PC, Filali-Mouhim A, Sekaly RP, Jenkins MK, Vezys V, Haining WN, Jameson SC, Masopust D. Normalizing the environment recapitulates adult human immune traits in laboratory mice. Nature 2016; 532 (7600), 512-516.
256. Gohl DM, Vangay P, Garbe J, MacLean A, Hauge A, Becker A, Gould TJ, Clayton JB, Johnson TJ, Hunter R, Knights D, Beckman KB. Systematic improvement of amplicon marker gene methods for increased accuracy in microbiome studies. Nat Biotechnol 2016; 34 (9), 942-949.
257. Martin M. Cutadapt removes adapter sequences from high-throughput sequencing reads. EMBnet.journal 2011; 17 (1), 3.
258. Callahan BJ, McMurdie PJ, Rosen MJ, Han AW, Johnson AJ, Holmes SP. DADA2: High-resolution sample inference from Illumina amplicon data. Nat Methods 2016; 13 (7), 581-583.

259. Oksanen J, Blanchet G, Friendly M, Kindt R, Legendre P. vegan: Community Ecology Package. 2017.
260. Love MI, Huber W, Anders S. Moderated estimation of fold change and dispersion for RNA-seq data with DESeq2. Genome Biol 2014; 15 (12), 550.
261. Langille MG, Zaneveld J, Caporaso JG, McDonald D, Knights D, Reyes JA, Clemente JC, Burkepile DE, Vega Thurber RL, Knight R, Beiko RG, Huttenhower C. Predictive functional profiling of microbial communities using 16S rRNA marker gene sequences. Nat Biotechnol 2013; 31 (9), 814-821.
262. Boyer EW. Management of opioid analgesic overdose. N Engl J Med 2012; 367 (2), 146-155.
263. Clapp M, Aurora N, Herrera L, Bhatia M, Wilen E, Wakefield S. Gut microbiota's effect on mental health: The gut-brain axis. Clin Pract 2017; 7 (4), 987.
264. Shreiner AB, Kao JY, Young VB. The gut microbiome in health and in disease. Curr Opin Gastroenterol 2015; 31 (1), 69-75.
265. Arndt A, Hoffacker P, Zellmer K, Goecer O, Recks MS, Kuerten S. Conventional housing conditions attenuate the development of experimental autoimmune encephalomyelitis. PLoS One 2014; 9 (6), e99794.
266. Letson HL, Morris J, Biros E, Dobson GP. Conventional and Specific-Pathogen Free Rats Respond Differently to Anesthesia and Surgical Trauma. Sci Rep 2019; 9 (1), 9399.
267. Abolins S, King EC, Lazarou L, Weldon L, Hughes L, Drescher P, Raynes JG, Hafalla JCR, Viney ME, Riley EM. The comparative immunology of wild and laboratory mice, Mus musculus domesticus. Nat Commun 2017; 8, 14811.
268. Zhang P, Yang M, Chen C, Liu L, Wei X, Zeng S. Toll-Like Receptor 4 (TLR4)/Opioid Receptor Pathway Crosstalk and Impact on Opioid Analgesia, Immune Function, and Gastrointestinal Motility. Front Immunol 2020; 11, 1455.
269. Kim YS, Unno T, Kim BY, Park MS. Sex Differences in Gut Microbiota. World J Mens Health 2020; 38 (1), 48-60.
270. Lockner JW, Ho SO, McCague KC, Chiang SM, Do TQ, Fujii G, Janda KD. Enhancing nicotine vaccine immunogenicity with liposomes. Bioorg Med Chem Lett 2013; 23 (4), 975-978.
271. Eisenstein TK. The Role of Opioid Receptors in Immune System Function. Front Immunol 2019; 10, 2904.
272. Dowling JK, Mansell A. Toll-like receptors: the swiss army knife of immunity and vaccine development. Clin Transl Immunology 2016; 5 (5), e85.